5-2007

Spatial Sensors for Quantitative Assessment of Retrieved Arthroplasty Bearings

Melinda Harman
Clemson University, melinda.harman@biomotion.org

SPATIAL SENSORS FOR QUANTITATIVE ASSESSMENT OF RETRIEVED ARTHROPLASTY BEARINGS

A Dissertation
Presented to
the Graduate School of
Clemson University

In Partial Fulfillment
of the Requirements for the Degree
Doctor of Philosophy
Bioengineering

---

by
Melinda Kay Harman
May 2007

Accepted by:
Martine Laberge, Ph.D., Academic Advisor
Scott A. Banks, Ph.D., Research Advisor
Karen J. L. Burg, Ph.D., Committee Member
Paul F. Joseph, Ph.D., Committee Member

ABSTRACT

Evaluation of retrieved joint arthroplasty bearings provides unique evidence related to the physiological environment in which bearing materials are expected to perform. This dissertation describes the development of novel spatial sensors and measurement strategies for standardized, quantitative assessments of arthroplasty bearings, including total knee replacements, unicompartmental knee replacements, and total hip replacements. The approach is to assess bearings that endured a finite duration of function in patients, with particular emphasis on expanding our understanding of the biomechanical conditions specific to bearing function and wear in the physiological environment. Several quantifiable parameters are identified that prove comparable to pre-clinical *in vitro* tibological evaluations, including knee wear simulation and analytical modeling. These comparisons provide clinical relevance to the existing methodologies, helping to verify that the biomechanical simulations accurately represent the *in vivo* conditions they are meant to simulate. The broad objective of this dissertation is to improve the longevity and function of arthroplasty bearing materials and designs. Assessments from the retrieved prostheses are discussed within the context of developing comprehensive approaches for the prospective evaluation of new materials and designs in joint replacements.

DEDICATION

To my extended family of friends and relatives who indulge my limitless desire to work hard and play hard.

ACKNOWLEDGEMENTS

The achievement of this professional goal is tribute to the support provided by my committee members, including Dr. Martine LaBerge (academic chairperson); Dr. Scott Banks (research chairperson); Dr. Karen Burg; and Dr. Paul Joseph. Thank you for being open to alternative pathways to success. I am thankful for the guidance of my mentors, past and present, including Kent Bacchus, PhD; Scott Banks, PhD; Roy Bloebaum, PhD; F. Robert Brueckmann, MD; Michael Ferrara, PhD; Linda Hicks; W. Andrew Hodge, MD; Marco Vicceconti, PhD; and Joanne Weatherbee. I acknowledge the substantial contributions of my collaborators and co-authors, including Scott A. Banks, PhD; Lisa C. Benson, PhD; Pat A. Campbell, PhD; John D. DesJardins, PhD; Benjamin J. Fregly, PhD; A. Seth Greenwald, D.Phil(Oxon); W. Andrew Hodge, MD; Martine LaBerge, PhD; George D. Markovich, MD; Akiko Mori, PhD; Edward A. Morra, MSME; Sven Rössing, MD; W. Gregory Sawyer, PhD; Hans-Peter Scharf, MD; Sabine Schmitt, MD; and Hiromasa Tanino, MD. Your input added magnitude and diversity to my work. Finally, I would like to acknowledge the institutional support of the Orthopaedic Research Laboratory and The BioMotion Foundation in West Palm Beach, Florida. The dynamic research environment provided to me was cultivated by an incredible team of people who worked with me over the years, including Scott Banks; Anne Banks; Sylvia Barnes; James Coburn; Lewjack Dorrance; Lauren Garrett; Andy Hodge; Scott Keiser; Kim Mitchell; Tammy Moore; Dave Morgan; Akiko Mori; Sharon Samsoondar; Heidi Anderson-Thomas; Dana Wilhelm; and all the former students; administrators; research fellows who contributed their time and talents.

TABLE OF CONTENTS

Table of Contents (Continued)

Table of Contents (Continued)

Table of Contents (Continued)

LIST OF TABLES

List of Tables (Continued)

List of Tables (Continued)

LIST OF FIGURES

List of Figures (Continued)

List of Figures (Continued)

List of Figures (Continued)

List of Figures (Continued)

List of Figures (Continued)

PREFACE

As the worldwide population continues to live longer, leading healthier and more active lives, the demand for technology to maintain mobility is increasing. Total joint arthroplasty (TJA) in the lower limb, including total knee replacement (TKR) and total hip replacement (THR), is widely recognized as a successful surgical procedure for treating arthritis and other congenital or degenerative musculoskeletal joint diseases. TJA survivorship is greater than 90% at 10 years,[67,75,123,144,145] providing significant improvement in social function, bodily pain, physical function, vitality, and general health in TJA patients.[100,122]

Over 1700 people receive a TKR or THR each day in the United States, and the number of those procedures performed is expected to double by the year 2016 for TKR and by the year 2026 for THR.[114,115] This increasing demand for primary TJA drives a parallel increase in the number of revision procedures which represent approximately 7% to 9% of the total number of TKR and 6% to 24% of the total number of THR performed in North America, Europe and Australia.[114,123] Survivorship of revision TJA is dramatically lower than primary TJA,[159] resulting in a tremendous amount of pain and morbidity to patients. Efforts to improve TJA longevity, especially in younger patients,[74] and decrease the incidence of revision TJA will have a positive socio-economic impact on both patients and society.

Historically, factors contributing to successful joint arthroplasty and those that limit longevity are documented in clinical outcome and survivorship studies. Clinical

pioneers in orthopaedics provided early empirical evidence supporting the use of biomaterials for TJA[126,129,148,161] and contributed, in part, to the modern used of cobalt-chrome alloys,[2,89] alumina and zirconia ceramics[5,92,93] and ultra-high molecular weight polyethylene (UHMWPE)[3,90,91] for TJA bearing materials. Improved understanding of the interface between of the implanted joint prostheses and human tissues has been gained through programs to procure and analyze joint prostheses after they have functioned in patients.[24,26,36,84,97,118,155] The biomechanical performance of TKR and THR has been evaluated in patients during activities of daily living using high-speed dynamic imaging for accurate measurement of *in vivo* joint motions[6-14,20,45-50,59,60,82,87,103,104,105,112,124,135,,138,139,143,161,164,167,171,173] and using instrumented prostheses for accurate measurement of *in vivo* joint forces and pressures.[23,54-56,81,109,115,168] These outcome, retrieval and biomechanical studies are used by the medical, engineering and manufacturing communities to characterize the *in vivo* conditions in which TJA prostheses are expected to function.

Quantitative assessments of retrieved TJA bearings provide unique evidence related to the physiological environment in which bearing materials are expected to perform. The rationale for many of the changes in bearing surfaces are linked to evidence of wear on UHMWPE articular bearings retrieved after *in vivo* function[25,28,30,39,40,42,57,62,77,78,96,98,99,101,108,110,120,128,137,140,169,176,179,183,184,185] and the submicron sized wear particles generated at the bearing surfaces during *in vivo* function.[15,21,32,40,44,37,41,44,61,79,80,140,177,185] The histological and biochemical responses to these wear particles can incite a cellular response leading to bone-resorbing osteolysis,[88,134] which dramatically limits the longevity of joint

prostheses.[65,70,77,78,85,102,111,125,131,153,156,182] Interest in reducing the number of revision TJA occurring due to bearing wear will continue to drive changes in bearing materials, designs and manufacturing processes.[116,119,121,141,152,170,174,186]

Studies of retrieved TJA bearings suggest that different articular wear mechanisms correspond to visibly different articular wear modes, surface deformation and different wear particle sizes.[1,17,29,31,43,71,73,77,79,83,86,117,125,131,133,146,157,165,176,180,181] However, identifying the relationships between articular damage and joint mechanics existing in TJA patients during activities of daily living can be difficult.[7,62,73,120,142,160,176,180,181] TJA function is greatly influenced by variability in surgical technique, prosthesis design and patient habitus, as well as the variety of activities of daily living performed by TJA patients.[136,178] One of the primary aims of this dissertation is to assess the performance of bearing materials after that have endured a finite duration of function. To this end, spatial sensors and measurement strategies were developed for standardized, quantitative assessment of arthroplasty bearings. These novel technologies generate quantitative wear evaluations complementary to existing methodologies.

Joint wear simulations[4,17,22,51,52,94,95,166] and analytical models[18,19,64,68] aim to mimic relevant biomechanics and physiologic conditions in an effort to reproduce clinical wear rates and wear mechanisms of the materials being tested.[34,35,131,132,152,172,175] Attempts to verify the clinical relevance of such methodology has included comparison of simulator wear rates with estimates of in vivo wear rates derived from radiographic films or direct measurement of worn bearings. While largely successful for THR bearing materials,[33,63,69,130,175] such comparisons have proven difficult for TKR

bearings.[38,76,107,147,149,158] Consequently, the clinical relevance of knee joint wear simulators has yet to be established to the same extent as hip simulators, and the orthopaedic community is in need of quantitative assessments applicable to both knee joint wear simulation and analytical models.

In well-functioning TJA, UHMWPE wear mechanisms are principally determined by the motion (kinematics) and load (pressure) conditions occurring at the bearing articular surface.[16,18,27,43,53,58,66,72,106,117,127,150,151,181] Considering that knee kinematics during patient activity contribute substantially to damage patterns on retrieved UHMWPE TKR bearings,[73]comparison of the damage patterns generated after simulation with damage patterns on retrieved bearings is one possible method for verifying the kinematic and load input parameters and the resulting UHMWPE damage after simulation or analytical modeling. It is hypothesized that quantitative wear assessments of retrieved TJA bearings can be made comparable to damage assessments after joint wear simulations and musculoskeletal models. It is intended that these comparisons will provide clinical relevance to the existing methodologies and advance the prospective evaluation of TJA bearing materials and designs.

Significance of Dissertation

The broad objective of this dissertation is to improve the longevity of arthroplasty bearing materials and designs. The approach used in this dissertation is to investigate the performance of bearings that have endured a finite duration of function in patients after TJA. The overall aim of this dissertation is to expand our understanding of bearing wear and the contributing biomechanical environment in which arthroplasty bearings function throughout their service in patients.

To this end, novel spatial sensors were developed for the quantitative assessment of arthroplasty bearings, as detailed in Chapter 1. These spatial sensors were applied to several groups of retrieved joint arthroplasty bearings, including TKR in Chapters 2-5, unicompartmental knee replacements (UKR) in Chapter 6, and THR in Chapter 7. Those chapters aim to characterize the bearings' performance under physiologic conditions by quantifying the cumulative damage that occurs at the bearing contact surfaces. These assessments of in vivo performance are then compared with results from contemporary joint wear simulation in Chapter 8 and contact modeling in Chapters 9-10. Those chapters aim to evaluate the in vitro test methodologies to verify that the biomechanical simulations and analytical models accurately represent the in vivo conditions they are meant to simulate. Chapter 11 explores the relationship between tibiofemoral kinematics and articular geometry

With the exception of Chapter 1, each chapter is presented as an individual study, with unique hypotheses originating from the context of retrieved bearing performance. The final chapter provides dissertation conclusions and recommendations for future work. The assessments from the retrieved prostheses are discussed within the context of developing comprehensive approaches for the prospective evaluation of new materials and designs in joint replacements. Continuing to expand the utility of the spatial sensors presented in this dissertation will result in useful, quantitative endpoints for comparison with simulation and analytical modeling of joint arthroplasty biomechanics and bearing tribology.

1 EXPERIMENTAL TECHNIQUES

1.1 Introduction

Joint prostheses used for orthopaedic hip and knee replacement arthroplasty were obtained through the Implant Retrieval Program established in 1992 by the Orthopaedic Research Laboratory at Good Samaritan Medical Center in West Palm Beach, Florida.[5,6] This program was initiated with approval from the Institutional Review Board, with written informed consent to retrieve the prostheses obtained from the patients' during follow-up visits at the clinical office or from patients' family members for those donating prostheses post-mortem. The Implant Retrieval Program has been directed by the candidate (MKH) since 1994 and approximately 1100 hip and knee prostheses consisting of various designs have been obtained through this program.

In the work reported herein, prostheses have sustained damage at the UHMWPE articular surface due to *in vivo* function in patients (retrieved inserts) or *in vitro* loading on a knee joint wear simulator (simulated inserts). Several sources of retrieved inserts and simulated inserts were available based on collaborative research projects established by the candidate (MKH). Retrieved inserts from hip and knee arthroplasty patients of W. Andrew Hodge, MD of West Palm Beach, Florida and Sabine Schmitt, MD of Mannheim, Germany were included. Retrieved inserts from knee arthroplasty patients of George D. Markovich, MD of Fort Myers, Florida and Aaron A. Hofmann, MD of Salt Lake City, Utah that were obtained through the Bone & Joint Research Lab at the Department of Veterans Affairs Medical Center in Salt Lake City, Utah were also

included. All simulator worn inserts were obtained from the Department of Bioengineering at Clemson University, Clemson, South Carolina.

Retrieved and simulated inserts were characterized according to design type, material (as reported by the manufacturer), and component size. The level of performance of the retrieved inserts was characterized using standard patient demographics (sex, age, weight, height, etc.), and reason for retrieval, depending on availability of such information in the patients' medical records. Duration of function for retrieved inserts was expressed as the number of months between the date of implantation and the date of retrieval. Clinical outcome scores[9] and retrospective radiographic review of radiolucent lines and component alignment[3,10] were assessed according to published guidelines. The level of performance of the simulator worn inserts was characterized based on kinematic and load input parameters from the knee joint wear simulator and duration of function (number of repetitions of one million cycles of loading).

All retrieved UHMWPE knee and hip components were handled according to written procedures established for the Implant Retrieval Program. Each component was assigned a unique identifying accession number and the condition at retrieval was recorded using written notes and gross photographs. UHMWPE components were gently cleaned with mild soap, soaked in a disinfectant solution, rinsed in running tap water and allowed to air dry. Inserts were stored in ambient air in sealed and labeled plastic bags.

1.2 Optical Sensor for Assessing Damage Modes on UHMWPE Tibial Inserts and UHMWPE Patellar Components

The articular and backside (modular components only) surfaces for retrieved and simulated UHMWPE tibial inserts and retrieved UHMWPE patellar components were assessed visually at 7 to 30 times magnification using an optical microscope (model Z30L, Cambridge Instruments, Cambridge, MA). The prevalence of eleven distinct damage modes was evaluated using published[7,8,13,17] visual identification methods (Figure 1.1). Abrasion is typically visualized as rough, tufted regions. Burnishing is visualized as smooth regions that are highly reflective of incident light. Delamination is visualized as thin layers of UHMWPE material separated from the surface. Subsurface delamination appears as cracks and/or discoloration located inferior and generally parallel to articular plane without discontinuity of the articular surface material. Dimpling is visualized as uniform, nearly circular indentations approximately 100 μm in diameter.[15] Non-articular deformation is visualized as a permanent change in shape from the original surface in regions not intended as a bearing surface. Embedded debris is visualized as particles that differed in color and/or texture relative to the surrounding UHMWPE surface, consistent with embedded particles of bone, cement fragments or metal particles. Pitting is visualized as depressions with rough surfaces typically 1 to 2 mm in diameter. Scratching is visualized as thin lines in irregular or ordered directions across the surface. Striations are visualized as highly oriented, longitudinal, smooth peaks and troughs on the articular surface.[17] Fractures are visualized as complete cracks or wear-through of the polyethylene insert, typically resulting in exposure of the metal baseplate in modular components.

1.3 Optical Sensor for Quantitative Measurement of Damage Patterns on UHMWPE Tibial Inserts and UHMWPE Patellar Components

Each UHMWPE tibial insert and UHMWPE patellar component was placed on a 20 mm^2 calibration grid. A digital image of each components' articular and backside (modular components only) surface was recorded at approximately 2.5X magnification. Actual dimensions were scaled using the calibration grid to convert pixels to millimeters (mm). Analysis software consisted of custom programs written in PV-Wave (version 6.21, Visual Numerics, Inc., Boulder, CO). PV-Wave is an array based programming language that is used to build visual data analysis applications with mathematical computations based on IMSL Numeric Libraries written in C/C++ and Fortran code.

A global coordinate system was established using the calibration grid in each image. A normalized, component-based coordinate system referencing the components' edges was established and a central origin for each component was determined. For tibial inserts, the medial-lateral (ML) and anterior-posterior (AP) edges of the articular surface were identified and the ML and AP midpoint were determined. The x-axis was directed in the AP direction, the y-axis was directed in the ML direction, and the z-axis was directed in the superior-inferior (SI) direction (Figure 1.2). The ML location is the distance from the medial (or lateral) edge of the component as a percentage of the total ML dimension, with 0% indicating the medial edge. The AP location is the distance from the posterior edge of the articular surface as a percentage of the total AP dimension, with 0% indicating the posterior edge. The AP centerline is the distance from a transtibial axis[7] bisecting the tibial component into anterior and posterior halves, with a positive sign for damage on the anterior tibial surface and a negative sign for damage on

the posterior tibial surface. For patellar components, the ML and SI edges were identified. The x-axis was directed in the SI direction, the y-axis was directed in the ML direction, and the z-axis was directed in the AP direction (Figure 1.3). The ML location is the distance from the medial edge of the component as a percentage of the total medial-lateral dimension, with 0% indicating the medial edge. The SI location is the distance from the inferior edge of the articular surface as a percentage of the total SI dimension, with 0% indicating the inferior edge. Algorithms were implemented to correct component rotational alignment such that the x-axis of the tibial inserts and patellar components was aligned with the global coordinate system.

The circumference of each identified damage region was outlined on the digital images[2] and the corresponding wear mode for each region was noted, as described in section 1.2. Surface damage on the medial and lateral articular surfaces of the tibial inserts was analyzed separately. The damage mode incidence was calculated as the number of inserts showing a given damage mode divided by the total number of inserts included in the group. The damage area was calculated as a percentage of the total medial or lateral articular or backside surface areas for tibial inserts or the total articular area for patellar components. The AP extent of the damage pattern region on the tibial inserts was calculated as the difference between the maximum anterior and posterior coordinate points. The area centroid for the sum of different damage regions was computed. The damage location was expressed as the location of the area centroid relative to the normalized component-based coordinate system.

The accuracy and repeatability for measuring damage area and location was evaluated using measurements on digital images of objects with known geometric sizes

(areas and linear dimensions) superimposed on a 20 mm^2 calibration grid. The circumference of each shape was outlined on the digital images and the area and linear dimensions of each shape were measured using custom analysis programs described above. Absolute error was calculated

$$\text{Error (absolute)} = |\text{true value} - \text{measured value}| \quad (1.1)$$

as the deviation of the measured value from the true value. Accuracy was calculated

$$\text{Accuracy} = 1 - (\text{absolute error} / \text{true value}) \quad (1.2)$$

as the degree to which the actual dimension agrees with a specified known value. Repeatability (precision) was the variation in repeated measurements taken by a single user on the same image using the same measurement tool. Based on these measurements, the damage pattern measurement technique had an average absolute error ranged from 0.41 mm to 0.48 mm for linear distances and from 3.3 mm^2 to 4.6 mm^2 for areas and was 98.6% accurate (Tables 1.1 and 1.2). Precision averaged 0.4 mm for linear distances and 3.9 mm^2 for areas based on repeated measurements taken by a single user (Tables 1.3 and 1.4).

1.4 Spatial Sensor for Quantitative Measurement of Articular Surface Deformation on UHMWPE Tibial Inserts

Surface deformation (depth) was measured using a hand-held digital stylus (Microscribe 3DX, Immersion Corp., San Jose, CA) interfaced with a computer and surfacing software (Rhinoceros, Robert McNeel & Associates, Seattle, WA). The digitizing stylus consisted of a 3.2 mm ball tip that was positioned in contact with the

UHMWPE insert and drawn across the articular surface (Figure 1.4). This system tracks the three-dimensional position of the stylus, output as x, y and z coordinate measurements. The instrument resolution is 0.13 mm and accuracy is 0.30 mm. A global coordinate system was established relative to the measuring surface. Surface topography was digitized on the articular surface of each retrieved UHMWPE insert and on unused control inserts of the same design. Approximately 4000 to 7000 points were digitized and exported to represent the three-dimensional articular geometry for each insert. Analysis software consisted of custom programs written in PV-Wave.

A contour grid for the retrieved and control inserts was generated in 0.5 mm increments across the articular surface, fitting a third-order polynomial least-squares fit line to the data points within the grid. Over-sampling of the point cloud optimized the estimate for the best fit surface contour grid lines. Algorithms were implemented to orient the contour grid lines for the retrieved and control inserts, correcting for specimen tilt and alignment within the same normalized coordinate system previously established. Rotations about the x-axis, y-axis and z-axis were implemented to align the contour grid lines of the retrieved and control inserts.

Surface deformation was calculated as the thickness difference between the best-fit contour grid lines defining the articular geometry of the worn inserts compared to unused control inserts. The magnitude of maximum deformation and its location relative to the normalized insert-based coordinate system was measured. The damage mode associated with the maximum deformation location was recorded using the methods in section 1.2. The deformation rate was calculated as maximum deformation divided by duration of function for each insert.

The accuracy of this surface deformation measurement technique (including error due to set-up, measurement and analysis) was determined using repeated measurements on a thin metal step wedge with discrete steps ranging from 0.25 mm to 1.02 mm. Approximately 4000 points were digitized and exported to represent the three-dimensional surface topography. Analysis routines were executed and the dimension (height) of the step wedge relative to the baseline surface was measured on four separate occasions (Table 1.5). Absolute error, accuracy and repeatability were calculated as previously defined relative to the known thickness of the step wedge (Table 1.6). Based on these measurements, the surface deformation technique had an average absolute error ranged from range, 0.087 mm to 0.115 mm and was 98.9% accurate. Precision averaged 0.103 mm based on repeated measurements taken by a single user.

In addition, the accuracy and precision of the surface deformation measuring technique was determined by comparing results using the hand-held digitizer to measurements on the same UHMWPE inserts measured using a laser scanner as previously reported by Fregly, et al.[4] Surface topography was digitized on the articular surface of a UHMWPE insert (Series 7000, Osteonics Corp., Allendale, NJ) retrieved from a right knee and on an unused control insert of the same size. Approximately 7600 points were digitized and exported to represent the three-dimensional articular geometry. Analysis routines were executed on seven separate occasions and the magnitude of maximum deformation on the medial and lateral surface were measured (Table 1.7). Based on these measurements, average absolute error for the hand-held stylus measurement technique was 0.025 mm, ranging from 0.001 mm to 0.072 mm. Average accuracy relative to measurements from the laser scan was 96.8%, ranging from 91.1% to 99.9%.

1.5 Spatial Sensor for Quantitative Measurement of Articular Surface Deformation on UHMWPE Acetabular Liners

UHMWPE acetabular liner THR designs were classified into three types depending on the presence of an inner rim chamfer or bevel (Figure 1.5). Peripheral rim damage consistent with impingement between the liner rim and the femoral head or stem neck[14,18] was assessed at up to 30 times magnification using an optical stereomicroscope. The extent of impingement damage into the liner rim was measured in the direction of the liner radius and graded as minimum if it extended <4 mm, moderate if it extended 4 mm to 7 mm; and severe if it extended to the outer edge or >7 mm.[18]

Liner articular geometry was measured using the hand-held digital stylus (MicroScribe 3DX) (Figure 1.4) interfaced with a computer and surfacing software (Rhinoceros). Each liner was secured to a horizontal work surface with the articular surface directed upward and the global coordinate system was established relative to the work surface (Figure 1.6). Three-dimensional coordinate points were digitized with the stylus tip contacting the inner liner rim and outer liner rim, taking care to avoid damaged regions. Surface deformation was measured using a spherical 28 mm or 32 mm diameter femoral head attached to the stylus tip, matching each liner's inner diameter (Figure 1.7). The sphere was positioned in two distinct contours for each liner, consistent with unworn and worn articular regions. The worn contour was visually distinguished by its highly reflective and polished appearance compared to the less polished and discolored unworn contour.[11,12] The worn contour was also distinguished by manually sensing the transition ridge creating a well-formed demarcation between the worn and unworn contour, as reported in previous retrieval studies.[11,12]

Geometric relationships between the liner rim and femoral head were characterized by lip height and head center inset (Figure 1.7). Analysis software consisted of custom programs written in PV-Wave. A curve fitting routine using the linear least-square method was applied to the outer and inner rim points, with a residual error of 0.018 mm. These points were used to establish the liner-based coordinate system with the origin at the geometric center of the circle defined by the outer rim and level with the liner opening (Figure 1.7). Image analysis routines were implemented to correct liner tilt about the x-axis and y-axis such that the outer rim curve was parallel with the horizontal plane of the work surface (cup tilt $< 0.01°$). All other digitized points were then transformed using the same rotation matrix and the geometric centroids of the outer rim and inner rim curves were calculated in the horizontal plane.

Lip height was the distance between the outer rim centroid and head center (ORu and ORw). Head center inset was the distance between the inner rim centroid and head center (IRu and IRw). The three-dimensional magnitude of head penetration into the polyethylene liner was calculated as the vector length between the head center positioned in the unworn and worn contours (HCw) and normalized to duration of function as penetration rate (HCw/year). The precision of the measurement technique for articular surface deformation was assessed by measuring six acetabular liners on seven different occasions (Table 1.8). Based on these measurements, average precision was 0.125 mm for lip height and head center inset and 0.203 mm for head center penetration (HCw), inclusive of error due to set-up, digitizing and image analysis (Table 1.9).

1.6 Spatial Sensor for Quantitative Measurement of Tibiofemoral Kinematics Using Guidance from the Articular Geometry of UHMWPE Tibial Inserts

This technique provides the mathematical algorithms to determine the relative positions and orientations of two rigid bodies within a calibrated spatial volume. These algorithms were applied to point clouds generated from a motion capture system tracking the movement of femoral and tibial TKA components that were positioned by hand using the damage patterns on the UHMWPE tibial inserts to guide the relative motions. The outputs of this technique are the kinematics of the femoral component relative to the tibial component, as given by the absolute translations and rotations of the component within a component-based coordinate system. Matrix and vector arrays were determined for the femoral and tibial components within the calibrated spatial volume defined by the global coordinate system. The position and orientation of the femoral and tibial marker arrays in laboratory coordinates are given by the time varying 4x4 matrices of

$$^{Lab}\mathbf{T}_{Fem\_array} \text{ and} \tag{1.3}$$

$$^{Lab}\mathbf{T}_{Tib\_array}, \tag{1.4}$$

respectively. The position and orientation of the femoral component in femoral array coordinates is given by the constant 4x4 matrix of

$$^{Fem\_array}\mathbf{T}_{Fem\_implant}. \tag{1.5}$$

The position and orientation of the tibial component in tibial array coordinates is given by the constant 4x4 matrix of

$$^{Tib\_array}\mathbf{T}_{Tib\_implant}. \quad (1.6)$$

The positions and orientations of the femoral and tibial components in laboratory coordinates are given by the 4x4 matrix of

$$^{Lab}\mathrm{T}_{Fem\_implant} = {}^{Lab}\mathrm{T}_{Fem\_array} * {}^{Fem\_array}\mathrm{T}_{Fem\_implant} \text{ and} \quad (1.7)$$

$$^{Lab}\mathrm{T}_{Tib\_implant} = {}^{Lab}\mathrm{T}_{Tib\_array} * {}^{Tib\_array}\mathrm{T}_{Tib\_implant}, \quad (1.8)$$

respectively. Finally, the position and orientation of the femoral component in tibial component coordinates is given by the 4x4 matrix of

$$^{Fem\_implant}\mathrm{T}_{Tib\_implant} = {}^{Fem\_implant}\mathrm{T}_{Lab} * {}^{Lab}\mathrm{T}_{Tib\_implant} = \left({}^{Lab}\mathrm{T}_{Fem\_array} * {}^{Fem\_array}\mathrm{T}_{Fem\_implant}\right)^{-1} * {}^{Lab}\mathrm{T}_{Tib\_array} * {}^{Tib\_array}\mathrm{T}_{Tib\_implant}. \quad (1.9)$$

Accurate measurements were obtained using the following sequence of data collection procedures. Femoral and tibial component kinematics were measured using a motion capture system consisting of four high-speed digital video cameras (MX-40, Vicon, Los Angeles, CA) interfaced with a computer and image capture software (Nexus 1.0, Vicon, Los Angeles, CA). This system optically tracked a series of 11 reflective 9.5 mm spheres rigidly attached to femoral components and tibial inserts (Figure 1.8) and output the three-dimensional coordinates of each marker sphere relative to a global coordinate system. The cameras were positioned on a rigid frame above the work surface creating an approximate 1 m^3 working volume (Figures 1.9 and 1.10). This volume was calibrated and a global coordinate system established using a small T-shaped wand fitted with five 9.5 mm reflective spheres in known positions relative to each other (Table 1.10,

Figure 1.11). The resolution of the optics for each camera was 0.343 mm/pixel, resulting in approximately 0.200 mm error when the markers were tracked by two or more cameras.

The geometric positions of the marker spheres were measured relative to identifiable landmarks on the femoral and tibial components using the hand-held digital stylus (MicroScribe 3DX) (Figure 1.4) interfaced with a computer and surfacing software (Rhinoceros). Analysis software consisted of custom programs written in PV-Wave and MatLab (version 7.3, MathWorks, Natick, MA). The stylus was positioned within the working volume and calibrated to align with the global coordinate system previously defined (Figures 1.9 and 1.10). Femoral component and tibial insert geometry were registered within the global coordinate system by digitizing specific landmarks on each component and the marker spheres. This established a static model of each component specific to geometry and size and a component-based coordinate system, according to previously established conventions[1] for TKA prostheses (Figures 1.12 and 1.13).

Once the static model was created, the femoral and tibial components were positioned in an anatomic configuration (femur component superior, tibial component inferior) and moved by hand using the damage patterns on the UHMWPE tibial inserts to guide the relative motions. The three-dimensional position coordinates (x, y, z) were recorded by the motion capture system, generating a point cloud of the incremental motions. The relative angles between the two components were determined using the Cardan angle convention as a 3-1-2 ordered sequence[16] from the computed tibiofemoral pose.

Accuracy and precision of the measurements were assessed using the mini T-wand rigidly secured to a precision rotation stage (Model 30 008-P, Daedal Inc., Harrison City, PA) and a precision translation stage (Exakt Medical Technologies, Oklahoma City,

OK) that were incremented in 0.01° of rotation and 0.01 mm of translation, respectively. A point cloud of the sphere locations relative to the global coordinate system was obtained. The technique was 92.5% accurate, with an average absolute error of 0.008 mm for linear translations (Table 1.11). Precision was 0.008 mm for linear translations based on repeated measurements taken by a single user (Table 1.11).

1.7 References Cited

1. Banks SA, Hodge WA. Accurate measurement of three-dimensional knee replacement kinematics using single-plane fluoroscopy. *IEEE Trans Biomed Eng*. 1996; 43:638-49.
2. Cornwall GB, Bryant JT, Hansson CM, Rudan J, Kennedy LA, Cooke TD. A quantitative technique for reporting surface degradation patterns of UHMWPE components of retrieved total knee replacements. *J Appl Biomater.* 1995;6:9-18.
3. Ewald FC. The Knee Society total knee arthroplasty roentgenographic evaluation and scoring system. *Clin Orthop*. 1989; 248:9-12.
4. Fregly BJ, Sawyer WG, Harman MK, Banks SA. Computational wear prediction of a total knee replacement from *in vivo* kinematics. *J Biomech*. 2005; 38:305-14.
5. Harman MK, Banks SA, Hodge WA. Organization of a post-mortem implant retrieval program. 68th Annual Meeting of the American Academy of Orthopaedic Surgeons. 2001; San Francisco, CA.
6. Harman MK, Banks SA, Hodge WA. Organization of a post-mortem implant retrieval program. 67th Annual Meeting of the American Academy for Orthopaedic Surgeons. 2000; Orlando, FL.
7. Harman MK, Banks SA, Hodge WA. Polyethylene damage and knee kinematics after total knee arthroplasty. *Clin Orthop*. 2001; 392:383-93.
8. Hood RW, Wright TM, Burstein AH. Retrieval analysis of total knee prostheses: A method and its application to 48 total condylar prostheses. *J Biomed Mater Res*. 1983; 17:829-42.
9. Insall JN, Dorr LD, Scott RD, Scott WN. Rationale of the Knee Society clinical rating system. *Clin Orthop*. 1989; 248:13-14.
10. Jonsson GT. Compartment arthroplasty for gonarthrosis. *Acta Orthop Scand*. 1981; 193-210.
11. Kabo JM, Gebhard JS, Loren G, Amstuz HC. In vivo wear of polyethylene acetabular components. *J Bone Joint Surg Br*. 1993; 75(2):254-8

12. Kelley SS, Lachiewicz PF, Hickman JM, Paterno SM. Relationship of femoral head and acetabular size to the prevalence of dislocation. *Clin Orthop.* 1998; 355:163-70

13. Rao A, Engh G, Collier M, Smain L. Tibial interface wear in retrieved total knee components and correlations with modular insert motion. *J Bone Joint Surg Am.* 2002; 84(10):1849-55.

14. Shon WY, Baldini T, Peterson MG, Wright TM, Salvati EA. Impingement in total hip arthroplasty: A study of retrieved acetabular components. *J Arthroplasty*. 2005; 20(4):427-35.

15. Silva M, Kabbash CA, Tiberi JV, Park SH, Reilly DT, Mahoney OM, Schmalzried TP. Surface damage on open box posterior stabilized polyethylene tibial inserts. *Clin Orthop.* 2003; 416:135-44.

16. Tupling S, Pierrynowski M. Use of Cardan angles to locate rigid bodies in three-dimensional space. *Med. & Biol. Eng. & Comp.* 1987; 25:527-32.

17. Wimmer M, Andriacchi T, Natarajan R, Loos J, Karlhuber M. A striated pattern of wear in ultrahigh-molecular-weight polyethylene components of Miller-Galante total knee arthroplasty. *J Arthroplasty*. 1998; 13(1):8-16.

18. Yamaguchi M, Akisue T, Bauer TW, Hashimoto Y. The spatial location of impingement in total hip arthroplasty. J Arthroplasty 2000; 15(3):305-13

Table 1.1: Accuracy of Linear Measurement of Damage Patterns

True Length (cm)	Measured length (cm)	Absolute error	Accuracy
2.30	2.458	0.158	0.931
1.85	1.899	0.049	0.974
3.00	3.017	0.017	0.994
1.85	1.877	0.027	0.985
3.80	3.777	0.023	0.994
3.30	3.330	0.030	0.991
3.30	3.307	0.007	0.998
1.60	1.654	0.054	0.966
1.60	1.609	0.009	0.994
4.10	4.067	0.033	0.992
Average		**0.041**	**0.982**

Table 1.2: Accuracy of Area Measurement of Damage Patterns

True Area (cm^2)	Measured area (cm^2)	Absolute error	Accuracy
2.42	2.47	0.05	0.979
2.78	2.75	0.03	0.989
8.55	8.56	0.01	0.999
4.00	4.04	0.04	0.990
3.52	3.51	0.01	0.997
3.76	3.75	0.01	0.997
4.56	4.44	0.12	0.974
8.00	8.020	0.02	0.998
2.42	2.525	0.105	0.957
2.78	2.763	0.017	0.994
3.52	3.498	0.022	0.994
8.55	8.572	0.022	0.997
3.76	3.773	0.013	0.997
4.56	4.543	0.017	0.996
Average		**0.035**	**0.990**

Table 1.3: Precision of Linear Measurement of Damage Patterns

	Day 1	Day 2	Day 1		Day 2	
True Length (cm)	Measured length (cm)	Measured length (cm)	Absolute error	Accuracy	Absolute error	Accuracy
2.30	2.458	2.422	0.158	0.931	0.122	0.947
1.85	1.899	1.889	0.049	0.974	0.039	0.979
3.00	3.017	2.978	0.017	0.994	0.022	0.993
1.85	1.877	1.911	0.027	0.985	0.061	0.967
3.80	3.777	3.755	0.023	0.994	0.045	0.988
3.30	3.330	3.311	0.030	0.991	0.011	0.997
3.30	3.307	3.267	0.007	0.998	0.033	0.990
1.60	1.654	1.689	0.054	0.966	0.089	0.944
1.60	1.609	1.622	0.009	0.994	0.022	0.986
4.10	4.067	4.067	0.033	0.992	0.033	0.992
Average			**0.041**	**0.982**	**0.048**	**0.978**

Table 1.4: Precision of Area Measurement of Damage Patterns

	Day 1	Day 2	Day 1		Day 2	
True area (cm^2)	Measured area (cm^2)	Measured area (cm^2)	Absolute error	Accuracy	Absolute error	Accuracy
2.42	2.525	2.421	0.105	0.957	0.001	1.000
2.78	2.763	2.692	0.017	0.994	0.088	0.968
3.52	3.498	3.539	0.022	0.994	0.019	0.995
8.55	8.572	8.460	0.022	0.997	0.090	0.989
3.76	3.773	3.701	0.013	0.997	0.059	0.984
4.56	4.543	4.578	0.017	0.996	0.018	0.996
Average			**0.033**	**0.989**	**0.046**	**0.989**

Table 1.5: Repeated Measurement of Surface Deformation Using the Hand-held Stylus

	Day 1	Day 2	Day 3	Day 4
True height (mm)	Measured height (mm)	Measured height (mm)	Measured height (mm)	Measured height (mm)
10.020	10.008	10.222	9.942	9.938
9.750	9.872	9.804	9.860	9.865
9.500	9.600	9.551	9.551	9.608
9.250	9.407	9.404	9.360	9.391

Table 1.6: Accuracy and Precision of Surface Deformation Measurement Technique

	Day 1	Day 2	Day 3	Day 4
	Absolute error	Absolute error	Absolute error	Absolute error
	0.012	0.202	0.078	0.082
	0.122	0.054	0.110	0.115
	0.100	0.051	0.051	0.108
	0.157	0.154	0.110	0.141
Average	**0.098**	**0.115**	**0.087**	**0.112**
	Accuracy	Accuracy	Accuracy	Accuracy
	0.999	0.980	0.992	0.992
	0.987	0.994	0.989	0.988
	0.989	0.995	0.995	0.989
	0.983	0.983	0.988	0.985
Average	**0.990**	**0.988**	**0.991**	**0.988**

Table 1.7: Comparison of Maximum Surface Deformation Measured Using a Laser Scan and a Hand-Held Stylus for Seven Different Trials

			Absolute Error		Accuracy	
	Medial (mm)	Lateral (mm)	Medial	Lateral	Medial	Lateral
Laser Scan	0.73	0.81				
Stylus						
Trial 1	0.718	0.809	0.012	0.001	0.983	0.999
Trial 2	0.771	0.882	0.041	0.072	0.944	0.911
Trial 3	0.721	0.799	0.009	0.011	0.988	0.987
Trial 4	0.724	0.831	0.006	0.021	0.991	0.974
Trial 5	0.717	0.833	0.013	0.023	0.982	0.971
Trial 6	0.673	0.745	0.057	0.065	0.922	0.920
Trial 7	0.734	0.821	0.004	0.011	0.994	0.987
Stylus Average	**0.723**	**0.817**	**0.020**	**0.029**	**0.972**	**0.964**

Table 1.8: Magnitude of Head Penetration (HcW) Measured in Separate Trials

Liner #	Trial 1	Trial 2	Trial 3	Trial 4	Trial 5
H3107_97L	0.303	0.593	0.516	0.457	0.419
H1097_99L	0.000	0.000	0.000	0.000	0.000
H1119_00L	1.438	2.324	2.028	2.109	2.256
H2134_95L	1.603	1.784	2.049	1.799	1.627
H1096_96L	2.019	2.274	2.251	2.319	2.213
H2067_00L	2.283	2.753	2.943	3.037	2.834

Table 1.9: Precision of Head Penetration (HcW) Measurement

Liner #	Trial 1-2	Trial 1-3	Trial 1-4	Trial 1-5	Trial 2-3
H3107_97L	0.290	0.214	0.077	0.154	0.136
H1097_99L	0.000	0.000	0.000	0.000	0.000
H1119_00L	0.886	0.591	0.296	0.671	0.215
H2134_95L	0.181	0.446	0.265	0.196	0.015
H1096_96L	0.254	0.231	0.023	0.300	0.046
H2067_00L	0.470	0.661	0.190	0.755	0.284
Average	**0.347**	**0.357**	**0.142**	**0.346**	**0.116**

Liner #	Trial 2-4	Trial 2-5	Trial 3-4	Trial 3-5	Trial 4-5
H3107_97L	0.060	0.116	0.174	0.097	0.038
H1097_99L	0.000	0.000	0.000	0.000	0.000
H1119_00L	0.081	0.818	0.068	0.227	0.147
H2134_95L	0.250	0.024	0.157	0.422	0.172
H1096_96L	0.069	0.194	0.061	0.038	0.107
H2067_00L	0.094	0.551	0.081	0.110	0.203
Average	**0.092**	**0.284**	**0.090**	**0.149**	**0.111**

Table 1.10: Marker Sphere Spacing for Mini Calibration T-Wand

Relative to Wand Origin

	X (mm)	Y (mm)	Z (mm)
Marker A	33.465	-12.488	7.849
Marker B	-11.187	-12.488	7.849
Marker C	-41.633	-12.488	7.849
Marker D	-11.187	35.565	7.849
Marker E	-11.187	83.618	7.849

Table 1.11: Accuracy and Precision of Linear Displacement Measurements

for the Motion Capture-based Technique

True (mm)	Measured (mm)	Absolute error	Accuracy	Measured (mm)	Absolute error	Accuracy
0.1	0.086	0.014	0.86	0.090	0.010	0.90
0.1	0.103	0.003	0.97	0.120	0.020	0.80
0.1	0.100	0.000	1.00	0.103	0.003	0.97
0.1	0.079	0.021	0.79	0.105	0.005	0.95
0.1	0.122	0.022	0.78	0.098	0.002	0.98
0.1	0.094	0.006	0.94	0.097	0.003	0.97
0.1	0.108	0.008	0.92	0.080	0.020	0.80
0.1	0.098	0.002	0.98	0.098	0.002	0.98
0.1	0.100	0.000	1.00	0.095	0.005	0.95
0.1	0.096	0.004	0.96	0.101	0.001	0.99
Average		**0.008**	**0.92**		**0.007**	**0.93**

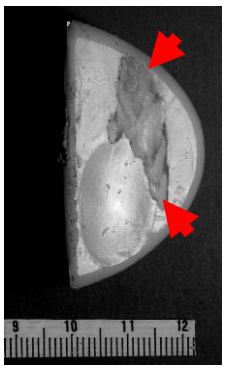

Abrasion

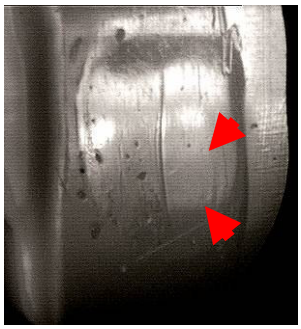

Burnishing

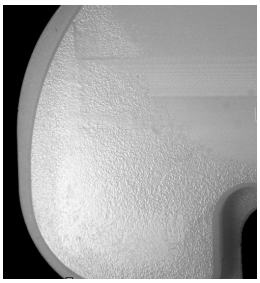

Dimpling

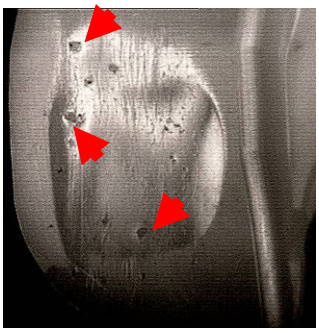

Pitting

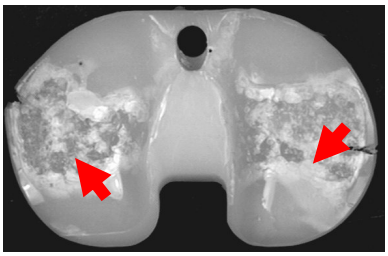

Delamination

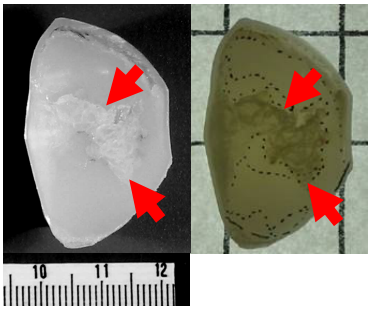

Subsurface Delamination

Fracture

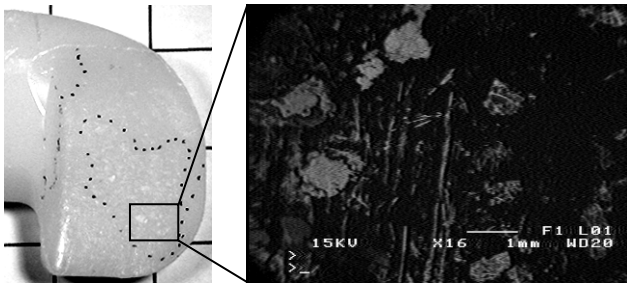

Embedded Debris

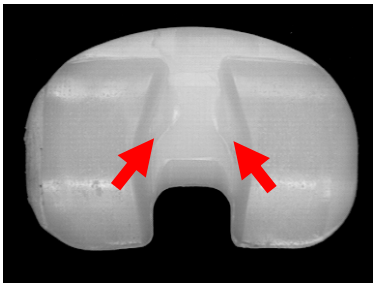

Non-articular deformation

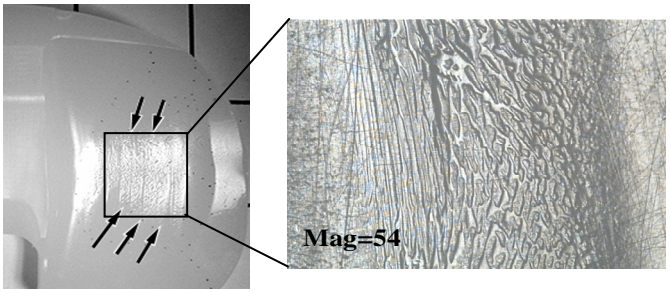

Striations

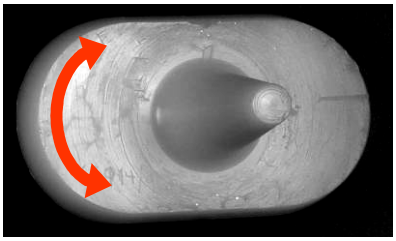

Scratching

Figure 1.1: Visual Appearance of 11 Different Damage Modes

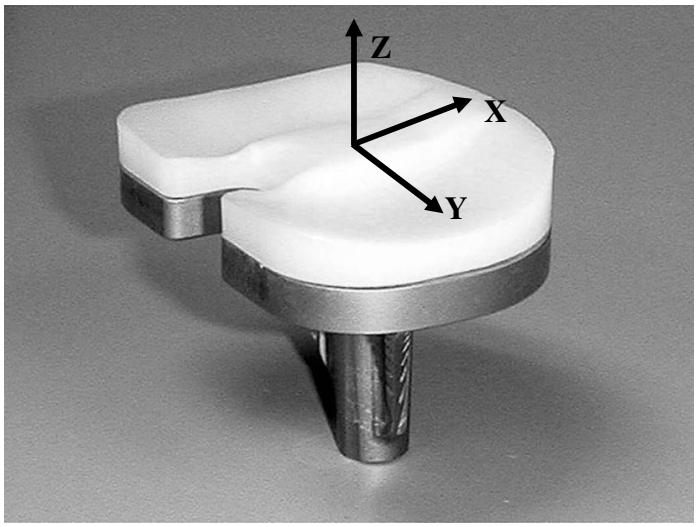

Figure 1.2: Coordinate Axes for Tibial Components in Damage Area and Surface Deformation Measurement Techniques

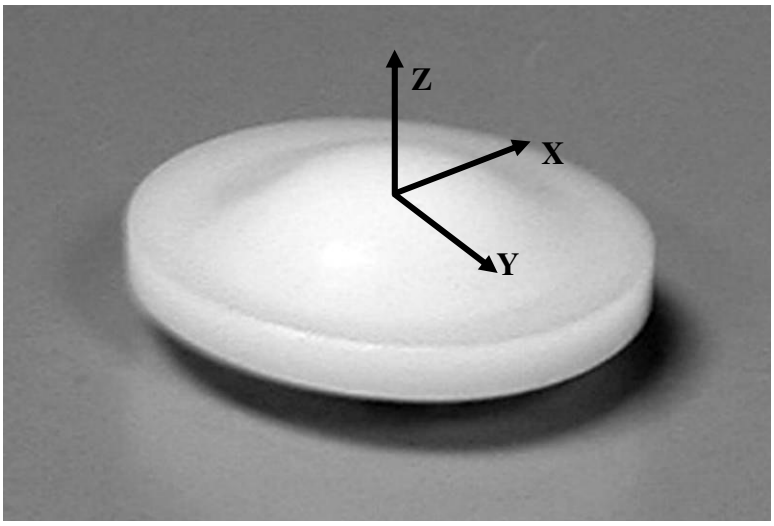

Figure 1.3: Coordinate Axes for Patella Components in Damage Area Measurement Technique

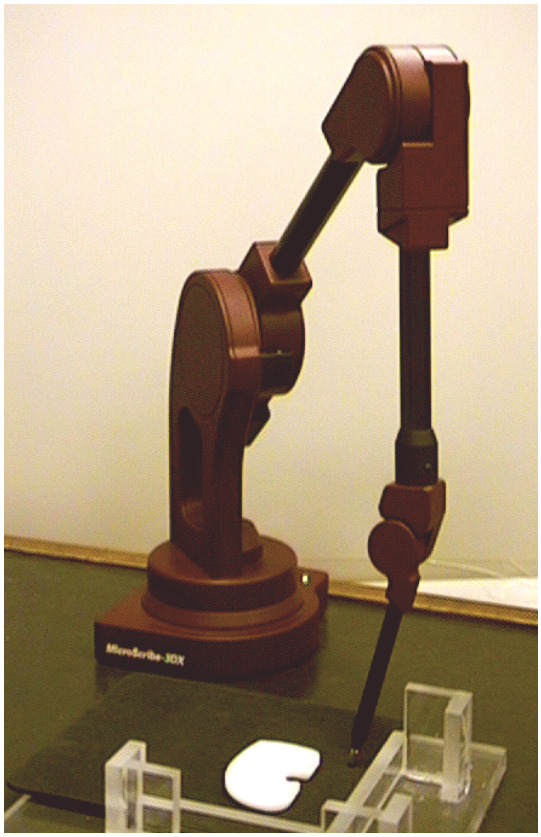

Figure 1.4: Hand-held Digital Stylus

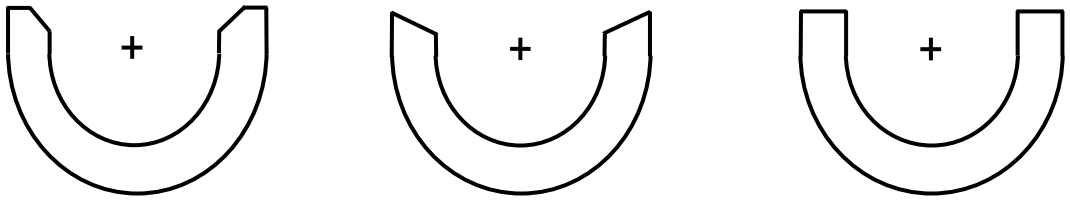

Figure. 1.5: Three Types of UHMWPE Liner Designs

Type A had an inner chamfer, Type B had a bevel and Type C had neither an inner chamfer nor bevel.

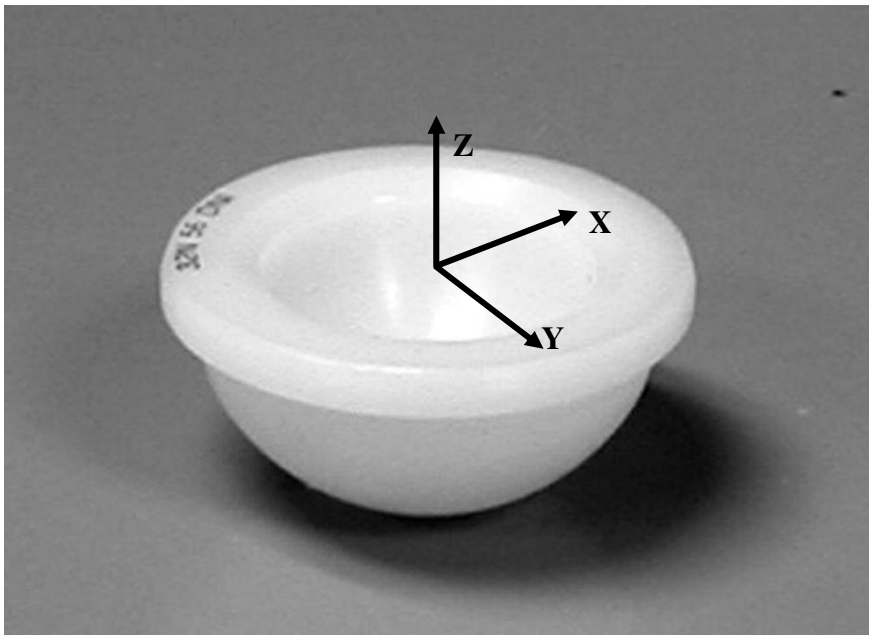

Figure 1.6: Coordinate Axes for Acetabular Liners in the Articular Surface Deformation Measurement Technique

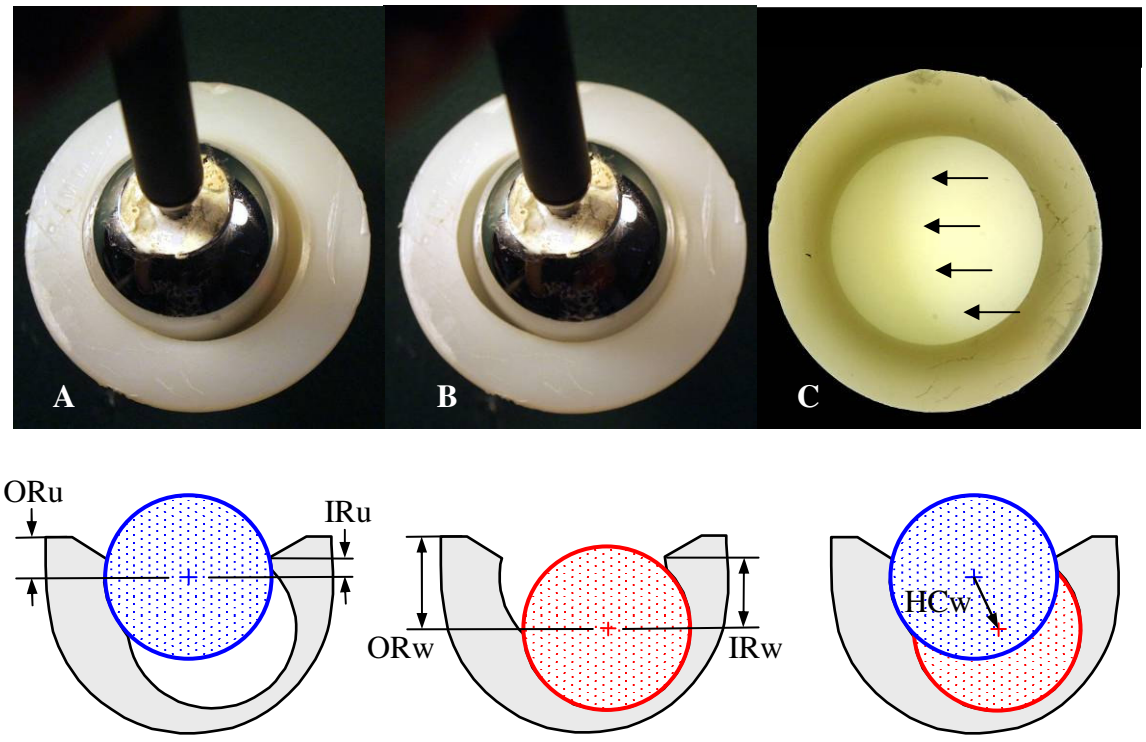

Figure. 1.7: Measurement of Articular Geometry and Head Penetration in UHMWPE Acetabular Liners

The measurement technique included locating a femoral head sphere in the unworn (A) and worn (B) contours of the polyethylene liner as demarked by a transitional ridge (C, arrows). Lip height was measured from the outer rim to the head center in the unworn (ORu) and worn (ORw) contours. Head center inset was measured from the inner rim to the head center in the unworn (IRu) and worn (IRw) contours. Head penetration (HCw) was the three-dimensional vector length between the sphere center in the unworn (shaded blue) and worn (shaded red) contours.

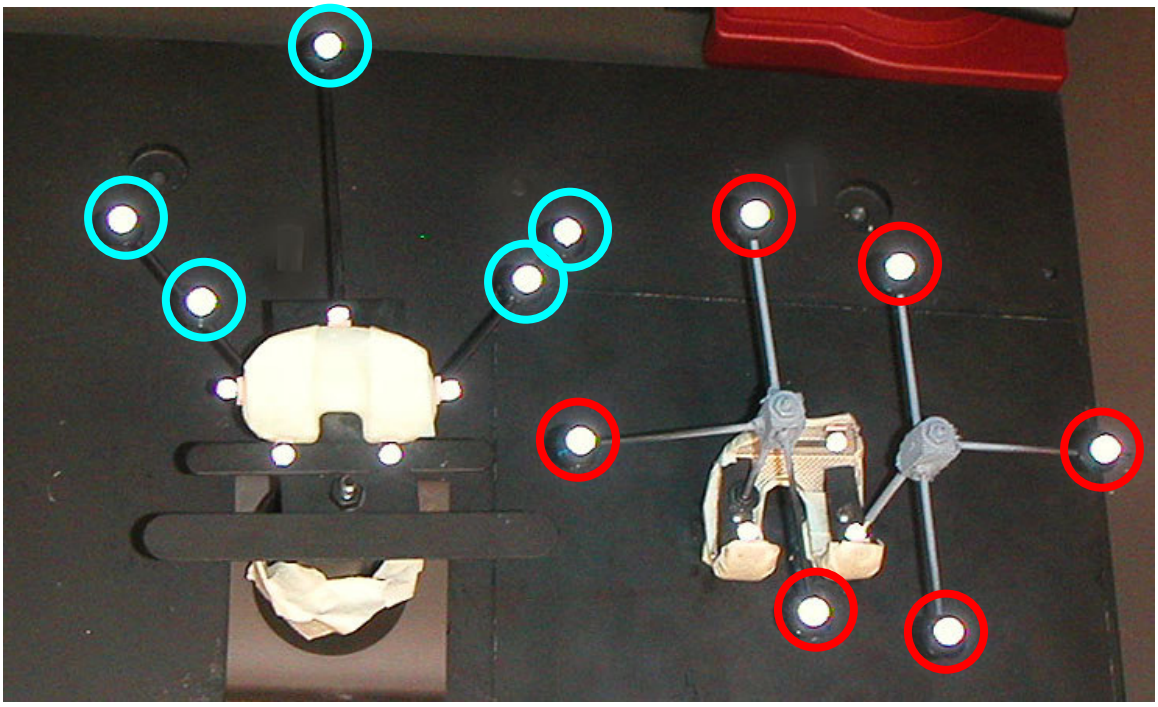

Figure 1.8: Marker Spheres Defining the Femoral and Tibial Components' Geometry Five markers (cyan) were oriented on rigid wire outriggers about the tibial insert and six markers (red) were oriented on rigid wire outriggers about the femoral component.

Figure. 1.9: Working Volume with Four Mounted Video Cameras, Digital Stylus and Mini T-Wand Defining the Global Coordinate System and Origin

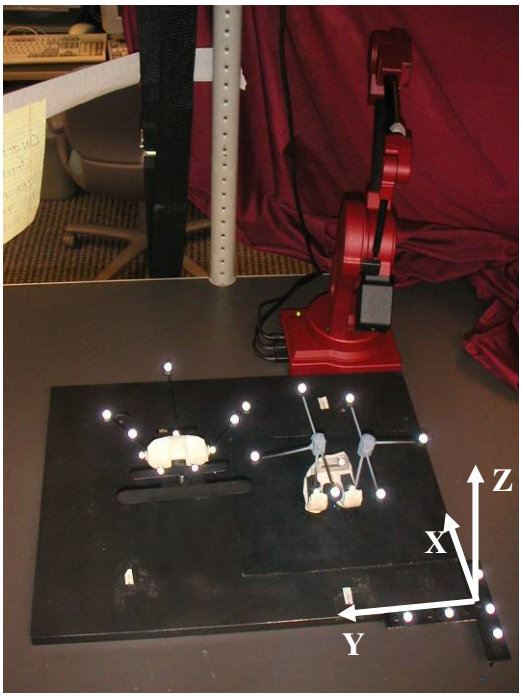

Figure. 1.10: Tibial and Femoral Components Mounted with Reflective Marker Spheres and Positioned within the Calibrated Global Coordinate System

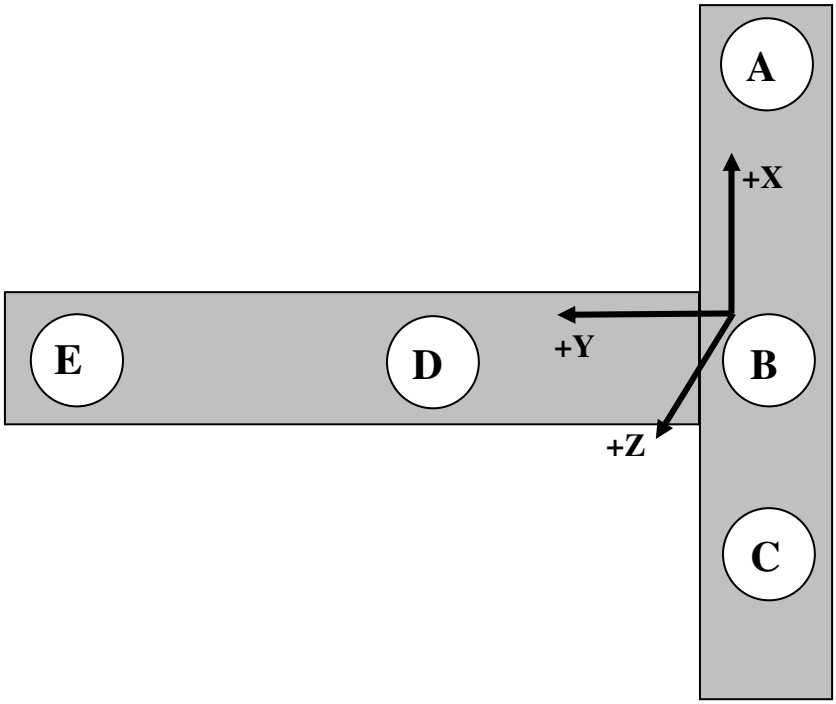

Figure 1.11: Five Marker Spheres and Origin for Mini Calibration T-Wand

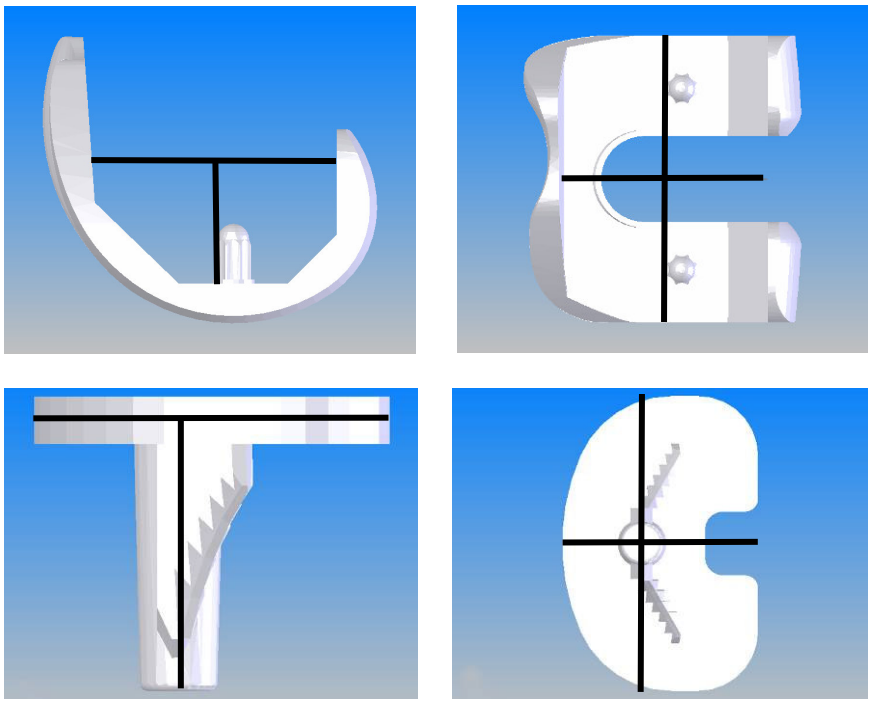

Figure 1.12: Femoral and Tibial Component Origins

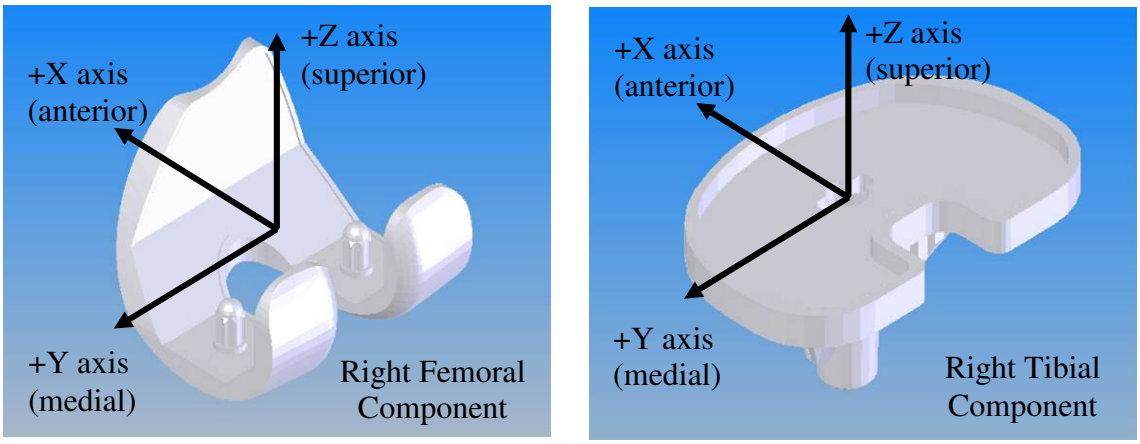

Figure. 1.13: Femoral and Tibial Component-Based Coordinate Systems

2 DOES BACKSIDE DAMAGE CORRESPOND TO ARTICULAR DAMAGE IN RETRIEVED TKA POLYETHYLENE INSERTS?

2.1 Introduction

Modularity between the metal tibial baseplate and polyethylene insert is a design feature common to many total knee arthroplasties (TKAs). However, its long-term wear performance has been questioned.[13] Evidence of motion between modular tibial baseplates and polyethylene inserts and damage on the backside of retrieved polyethylene inserts led to suggestions that the modular capture mechanism degrades with physiologic loading.[13] However, a correlation between insert motion and in vivo time has not been reported,[8,26] and data from autopsy retrievals do not support the relationship.[13,26]

The magnitude of insert motion varies greatly among TKAs, and some modular capture designs appear more susceptible to disruption and backside damage.[1,13,21,24,26] The majority of components included in mechanical studies of capture mechanism performance were obtained at revision surgery, with disassembly and reassembly of the modular junction before testing.[8,13,26] Unfortunately, this disrupts the area of contact between the insert and baseplate and some designs incur irreparable damage to the capture mechanism with disassembly during revision surgery, precluding further assessment. For those designs, autopsy-retrieved components that have not been disassembled may provide a more accurate indication of the amount of insert motion that was occurring in vivo.

Motion between the polyethylene insert and the metal tibial baseplate is one probable cause of backside wear, and significant positive correlations between insert motion and backside wear have been reported.[8,26] At the articular surface, femoral component motion and contact on the tibial polyethylene insert is a significant predictor of articular damage patterns.[15] If kinematic conditions and contact stresses at the articular surface may be transmitted to the modular baseplate interface,[3,22,30] then backside damage patterns should correspond to articular patterns. However, comparisons of articular and backside damage patterns are limited,[1,27,32] and the effects of different wear mechanisms at the articular and backside interfaces remain unclear.[13]

The primary research objective was to determine the effect of physiological loading on the modular capture mechanism and the distribution of articular and backside surface damage patterns. It was hypothesized: (1) in autopsy-retrieved modular tibial components that have not been previously disassembled, polyethylene insert motion increases with time in vivo with a corresponding increase in backside surface damage; (2) the articular and backside surface damage area for polyethylene inserts retrieved at autopsy and revision surgery increases with time in vivo; and 3) backside damage patterns correspond to articular damage patterns.

2.2 Materials and Methods

Thirty seven consecutive posterior cruciate ligament-retaining tibial components (Series 7000, Stryker Orthopaedics, Mahwah, NJ) were retrieved at autopsy (12 knees) and revision knee arthroplasty (25 knees) over 8 years (Table 2.1). Mechanical testing was used to measure insert motion for six of the 12 autopsy-retrieved tibial components and for six similarly sized, unused control components. The other six autopsy-retrieved

components and 25 revision components were excluded from the insert motion evaluations because previous disassembly caused permanent damage to the locking mechanism. Articular and backside surface damage patterns were visually assessed on all polyethylene tibial inserts and the damage area and damage location were measured.

The reasons for revision included infection (7 knees), resurfacing of a previously unresurfaced patella (5 knees), patellar component wear (3 knees), patellar component loosening (2 knees), tibial component loosening (3 knees), tibial osteolysis (2 knees), femoral component loosening (1 knee), patellar component subluxation (1 knee), and supracondylar fracture (1 knee). The TKAs functioned an average duration of 41 ± 21 months (range, 15–74 months) for the autopsy group and 26 ± 21 months (range, 1–71 months) for the revision group. Written informed consent to retrieve the components at autopsy was obtained through our established Implant Retrieval Program.[15]

All prostheses were implanted using cement fixation by the same surgeon from November 1991 to April 1998 during index TKA in 31 knees and during revision TKA in six knees. This prosthesis was utilized in approximately 75 knees annually during this period. Patellar components were implanted in 19 of 37 (51%) knees. The polyethylene tibial inserts were machined from compression-molded slabs (GUR 1120), maintaining a minimum polyethylene thickness of 6.8 mm (20 inserts), 8.5 mm (9 inserts), 9.5 mm (1 insert), and 13 mm (7 inserts), and sterilized with gamma radiation in air.

The full peripheral rim snap-fit modular locking mechanism consisted of a lipped edge around the tibial tray circumference that captured a recessed edge around the polyethylene insert periphery and three metal barbs that captured a wire in the anterior insert rim (Figure 2.1). The cobalt-chrome alloy tibial baseplate lacked screw holes and

had a nonpolished surface finish (Ra=0.8 μm, personal communication, Peter Krijger, Stryker Orthopaedics). We are unaware of any changes to resin type, surface finish, or manufacturing tolerances implemented by the manufacturer during the 8-year study period.

Before mechanical testing, the assembled control components and retrieved components were soaked in a 37° C water bath for 2 weeks to allow fluid absorption[6] and achieve temperature equilibration. Each polyethylene insert was secured in a metal frame mold and backfilled with urethane (Smooth-Cast 300, Smooth-On, Easton, PA). Each tibial baseplate was rigidly clamped to the test table. Static loads from 0 to 98 N were incrementally applied to the metal frame at a rate of 2 N/second according to methods used by Engh et al[13] and Parks et al.,[24] displacing the polyethylene insert in the anteroposterior (AP) and mediolateral (ML) directions. Loading was repeated for at least three cycles to ensure measuring the total slack of the locking mechanism.[13] Insert motion was measured throughout the loading cycles using a digital dial gauge (resolution, 12.7 μm) that was rigidly attached to the tibial baseplate frame. Insert motion was defined as the fully reversible linear motion that occurred at loads of 11 N with the insert captured in the locking mechanism before elastic/plastic deformation was induced.[13,26] Total motion for each insert was calculated as[13]

$$\text{insert motion index} = (AP^2 + ML^2)^{1/2}. \quad (2.1)$$

An observer evaluated the polyethylene backside and articular surfaces on all 37 inserts using optical (model Z30L, Cambridge Instruments, Cambridge, MA) and

scanning electron (JSM 6100, JEOL USA, Peabody, MA) microscopy and visual identification methods.[17,26,33] One revised insert was excluded from the backside damage assessment because of insert destruction that occurred during an unrelated study. The prevalence of nine damage modes was determined. Abrasion was visualized as rough, tufted regions. Burnishing was visualized as smooth regions highly reflective of incident light. Surface deformation included regions not intended as a bearing surface that had a permanent change in shape from the original surface. On the backside surface, deformation is typically observed around protrusions (lettering) or screw holes that exist on the metal tibial baseplate.[19,28] On the articular surface, deformation not associated with condylar articulation is typically observed on the tibial eminence.[2,15] Delamination was visualized as thin sheets of material separated from the surface. Dimpling was visualized as smooth, nearly circular indentations that lacked orientation (Figure 2.2), making them visibly distinguishable from pitting and scratching.[27] Embedded debris were visualized as particles that differed in color and/or texture relative to the surrounding polyethylene surface. Pitting was visualized as depressions with rough surfaces typically 1 to 2 mm in diameter. Scratching was visualized as thin lines in irregular or ordered directions across the surface. Striations were visualized as highly oriented, longitudinal, smooth peaks and troughs on the articular surface.[33]

The circumference of the damage regions was outlined on calibrated digital images of the articular and backside surfaces for all inserts, and we measured the damage area using digital image analysis techniques.[10,15,16] Absolute error and accuracy were determined based on measurement of calibrated images of shapes with known dimensions. The technique is 98.6% accurate with a precision of 0.4 mm for linear

distances and 3.9 mm^2 for areas. Damage area was calculated as a percentage of the medial and lateral articular and backside surface areas. The damage location (area centroid) for the articular and backside damage regions was determined relative to a transtibial axis bisecting the tibial insert into equal anterior and posterior halves.

The association between variables was determined using Spearman's bivariate rank order correlation. Statistical power for damage pattern correlations was sufficient ($\beta = 0.8$) based on the available sample size of 37 inserts and $\alpha = 0.05$. Correlation coefficients greater than 0.6 indicated a strong correlation and correlation coefficients 0.4 to 0.6 indicated a moderate correlation. Statistical power for insert motion measurements was limited ($\beta = 0.5$) based on the sample size of six autopsy-retrieved tibial components available for mechanical testing. Given the possibility for a type 2 error, only descriptive statistics for mechanical testing are provided.

2.3 Results

Physiological loading affected the modular capture mechanism and the size of backside surface damage in the autopsy-retrieved components that had not been previously disassembled. Inserts with the largest backside damage area had the least motion and the longest in vivo duration (Figures 2.3, 2.4). The insert motion index was negatively correlated with backside damage area ($r = -0.94$, $p = 0.017$) and in vivo time ($r = -0.94$, $p = 0.017$). The insert motion index averaged 154 ± 121 μm for the six autopsy-retrieved components, which was 2.48 times greater than the 62 ± 53 μm average insert motion index for the unused controls.

The duration of physiological loading affected the size of the damage area on the backside surface of the polyethylene insert but not on the articular surface. Backside

damage size was 48% ± 17% of the medial insert and 42% ± 15% of the lateral insert (Table 2.2). Articular damage size was 51% ± 18% of the medial insert and 49% ± 15% of the lateral insert (Table 2.2). There was a moderate positive correlation ($r = 0.48$, $p = 0.004$) between in vivo time and backside damage area but not articular damage area. Inserts with longer in vivo functional duration had greater backside damage areas.

Damage areas and damage locations were similar for the backside and articular surfaces on the polyethylene inserts (Table 2.2). Damage locations were concentrated on the posterior half of the polyethylene inserts (Figure 2.6), with similar damage areas occupying approximately 40% to 50% of the medial and lateral compartments on both the backside and articular surfaces (Table 2.2). The average area centroid location was 2.2 mm to 4.8 mm posterior to the central transtibial axis for both the backside and articular surfaces, with damage more posterior on the lateral compartment than the medial compartment. Patient weight was moderately positively correlated (correlation coefficient = 0.44, $p = 0.006$) with articular damage area but not backside damage area.

Observed damage modes were substantially different for the articular and backside surfaces. The predominant backside damage mode was dimpling, occurring on 94% of the inserts (Figure. 2.5). Six inserts (17%) had dimpling alone without evidence of other damage modes. Scanning electron microscopy showed the dimples were circular indentations approximately 100 μm in diameter that appeared consistent with a cast impression of the textured metal baseplate against the polyethylene rather than material loss (Figure 2.2). The most frequent articular damage modes were burnishing, scratches, and striations, each observed on more than 60% of the inserts (Figure 2.5). Damage resulting from contact with surfaces other than the smooth metal articular surface of the

femoral condyles included deformation on the anterior tibial eminence[2,15] in 65% of the inserts and abrasive damage on the polyethylene insert rim[15,23] in 51% of the inserts. Articular surface delamination occurred on four (11%) inserts, but had areas less than 2%. None of the inserts had abrasion, delamination or striations on the backside surface. Backside surface deformation was noted around the periphery of a shallow rectangular recess in the center of the metal baseplate,[27] but deformation into screw holes did not occur as the cemented tibial baseplates did not have screw holes. Third-body debris consisted of a small number of metal particles that likely originated from the anterior wire locking feature during disassembly.

2.4 Conclusions

Substantial performance variations for different locking mechanism designs have been reported for a wide variety of TKAs.[8,9,12,13,19,21,24,25,26,28,31] It has been suggested the modular capture mechanism of some modular tibial components degrades with physiologic loading.[13] However, careful reviews of previous mechanical studies of knee prostheses retrieved at autopsy[13,26] and revision surgery[8] revealed no correlation between insert motion and in vivo time. In our study, autopsy-retrieved components used for the mechanical testing were not previously disassembled to maintain the physiological interface conditions and capture mechanism. The duration of physiological loading affected the modular capture mechanism and the size of the damage area on the backside surface of the polyethylene insert, but not on the articular surface.

Some limitations are noted. Autopsy retrieval of knee components is a time-intensive experimental model, limiting the number of components available for evaluation. Statistical power was limited for the insert motion data. The tolerance for the

insert locking mechanism reported by the manufacturer is ±0.003 inches (±76 microns). This is reflected, to some extent, by the observed variability in insert motion of control and retrieved inserts. Additional destructive testing to characterize material properties related to gamma radiation sterilization and associated polyethylene damage has not been completed, and the inserts' shelf ages are unknown. However, delamination or other damage modes typically associated with gamma radiation[7] occurred infrequently on these inserts retrieved after 1 to 74 months (Figure 2.5).

The full peripheral rim locking mechanism (Figure 2.1) we evaluated did not become increasingly unstable with in vivo function. Contrary to the hypothesis, autopsy-retrieved components with the longest time in vivo had the least amount of motion and the greatest backside damage area (Figures 2.3, 2.4). These data support previously reported lower than average insert motion for components retrieved after a long duration of function.[8] The insert motion index averaged 62 μm for the unused tibial components, similar to the 64 μm average motion index reported for other designs similarly tested.[13] After 2 to 6 years of in vivo physiological loading, the insert motion index averaged 154 μm for autopsy-retrieved components. Although average insert motion more than doubled after physiological loading, the magnitude was approximately 60% lower than the motion for other designs obtained at autopsy after a similar duration of function.[13,26] These differences may be from variations in the modular capture mechanism design and manufacturing tolerance.[1,13,24] The majority of autopsy-retrieved components similarly tested in previous studies[13,26] utilized tongue-and-groove capture mechanisms, which do not effectively restrict motion in the direction of the groove.[8,13]

Considering a cold flow of polyethylene can occur with cyclic loading,[5,11,20] one possible explanation for the decreased insert motion is that polyethylene expansion in the transverse plane during physiologic loading reduced the clearance between the insert and metal tray.[8] Similarities in feature morphology for the inferior insert and superior baseplate surfaces suggest that compressive forces from contact at the articular surface were transmitted to the backside surface, such that the textured pattern on the metal baseplate was transferred as an indented dimpled pattern onto the polyethylene backside surface (Figure 2.2). Silva, et al[27] reported plastic deformation of the polyethylene insert could result in tray transfer indentations. These observations suggest that insert motion was affected by mechanical interlock between the polyethylene insert and the full peripheral rim capture mechanism and grit-blasted metal tibial baseplate.

Dimpling was the most common backside damage mode, and it is possible mechanisms other than interface motion produced the well-distributed dimpled pattern and low prevalence of scratching. The dimpling was characterized as uniform, nearly circular indentations approximately 100 μm in diameter that lacked orientation (Figure 2.2). The magnitude of axial compressive force during daily activity is approximately five times greater than peak shear force,[29] with the location of articular load corresponding to the location of articular and backside deformation.[1,28] Loading perpendicular to the articular surface, with limited motion in the shear plane (parallel to the articular surface), can contribute to backside surface deformation without appreciable disruption of machining marks or wear debris production.[1,32] In contrast, stippling damage has been attributed to motion in the shear plane, possibly combined with third-body debris.[1,13,26] Stippling is characterized by small unidirectional scratches greater than 1 mm in length

on polyethylene backside surfaces. The dimpling patterns were visibly distinguishable from such scratches, which occurred infrequently on the backside surface.

Physiological loading affected the distribution of surface damage on the polyethylene inserts. The damage area centroid locations for both the articular and backside surfaces were located on the posterior half of the polyethylene insert (Figure 2.6), consistent with the reported location of tibiofemoral contact during activities of daily living in patients with this TKR design.[17] Articular damage area was not correlated with time in vivo, but backside damage area increased with time in vivo; consistent with data from other retrieval studies.[26,31] Substantial differences between the articular and backside damage modes suggest different wear mechanisms at the two interfaces. Compared with the polyethylene backside surfaces, the articular surfaces had a higher prevalence of abrasion, burnishing, delamination, pitting, scratching, and striated damage modes (Figure 2.5). Such damage was consistent with abrasive/adhesive wear mechanisms and tibiofemoral articular motion.[4,15,33,34] In contrast, fewer than 20% of inserts had abrasion, delamination, pitting, or scratches on the backside surface. Backside damage on six inserts consisted solely of dimpled indentations. These data are consistent with articular damage contributing to a substantially greater proportion of the total damage score.[1,27]

In summary, in vivo physiological loading affected the modular capture mechanism and damage patterns on the retrieved polyethylene inserts. Articular and backside damage patterns were concentrated on the posterior half of the inserts, consistent with the reported location of tibiofemoral articulation for this TKA design[15] and transmission of articular contact stresses to the backside surface.[22,30] Backside

damage revealed evidence of a mechanical interlock between the polyethylene insert and tibial tray, consistent with the measured insert motion. Although motion between the polyethylene insert and the metal baseplate can contribute to the overall particulate load,[19,26,28,31] adhesive/abrasive wear mechanisms on the polyethylene articular surface were dominant on these tibial inserts retrieved at autopsy and revision surgery.

2.5 Acknowledgement

The author thanks Scott A. Banks, PhD and W. Andrew Hodge, MD for co-authoring publication of this work; W. Andrew Hodge, MD for providing retrieved TKA components; Sylvia Barnes, Lewjack Dorrance, and Tammy Moore for cooperation in obtaining autopsy retrieved TKA and donor patient information; Carolyn Jones for technical assistance obtaining radiographs of autopsy retrieved knees. The author acknowledges Mark Kester and Amy Belisle for support in obtaining unused prostheses. This work was supported by funding from The BioMotion Foundation in Palm Beach, Florida, with partial funding provided by an institutional research grant from Osteonics Corp. (now Stryker Orthopaedics), Mahwah, New Jersey.

Note: This work has been accepted for publication and is referenced as follows.

Harman MK, Banks SA, Hodge WA: Does backside damage correspond to articular damage in retrieved TKR polyethylene inserts? Clin Orthop 2007; in press.

2.6 References Cited

1. Akisue T, Yamagushi M, Bauer TW, Takikawa S, Schils JP, Yoshiya S, Kurosaka M. Backside polyethylene deformation in total knee arthroplasty. *J Arthroplasty*. 2003;18:784-791.

2. Banks SA, Harman MK, Hodge WA. Mechanism of anterior impingement damage in total knee arthroplasty. *J Bone and Joint Surg Am.* 2002;84:37-42.

3. Bartel DL, Bicknell VL, Wright TM. The effect of conformity, thickness, and material on stresses in ultra-high molecular weight components for total joint replacement. *J Bone Joint Surg Am*. 1986;68:1041-1051.

4. Blunn GW, Walker PS, Joshi A, Hardinge K. The dominance of cyclic sliding in producing wear in total knee replacement. *Clin Orthop Relat Res.* 1991;273:253-60.

5. Chang DC, Goh JC, Teoh SH, Bose K: Cold extrusion deformation of UHMWPE in total knee prostheses. *Biomaterials*. 1995:16:219-23.

6. Clarke IC, Starkebaum W, Hosseinian A, McGuire P, Okuda R, Salovey R, Young R. Fluid-sorption phenomena in sterilized polyethylene acetabular prostheses. *Biomaterials*. 1985;6:184-8.

7. Collier JP, Sperling DK, Currier JH, Sutula LC, Saum KA, Mayor MB. Impact of gamma sterilization on clinical performance of polyethylene in the knee. *J Arthroplasty*. 1996;11(4):377-89.

8. Conditt MA, Ismaily SK, Alexander JW, Noble PC. Backside wear of modular ultra-high molecular weight polyethylene tibial inserts. *J Bone Joint Surg Am.* 2004;86:1031-7.

9. Conditt MA, Stein JA, Noble PC. Factors affecting the severity of backside wear of modular tibial inserts. *J Bone Joint Surg Am.* 2004;86:305-311.

10. Cornwall GB, Bryant JT, Hansson CM, Rudan J, Kennedy LA, Cooke TD. A quantitative technique for reporting surface degradation patterns of UHMWPE components of retrieved total knee replacements. *J Appl Biomater.* 1995;6:9-18.

11. Cuckler JM, Lemmons J, Tamarapalli JR, Beck P. Polyethylene damage on the nonarticular surface of modular total knee prostheses. *Clin Orthop.* 2003;410:248-53.

12. Engh G, Dwyer K, Hanes C. Polyethylene wear of metal-backed tibial components in total and unicompartmental knee prostheses. *J Bone and Joint Surg Br.* 1992;74(1):9-17.

13. Engh G, Smain L, Rao A, Collier M. In vivo deteriation of tibial baseplate locking mechanisms in contemporary modular total knee components. *J Bone and Joint Surg Am.* 2001;83:1660-65.

14. Ezzet KA, Garcia R, Barrack RL. Effect of component fixation method on osteolysis in total knee arthroplasty. *Clin Orthop.* 1995;321:86-91.

15 Harman MK, Banks SA, Hodge WA. Polyethylene damage and knee kinematics after total knee arthroplasty. *Clin Orthop.* 2001;392:383-93.

16. Harman MK, Markovich GD, Banks SA, Hodge WA. Wear patterns on tibial plateaus from varus and valgus osteoarthritic knees. *Clin Orthop.* 1998;352:149-58.

17. Hood RW, Wright TM, Burstein AH. Retrieval analysis of total knee prostheses: A method and its application to 48 total condylar prostheses. *J Biomed Mater Res.* 1983;17:829-42.

18. Lewis P, Rorabeck CH, Bourne RB. Screw osteolysis after cementless total knee replacement. *Clin Orthop.* 1995;321:173-7.

19. Li S, Scuderi G, Furman BD, Bhattacharyya S, Schmieg JJ, Insall JN. Assessment of backside wear from the analysis of 55 retrieved tibial inserts. *Clin Orthop.* 2002;404:75-82.

20. McDonald MD, Bloebaum RD. Distinguishing wear and creep in clinically retrieved polyethylene inserts. *J Biomed Mater Res*. 1995;29:1-7.

21. Mikulak SA, Mahoney OM, Dela Rosa MA, Schmalzried TP. Loosening and osteolysis with the press-fit condylar posterior-cruciate-substituting total knee replacement. *J Bone and Joint Surg Am.* 2001;83(3):398-403.

22. Morra EA, Harman MK, Greenwald AS. Computational Models Can Predict Polymer Insert Damage in Total Knee Replacements. In *Insall & Scott Surgery of the Knee, 4th edition*, Vol. 1 (13):271-283, Scott WN (ed.) Elsevier Inc., Philadelphia, PA, 2005.

23. Noble PC, Conditt MA, Thompson MT, Stein JA, Kreuzer S, Parsley BS, Mathis KB. Extraarticular abrasive wear in cemented and cementless total knee arthroplasty. *Clin Orthop.* 2003;416:120-8.

24. Parks N, Engh G, Topoleski L, Emperado J. Modular tibial insert micromotion: A concern with contemporary knee implants. *Clin Orthop.* 1998;356:10-15.

25. Peters PC, Engh GA, Dwyer K, Vinh T. Osteolysis after total knee arthroplasty without cement. *J Bone and Joint Surg Am.* 1992;74(6):864-76.

26. Rao A, Engh G, Collier M, Smain L. Tibial interface wear in retrieved total knee components and correlations with modular insert motion. *J Bone and Joint Surg Am.* 2002;84(10):1849-55.

27. Silva M, Kabbash CA, Tiberi JV, Park SH, Reilly DT, Mahoney OM, Schmalzried TP. Surface damage on open box posterior stabilized polyethylene tibial inserts. *Clin Orthop.* 2003;416:135-44.

28. Surace MF, Berzins A, Urban RM, Jacobs JJ, Berger RA, Natarajan RN, Andriacchi TP, Galante JO. Back surface wear and deformation in polyethylene tibial inserts retrieved postmortem. *Clin Orthop.* 2002;404:14-23.

29. Taylor SJ, Walker PS, Perry JS, Cannon SR, Woledge R. The forces in the distal femur and the knee during walking and other activities measured by telemetry. *J Arthroplasty*. 1998;13(4):428-37.

30. Wasielewski RC. The causes of insert backside wear in total knee arthroplasty. *Clin Orthop*. 2002;404:232-46.

31. Wasielewski RC, Parks N, Williams I, Surprenant H, Collier JP, Engh GA. Tibial insert undersurface as a contributing source of polyethylene wear debris. *Clin Orthop.* 1997;345: 53-9.

32. Wasielewski RC, Galante JO, Leighty RM, Natarajan RU, Rosenberg AG. Wear patterns on retrieved polyethylene tibial inserts and their relationship to technical considerations during total knee arthroplasty. *Clin Orthop.* 1994;299:31-43.

33. Wimmer M, Andriacchi T, Natarajan R, Loos J, Karlhuber M. A striated pattern of wear in ultrahigh-molecular-weight polyethylene components of Miller-Galante total knee arthroplasty. *J Arthroplasty.* 1998;13(1):8-16.

34. Wimmer, MA., and Andriacchi, T. P.: Tractive forces during rolling motion of the knee implications for wear in total knee replacement. *J. Biomech.*, 30(2): 131-137, 1997.

Table 2.1: Patient Demographics*

Parameters	Autopsy	Revision	Total
n	12	25	37
Gender (male, female)	11, 1	13, 12	24, 13
Age at surgery (years)	69 ± 4	67 ± 8	68 ± 7
Age at retrieval (years)	73 ± 4	70 ± 8	71 ± 7
Height (cm)	180 ± 10	173 ± 13	175 ± 13
Weight (kg)	90 ± 15	85 ± 18	86 ± 17
Body mass index (kg/m^2)	28 ± 2	29 ± 5	28 ± 5
In situ time (months)	41 ± 21	26 ± 21†	31 ± 22

*values provided as mean and standard deviation

†$p < 0.05$ compared with autopsy knees

Table 2.2: Articular and Backside Damage Areas and Locations for Polyethylene Inserts*

	Damage Area		Damage Location†	
Surface	Medial (percent)	Lateral (percent)	Medial (mm)	Lateral (mm)
Articular	51 ± 18	49 ± 15	3.0 ± 3.0	4.8 ± 3.3
Backside	48 ± 17	42 ± 15	2.2 ± 3.4	2.9 ± 2.6

* values provided as mean and standard deviation

†distance posterior to the transtibial axis

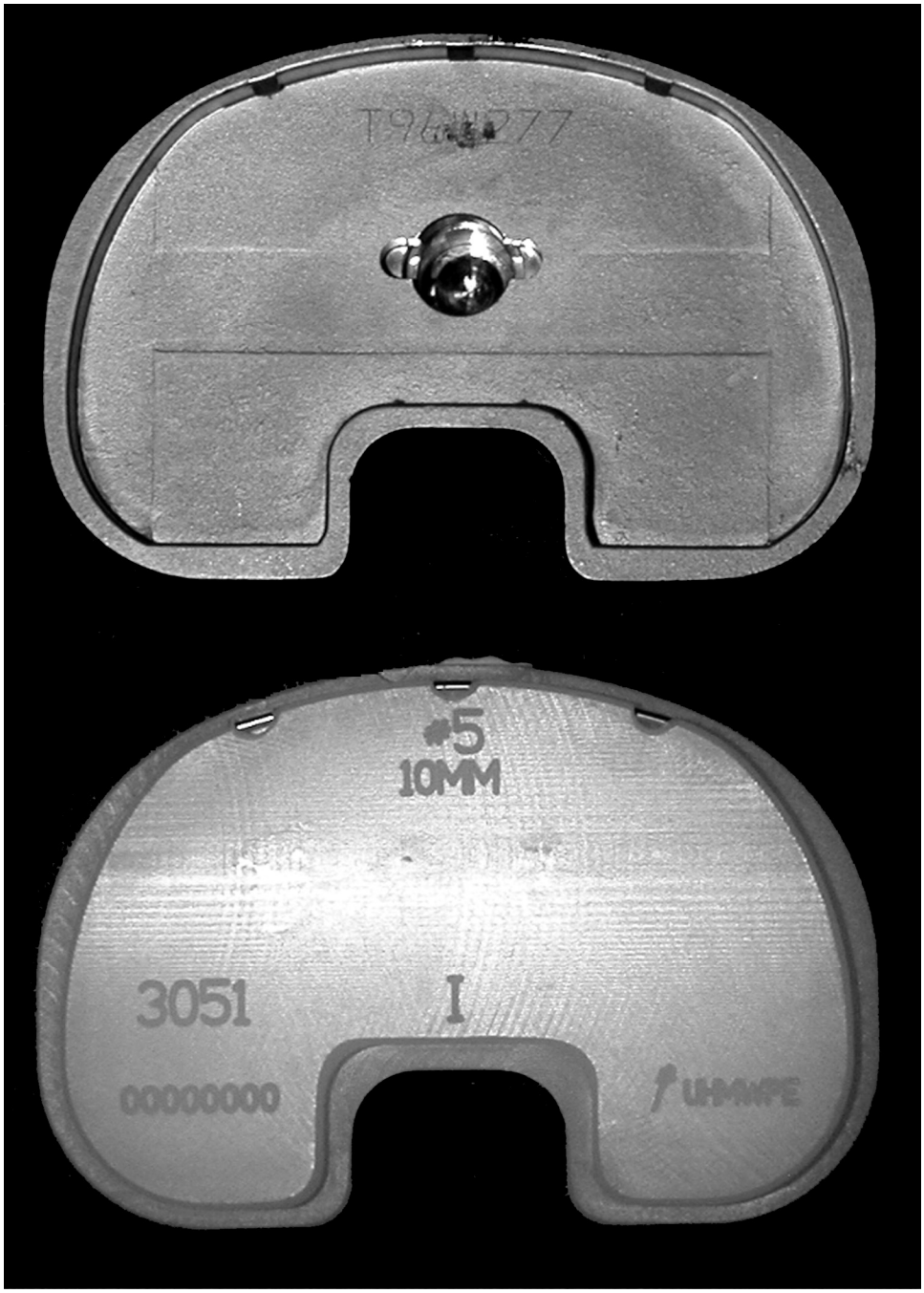

Figure 2.1: Full Peripheral Rim Locking Mechanism for Modular TKA

There was a lipped edge around the metal tibial baseplate circumference and a recessed edge around the periphery of the polyethylene insert. Three metal barbs on the anterior baseplate captured a wire in the anterior insert.

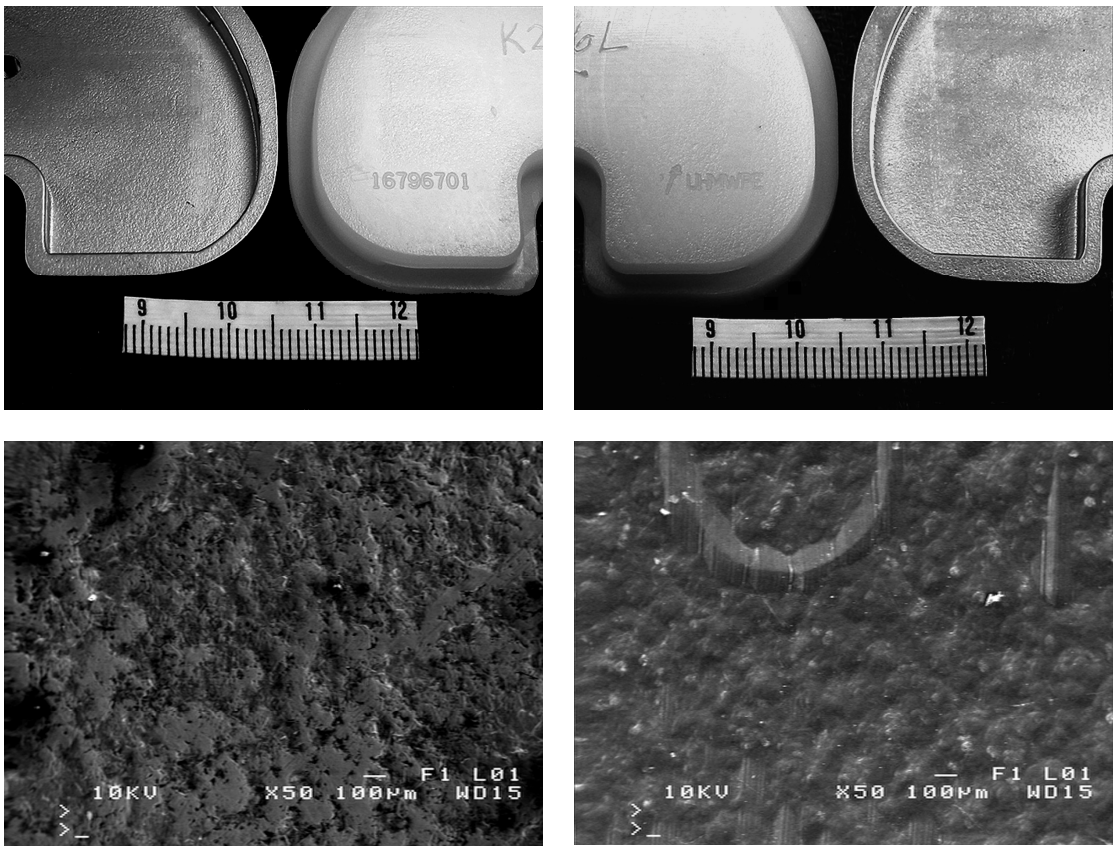

Figure 2.2: Surface Texture of the Metal Baseplate and Polyethylene Insert

The metal baseplate had a textured surface with smooth rectangular regions on the (A) medial and (B) lateral plateau that were transferred to the backside surface of the polyethylene insert. Scanning electron microscopy revealed a similar scale for the (C) grit-blasted metal surface and the (D) dimpling on the polyethylene insert. Stamped alphanumerics on the polyethylene insert were well preserved in the macroscopic photos and micrographs, consistent with the low prevalence of abrasive wear mechanisms on the backside surfaces.

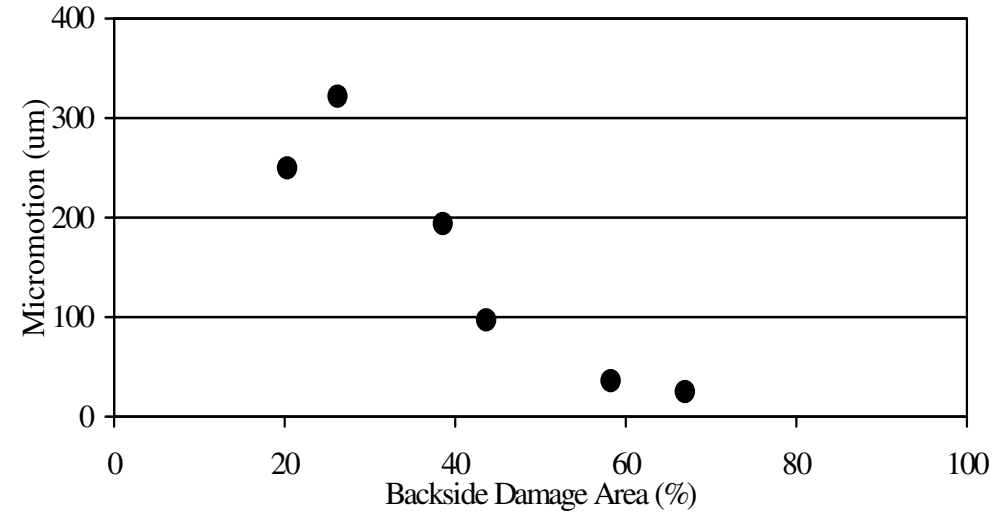

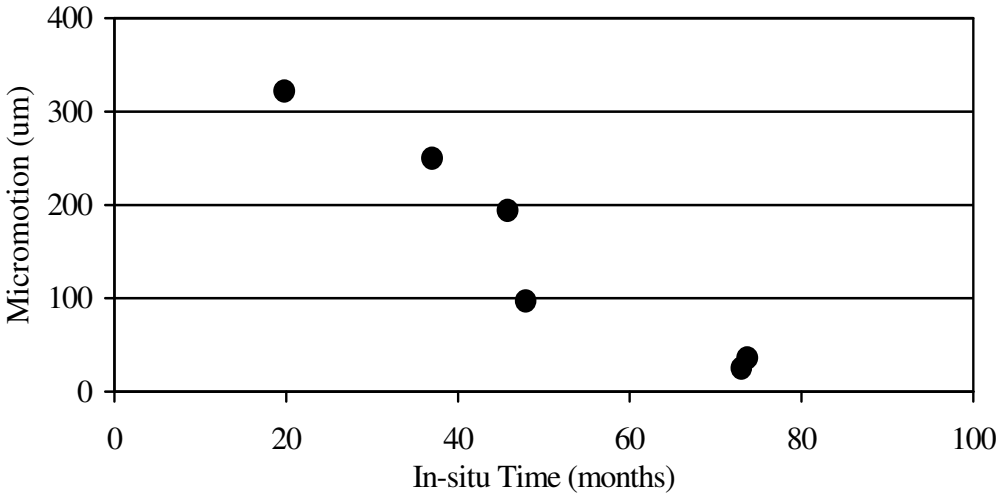

Figure 2.3: Insert Motion Versus Backside Damage Area and *In situ* Time

Inserts with the least motion had the most backside damage area and were in situ longest for the six autopsy-retrieved tibial components.

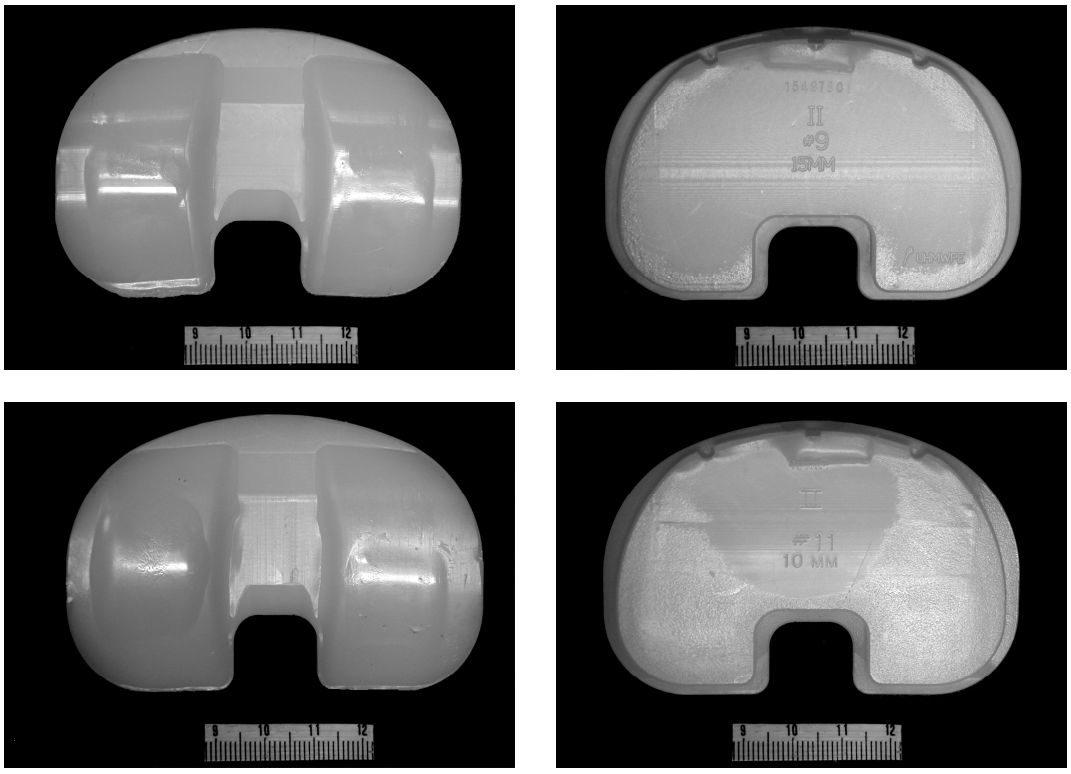

Figure 2.4: Articular and Backside Damage for Two Autopsy Retrieved TKA

A photograph shows (A) articular and (B) backside damage on an insert retrieved at autopsy from the left knee of a 70 kg male after 20 months of in vivo function. There was damage on 40% of the articular surface and 26% of the backside surface. The motion index was 322 μm. A photographs shows (C) articular and (D) backside damage on an insert retrieved at autopsy from the right knee of a 100 kg male after 73 months of in vivo function. There was damage on 53% of the articular surface and 67% of the backside surface. The motion index was 25 μm.

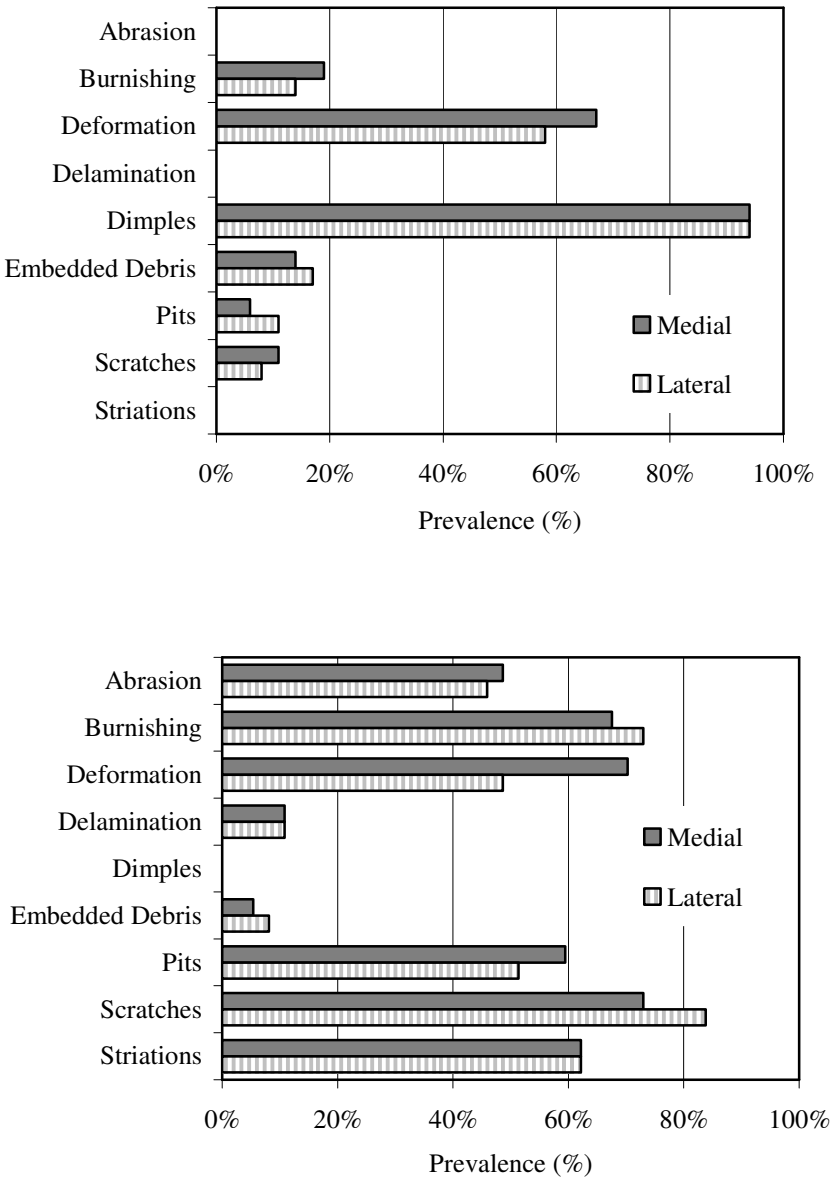

Figure 2.5: Prevalence of Different Damage Modes on the Backside and Articular Surfaces of Retrieved Polyethylene Inserts

Abrasive/adhesive wear mechanisms were largely absent on the backside surface (top) compared to the articular surface (bottom), suggesting different wear mechanisms occurred during physiological loading.

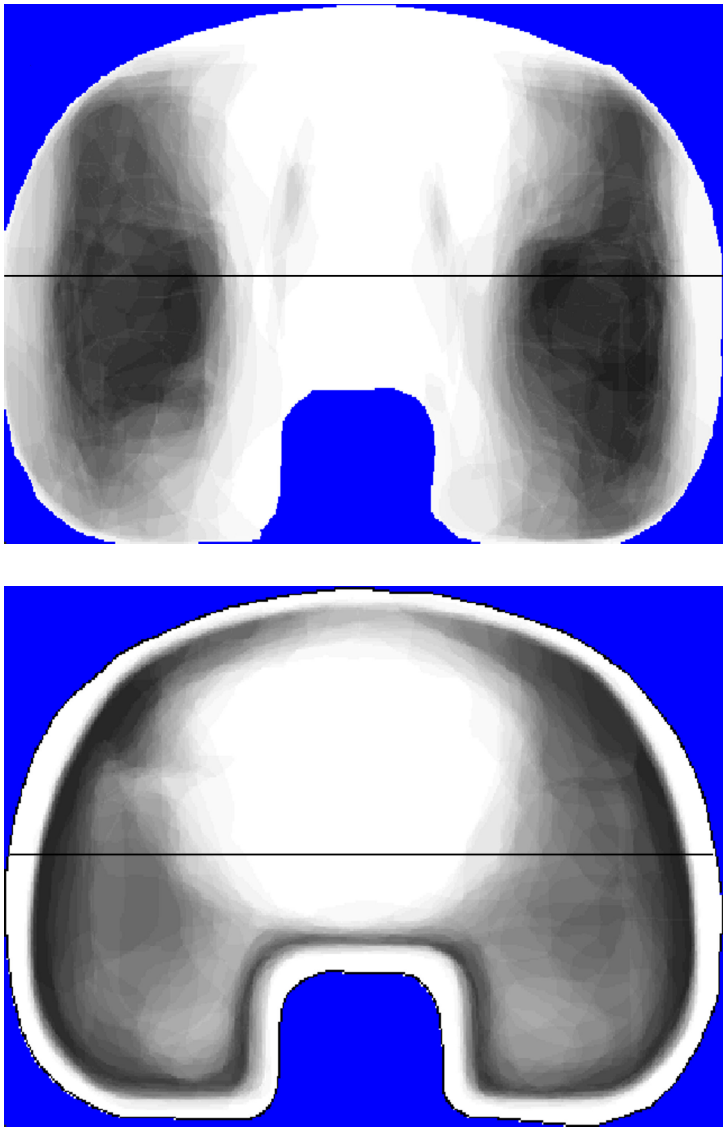

Figure 2.6: Graphic Overlay Showing Articular and Backside Damage Regions

Damage regions on the (A) articular and (B) backside surfaces of all retrieved polyethylene inserts were normalized to a medium-sized right insert. Darker grayscale indicates more damage. Backside damage locations were concentrated on the posterior half of the insert, corresponding to the articular damage location and the reported location of tibiofemoral contact during activities of daily living in patients with this TKA design.[1]

3 DAMAGE PATTERNS ON RETRIEVED MOBILE BEARING POLYETHYLENE INSERTS: DO ANALYTICAL MODELS PREDICT IN VIVO PERFORMANCE?

3.1 Introduction

Enthusiasm for using mobile polyethylene bearings in total knee arthroplasty (TKA) is based, in part, on early outcomes of the Oxford bi-compartmental and Low Contact Stress (LCS) meniscal-bearing and rotating-platform designs.[8,17] Early survivorship was greater than 95% at the 6 to 10 year follow-up interval for LCS TKA[6,27] and revision rates ranged from 0% to 7% after 7 to 12 years of function in patients.[11,28,29,37] Over the long-term, these generally favorable clinical outcomes have been maintained,[9,10,12] with outcomes comparable to the best results of fixed-bearing TKA in terms of wear, loosening, and osteolysis.[12,36]

Despite these successes, initial widespread use of these mobile-bearing TKA was tempered by some reports of complications. Patient selection and assessment of instability proved critical, as poor survivorship (81%) occurred with the Oxford design when implanted in patients with a ruptured anterior cruciate ligament at index TKA[18] and bearing dislocation and/or gross fracture was reported in 1% to 9% of LCS meniscal bearing TKA.[2,7,25,26] In addition, there are concerns that polyethylene wear debris generated at the conforming articular surface and mobile "backside" surface will adversely effect the longevity of mobile-bearing TKA.[3,22,24,25]

One of the theoretical advantages of the mobile bearing concept put forth by the early innovators[8,17] is that large tibial-femoral contact areas and lower contact stresses will diminish the likelihood of bearing wear. Finite element models for a variety of mobile bearing TKA, including the LCS rotating platform, show contact areas that are approximately double the size of contact for non-conforming fixed bearing designs (Figure 3.1).[3,30-35] This contributes to contact stresses that are below the yield stress of polyethylene, reducing the potential for polyethylene material fatigue. These analytical predictions of bearing performance are supported by retrieved LCS bearings, with Collier, et al.[14] concluding the "benefits of highly congruent, tibiofemoral configuration were evident from lack of deep pitting, delamination, or cracking in the majority of LCS meniscal bearing and rotating platform prostheses".

The objective of this study is to evaluate articular and backside wear on retrieved polyethylene mobile bearing TKA for comparison with published analytical models for the LCS TKA design. It was hypothesized that damage patterns would correspond to predicted contact areas and contact stress patterns in the analytical models. Furthermore, it was hypothesized that TKA revised for polyethylene wear would have distinct damage patterns and associated adverse biological responses noted at revision TKA.

3.2 Materials and Methods

Forty consecutively retrieved mobile bearing TKA tibial components were evaluated, including 27 pair of meniscal bearing inserts and 13 rotating platform inserts (Figure 3.2). All components were posterior cruciate ligament sacrificing mobile bearing TKA (LCS, DePuy, Warsaw, IN) with cementless fixation. The tibial bearings

articulated with femoral components having multiple radii in the sagittal plane and all polyethylene inserts were sterilized using gamma radiation in air.

The index TKA surgical procedures were operated by multiple surgeons prior to referral to two medical centers contributing retrievals to an established Implant Retrieval Program.[19] Patient demographics and reasons for revision are provided in Tables 3.1 and 3.2. Among the 38 components obtained at revision TKA, bearing exchange without revision of any metal component was possible in 28 knees (74%). The femoral component was not revised in 32 (84%) knees, the tibial baseplate was not revised in 29 (76%) knees, and the patellar metal-back was not revised in 31 (82%) knees.

One observer visually assessed damage on the superior tibial-femoral articular surface (henceforth, articular surface) and inferior mobile bearing surface (henceforth, backside surface) of the retrieved tibial inserts using an optical microscope (model Z30L, Cambridge Instruments, Cambridge, MA) at 7 to 30 times magnification. The prevalence of ten distinct damage modes was evaluated using published visual identification methods.[20,23,38] Abrasion is typically visualized as rough, tufted regions. Burnishing is visualized as smooth regions that are highly reflective of incident light. Delamination is visualized as thin layers of polyethylene material separated from the surface. Subsurface delamination appears as cracks and/or discoloration located inferior and generally parallel to articular plane without discontinuity of the articular surface material. Creep deformation is visualized as a permanent change in shape from the original surface. Embedded debris is visualized as particles that differed in color and/or texture relative to the surrounding polyethylene surface, consistent with embedded particles of bone, cement fragments or metal particles. Pitting is visualized as depressions with rough

surfaces typically 1 to 2 mm in diameter. Scratching is visualized as thin lines in irregular or ordered directions across the surface. Striations are visualized as highly oriented, longitudinal, smooth peaks and troughs on the articular surface.[38] Fractures are visualized as complete cracks or wear-through of the polyethylene.

Each insert was placed on a 20 mm^2 calibration grid and digital images of the articular and backside surfaces were recorded. A normalized, component-based coordinate system was established, dividing the articular and backside surfaces into four anterior, poster, medial and lateral quadrants. Algorithms were implemented to correct component rotational alignment within the global coordinate system. The circumference of each identified damage region was outlined on the digital images[16,20,21] using custom digital image analysis programs and the corresponding wear mode for each region was recorded. The technique is 98.6% accurate with a precision of 0.4 mm for linear distances and 3.9 mm^2 for areas. The damage mode incidence was calculated as the number of inserts showing a given damage mode divided by the total number of inserts included in the group. The damage area was calculated as a percentage of the total articular or backside area and the area centroid was computed. The damage location was expressed as the location of the area centroid relative to the normalized component-based coordinate system. The AP extent of the damage pattern region on the tibial inserts was calculated as the difference between the maximum anterior and posterior coordinate points. Bearing orientation was not preserved during revision surgery and therefore, no distinction between medial and lateral bearing surfaces could be determined.

Strength of association between variables was determined using Spearman's bivariate rank order correlation. Correlation coefficients >0.6 were considered to indicate

strong correlation, and values of 0.4 to 0.6 were considered to indicate moderate correlation. Differences between groups were analyzed using analysis of variance with appropriate post hoc multiple comparisons.

3.3 Results

Revision surgery was indicated for reasons of polyethylene wear in 21 of the 40 (53%) TKA in this series, including seven TKA revised for patella bearing wear and 14 TKA revised for tibial bearing wear. TKA revised for polyethylene wear had significantly longer duration of function compared to TKA revised for other reasons (ANOVA, $p<0.001$) Average duration of function for the meniscal bearings was 6 years longer than the duration for rotating platforms (ANOVA, $p<0.001$).

Delamination and subsurface changes were evident on more than 75% of meniscal bearings and more than 35% of rotating platforms, consistent with fatigue related damage mechanisms (Figures 3.3, 3.4). Duration of function was strongly correlated to damage size (correlation coefficient = 0.62, $p<0.001$) and the presence of delamination (correlation coefficient = 0.62, $p<0.001$), fracture (correlation coefficient = 0.52, $p<0.001$), and subsurface delamination (correlation coefficient = 0.69, $p<0.001$) damage modes. Duration of time in storage prior to implantation was known for 20 of the retrieved inserts and averaged 1.6 (range, 0.1 to 7.3) years, resulting in an average total age of 12.5 (range, 5.2 to 16.6) years. However, there were no correlations between shelf age and damage area or type ($p>0.05$)

Damage areas were significantly different between the two types of mobile bearing inserts (Mann-Whitney, $p<0.001$). Median damage area was 96.9% and 70.4% for the meniscal bearing and rotating platform inserts, respectively (Figure 3.5).

Subsurface delamination was strongly correlated with having a meniscal bearing insert (Figure 3.3), pitting was correlated with having a rotating platform insert (correlation coefficient=0.57, $p<0.05$). Bearing fracture occurred in 38% of the meniscal bearing inserts compared to 8% of the rotating platform inserts, likely due to the thinner polyethylene bearing thickness for the meniscal bearings (Figure 3.2). Backside surface scratches were oriented in a linear pattern on meniscal bearings and in a rotational pattern on rotating platforms (Figure 3.6), consistent with the constraint mechanisms at the bearing interface.

3.4 Conclusions

A perceived disadvantage of mobile bearings TKA is that osteolysis will become more prevalent with longer duration of function. Huang, et al.[25] reported a 47% incidence of osteolysis after an average follow-up of 8.5 years in TKA patients with LCS mobile bearing and rotating platform bearings. Histological analysis of tissues surrounding failed TKA show a significantly higher rate of wear debris production and a higher volume of smaller diameter wear particles for mobile bearing TKA compared to fixed bearing TKA.[22,24] A knee joint wear simulator study demonstrate a 10-fold increase in wear volume for mobile bearing TKA compared to the same design with a fixed bearing insert.[3] In the current study, adverse biological consequences of severe bearing wear did not occur after 1 to 15 years in-situ. Bearing wear and fracture, not osteolysis, were the predominant reasons for revision. Despite substantial polyethylene damage patterns on the articular and backside surfaces, the incidence of osteolysis noted at retrieval was low (5%). Polyethylene bearing exchange was used successfully to treat 74% of these patients at revision TKA. In the ten patients requiring revision of the metal

components, revision occurred early (within 48 months) and for reasons associated with pain and lack of range of motion, not wear or osteolysis. It remains to be seen whether improved materials and less degrading sterilization methods will benefit the mobile bearing design concept for TKA.

The theoretical advantages of large contact area and low contact stresses[3,8,14,17] (Figure 3.1) were not realized for the LCS bearings included in the current study. Approximately one-third of the retrieved bearings were fractured, with delamination and subsurface cracking evident on more than 75% of meniscal bearings and more than 35% of rotating platforms. Areas of delamination and subsurface cracking ranged from 21%-25% and 34%-45%, respectively. These wear modes are characteristic of fatigue related damage mechanisms. Analytical models inclusive of kinematics and loading conditions that are representative of a dynamic range of motion may better predict the types of damage observed on these inserts.

Possible explanations for the apparent contradiction between the predicted performance of the LCS bearings (Figure 3.1) and the actual performance are related to articular geometry and bearing materials. The multi-radius geometry of the LCS femoral component allows the contact area on the tibial bearing to vary appreciably throughout the active knee flexion range. During knee extension, the LCS and other mobile bearing designs have large tibial-femoral contact areas contributing to relatively low contact stresses under physiologic loads (Figure 3.1).[3,30-35] However, after approximately 20° of knee flexion, the contact area decreases dramatically (Figure 3.7) as the sagittal radius of the femoral condyles decrease.[3,13] Contact stresses at the tibial-femoral articular surface are further exacerbated with the high joint loads that occur during knee flexion activities,

such as descending stairs and rising from a seated position.[33-35] When combined with poor material properties associated with gamma sterilization,[4,15] these loading conditions can result in contact stresses that exceed the yield stress of the polyethylene material, as evidenced by the damage modes in this series of retrieved inserts. TKA designs that maintain a large contact area throughout the range of motion occurring during activities of daily living may prove beneficial.

Abrasive wear due to sliding contact on the inferior polyethylene surface remains a concern in mobile bearing knees.[22,24] Despite the highly polished metal tibial surface used in the LCS design, scratching was the dominant backside wear mode on these retrieved inserts, appearing in a relatively linear pattern on the meniscal bearing inserts and in a rotational pattern on the rotating platform inserts (Figure 3.6). These findings are consistent with in vivo kinematic data showing anterior-posterior translations of LCS meniscal bearings during knee flexion activities.[1,5] However, the clinical significance of this backside damage was not apparent in this series, as complications due to particulate debris were not a factor in the revision reasons and bearing failure occurred with changes at the articular surface rather than the backside surface.

In summary, severe bearing wear and abrasive backside wear were not associated with osteolysis in these patients. Fixation of these uncemented mobile-bearing components was largely unaffected by gross bearing wear in these patients after 9 years of physiologic loading in patients. In cases of extreme polyethylene wear, bearing exchange provided a simple solution at revision TKA while limiting the destructive bone loss that can occur with revision of metal TKA prostheses.

3.5 Acknowledgements

The author thanks George D. Markovich, MD, Scott A. Banks, PhD, and W. Andrew Hodge, MD for co-authoring this work; and George D. Markovich, MD for providing retrieved mobile bearing TKA components and clinical data. This work was supported by funding from The BioMotion Foundation in Palm Beach, Florida.

Note: This work has been presented at an international scientific conference is referenced as follows.

Harman MK, Markovich GD, Banks SA, Hodge WA: Cementless LCS total knee arthroplasty after 9 years in-situ: Articular and backside wear on retrieved meniscal and rotating platform polyethylene bearings. 71st Annual Meeting of the American Academy of Orthopaedic Surgeons, San Francisco, CA, March 2004.

3.6 References Cited

1. Banks SA, Hodge WA. Design and activity dependence of kinematics in fixed and mobile-bearing knee arthroplasties. *J Arthroplasty*, 2004; 19(7):809-16.
2. Bert JM. Dislocation/subluxation of meniscal bearing elements after New Jersey low-contact stress total knee arthroplasty. *Clin Orthop*. 1990; 254:211-5.
3. Bourne RB, Masonis J, Anthony M. An analysis of rotating-platform total knee replacements. *Clin Orthop*. 2003; 410:173-80.
4. Bohl JR, Bohl WR, Postak PD, Greenwald AS. The Coventry Award. The effects of shelf life on clinical outcome for gamma sterilized polyethylene tibial components *Clin Orthop.* 1999; 367:28-38.
5. Bradley J, Goodfellow JW, O'Connor JJ. A radiographic study of bearing movement in unicompartmental Oxford knee replacements. *J Bone Joint Surg Br*. 1987; 69(4):598-601.
6. Buechel FF, Pappas MJ. Long-term survivorship analysis of cruciate-sparing versus cruciate-sacrificing knee prostheses using meniscal bearings. *Clin Orthop*. 1990; 260:162-9.

7. Buechel FF, Pappas MJ. New Jersey low contact stress knee replacement system. Ten-year evaluation of meniscal bearings. *Orthop Clin North Am*. 1989; 20(2):147-77.

8. Buechel FF, Pappas MJ. The New Jersey Low-Contact-Stress Knee Replacement System: biomechanical rationale and review of the first 123 cemented cases. *Arch Orthop Trauma Surg*. 1986; 105(4):197-204.

9. Buechel FF Sr, Buechel FF Jr, Pappas MJ, D'Alessio J. Twenty-year evaluation of the New Jersey LCS Rotating Platform Knee Replacement. *J Knee Surg*. 2002; 15(2):84-9.

10. Buechel FF Sr, Buechel FF Jr, Pappas MJ, D'Alessio J. Twenty-year evaluation of meniscal bearing and rotating platform knee replacements. *Clin Orthop*. 2001; 388:41-50.

11. Callaghan JJ; Squire MW; Goetz DD; Sullivan PM; Johnston RC. Cemented rotating-platform total knee replacement : A nine to twelve-year follow-up study. *J Bone Joint Surg Am*. 2000; 82(5):705-11.

12. Callaghan JJ, O'Rourke MR, Iossi MF, Liu SS, Goetz DD, Vittetoe DA, Sullivan PM, Johnston RC. Cemented rotating-platform total knee replacement: A concise follow-up, at a minimum of fifteen years, of a previous report. *J Bone Joint Surg Am*. 2005; 87(9):1995-8.

13. Chapman-Sheath PJ, Bruce WJ, Chung WK, Morberg P, Gillies RM, Walsh WR. In vitro assessment of proximal polyethylene contact surface areas and stresses in mobile bearing knees. *Med Eng Phys*. 2003; 25(6):437-43.

14. Collier JP, Mayor MB, McNamara JL, Surprenant VA, Jensen RE. Analysis of the failure of 122 polyethylene inserts from uncemented tibial knee components. *Clin Orthop*. 1991; 273:232-42.

15. Collier JP, Sperling DK, Currier JH, Sutula LC, Saum KA, Mayor MB. Impact of gamma sterilization on clinical performance of polyethylene in the knee. *J Arthroplasty*. 1996; 11(4):377-89.

16. Cornwall GB, Bryant JT, Hansson CM, Rudan J, Kennedy LA, Cooke TD. A quantitative technique for reporting surface degradation patterns of UHMWPE components of retrieved total knee replacements. *J Appl Biomater*. 1995; 6:9-18.

17. Goodfellow JW; O'Connor JJ. Clinical results of the Oxford knee. Surface arthroplasty of the tibiofemoral joint with a meniscal bearing prosthesis. *Clin Orthop*. 1986; 205:21-42.

18. Goodfellow JW, Kershaw CJ, Benson MK, O'Connor JJ. The Oxford Knee for unicompartmental osteoarthritis: The first 103 cases. *J Bone Joint Surg Br*. 1988; 70(5):692-701.

19. Harman MK, Banks SA, Hodge WA. Organization of a post-mortem implant retrieval program. 67th Annual Meeting of the American Academy for Orthopaedic Surgeons, Orlando, FL, 2000.

20. Harman MK, Banks SA, Hodge WA. Polyethylene damage and knee kinematics after total knee arthroplasty. *Clin Orthop*. 2001; 392:383-93.

21. Harman MK, Markovich GD, Banks SA, Hodge WA. Wear patterns on tibial plateau from varus and valgus osteoarthritic knees. *Clin Orthop*. 1998; 352:149-58.

22. Hirakawa K, Bauer TW, Stulberg BN, Wilde AH, Borden LS. Characterization of debris adjacent to failed knee implants of 3 different designs. *Clin Orthop*. 1996; 331:151-8.

23. Hood RW, Wright TM, Burstein AH. Retrieval analysis of total knee prostheses: A method and its application to 48 total condylar prostheses. *J Biomed Mater Res*. 1983;17: 829-42.

24. Huang CH, Ho FY, Ma HM, Yang CT, Liau JJ, Kao HC, Young TH, Cheng CK. Particle size and morphology of UHMWPE wear debris in failed total knee arthroplasties--a comparison between mobile bearing and fixed bearing knees. *J Orthop Res*. 2002; 20(5):1038-41.

25. Huang CH; Ma HM; Liau JJ; Ho FY; Cheng CK. Osteolysis in failed total arthroplasty: A comparison of mobile-bearing and fixed-bearing knees. *J Bone Joint Surg Am*. 2002; 84:2224-9.

26. Huang CH; Ma HM; Liau JJ; Lee YM; Ho FY. Long-term results of Low Contact Stress mobile-bearing total knee replacements. *Clin Orthop*. 2003; 416:265-70.

27. Jordan LR, Olivo JL, Voorhorst PE. Survivorship analysis of cementless meniscal bearing total knee arthroplasty. *Clin Orthop*. 1997; 338:119-23.

28. Lidgren L, Knutson K, Robertsson O. The Swedish knee arthroplasty register: Annual report 2003. www.ort.lu.se/knee/

29. Lidgren L, Knutson K, Robertsson O. The Swedish knee arthroplasty register: Annual report 2004. www.ort.lu.se/knee/

30. Morra EA, Postak PD, Greenwald AS. The influence of mobile bearing knee geometry on the wear of UHMWPE tibial inserts: A finite element study. Presented at the annual meeting of the American Academy of Orthopaedic Surgeons, 1998.

31. Morra EA, Postak PD, Greenwald AS. The influence of mobile bearing knee geometry on the wear of UHMWPE tibial inserts II: A finite element study. Presented at the annual meeting of the American Academy of Orthopaedic Surgeons, 1999.

32. Morra EA, Postak PD, Greenwald AS. The influence of mobile bearing knee geometry on the wear of UHMWPE tibial inserts III: A finite element study. Presented at the annual meeting of the American Academy of Orthopaedic Surgeons, 2000.

33. Morra EA, Postak PD, Greenwald AS. Tibial plateau abrasion in mobile bearing knee systems during walking gait: A finite element study. Presented at the annual meeting of the American Academy of Orthopaedic Surgeons, 2001.

34. Morra EA, Postak PD, Heim CS, Greenwald AS. Tibial plateau abrasion in mobile bearing knee systems during walking gait II: A finite element study. Presented at the annual meeting of the American Academy of Orthopaedic Surgeons, 2002.

35. Morra EA, Greenwald AS. Tibial plateau abrasion in mobile bearing knee systems during walking gait III: A finite element study. Presented at the annual meeting of the American Academy of Orthopaedic Surgeons, 2004.

36. Rand JA, Trousdale RT, Ilstrup D, Harmsen WS. Factors affecting the durability of primary total knee prostheses. *J Bone Joint Surg Am*. 2003; 85:259-65.

37. Stiehl JB, Voorhorst PE. Total knee arthroplasty with a mobile-bearing prosthesis: comparison of retention and sacrifice of the posterior cruciate ligament in cementless implants. *Am J Orthop*. 1999; 28(4):223-8.

38. Wimmer MA, Andriacchi TP, Natarajan RN, Loos J, Karlhuber M, Petermann J, Schneider E, Rosenberg AG. A striated pattern of wear in ultrahigh-molecular-weight polyethylene components of Miller-Galante total knee arthroplasty. *J Arthroplasty*. 1998; 13:8-16.

Table 3.1: Patient Demographics (mean, standard deviation)

n	41
Male / Female	22 / 19
Age at index TKR (yrs.)	65±8 (range, 41-79)
Age at retrieval (yrs.)	74±11 (range, 48-90)
Functional Duration (yrs.)	8.6±4.7 (range, 0.8-14.9)

Table 3.2: Reasons for Revision

Autopsy	2
Patellar bearing wear	7
Tibial bearing wear	14
Instability	2
Patellar / tibial loosening	4
Osteolysis	2
Pain / Stiffness	5
Patella Arthritis	1
Infection	1
Unknown	2

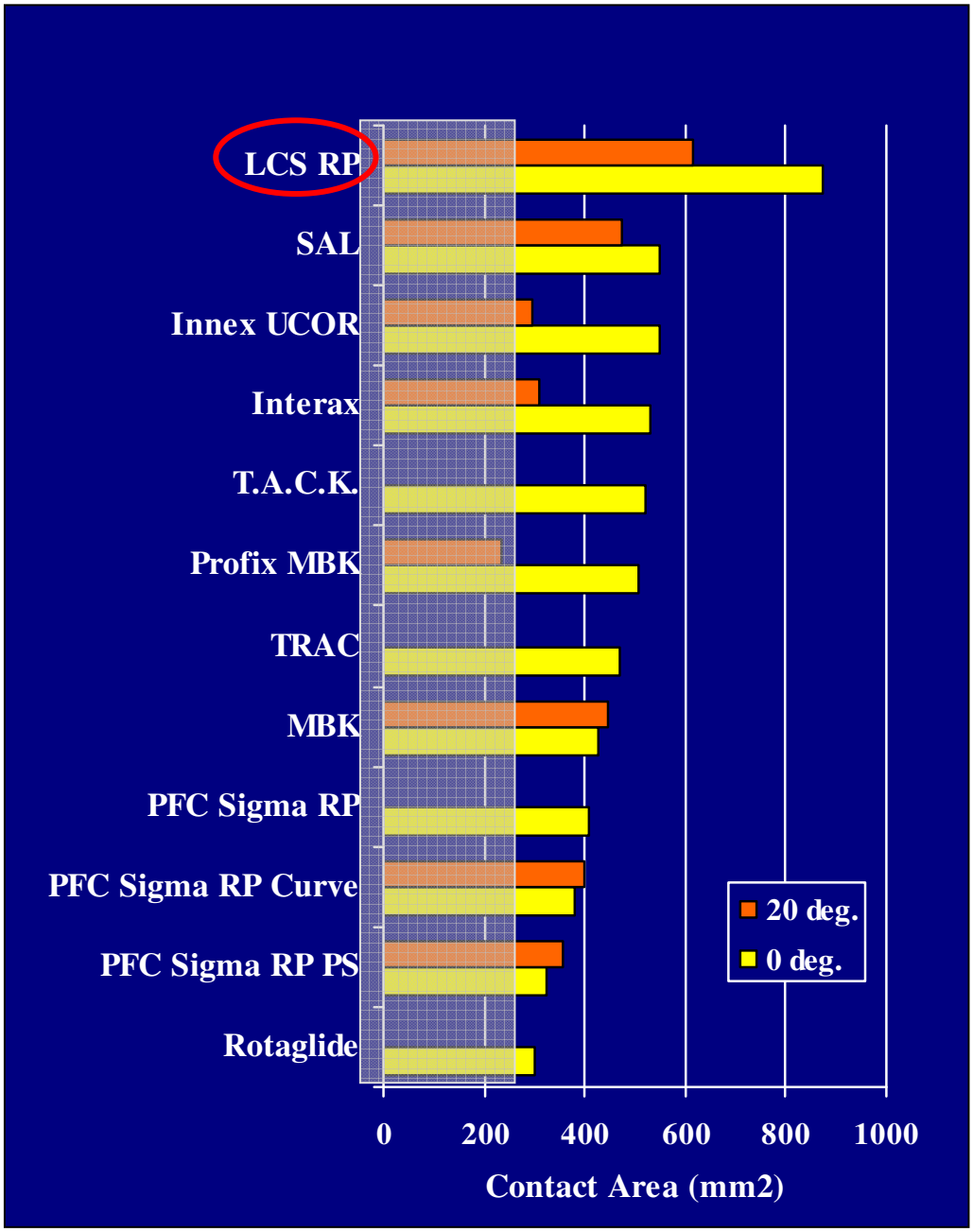

Figure 3.1: Contact Areas for Contemporary Mobile Bearing TKA[30-35]

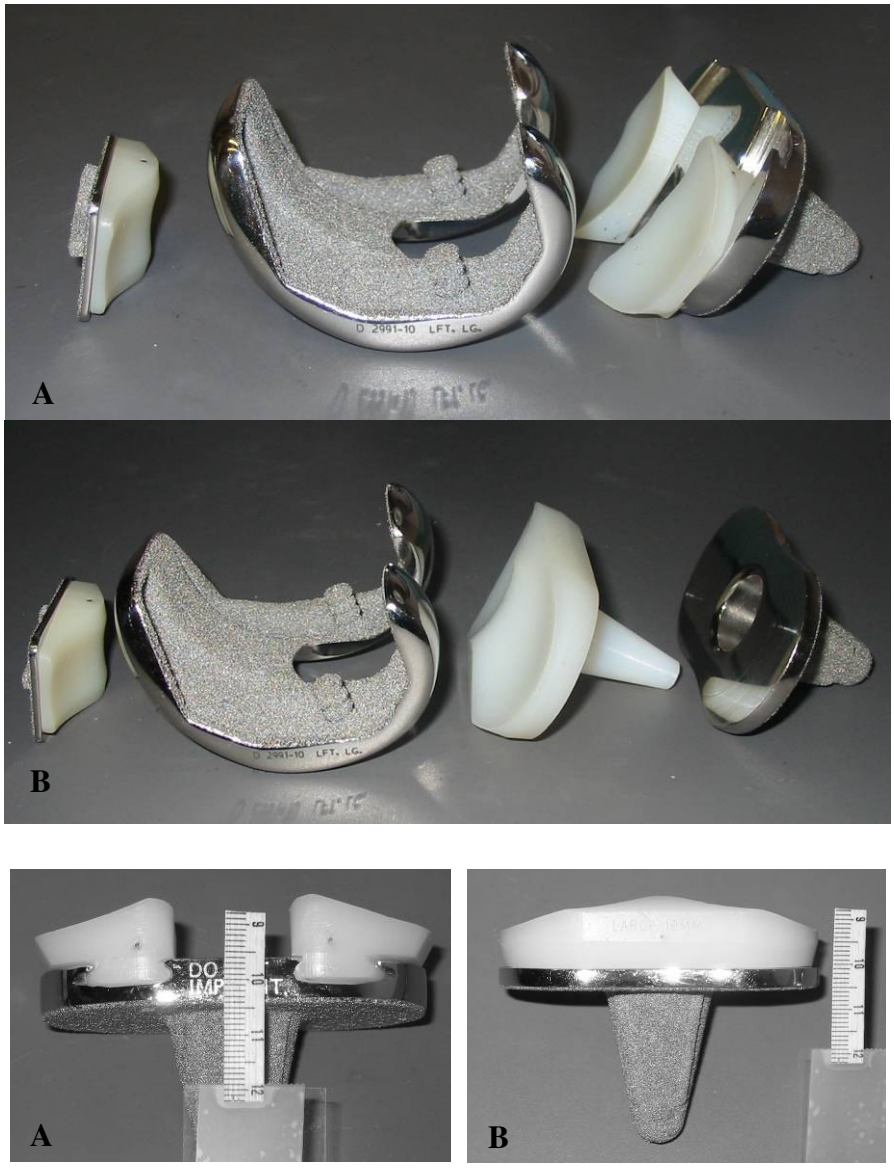

Figure 3.2: Femoral, Tibial and Patellar Components

for the Meniscal Bearing (A) and Rotating Platform (B) TKA

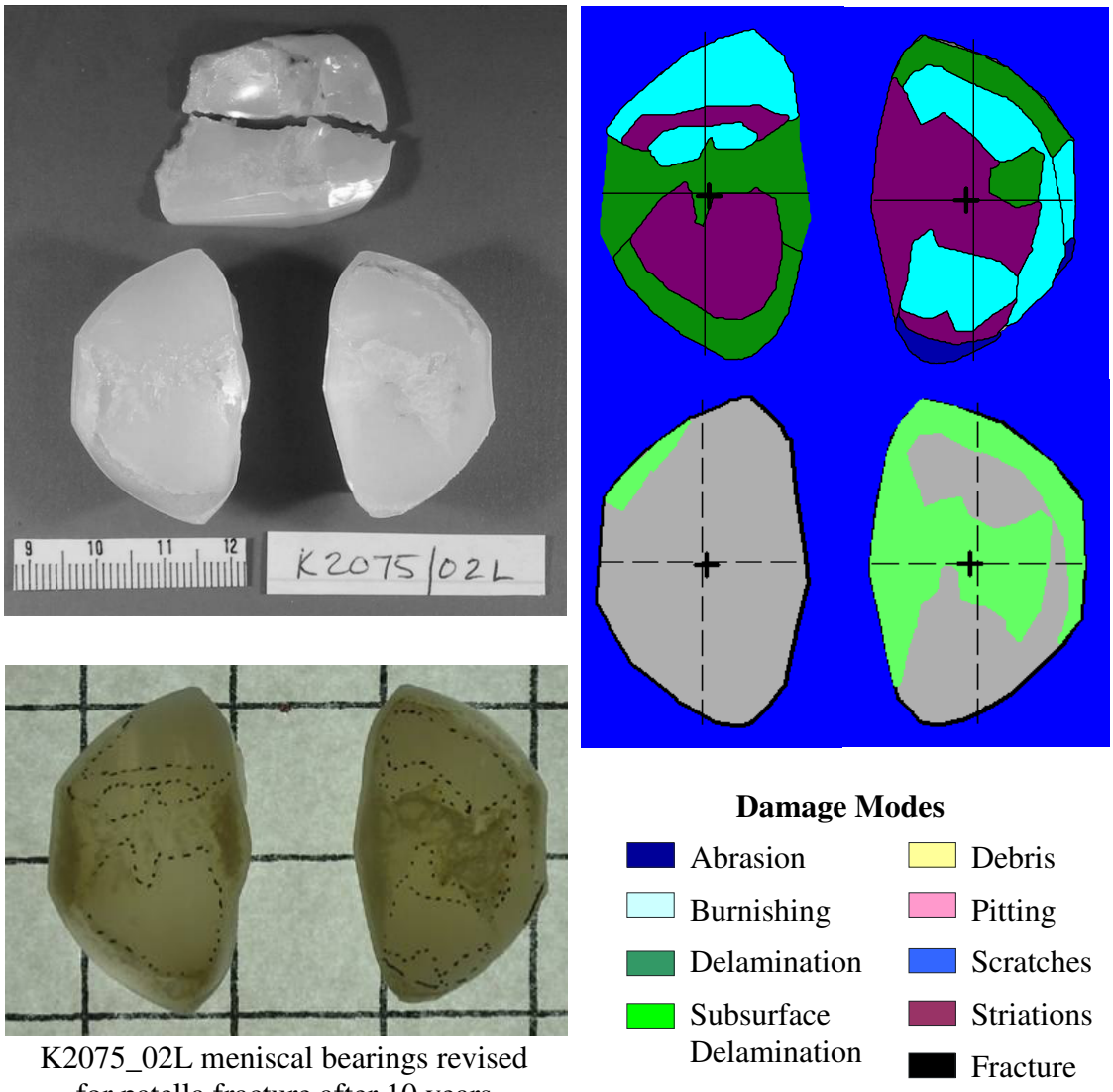

K2075_02L meniscal bearings revised for patella fracture after 10 years of in vivo function

Figure 3.3: Damage Patterns on Retrieved Meniscal Bearings

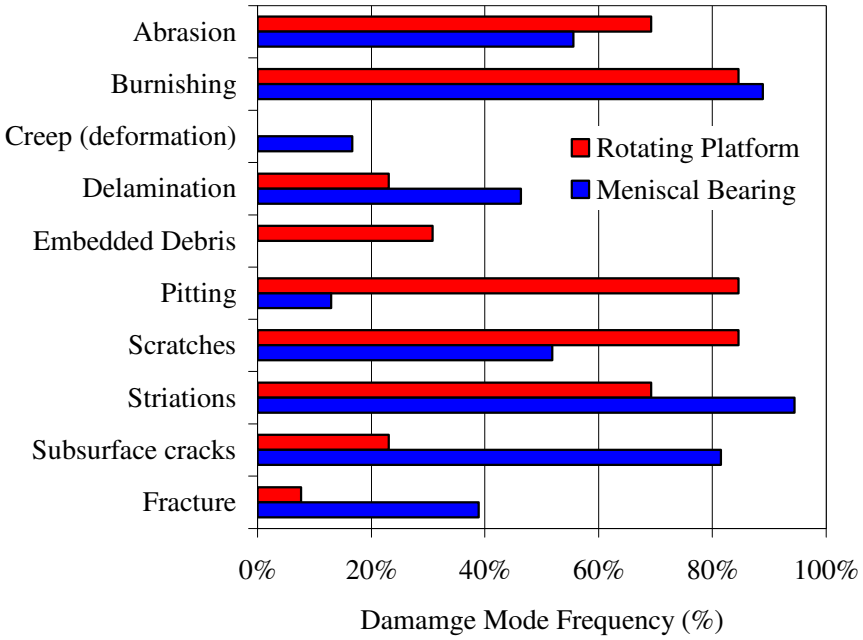

Figure 3.4: Comparison of Frequency for Different Damage Modes

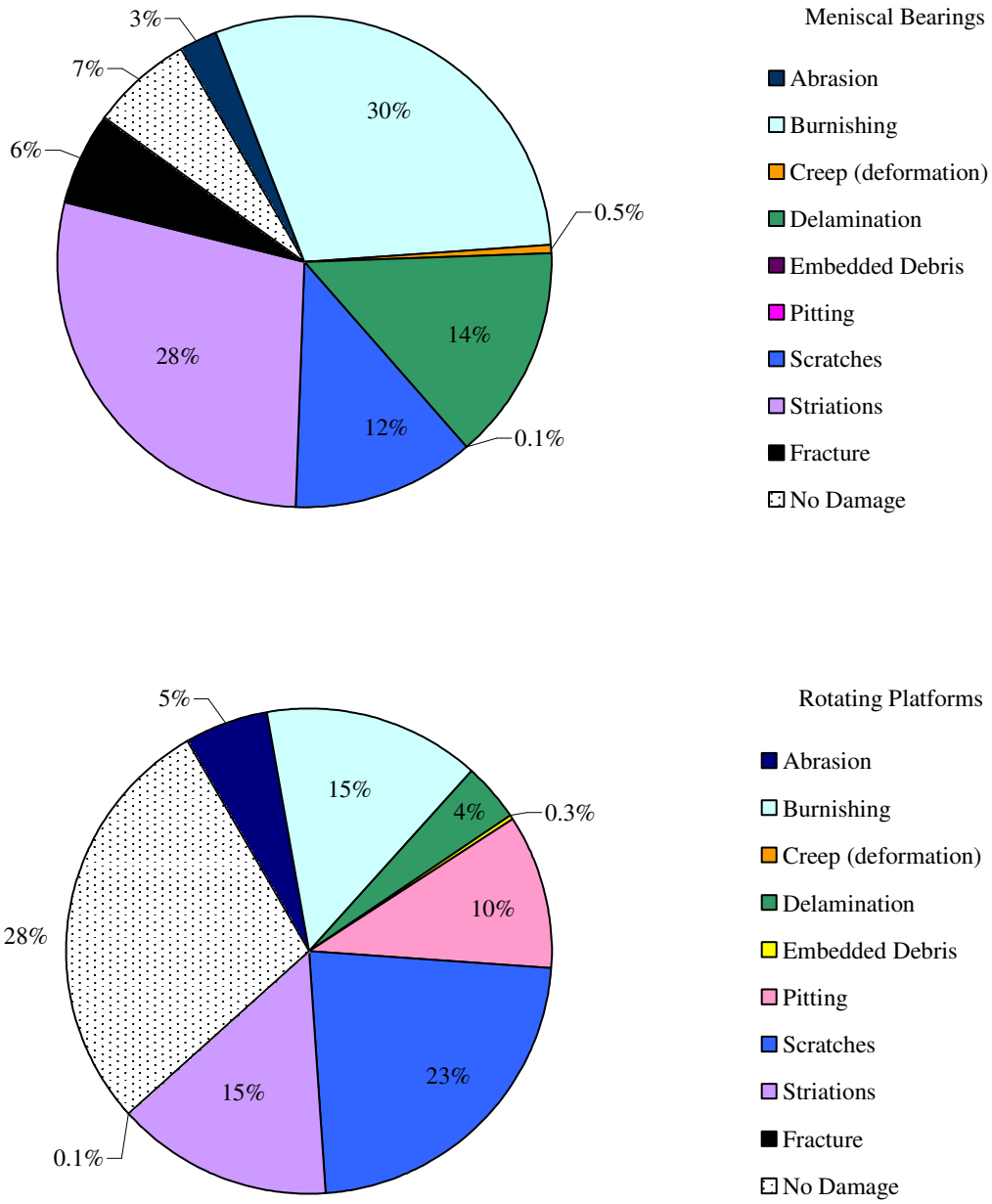

Figure 3.5: Comparison of Damage Areas for Retrieved Meniscal Bearing and Rotating Platform Polyethylene Inserts

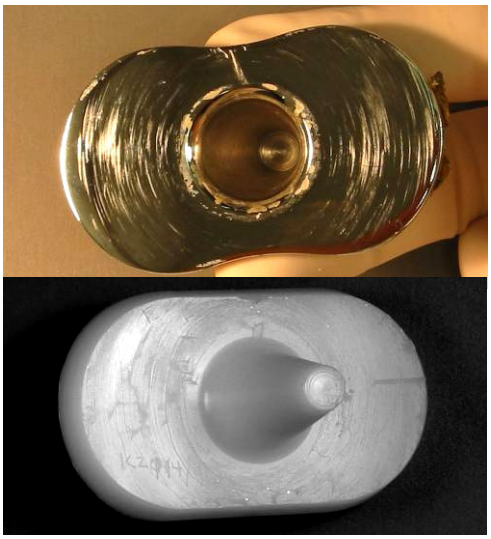

Rotating platform (K2114/96R)
revised for loosening at 2 yrs.

Meniscal bearing (K2073/02R)
revised for bearing fracture at 15 yrs.

Figure 3.6: Scratching Pattern on Backside Surface of Retrieved Mobile Bearing TKA Tibial Components

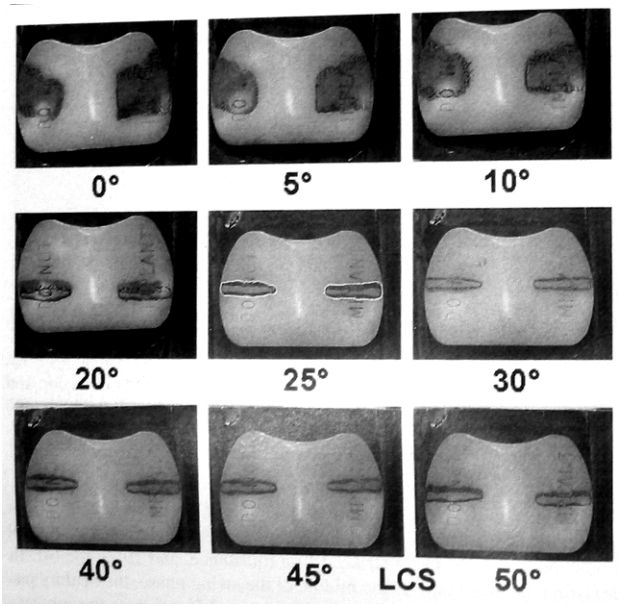

Figure 3.7: Contact Area versus Knee Flexion for the LCS Mobile Bearing TKA[3]

4 DAMAGE PATTERNS ON PATELLAR BEARINGS RETRIEVED AFTER TOTAL KNEE ARTHROPLASTY: CONSIDERATIONS FOR DESIGN AND BIOMECHANICAL FUNCTION

4.1 Introduction

Achieving adequate extensor mechanism function after total knee arthroplasty (TKA) remains a challenge. Surgical techniques, such as release of lateral soft tissues and aligning the femoral component with relative external rotation, are used to aid patellar tracking.[5,13,19] Gradual changes in femoral component designs also have been introduced, featuring a more anatomic geometry, a raised lateral eminence, and a deeper, more lateralized femoral sulcus.[9] Similarly, there has been a shift toward widespread use of all-polyethylene patellar components as 10 year survivorship of those designs is 93% compared to 76% for metal-backed patellar components.[27] Despite these efforts, patellar complications continue to be associated with poor outcomes in primary TKA.[1,27,29]

Design rationales for the patellar-femoral articulation in TKA attempt to harness the advantages of conformity and alignment necessary for optimized patellar tracking and load distribution at the articular surface. Greater patellar-femoral articular conformity lowers the contact stresses[4,7,26,33] and associated bearing wear.[18,20] However, contact pressures and contact stresses for many designs are substantially increased compared to the natural patellar-femoral joint.[22,26] Patellar components with mobile bearings can accommodate axial rotation of the articular surface during knee motion, reducing shear stresses at the articular surface and maintaining articular congruency with the femoral component.

Knee kinematics contribute substantially to the biomechanical function of patellar components after TKA. In vitro biomechanical simulations show substantial increases in patellar-femoral contact stresses with increasing knee flexion.[22,24] Singerman, et al.[30] reported increased patellar strain with anterior displacement of the femoral component relative to the tibial component during flexion-extension. Some designs exhibiting anterior femoral displacement during knee flexion[2,3,15] have an anterior center of rotation and incorporate multiple radii of curvature in the sagittal plane.(Figure 4.1) That geometry is based upon traditional descriptions of knee flexion occurring about multiple instantaneous centers of rotation when viewed in the sagittal plane.[14,31,32] An anterior center of rotation can decrease the quadriceps moment arm, resulting in increased quadriceps loading and associated increased patellar-femoral compressive forces in TKA patients during activities of daily living.[12,23,34]

Analysis of damage patterns on retrieved patellar components is one method of evaluating relationships between the TKA patellar-femoral geometry and the biomechanics associated with the in vivo function of the different designs. The purpose of this study was to assess damage patterns occurring on retrieved polyethylene articular bearings from two different groups of patellar components. Included components had nonconforming, dome-shaped all-polyethylene bearings or asymmetric, conforming metal-backed polyethylene bearings. It was hypothesized that damage modes and damage areas would be significantly different for conforming bearings compared to nonconforming bearings.

4.2 Materials and Methods

Two groups of consecutively retrieved patellar components were evaluated, including 18 all-polyethylene patellae (Group AP) and 26 metal-backed patellae (Group MB). The index TKR for Group AP were operated by one surgeon using a single posterior cruciate ligament retaining TKR design (Series 7000, Osteonics Corp., Allendale, NJ) with cement fixation. These revisions represent approximately 3% of the estimated 525 Series 7000 TKA performed in that clinical practice over a 7 year period. The index TKR for Group MB were operated by a second surgeon using a single posterior cruciate ligament sacrificing mobile bearing TKR (LCS, DePuy, Warsaw, IN) with cementless fixation. These revisions represent approximately 0.5% of the estimated 5000 LCS TKA performed in that clinical practice over a 17 year period. Patient demographics and reasons for revision are provided in Tables 4.1-4.2.

Differences in the patella-femoral geometry were noted. Group AP patellae were all-polyethylene, oval-shaped fixed bearings with a medialized articular dome. Group AP patellae articulated with femoral components having multiple radii in the sagittal plane and a single radius in the coronal plane (Figure 4.1, 4.2). Group MB patellae were metal-backed, rectangular-shaped polyethylene mobile bearings with a conforming articular surface. mobile bearing polyethylene articulation. Group MB patellae articulated with femoral components having multiple radii in the sagittal plane and divergent radii in the coronal plane (Figure 4.1, 4.2). The polyethylene components in both groups had been sterilized using gamma radiation in air.

One observer visually assessed articular surface damage on the retrieved patellar components using an optical microscope (model Z30L, Cambridge Instruments,

Cambridge, MA) at 7 to 30 times magnification. The prevalence of ten distinct damage modes was evaluated using published visual identification methods.[15,17,35] Abrasion is typically visualized as rough, tufted regions. Burnishing is visualized as smooth regions that are highly reflective of incident light. Delamination is visualized as thin layers of polyethylene material separated from the surface. Subsurface delamination appears as cracks and/or discoloration located inferior and generally parallel to articular plane without discontinuity of the articular surface material. Creep deformation is visualized as a permanent change in shape from the original surface. Embedded debris is visualized as particles that differed in color and/or texture relative to the surrounding polyethylene surface, consistent with embedded particles of bone, cement fragments or metal particles. Pitting is visualized as depressions with rough surfaces typically 1 to 2 mm in diameter. Scratching is visualized as thin lines in irregular or ordered directions across the surface. Striations are visualized as highly oriented, longitudinal, smooth peaks and troughs on the articular surface.[35] Fractures are visualized as complete cracks or wear-through of the polyethylene.

Each patella was placed on a 20 mm^2 calibration grid and a digital image of the articular surface was recorded. A normalized, component-based coordinate system was established, dividing the articular surface into four superior, inferior, medial, and lateral quadrants. Algorithms were implemented to correct component rotational alignment within the global coordinate system. The circumference of each identified damage region was outlined on the digital images[11,15,16] using custom digital image analysis programs and the corresponding wear mode for each region was recorded. The technique is 98.6% accurate with a precision of 0.4 mm for linear distances and 3.9 mm^2 for areas. The damage mode incidence was calculated as the number of patellae showing a given

damage mode divided by the total number of inserts included in the group. The damage area was calculated as a percentage of the total articular area and the damage location was expressed relative to the normalized component-based coordinate system.

Strength of association between variables was determined using Spearman's bivariate rank order correlation and multiple regression. Correlation coefficients >0.6 were considered to indicate strong correlation, and values of 0.4 to 0.6 were considered to indicate moderate correlation. Differences between groups were analyzed using analysis of variance with appropriate post hoc multiple comparisons.

4.3 Results

The damage area for Group MB inserts was significantly greater than Group AP inserts (Tukey test, $p<0.001$), consistent with the more conforming patellar-femoral articulation in Group MB. Damage area averaged 29%$\pm$14% for Group AP and 70%$\pm$15% for Group MB. There was a significant correlation between the bearing type and the observed damage modes (Spearman Correlation, $p<0.05$), with unique modes identified within the different damage areas for each group. Creep deformation and burnishing were the largest and most prevalent damage modes observed in Group AP, compared to burnishing, scratching, delamination, and striations for Group MB (Figures 4.3-4.4). Damage area was linearly related to duration of function (linear regression, $R^2=0.38$, $p<0.001$) when all retrieved bearings were considered (Figure 4.5). However, there was no statistical relationship between damage area and time within each group. There were no correlations between patella damage area, damage modes and recorded patient demographics

Damage patterns were concentrated in the superior half of the articular surface for both groups (Figure 4.6) For Group AP, surface deformation (creep) was observed on each patella (100%) and was located in the superior-lateral quadrant on 11 of the 14 (79%) patellae. Delamination was observed on 5 patellae, including 4 revised for patellar complications and 1 retrieved at autopsy. This delamination exhibited a "horse-shoe shaped" pattern in three knees revised for patellar component wear, including two knees with notable patellar clunk occurring before revision surgery. The damage radius was consistent with the radius of the femoral component intracondylar notch, suggesting that this damage occurred with the knee in a relatively flexed position (Figure 4.7).

Damage patterns for Group MB included delamination and subsurface cracking on 23 (88%) patellae that was concentrated in the superior-medial and inferior-medial quadrants (Figure 4.6). There were 10 (38%) fractured patellar bearings in Group MB, including six (23%) with the fracture plane oriented in the medial-lateral direction (Figure 4.8). Ten (38%) Group MB patellae had a band of subsurface delamination oriented along the superior-inferior axis in the lateral quadrant. Subsurface cracks oriented along the medial-lateral axis were noted to originate from this region.

4.4 Conclusions

The relationships between patellar-femoral geometry and TKA biomechanics were explored using analysis of damage patterns on two different patellar component designs retrieved after in vivo function. Damage areas and damage modes for the more conforming Group MB patellae were significantly different from the damage observed on the nonconforming, dome-shaped Group AP patellae, supporting the stated hypothesis.

Patellar-femoral biomechanics during physiologic loading contributed to some of the damage patterns that were observed. In normal knees and after TKA, the contact zone moves from distal to proximal and the patella shifts laterally and internally rotates (distal pole moves laterally) with increasing knee flexion.[9] The bearing surface geometry of the LCS patellar component is designed to accommodate this rotational motion, while allowing for full congruency in both 0º and 90º of flexion. However, the delamination patterns on the retrieved Group MB patellae in the current study are consistent with rotation into an incongruent bearing position during knee flexion, with presumably high contact stresses occurring in the superior-medial quadrant. These data suggest that the mobility of the polyethylene articular surface was compromised for some duration of in-vivo function, resulting in unsupported corners of thin polyethylene bearing material (Figure 4.9). Fractured bearings occurred in 38% of Group MB. Cyclic compressive and tensile forces likely caused initiation and/or propagation of the cracks oriented along the medial-lateral axis.

The theoretical advantage of the mobile bearing patellar design concept in TKA is the ability to maintain congruency at the patellar-femoral articulation while allowing axial rotation to reduce shear stresses at the interface. These bearings potentially minimize loosening and patellar fracture problems through the use of a metal backing, while increasing contact area and decreasing shear stress through the use of a rotating bearing.[7] Clinical outcomes and analysis of retrieved mobile bearing patellae support this rationale. Beuchel, et al.[8] report no revisions for patellar bearing wear or fracture in 331 TKA with 2 to 11 years of follow-up. Collier, et al.[10] evaluated 115 retrieved metal-backed patellae and reported significantly lower wear scores for fully congruent patellar

designs. However, retrieved Group MB components in the current study suggest that bearing mobility was compromised for some duration of in vivo function, resulting in deleterious loading conditions and severe polyethylene wear. Optimal bearing alignment may not always exist in TKA patients and the advantages of a fully congruent mobile-bearing patella may not always be realized.

The damage patterns on both Group AP and Group MB bearings are consistent with a small areas of contact enduring high contact stresses. Laboratory assessments have shown that patellar contact stresses often exceed the 21 MPa yield strength of polyethylene at flexion angles greater than 90°.[12,22,24,26,33] However, assuming proper articular alignment, contact areas for LCS mobile bearing patella are 2 to 3 times greater than dome patellae (Figure 4.10), with contact stresses below 10 MPa.[33] The high incidence of surface deformation (creep) in Group AP is consistent with contact stresses exceeding the yield strength of the material. Similarly, the high incidence of delamination and brittle polyethylene fracture in Group MB suggests that the contact stresses exceeded the ultimate strength of the material. Improved pre-clinical evaluation methods are needed to better replicate the physiologic environment contributing to these observed damage patterns.

Weight-bearing at the patellar-femoral joint is complex. Loads at the articular surface range have been estimated to range from 0.5 to 1.8 times body weight for level walking, 2.1 to 5.6 times body weight for maneuvering stairs, over 3 times body weight for rising from a chair, and 1.8 to 7 times body weight for downhill walking.[21,25,28] D'Lima, et al.[12] measured in-vitro patellar compressive forces of more than 450N for Series 7000 components at flexion angles greater than 75º. Such loads, combined with

contact between the patella and the posterior-inferior edge of the femoral sulcus, likely contributed to the horseshoe-shaped delamination in Group AP (Figure 4.7). One possible design strategy to avoid this type of damage is to deepen the femoral sulcus and effectively limit the patellar articular surface from contacting this edge during deep flexion.

Although material properties of the polyethylene bearings were not evaluated in this study, a brief comment on the possible role of material degradation is necessary since all retrieved bearings were sterilized using gamma radiation in air. It has been shown that gamma radiated polyethylene exhibits increased density and increased elastic modulus, resulting in increased contact stresses for a given load and reduced fatigue strength. Previous studies of TKA failure due to polyethylene wear have shown increased failure rates associated with increased component aging prior to implantation.[6] In that study, five year survivorship declined 21% when the total age of the components increased from nine years (five years of function plus four years of storage) to over 13 years (five years of function plus eight to 11 years of storage). In the current study, shelf age was not known for the retrieved patellar components in either group and it was difficult to distinguish between wear due to degraded material properties versus wear associated with high contact stresses in these thin polyethylene bearings.

In conclusion, fully congruent mobile-bearing patellar components must maintain mobility during physiologic loading to avoid incongruent contact and associated high contact stresses. It remains to be seen whether modified femoral component designs incorporating a deeper sulcus to better accommodate patellar tracking or a single sagittal radius to increase the quadriceps moment arm and reduce patellar-femoral compressive forces[12,23,34] contribute to improved patellar component longevity.

4.5 Acknowledgements

The author thanks George D. Markovich, MD, Scott A. Banks, PhD, and W. Andrew Hodge, MD for co-authoring this work; and George D. Markovich, MD and W. Andrew Hodge, MD for providing retrieved mobile bearing TKA components and clinical data. This work was supported by funding from The BioMotion Foundation in Palm Beach, Florida.

Note: This work has been presented at international national scientific conferences and is referenced as follows.

Harman MK, Banks SA, Hodge WA: Damage on retrieved all-polyethylene patellar components after total knee arthroplasty. The 49th Annual Meeting of the Orthopaedic Research Society, New Orleans, LA, 2003.

Harman MK, Markovich, GD, Banks SA, Hodge, WA: The relationship between polyethylene damage and function of metal-backed patellar components retrieved after mobile bearing total knee arthroplasty. 7th Congress of the European Federation of National Associations of Orthopaedics and Traumatology (EFORT), Lisbon, Portugal, 2005.

4.6 References Cited

1. Ayers DC, Dennis DA, Johanson NA, Pellegrini VD. Common complications of total knee arthroplasty. *J Bone Joint Surg Am*. 1977; 79(2):278-311.
2. Banks SA, Hodge WA. Implant design affects knee arthroplasty kinematics during stair-stepping. *Clin Orthop*. 2004; 426:187-93.
3. Banks SA, Markovich GD, Hodge WA. In Vivo kinematics of cruciate-retaining and -substituting knee arthroplasties. *J Arthroplasty*, 1997; 12(3):297-304.

4. Benjamin JB, Szivek JA, Hammond AS, Kubchandhani Z, Matthews AI, Anderson P. Contact areas and pressures between native patellas and prosthetic femoral components. *J Arthroplasty*. 1998;13(6):693-8.

5. Berger RA, Crossett LS, Jacobs JJ, Rubash HE. Malrotation causing patellofemoral complications after total knee arthroplasty. *Clin Orthop*. 1998; 356:144-53.

6. Bohl JR, Bohl WR, Postak PD, Greenwald AS. The effects of shelf life on clinical outcome for gamma sterilized polyethylene tibial components. *Clin Orthop.* 1999; 367:28-38.

7. Buechel FF, Pappas MJ, Makris G. Evaluation of contact stress in metal-backed patellar replacements: A predictor of survivorship. *Clin Orthop*. 1991; 273:190-7.

8. Buechel FF, Rosa RA, Pappas MJ. A metal-backed rotating-bearing patellar prosthesis to lower contact stress: An 11-year clinical study. *Clin Orthop*. 1989; 248:34-49.

9. Chew JTH, Stewart NJ, Hanssen AD, Luo ZP, Rand JA, An KN. Differences in patellar tracking and knee kinematics among three different total knee designs. *Clin Orthop*. 1997; 345:87-98.

10. Collier JP, McNamara JL, Surprenant VA, Jensen RE, Surprenant HP. All-polyethylene patellar components are not the answer. *Clin Orthop*. 1991; 273:198-203.

11. Cornwall GB, Bryant JT, Hansson CM, Rudan J, Kennedy LA, Cooke TD. A quantitative technique for reporting surface degradation patterns of UHMWPE components of retrieved total knee replacements. *J Appl Biomater.* 1995; 6:9-18.

12. D'Lima DD, Poole C, Chadha H, Hermida JC, Mahar A, Colwell CW. Quadriceps moment arm and quadriceps forces after total knee arthroplasty. *Clin Orthop*. 2001; 392:213-20.

13. Figgie M, Goldberg V, Figgie H. The effects of alignment of the implant on fracture of the patella after total condylar knee arthroplasty. *J Bone Joint Surg Am*. 1989; 71:1031-9.

14. Frankel VH, Burstein An, Brooks DB. Biomechanics of internal derangement of the knee: Pathomechanics as determined by analysis of instant centers of motion. *J Bone Joint Surg Am*. 1971; 53:945-62.

15. Harman MK, Banks SA, Hodge WA. Polyethylene damage and knee kinematics after total knee arthroplasty. *Clin Orthop*. 2001; 392:383-93.

16. Harman MK, Markovich GD, Banks SA, Hodge WA. Wear patterns on tibial plateau from varus and valgus osteoarthritic knees. *Clin Orthop*. 1998; 352:149-58.

17. Hood RW, Wright TM, Burstein AH. Retrieval analysis of total knee prostheses: A method and its application to 48 total condylar prostheses. *J Biomed Mater Res.* 1983; 17:829-42.

18. Hsu HP, Walker PS: Wear and deformation of patellar components in total knee replacement. *Clin Orthop*. 1989; 246:260-5.

19. Kaper BP, Woolfrey M, Bourne RB. The effect of built-in external femoral rotation on patellofemoral tracking in the Genesis II total knee arthroplasty. *J Arthroplasty*. 2000; 15(8):964-9.

20. Kray MJ, Darr OJ, Salata MJ, Goldberg VM. Outcome of metal-backed cementless patellar components: The effect of implant design. *Clin Orthop*. 2001; 392:239-44.

21. Kuster MS; Wood GA, Stachowiak GW Gachter A. Joint load considerations in total knee replacement. *J Bone Joint Surg Br*. 1997; 79(1):109-13.

22. Lee TQ, Gerken AP, Glaser FE, Kim WC, Anzel SH. Patellofemoral joint kinematics and contact pressures in total knee arthroplasty. *Clin Orthop.* 1997; 340:257-66.

23. Mahoney OM, McClung CD, dela Rosa MA, Schmalzried TP. The effect of total knee arthroplasty design on extensor mechanism function. *J Arthoplasty*. 2002; 17(4):416-21.

24. Matsuda S, Ishinishi T, White SE, Whiteside LA. Patellofemoral joint after total knee arthroplasty: Effect on contact area and contact stress. *J Arthroplasty*. 1997; 12(7):790-7.

25. Matthews LS, Sonstegard DA, Henke JA. Load bearing characteristics of the patello-femoral joint. *Acta Orthop Scand*. 1977; 48(5):511-6.

26. McNamara JL, Collier JP, Mayor MB, Jensen RE. A comparison of contact pressures in tibial and patellar total knee components before and after service in vivo. *Clin Orthop*. 1994; 299:104-13.

27. Rand JA, Trousdale RT, Ilstrup D, Harmsen WS. Factors affecting the durability of primary total knee prostheses. *J Bone Joint Surg Am*. 2003; 85:259-65.

28. Reilly DT, Martens M. Experimental analysis of the quadriceps muscle force and patello-femoral joint reaction force for various activities. *Acta Orthop Scand*. 1972; 43(2):126-37.

29. Sharkey PF, Hozack WJ, Rothman RH, Shastri S, Jacoby SM. Insall Award Paper: Why are total knee arthroplasties failing today? *Clin Orthop*. 2002; 404:7-13.

30. Singerman R, Heiple KG, Davy DT, Goldberg VM. Effect of tibial component position on patellar strain following total knee arthroplasty. *J Arthroplasty*. 1995; 10(5):651-6.

31. Smidt GL. Biomechanical analysis of knee flexion and extension. *J Biomech.* 1973; 6:79-92.

32. Soudan K, Van Audekercke R, Martens M. Methods, difficulties and inaccuracies in the study of human joint kinematics and pathomechanics by the instant axis concept: Example the knee joint. *J Biomech* 1979, 12:27-33.

33. Szivek JA, Anderson PL, Benjamin JB. Average and peak contact stress distribution evaluation of total knee arthroplasties. *J Arthroplasty*. 1996; 11(8):952-63.

34. Wang H, Simpson KJ, Chamnongkich S, Kinsey T, Mahoney OM. A biomechanical comparison between the single-axis and multi-axis total knee arthroplasty systems for the stand-to-sit movement. *Clin Biomech.* 2005; 20:428-33.

35. Wimmer M, Andriacchi T, Natarajan R, Loos J, Karlhuber M. A striated pattern of wear in ultrahigh-molecular-weight polyethylene components of Miller-Galante total knee arthroplasty. *J Arthroplasty.* 1998; 13(1):8-16.

Table 4.1: Patient Demographics (mean, standard deviation)

	Group AP	Group MB
n	14	26
Male / Female	9 / 5	12 / 14
Age at index TKR (yrs.)	69±7 (range, 59-80)	64±9 (range, 41-75)
Age at retrieval (yrs.)	72±7 (range, 61-83)	75±11 (range, 48-90)
Functional Duration (yrs.)	3.1±1.8 (range, 0.2-5.9)	10.8±3.6 (range, 1.7-14.9)

Table 4.2: Reasons for Revision

	Group AP	Group MB
Autopsy	5	0
Patellar bearing wear	3	7
Tibial bearing wear	0	11
Instability	1	2
Patellar / tibial loosening	2	1
Osteolysis	1	1
Pain	0	3
Infection	2	0
Unknown	0	1

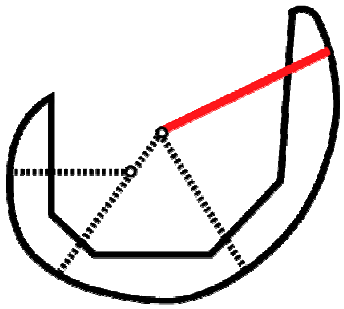

Figure 4.1: Sagittal Profile of a Multi-radius Femoral Component Geometry

The quadriceps moment arm (red line) is the distance from the center of rotation of the component to the patellar articular surface, as determined by the articular radii.

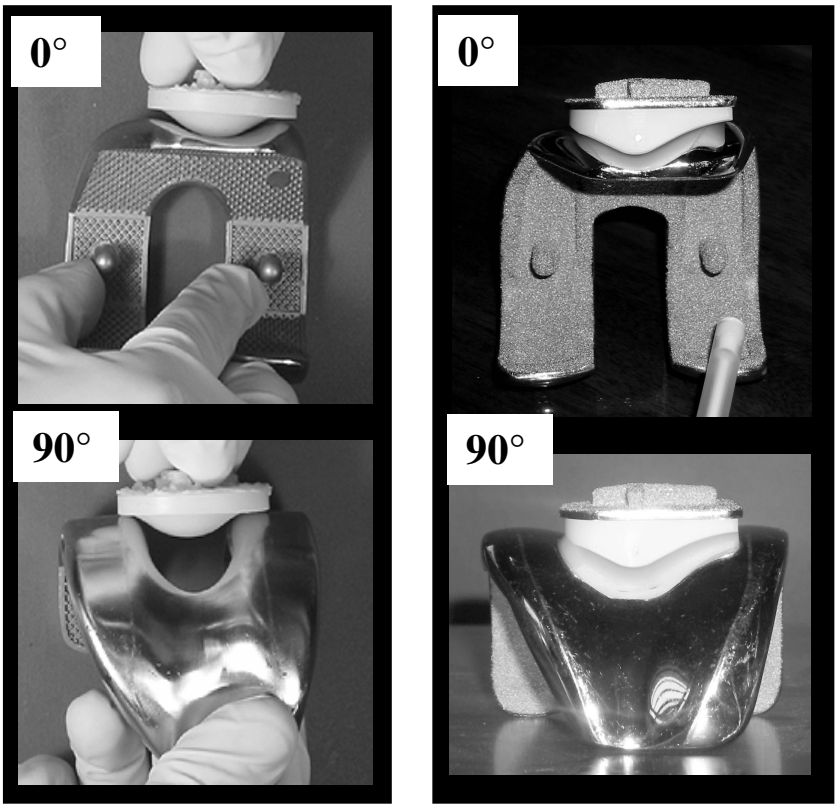

Figure 4.2: Patella-Femoral Articulations

Group AP (left) and Group MB (right) components at 0° and 90° of flexion

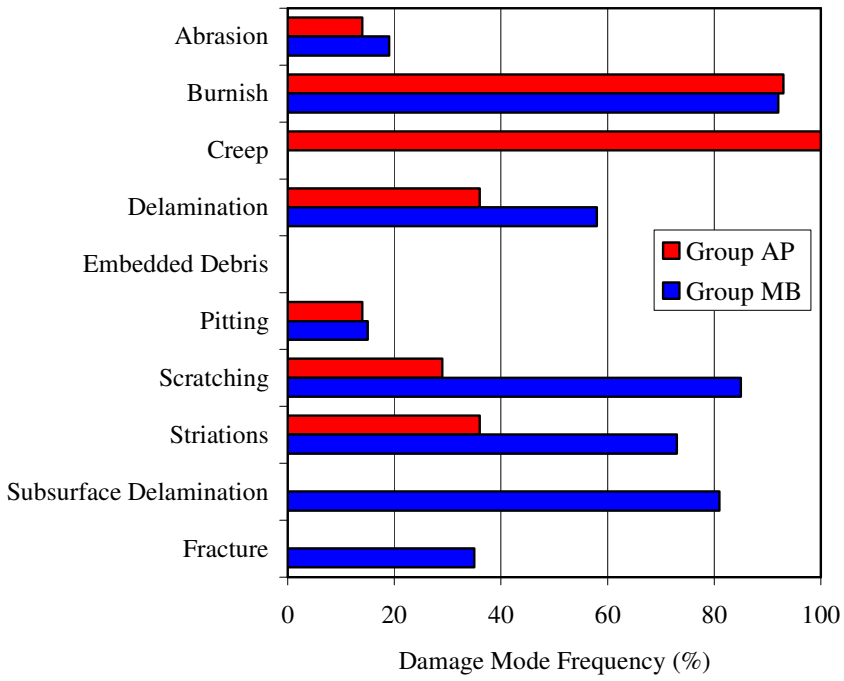

Figure 4.3: Comparison of Damage Mode Frequency

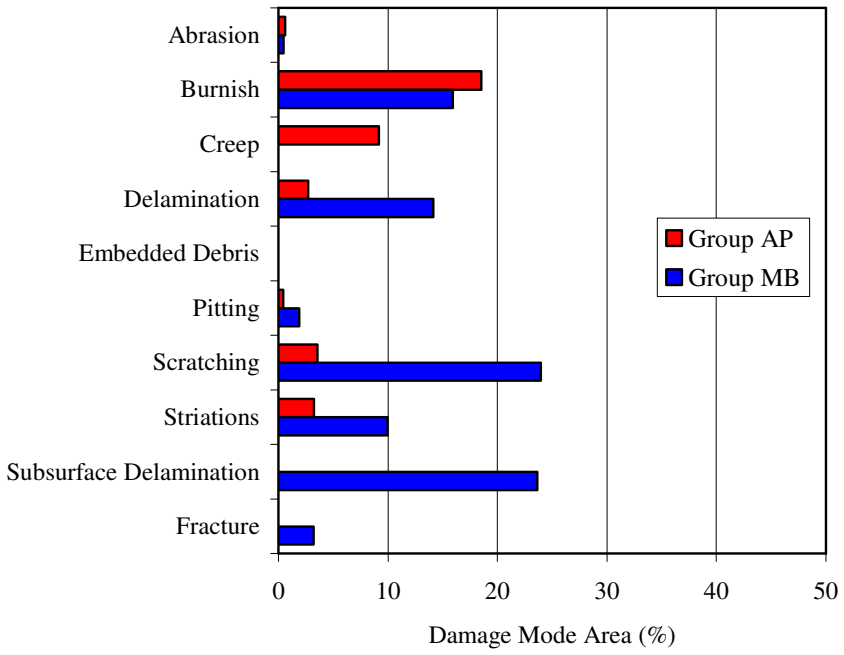

Figure 4.4: Comparison of Damage Areas for Different Damage Modes

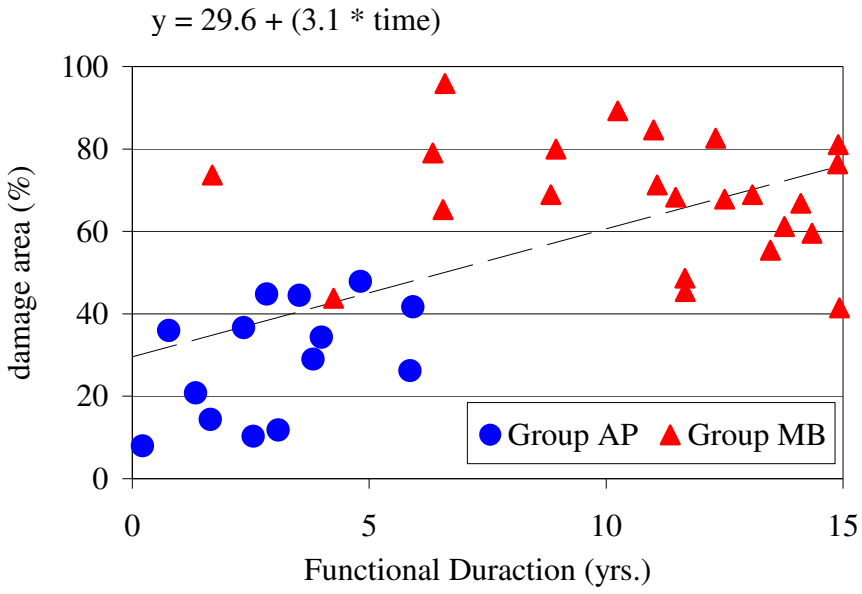

Figure 4.5: Damage Area versus Functional Duration

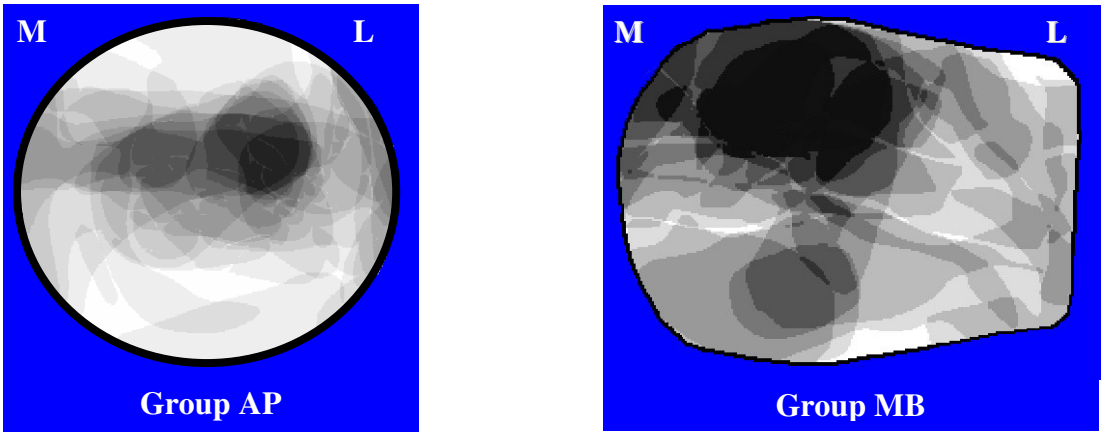

Figure 4.6: Graphic Overlay of Damage Patterns on Retrieved Patellar Bearings All damage modes are depicted for Group AP (left) and delamination modes for Group MB. Darker shading density indicates a greater number of bearings had damage in a given region.

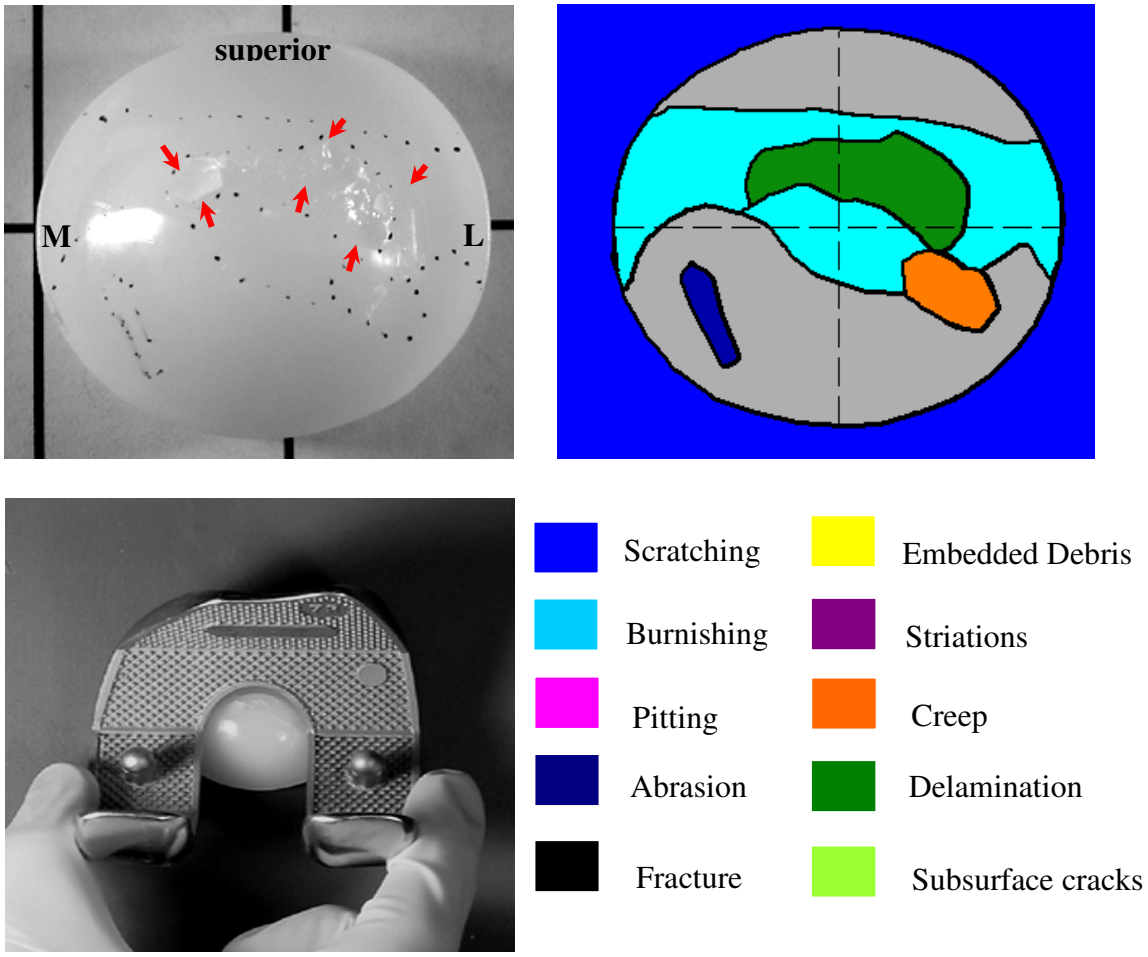

Figure 4.7: Group AP Patella Retrieved After 34 Months of Function in Right TKA Delamination was consistent with contact on the posterior-inferior edge of the femoral sulcus.

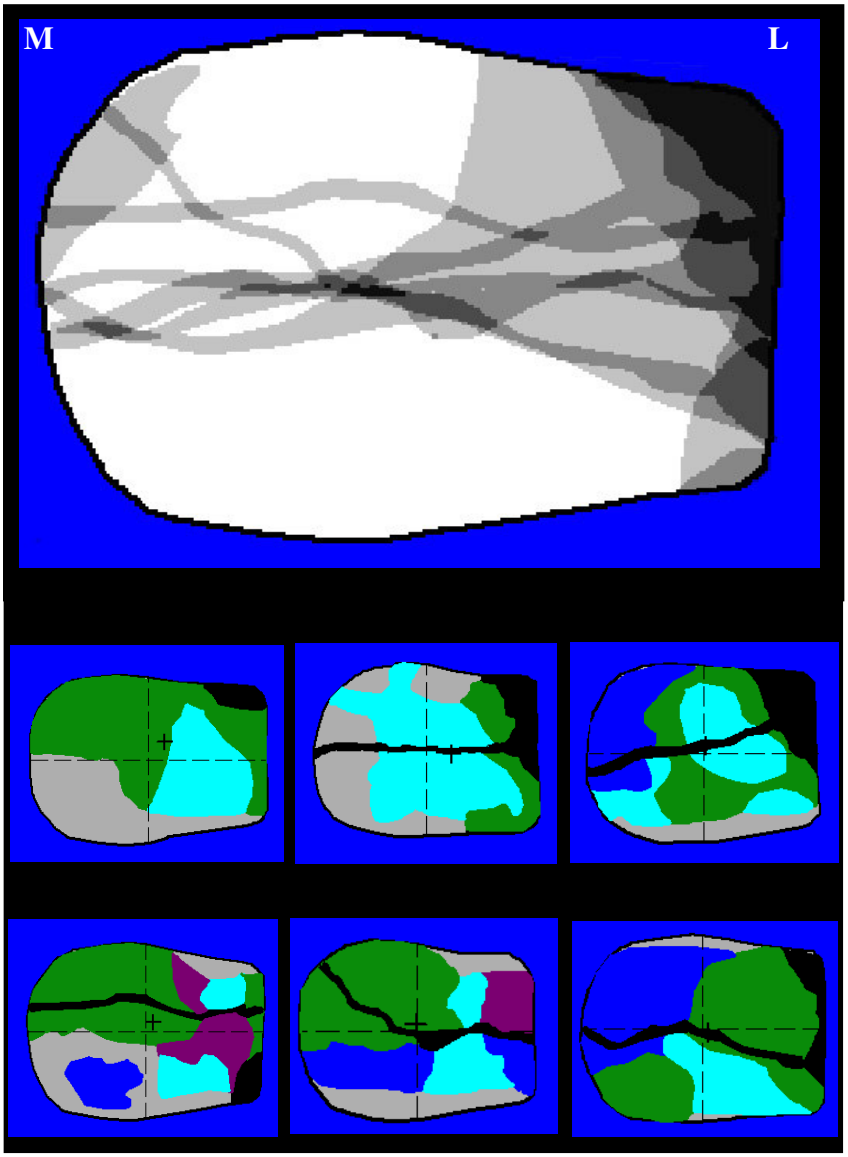

Figure 4.8: Graphic Overlay of Fractured Bearings for Group MB with Representative Damage Patterns from Six Patellae

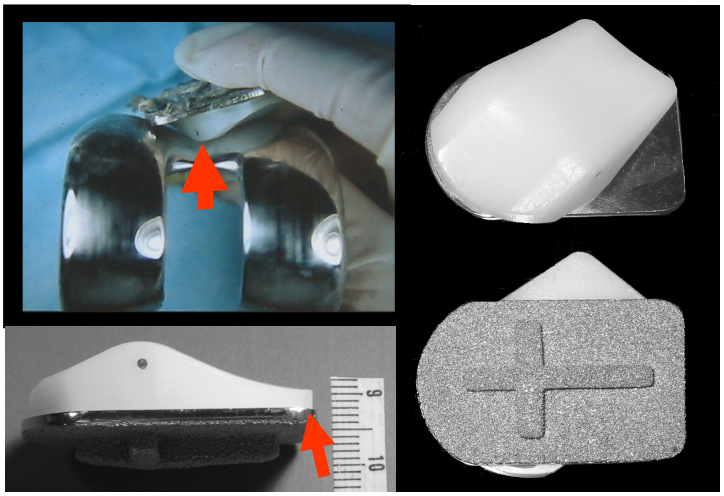

Figure 4.9: Restricted Bearing Rotation Resulted in Incongruent Bearing Contact and Exposed Thin Polyethylene for Group MB

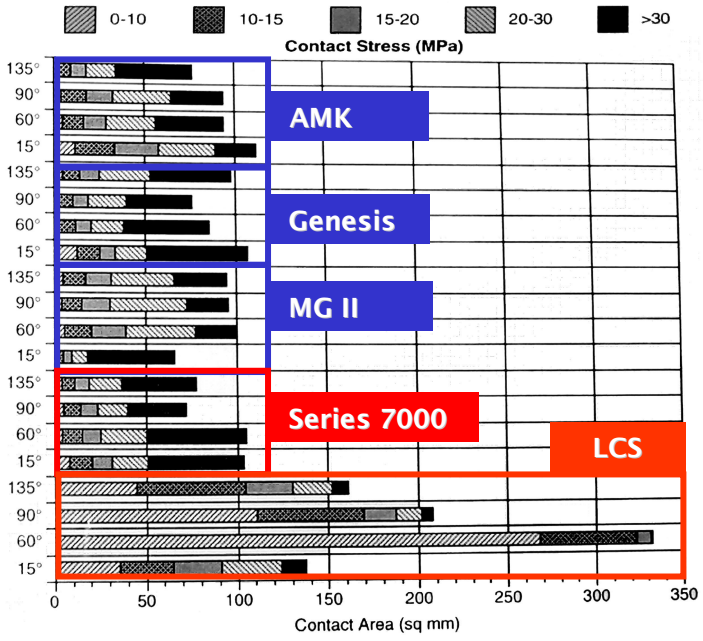

Figure 4.10: Comparison of Contact Areas Versus Knee Flexion for Different Patellar Component Designs[33]

5 COMPARISON OF HISTOLOGY, PARTICULATE DEBRIS AND POLYETHYLENE WEAR IN AUTOPSY RETRIEVED TOTAL KNEE REPLACEMENTS

5.1 Introduction

Damage patterns, such as changes due to material loss (wear) and plastic deformation, are easily visualized on ultra-high molecular weight polyethylene (UHMWPE) components retrieved from the articulating surfaces of joint replacements. Loss of material during in vivo function can introduce UHMWPE wear particles to the periprosthetic tissues. The histological and biochemical responses to these wear particles strongly affect the longevity of the joint prostheses, as characterized in analysis of failed hip, knee and shoulder replacements.[13,18,19,21,25,27,30,33,45,48,53] However, the failure cascade that occurs with revised joint components can alter the wear accumulation and may complicate the histological response in periprosthetic tissues. Characterization of UHMWPE wear debris in well-functioning joint replacements remains poorly understood since few studies have included joint replacements retrieved at autopsy.[43,40]

After total knee replacement (TKR), potential sources for UHMWPE wear particles include the articular surfaces of UHMWPE tibial inserts and patellar components, as well as the backside surface of modular tibial inserts. Qualitative description of damage patterns and wear modes from retrieved UHMWPE TKR components have been associated with an adverse biological response.[5,8,10,26,36,51]

However, quantitative comparisons of damage patterns and UHMWPE wear particles that accumulate in periprosthetic tissues are infrequently reported.[7]

The primary objective of this study is to evaluate twelve well-functioning knee prostheses retrieved at autopsy from TKR patients. Histology and UHMWPE wear particulate characteristics are compared with articular and backside damage patterns on retrieved UHMWPE components for each case. It is hypothesized that different wear modes would correspond to wear particle size and shape and the corresponding histological responses in well-functioning knees.

5.2 Materials and Methods

Twelve knees in nine patients (six men and three women) received primary TKR by the same surgeon (Table 5.1). At the time of index TKR, the mean patient age and weight were 70.2±4.6 years (range, 66.2-80.2 years) and 83.9±13.8 kg (range, 64.5-101.8 kg), respectively. Surgical technique included retention of the posterior cruciate ligament and cement fixation of all components. The implanted prostheses included ten modular (Series 7000, Stryker, Howmedica, Osteonics, Inc., Allendale, NJ) and two all-polyethylene (Series 7000 & 3000, Stryker, Howmedica, Osteonics, Inc.) tibial components. Five knees had patellar resurfacing using an all-polyethylene patellar component. UHMWPE components were machined from compression molded stock and were gamma radiation sterilized in air.

The twelve knee prostheses were retrieved at autopsy after a mean functional duration of 53.1±24.8 months (range, 19.8-97.0 months) in vivo. All patients previously signed informed consent to participate in this established Implant Retrieval Program.[15] Knee Society pain and function scores[24] were consistent with well-functioning TKR and

averaged 94 and 86, respectively, at last follow-up prior to retrieval. Radiographs obtained at autopsy were examined for evidence of osteolysis.[11]

At autopsy, periprosthetic soft tissue samples were obtained from the twelve knees for semi-quantitative histological analysis and quantitative UHMWPE wear particle analysis. Using routine methods[3], the tissue samples were embedded in glycol methacrylate (GMA) or paraffin wax and sectioned at 3 or 5 μm. The GMA sections were stained with oil red O, a marker for UHMWPE, and the paraffin sections were stained with hematoxylin and eosin (H&E).[42,44] The sections were visually examined using a light microscope (Olympus BHS, Olympus America Inc., Melville, NY) with plain and polarized light. The presence of macrophages and giant cells were graded using a semiquantitative rating scale from 0+ to 3+.[3,43] Cells received a grade of 0+ if they were not observed in the section; 1+ if they were present in a limited amount or not readily apparent; 2+ if they were a general feature in the section; and 3+ if their amount was striking and dominated the section.

UHMWPE wear particles were isolated from periprosthetic tissues using published techniques.[9] The collected sample of particle solution was diluted with varying amounts of 0.2-μm filtered deionized water, depending on the viscosity of the solution, and then vacuum filtered through 0.2-μm Isopore™ polycarbonate membrane filters (Cat.No. GTTP04700, Millipore Corp., Bedford, MA). The filters were dried, sputter coated with gold and imaged using a scanning electron microscope (SEM: JSM 6100, JEOL Inc., Peabody, MA) at 250×-5000× magnifications, depending on the size of the particle. Thirty fields of view were randomly obtained on each of the 32 filters, with at least one filter analyzed per knee. Aggregated submicron-sized particles without clearly

defined individual shapes were excluded from the particle analysis. Particles were verified as UHMWPE material using Raman spectroscopy (inVia Raman Microscope, Renishaw Inc., Hoffman Estates, IL) with an attached microscope (Leica DM LM, Leica Microsystems Inc., Bannockburn, IL) in reflectance mode.

The size and shape of each particle in the digital images were analyzed using digital image processing software (ImageJ, NIH Image, National Institutes of Mental Health, Bethesda, MD) . Equivalent circle diameter (ECD), aspect ratio (AR), roundness (R) and form factor (FF) were calculated in accordance with ASTM F1877-98.[2] ECD is defined as a circle diameter with an area equivalent to the actual particle area. AR is defined as the ratio of the major to minor particle diameter. R is a measure of how closely a particle resembles a circle, based on the area and the maximum particle diameter and varies from 0 to 1, with a perfect circle having a value of 1. FF is similar to R, but is based on the perimeter of the particle outline. Particle shapes were classified[37] as spheroidal ($AR \leq 2$, $R \geq 0.6$), granular ($2 < AR < 4$, $0.4 < R < 0.6$), fibrillar ($AR \geq 3$, $R \leq 0.4$), or others (Figure 5.1).

The retrieved UHMWPE tibial inserts and patellar components were gently cleaned in a mild detergent. The prevalence of eight distinct damage modes was assessed on the UHMWPE surfaces using an optical microscope (model Z30L, Cambridge Instruments, Cambridge, MA) at 30× magnification and previously published visual identification methods.[15,20,39,52] Abrasion (evaluated on the articular surfaces only) was visualized as rough, tufted regions. Burnishing was visualized as smooth regions that were highly reflective of incident light. Delamination was visualized as thin layers of UHMWPE material separated from the surface. Dimpling (evaluated on the backside

surface only) was visualized as uniform, nearly circular indentations approximately 100 μm in diameter.[49] Embedded debris was visualized as particles that differed in color and/or texture relative to the surrounding UHMWPE surface, consistent with embedded particles of bone, cement fragments or metal particles. Pitting was visualized as depressions with rough surfaces typically 1 to 2 mm in diameter. Scratching was visualized as thin lines in irregular or ordered directions across the surface. Striations (evaluated on the articular surfaces only) were visualized as highly oriented, longitudinal, smooth peaks and troughs on the articular surface. The circumference of damage regions was outlined on calibrated digital images of the articular surfaces (tibial inserts and patellar components) and backside surfaces (tibial inserts only). The damage area was calculated as a percentage of the total surface area using custom image analysis software.[15]

The association between variables was determined using Spearman's bivariate rank order correlation and linear regression statistical analysis. Correlation coefficients greater than 0.6 indicated a strong correlation and correlation coefficients 0.4 to 0.6 indicated a moderate correlation.

5.3 Results

A total of 20,351 particles were analyzed, including at least 285 particles from each knee. Isolated UHMWPE particle size (ECD), showed a wide variation for all knees (Figure 5.1), ranging from 0.08 μm to 190.6 μm (Table 5.2). Mean particle size was 2.94±6.55 μm, with 44% less than 1μm, 84 % less than 4 μm and 94 % less than 10 μm in size. The frequency of the smaller UHMWPE wear particles was substantially higher than that of large particles in ten of twelve cases, including seven knees with the highest

frequency of particles in the 1 μm to 4 μm range (Figure 5.2). However, two knees showed a high frequency of larger particles (knees 4 and 11).

The histological responses in the tissues from these well-functioning TKR corresponded to the wear particle size. Particle size greater than 4 μm was significantly correlated with a higher grade for giant cells (Table 5.2, correlation coefficient=0.58, p=0.04). A significant correlation between particle size and macrophage response was not detected (p>0.05). Radiological evidence of osteolysis was not observed in any knee.

The vast majority (94%) of wear particles were within the phagocytable range and capable of stimulating macrophages. Histology showed a relatively consistent macrophage response to UHMWPE particulate debris, with all knees having at least a grade 1+ macrophage response (Table 5.2). In nine (75%) of the twelve knees, a maximum grade of 3+ macrophage response was observed in multiple sections. In some cases with a high frequency of large wear particles, grade 1+ to 2+ multinucleated giant cells were associated with occasional big (10-100 μm) UHMWPE flakes and fibers (Figure 5.3). However, no sections produced a 3+ giant cell formation in response to UHMWPE particles. Among the 36 histological sections, the macrophage response was graded 3+ in 45%, 2+ in 8%, 1+ in 36% and 0+ in 11% and the giant cell response was graded 3+ in 0%, 2+ in 8%, 1+ in 42% and 0+ in 50%.

In terms of shape descriptors, 50% of the particles were categorized as spheroidal, compared to 16% and 7% of the particles categorized as granular or fibrillar, respectively (Tables 5.3 and 5.4). The majority of particles had a rounded appearance, independent of size, with an AR between 1 and 2 (Table 5.3, Figure 5.4). However, a greater proportion of elongated particles (higher AR) consisted of larger sized particles (Figure 5.4). There

were no significant correlations between particle shape and either macrophage response or giant cell response ($p>0.05$). There were no correlations between duration of in vivo function and either UHMWPE particle size or shape ($p>0.05$).

Different wear modes on the retrieved UHMWPE components corresponded to wear particle size and histological response. There was a significant positive relationship between articular abrasion area and both the frequency of particles ≥4 μm in size (linear regression, $R^2=0.55$, $p=0.005$) and the average ECD (linear regression, $R^2=0.52$, $p=0.008$) (Figure 5.5). Larger regions of abrasive damage were significantly correlated with higher giant cell grade (correlation coefficient =0.63, $p=0.026$). Pitting and scratching areas were negatively correlated with macrophage response (correlation coefficient =-1.0, $p=0.017$). Also, pitting on the tibial articular surface was significantly correlated with giant cell grade (correlation coefficient =0.708, $p=0.009$).

Articular surface damage size on the tibial inserts and patellar components averaged 49%±11% and 25%±12%, respectively (Table 5.5). Tibial backside damage size averaged 48%±16%. Duration of in vivo function was significantly correlated with articular surface damage size (correlation coefficient =0.73, $p=0.005$). The predominant damage modes occupying the largest areas on the tibial articular surfaces were burnishing, scratching and striations, each visible on 10 or more inserts (Table 5.6, Figure 5.6). Similarly, all 5 patellar components had visible burnishing (Table 5.7). Eight (67%) tibial inserts had abrasive damage on the posterior medial and/or lateral edges of the articular surfaces. The mechanism for such abrasive damage was confirmed at autopsy for knees 4, 6, 8, 10, 11 and consisted of visible contact between the UHMWPE inserts and femoral condylar bone or posterior osteophytes (Figure 5.7). Delamination

was observed on fewer than 25% of the tibial (3/12) or patellar (1/5) components. However, one knee (knee 12) had 21.8% tibial articular delamination but all layers of UHMWPE material remained attached. Embedded debris was not observed on any component. The predominant damage mode on the tibial backside surfaces was dimpling on 100% of the modular inserts (Figure 5.6). The dimples had relatively smooth surfaces, consistent with an impression of the textured surface of the metal baseplate.[49] The other damage modes occurred on 20% or fewer inserts' backside surfaces. Correlations between particle size and shape and damage modes other than abrasion were not detected ($p>0.05$).

6.4 Conclusions

Although it is generally accepted that both total hip replacements (THR) and TKR generate a substantial proportion of UHMWPE particles that are submicron in size, a higher frequency of larger UHMWPE elongated debris and flakes are considered typical of wear debris in failed TKR.[19,30,42,45,46] However, few studies[43,50] have included joint replacements retrieved at autopsy and characterization of UHMWPE wear debris in well-functioning joint replacements remains poorly understood.

In the current study, all knee replacements were well-functioning at last follow-up prior to autopsy retrieval, without radiological evidence of osteolysis. Therefore, the histology, quantitative descriptors of UHMWPE wear debris, and the articular and backside damage pattern measurements are descriptive of normal wear in well-functioning TKR of this implant type with UHMWPE components sterilized with gamma irradiation in air. The observed particle sizes and shapes are comparable to previously reported studies[22,30,42,46] inclusive of tissues from failed TKR (Table 5.8).

Limitations with this study are typical for analysis of retrieved prostheses. Comparisons between different studies are difficult due to variations in patients, surgical technique, implant design, UHMWPE material, and the randomness of the tissue sampling technique. Nevertheless, the components included in the current study represent a homogenous group since all components were from the same manufacturer and all index surgeries were performed by the same surgeon using a uniform surgical technique. These well-functioning, autopsy-retrieved TKR present a unique opportunity for understanding the relationship between UHMWPE damage patterns occurring after in vivo function and particulate debris accumulated in tissues.

Different wear particle sizes and shapes have been attributed to different articular contact and wear mechanisms,[17,29,30,42,46] sometimes resulting in visibly different damage modes.[6,33] However, direct comparisons of damage modes observed on retrieved UHMWPE components and wear particle morphology are infrequently reported.[18,22,33] Hirakawa, et al.,[18] found a significant positive correlation between UHMWPE tibial surface damage area and the number of wear particles larger than 10 μm in diameter. Huang, et al.,[22] suggest that different wear mechanisms for mobile bearing and fixed bearing components contribute to differences in UHMWPE debris size at retrieval. However, the frequency of different damage modes was not quantified for the retrieved inserts in those studies.[18,22] In the current study, abrasive articular damage existed on eight (67%) tibial inserts, with larger regions of abrasive damage corresponding to a significantly greater frequency of large particles and a corresponding higher grade for giant cells. Burnishing, scratching and striations were the largest and most predominant articular damage modes.

The mechanism contributing to the abrasive damage consisted of impingement contact between the UHMWPE inserts and femoral condylar bone or posterior osteophytes (Figure 5.7). However, osteophytes were not present on radiographs obtained immediately after TKR, suggesting that bone growth can occur in the postoperative period and ultimately affect UHMWPE wear. The prevalence of this abrasive damage is similar to the prevalence reported for retrieved mobile bearing[1,32,38] and fixed bearing components[14-16,35] and is not considered unique to one particular knee replacement design. Such impingement has been linked to decreased range of knee flexion,[4,31] pain and instability[35] and an associated increase in polyethylene deformation.[16,38] The estimated wear rate for inserts with impingement and abrasive damage is five times higher than inserts without such damage.[38] These results demonstrate that articular damage mechanisms impact the accumulation of UHMWPE debris in periprosthetic tissues and can have histological consequences.

It is generally accepted that sub-micrometer-sized particles produce a relatively uniform macrophage response, thus initiating cellular events that lead to bone-resorbing osteolysis.[23,34] Although the variety in shape and texture of the large particles was striking on SEM observation, the vast majority (84%) of particles were <4 μm in diameter in the current study, and tissues from all 12 knees demonstrated a uniform macrophage response. Only three knees had a giant cell response graded higher than 1+ and this was associated with a higher proportion of larger particles and larger abrasive articular damage. Despite these histological results and the high frequency of small particles, there was a notable absence of osteolysis at the bone/implant interfaces of these cemented components. Green et al.[12] reported that UHMWPE particle with a mean size

of 0.49 or 4.3 μm stimulated macrophages for generating bone resorbing cytokines and concluded that the most biologically active UHMWPE particles are in the phagocytable size range 0.3-10 μm. Additional factors, such as particle shape and composition, number, surface area, and volumetric concentration accumulated with time also can contribute to the foreign body macrophage response and the extent of periprosthetic osteolysis.[23,41,47] Similarly, osteolysis may not only be a dose-dependent disease but also one that may be prevented by reducing the particle dose below a certain threshold concentration ($<1\times10^{10}$/g)[23,28,40] and by limiting access to the periprosthetic bone interface.[43] Although the relative contributions of these additional factors cannot be distinguished in the current study, the short duration of in vivo function may have contributed to a low particle concentration below that threshold, and the use of cement fixation may have provided an effective barrier to the periprosthetic tibial, femoral and patellar bone interfaces.

In conclusion, a wide variation of particle sizes accumulated in the periprosthetic tissues of these autopsy-retrieved TKR. Some knees showed a higher frequency of smaller UHMWPE wear particles and other knees showed a higher frequency of larger particles (Figure 5.2). The histological response was correlated to wear particle size and a vast majority (94%) of particles was within the phagocytable range capable of stimulating macrophages. Most particles were spheroidal or granular in shape. Different articular wear modes corresponded to wear particle size, with abrasive articular damage mechanisms impacting the accumulation of UHMWPE debris in periprosthetic tissues with histological consequences.

5.5 Acknowledgement

The author thanks Akiko Mori, PhD, Pat Campbell, PhD, Scott A. Banks, PhD and W. Andrew Hodge, MD for co-authoring publication of this work; The author thanks W. Andrew Hodge, MD for providing retrieved TKA components; Sylvia Barnes, Lewjack Dorrance, and Tammy Moore for cooperation in obtaining retrieved implants and donor patient information; Carolyn Jones for technical assistance obtaining radiographs of autopsy retrieved knees; Akiko Mori, PhD for completing particle analysis; and Pat Campbell, PhD for completing tissue digestion and histological analysis. This work was supported by funding from The BioMotion Foundation in Palm Beach, Florida, with partial funding provided by an institutional research grant from Osteonics Corp. (now Styker Orthopaedics), Mahwah, New Jersey, and Orthopaedic Hospital/UCLA in Los Angeles, California.

Note: This work has been submitted for publication and is referenced as follows.

Mori A, Harman MK, Campbell P, Banks SA, Hodge WA: Polyethylene wear in autopsy retrieved total knee replacements. J Bone Joint Surg 2007, submitted March 2007.

5.6 References Cited

1. Argenson J-N, O'Connor JJ. Polyethylene wear in meniscal knee replacement: A one to nine-year retrieval analysis of the oxford knee. *J Bone Joint Surg Br*. 1992; 74(2):228-32.
2. ASTM subcommittee F04.16. F1877-98 Standard Practice for Characterization of Particles. In: Annual Book of ASTM Standards 2002, Vol.13.01. West Conshohocken, PA: American Society for Testing and Materials; 2002. 13:01:1397-408.
3. Beaulé PE, Campbell PA, Walker PS, Schmalzried TP, Dorey FJ, Blunn GW, Bell CJ, Yahia L'H, Amstutz HC. Polyethylene wear characteristics in vivo and in a knee simulator. *J Biomed Mater Res*. 2002; 60:411-9.

4. Bellemans J, Robijns F, Duerinckx J, Banks A, Vandenneucker. The influence of tibial slope on maximal flexion after total knee arthroplasty. *Knee Surg Sports Traumatol Arthrosc.* 2005; 13:193-6.

5. Benevenia J, Lee FY-I, Buechel F, Parsons JR. Pathologic supracondylar fracture due to osteolytic pseudotumor of knee following cementless total knee replacement. *J Biomed Mater Res (Appl Biomater).* 1998; 43:473-7.

6. Blunn GW, Walker PS, Joshi A, Hardinge K. The dominance of cyclic sliding in producing wear in total knee replacements. *Clin Orthop*. 1991; 273:253-60.

7. Bosco J, Benjamin J, Wallace D. Quantitiative and qualitative analysis of polyethylene wear particles in synovial fluid of patients with total knee arthroplasty. *Clin Orthop*. 1994; 309:11-9.

8. Cadambi A, Engh GA, Dwyer KA, Vinh TN. Osteolysis of the distal femur after total knee arthroplasty. *J Arthroplasty*. 1994; 9(6):579-94.

9. Campbell P, Ma S, Yeom B, McKellop H, Schmalzried TP, Amstutz HC. Isolation of predominantly submicron-sized UHMWPE wear particles from periprosthetic tissues. *J Biomed Mater Res.* 1995; 29:127-31.

10. Dannenmaier WC, Haynes DW, Nelson CL. Granulomatous reaction and cystic bony destruction associated with high wear rate in a total knee prosthesis. *Clin Orthop*. 1985; 198:224-30.

11. Ewald FC. The Knee Society total knee arthroplasty roentgenographic evaluation and scoring system. *Clin Orthop*. 1989; 248:9-12.

12. Green TR, Fisher J, Stone M, Wroblewski BM, Ingham E. Polyethylene particles of a 'critical size' are necessary for the induction of cytokines by macrophages in vitro. *Biomaterials*. 1998; 19: 2297-302.

13. Hahn DW, Wolfarth DL, Parks NL. Characterization of submicron polyethylene wear debris from synovial-fluid samples of revised knee replacements using a light-scattering technique. *J Biomed Mater Res*. 1996; 31:355-63.

14. Harman MK, Banks SA, Hodge WA. Does backside damage correspond to articular damage in retrieved TKA polyethylene inserts? *Clin Orthop*. 2007; in press.

15. Harman MH, Banks SA, Hodge WA. Polyethylene damage and knee kinematics after total knee arthroplasty. *Clin Orthop*. 2001; 392:383-93.

16. Harman MK, Schmitt S, Roessing S, Banks SA, Scharf HP, Hodge WA. Predicting progressive degeneration, component fixation and polyethylene wear from radiographs of 27 UKR retrieved after 2 to 13 years of functional duration. *ACTA Orthop.* 2007; in review.

17. Hirakawa K, Bauer TW, Hashimoto Y, Stulberg BN, Wilde AH, Secic M. Effect of femoral head diameter on tissue concentration of wear debris. *J Biomed Mater Res*. 1997; 36:529-35.

18. Hirakawa K, Bauer TW, Stulberg BN, Wilde AH, Borden LS. Characterization of debris adjacent to failed knee implants of 3 different designs. *Clin Orthop*. 1996; 331:151-8.

19. Hirakawa K, Bauer TW, Stulberg BN, Wilde A. Comparison and quantitation of wear debris of failed total hip and total knee arthroplasty. *J Biomed Mater Res*. 1996; 31:257-63.

20. Hood RW, Wright TM, Burstein AH. Retrieval analysis of total knee prostheses: A method and its application to 48 total condylar prostheses. *J Biomed Mater Res*. 1983; 17: 829-42.

21. Howling GI, Barnett PI, Tipper JL, Stone MH, Fisher J, Ingham E. Quantitative characterization of polyethylene debris isolated from periprosthetic tissue in early failure knee implants and early and late failure Charnley hip implants. *J Biomed Mater Res (Appl Biomater).* 2001; 58:415-20.

22. Huang C-H, Ho F-Y, Ma H-M, Yang C-T, Liau J-J, Kao H-C, Young T-H, Cheng C-K. Particle size and morphology of UHMWPE wear debris in failed total knee arthroplasties- a comparison between mobile bearing and fixed bearing knees. *J Orthop Res*. 2002; 20:1038-41.

23. Ingham E, Fisher J. The role of macrophages in osteolysis of total joint replacement. *Biomaterials*. 2005; 26:1271-86.

24. Insall JN, Dorr LD, Scott RD, Scott WN. Rationale of the Knee Society clinical rating system. *Clin Orthop.* 1989; 248:13-14.

25. Kadoya Y, Revell PA, Al-Saffar N, Kobayashi A, Scott G, Freeman MAR. Bone formation and bone resorption in failed total joint arthroplasties: Histomorphometric analysis with histochemical and immunohistochemical technique. *J Ortho Res*. 1996; 14(3):473-82.

26. Kilgus DJ, Funahashi TT, Campbell PA. Massive femoral osteolysis and early disintegration of a polyethylene-bearing surface of a total knee replacement: A case report. *J Bone Joint Surg Am*. 1992; 74(5):770-4.

27. Kobayashi A, Bonfield W, Kadoya Y, Yamac T, Freeman MAR, Scott G, Revell PA. The size and shape of particulate polyethylene wear debris in total joint replacements. *Proc Instn Mech Engrs [H]*. 1997; 211:11-5.

28. Kobayashi A, Freeman MAR, Bonfield W, Kadoya Y, Yamac T, Al-Saffar N, Scott G, Revell PA. Number of polyethylene particles and osteolysis in total joint replacements. *J Bone Joint Surg Br*. 1997; 79(5):844-8.

29. Landry ME, Blanchard CR, Mabrey JD, Wang X, Agrawal CM. Morphology of in vitro generated ultrahigh molecular weight polyethylene wear particles as a function of contact conditions and material parameters. *J Biomed Mater Res (Appl Biomater).* 1999; 48:61-9.

30. Mabrey JD, Afsar-Keshmiri A, Engh GA, Sychterz CJ, Wirth MA, Rockwood CA, Agrawa CM. Standardized analysis of UHMWPE wear particles from failed total joint arthroplasties. *J Biomed Mater Res (Appl Biomater).* 2002; 63:475-83.

31. Majewski M, Weining G, Friederich NF. Posterior femoral impingement causing polyethylene failure in total knee arthroplasty. *J Arthroplasty*. 2002; 17(4):524-6.

32. Markovich GD, Harman MK, Banks SA, Hodge WA. Cementless LCS total knee arthoplasty after 9 years in-situ: Articular and backside damage on retrieved meniscal and rotating platform polyethylene bearings. *Proceedings of the American Academy of Orthopaedic Surgeons*, 2004.

33. McKellop HA, Campbell P, Park S-H, Schmalzried TP, Grigoris P, Amstutz HC, Sarmiento A. The origin of submicron polyethylene wear debris in total hip arthroplasty. *Clin Orthop*. 1995; 311: 3-20.

34. Murray DW, Rushton N. Macrophages stimulate bone resorption when they phagocytose particles. *J Bone Joint Surg Br*. 1990; 72(6):988-92.

35. Noble PC, Conditt MA, Thompson MT, Stein JA, Kreuzer S, Parsley BS, Mathis KB. Extraarticular abrasive wear in cemented and cementless total knee arthroplasty. *Clin Orthop*. 2003; 416:120-8.

36. Peters PC, Engh GA, Dwyer KA, Vinh TN. Osteolysis after total knee arthroplasty without cement. *J Bone Joint Surg Am*. 1992;74(6):864-76.

37. Popoola OO, Johnson TS, Bhambri S. Morphology and size distribution of polyethylene debris generated during multiple activity knee wear testing. *Transactions of the 52nd Annual Meeting of the Orthopaedic Research Society*. 2006; 31:634.

38. Psychoyios V, Crawford RW, O'Connor JJ, Murray DW. Wear of congruent meniscal bearings in unicompartmental knee arthroplasty: A retrieval study of 16 specimens. *J Bone Joint Surg Br*. 1998;80(6):976-82.

39. Rao AR, Engh GA, Collier MB, Lounici S. Tibial interface wear in retrieved total knee components and correlations with modular insert motion. *J Bone Joint Surg Am*. 2002; 84(10):1849-55.

40. Revell PA. Biological reaction to debris in relation to joint prostheses. *Proc Instn Mech Engrs J Engrs Med.* 1997; 211:187-97.

41. Sabokbar A, Pandey R, Athanasou NA. The effect of particle size and electrical charge on macrophage-osteoclast differentiation and bone resorption. *J Mater Sci Mater Med*. 2003; 14:731-8.

42. Schmalzried TP, Campbell P, Schmitt AK, Brown IC, Amstutz HC. Shapes and dimensional characteristics of polyethylene wear particles generated in vivo by total knee replacements compared to total hip replacements. *J Biomed Mater Res (Appl Biomater).* 1997; 38:203-10.

43. Schmalzried TP, Jasty M, Harris WH. Periprosthetic bone loss in total hip arthroplasty: Polyethylene wear debris and the concept of effective joint space. *J Bone Joint Surg Am*. 1992; 74(6):849-63.

44. Schmalzried TP, Jasty M, Rosenberg A, Harris WH. Histologic identification of polyethylene wear debris using oil red o stain. *J Appl Biomater.* 1993; 4:119-25.

45. Schmalzried TP, Jasty M, Rosenberg A, Harris WH. Polyethylene wear debris and tissue reactions in knee as compared to hip replacement prostheses. *J Appl Biomater* 1994; 5:185-90.

46. Shanbhag AS, Bailey HO, Hwang D-S, Cha CW, Eror NG, Rubash HE. Quantitative analysis of ultrahigh molecular weight polyethylene(UHMWPE) wear debris associated with total knee replacements. *J Biomed Mater Res (Appl Biomater).* 2000; 53:100-10.

47. Shanbhag AS, Jacobs JJ, Black J, Galante JO, Glant TT. Macrophage/particle interactions: Effect of size, composition and surface area. *J Biomed Mater Res*. 1994; 28:81-90.

48. Shanbhag AS, Jacobs JJ, Glant TT, Gilbert JL, Black J, Galante JO. Composition and morphology of wear debris in failed uncemented total hip replacement. *J Bone Joint Surg Br*. 1994; 76-B(1):60-7.

49. Silva M, Kabbash CA, Tiberi JV III, Park SH, Reilly DT, Mahoney OM, Schmalzried TP. Surface damage on open box posterior-stabilized polyethylene tibial inserts. *Clin Orthop*. 2003; 416: 135-44.

50. Surace MF, Berzins A, Urban RM, Jacobs JJ, Berger RA, Natarajan RN, Andriacchi TP, Galante JO. Backsurface wear and deformation in polyethylene tibial inserts retrieved postmortem. *Clin Orthop*. 2002; 404:14-23.

51. Wasielewski RC, Parks N, Williams I, Surprenant H, Collier JP, Engh G. Tibial insert undersurface as a contributing source of polyethylene wear debris. *Clin Orthop*. 1997; 345:53-9.

52. Wimmer MA, Andriacchi TP, Natarajan RN, Loos J, Karlhuber M, Petermann J, Schneider E, Rosenberg AG. A striated pattern of wear in ultrahigh-molecular-weight polyethylene components of Miller-Galante total knee arthroplasty. *J Arthroplasty*. 1998; 13:8-16.

53. Wolfarth DL, Han DW, Bushar G, Parks NL. Separation and characterization of polyethylene wear debris from synovial fluid and tissue samples of revised knee replacements. *J Biomed Mater Res*. 1997; 34:57-61.

Table 5.1: Patient Demographics

Knee	Sex	Age at Index (yrs)	Weight at Index (kg)	Months in Vivo	Implant Type
1[a]	M	67.8	70.5	19.8	Series 7000
2[†]	M	67.9	77.3	20.1	Series 7000
3[†,a]	M	67.2	77.3	28.2	Series 7000
4[a]	M	80.2	86.4	37.0	Series 7000
5[‡,a]	M	66.4	101.8	45.8	Series 7000
6[‡,a]	M	66.2	101.8	47.9	Series 7000
7	F	66.7	69.1	51.2	Series 7000
8	M	74.0	78.2	62.9	Series 7000
9[+]	M	67.9	100.0	73.0	Series 7000
10[+]	M	67.8	100.0	73.7	Series 7000
11[b]	F	75.5	64.5	80.7	Series 7000
12[b]	F	74.0	79.5	97.0	Series 7000
Mean ± Std.	—	70.2±4.6	83.9±13.8	53.1±24.8	—

[†, ‡, +]These patients had bilateral total knee replacements.

[a] Patella resurfaced with an all-polyethylene patellar component.

[b] These patients had an all-polythylene tibial component.

Table 5.2: Sizes of UHMWPE Wear Particles Recovered from the Tissues and Maximum Histological Grade

Knee	Particle Count	Equivalent Circle Diameter (ECD)			Histological Grade	
		Size Range (μm)	Mean±Std. (μm)	Frequency (%) ≥4 μm	Macrophages	Giant Cells
1	501	0.27~ 28.09	3.67± 3.88	25.7	3	1
2	921	0.08~ 82.23	3.25± 5.27	20.6	3	1
3	986	0.23~ 73.09	3.01± 4.38	16.7	2	1
4	1,502	0.17~170.46	6.95±10.91	43.5	3	2
5	1,086	0.24~ 53.45	2.71± 4.37	12.4	3	1
6	3,911	0.09~108.38	1.65± 4.88	6.5	3	1
7	1,176	0.20~ 33.69	1.81± 2.97	7.0	3	0
8	3,046	0.08~ 82.51	3.62± 4.62	24.5	1	1
9	285	0.37~ 24.48	2.61± 3.42	10.9	3	2
10	4,837	0.08~186.73	1.68± 6.01	7.4	3	1
11	1,065	0.20~ 98.83	6.93±11.54	45.4	3	2
12	1,035	0.17~190.64	2.70± 8.48	9.5	1	0
Total	20,351	0.08~190.64	2.94± 6.55	16.4	—	—

Table 5.3: UHMWPE Particle Shape Descriptors (mean ± standard deviation)

Knee	Particle Count	Aspect Ratio (AR)	Roundness (R)	Form Factor (FF)
1	501	1.93±0.70	0.42±0.13	0.53±0.22
2	921	1.99±0.74	0.39±0.13	0.42±0.21
3	986	1.94±0.76	0.39±0.12	0.43±0.19
4	1,502	1.69±0.69	0.53±0.16	0.65±0.19
5	1,086	1.99±0.82	0.41±0.13	0.56±0.22
6	3,911	1.78±0.66	0.46±0.12	0.64±0.20
7	1,176	1.86±0.64	0.43±0.12	0.59±0.21
8	3,046	1.90±0.70	0.42±0.13	0.50±0.20
9	285	1.87±0.76	0.43±0.14	0.43±0.20
10	4,837	1.82±0.64	0.44±0.12	0.54±0.20
11	1,065	2.18±0.92	0.36±0.13	0.41±0.22
12	1,035	1.76±0.66	0.46±0.13	0.52±0.20
Total	20,351	1.86±0.71	0.44±0.13	0.54±0.21

Note. AR is a ratio of the major to the minor diameter of a particle; R is a measure of how closely a particle resembles a circle, based on the major diameter; and FF is a measure of how closely a particle resembles a circle, based on the perimeter of the particle.

Table 5.4: Morphology Distributions of UHMWPE Wear Particles

Knee	Particle Count	Spheroidal (%)	Granular (%)	Fibrillar (%)	Others (%)
1	501	44.7	18.4	8.4	28.5
2	921	40.8	20.5	10.0	28.7
3	986	45.2	18.5	9.1	27.2
4	1,502	62.9	10.7	4.9	21.5
5	1,086	43.4	15.6	9.7	31.3
6	3,911	54.8	14.7	4.8	25.7
7	1,176	48.8	17.1	6.5	27.6
8	3,046	46.5	17.2	7.7	28.6
9	285	50.5	16.9	7.0	25.6
10	4,837	50.0	15.7	5.4	28.9
11	1,065	34.8	20.9	15.8	28.5
12	1,035	56.1	15.8	4.3	23.8
Total	20,351	49.7	16.1	6.9	27.3

Table 5.5: Total Damage Area on Articular and Backside Surfaces of UHMWPE Components

Knee	Tibia (Articular)	Patella (Articular)	Tibia (Backside)
1	41.2	14.4	26.2
2	40.7	—[a]	57.8
3	36.4	36.7	58.2
4	45.9	11.8	20.3
5	47.9	29.0	38.6
6	54.6	34.3	43.6
7	33.7	—[a]	57.6
8	46.8	—[a]	56.8
9	52.6	—[a]	67.0
10	48.9	—[a]	58.2
11	68.7	—[a]	—[b]
12	68.7	—[a]	—[b]
Mean ± Std.	48.7±10.8	25.2±11.5	48.4±15.6

[a] *These patients did not have a resurfaced patella.*

[b] *These patients had an all-polyethylene tibial component.*

Table 5.6: Damage Area (%) on UHMWPE Articular Surfaces of Tibial Inserts

Knee	Abrasion	Burnishing	Delamination	Embedded Debris	Pitting	Scratching	Striations
1	1.2	16.1	0.0	0.0	0.9	3.9	19.2
2	4.2	8.6	0.0	0.0	0.0	8.1	19.7
3	0.0	13.9	0.0	0.0	0.0	0.0	22.5
4	5.7	10.1	0.0	0.0	1.9	28.2	0.0
5	0.0	16.2	0.2	0.0	1.2	7.3	23.0
6	3.6	18.6	2.1	0.0	2.8	7.0	20.5
7	0.0	7.9	0.0	0.0	0.0	18.5	7.2
8	6.7	21.7	0.0	0.0	0.3	13.0	5.1
9	1.9	15.1	0.0	0.0	1.2	8.6	25.8
10	3.4	16.8	0.0	0.0	0.0	6.6	22.1
11	16.4	20.8	0.0	0.0	5.7	17.4	8.4
12	0.0	20.2	21.8	0.0	0.0	24.7	0.0
Mean	5.4	15.5	8.0	0.0	2.0	13.0	17.4
Frequency (%)	66.7	100.0	25.0	0.0	58.3	91.7	83.3

Table 5.7: Damage Area (%) on UHMWPE Articular Surfaces of Patellar Components

Knee	Abrasion	Burnishing	Delamination	Embedded Debris	Pitting	Scratching	Striations
1	0.0	6.9	7.6	0.0	0.0	0.0	0.0
2	—	—	—	—	—	—	—
3	0.0	22.3	0.0	0.0	0.1	4.2	10.1
4	0.0	11.8	0.0	0.0	0.0	0.0	0.0
5	0.0	18.6	0.0	0.0	0.0	0.0	10.4
6	0.0	29.2	0.0	0.0	0.0	0.0	5.1
7	—	—	—	—	—	—	—
8	—	—	—	—	—	—	—
9	—	—	—	—	—	—	—
10	—	—	—	—	—	—	—
11	—	—	—	—	—	—	—
12	—	—	—	—	—	—	—
Mean	0.0	17.8	7.6	0.0	0.1	4.2	8.5
Frequency (%)	0.0	100.0	20.0	0.0	20.0	20.0	60.0

Table 5.8: UHMWPE Particle Comparison of Current Study for Autopsy TKR and Previous Reports for Failed TKR

Report	Particle Size		Particle Shape
	Mean (μm) [range]	Distribution	
Mori, et al. (Current Study)	2.94 [0.08-190.6]	44% <1μm 84% <4μm 94% <10μm	AR=1.86 R=0.44 FF=0.54
Mabrey, et al.[30]	1.19	43% <1μm	AR=1.935 R=0.612 FF=0.764
Huang, et al.[22]	LCS(Mobile)=0.58 PCA(Fixed)=1.17 M/G(Fixed)=5.23		
Shanbhag, et al.[46]	1.7 [0.1-18]	36% <1μm 90% <3μm 98% <10μm	AR=1.7
Schmalzried, et al.[42]	0.52	71% <1μm	AR=7.5

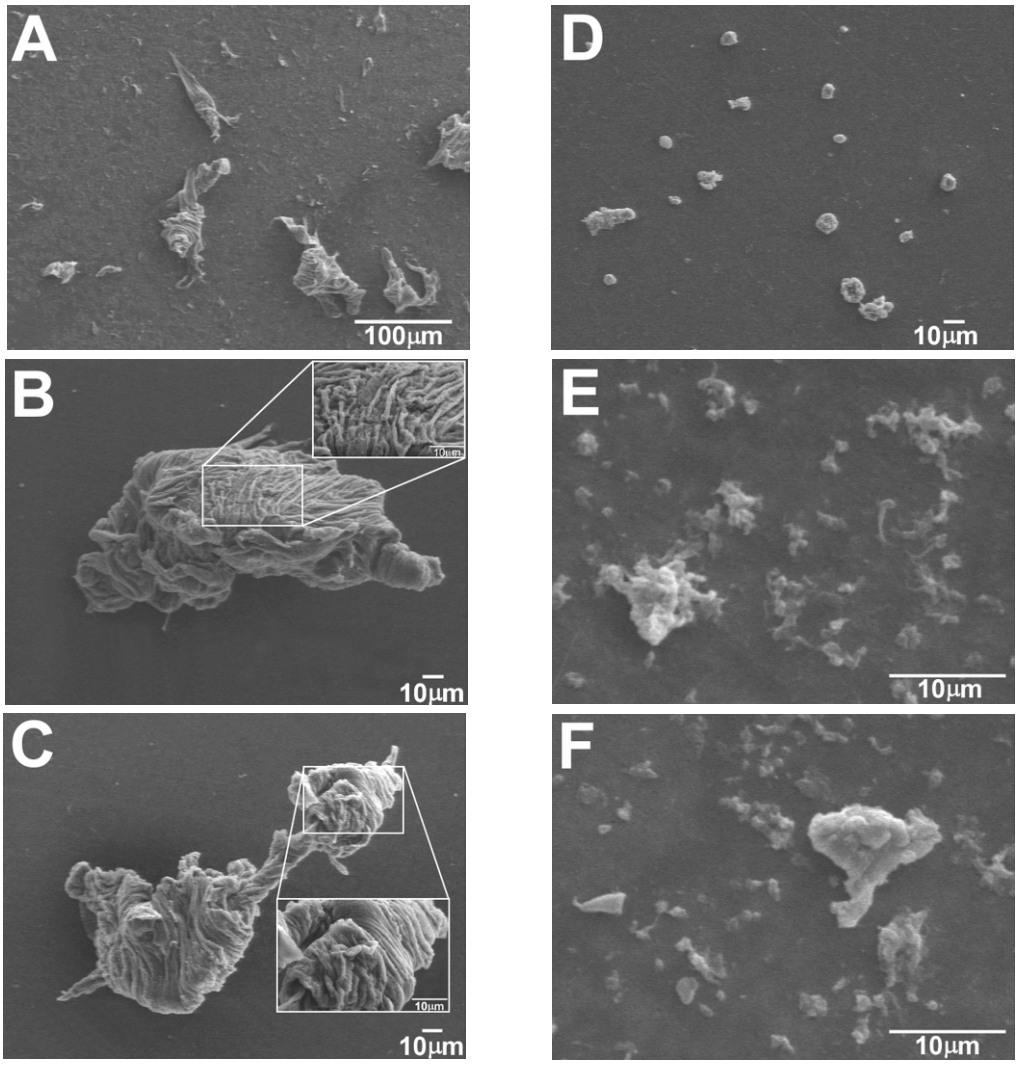

Figure 5.1: Scanning Electron Micrographs of UHMWPE Wear Particles

[A] Large (100 μm) flake-like particles with a ripple-textured surface were striking in knee 11. Submicron-size fine particles covered the filter surface; [B,C] Ripple-textured particles were seen in knee 4; [D] Knee 4 also showed rounded spheroidal particles with mixed surface texture (smooth and irregular), ranging from several microns to 30 μm in diameter; [E,F] Small spheroidal and granular particles with occasional attached fine fibrils were predominantly seen in most knees, [E] knee 2, [F] knee 8.

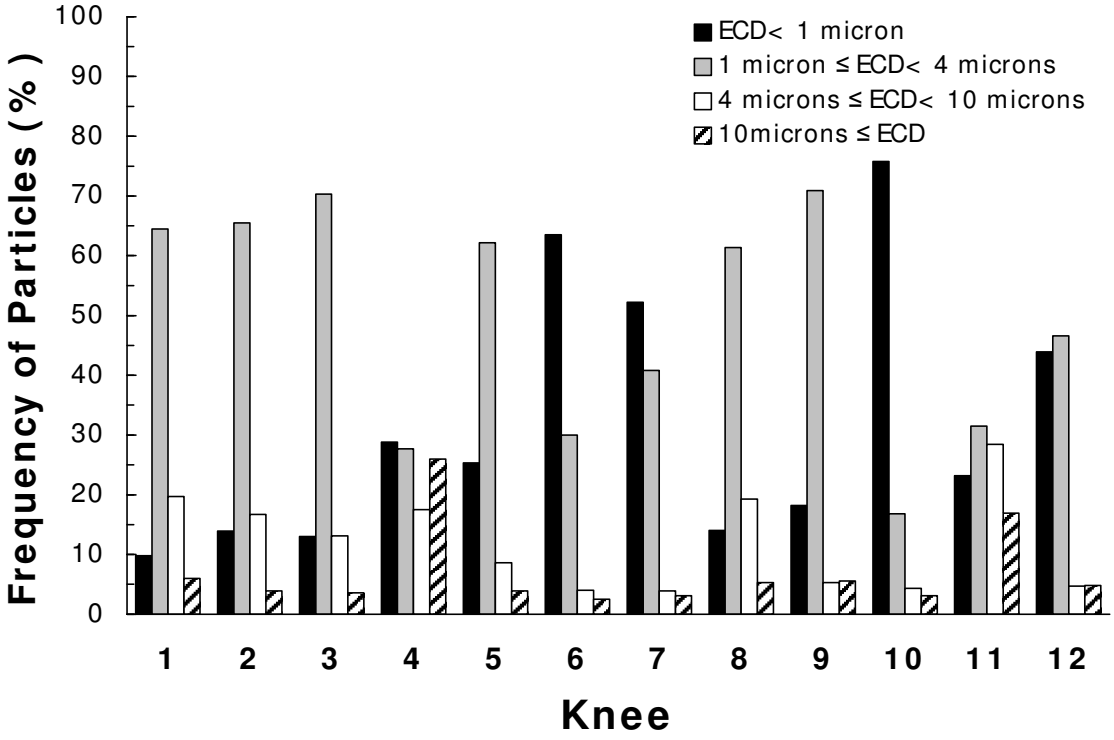

Figure 5.2: Frequency Distributions of UHMWPE Wear Particle Size

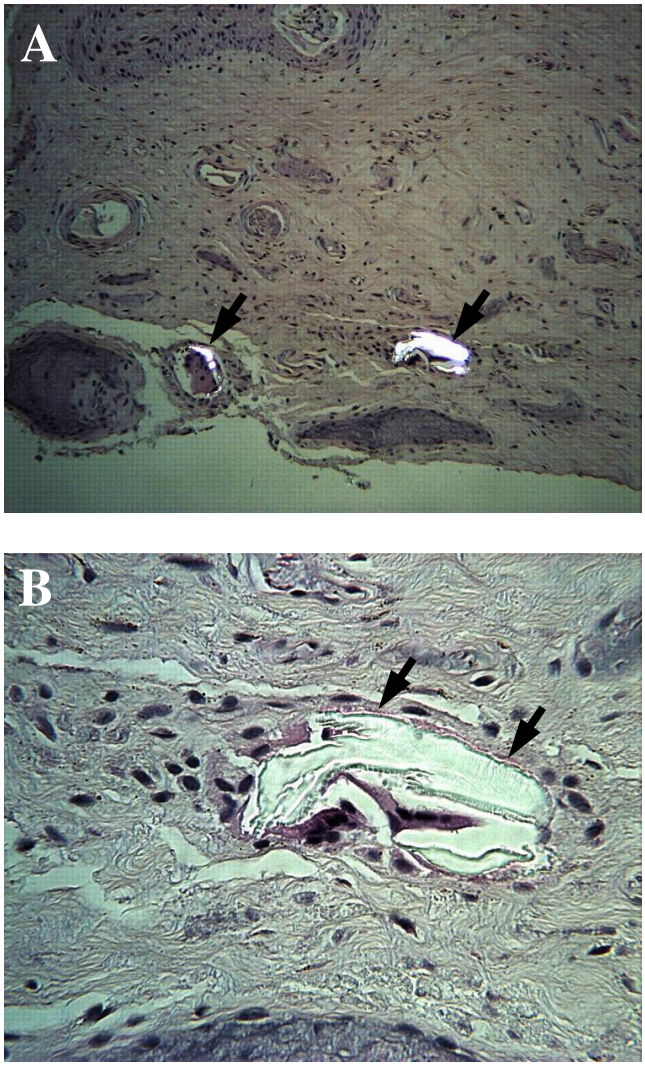

Figure 5.3: Photomicrographs of a Histological Section of Periprosthetic Tissues [A] Under polarized light, large UHMWPE wear particles in knee 4 were birefringent (arrows, original magnification, x100); [B] At higher magnification, a non-phagocytable UHMWPE flake from knee 4 (arrow) is surrounded by a multinucleated giant cell (original magnification, x400).

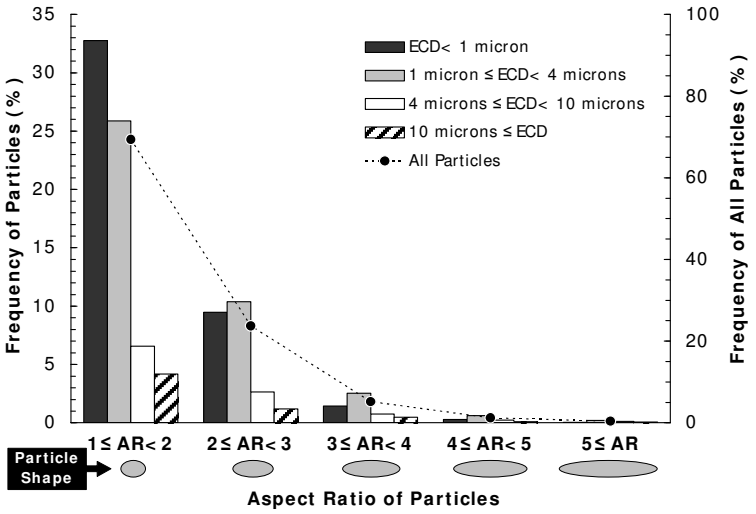

Figure 5.4: Frequency Distributions of UHMWPE Particles

with Respect to Size and Particle Aspect Ratio

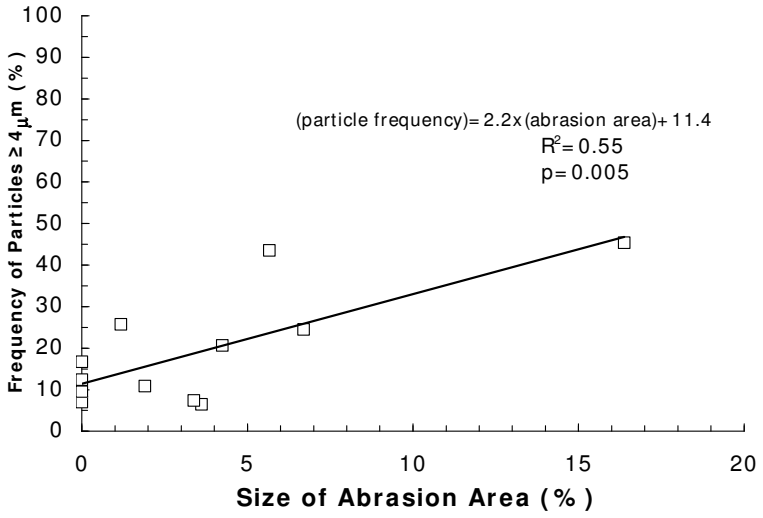

Figure 5.5: Relationship Between Abrasive Damage Area on Tibial Articular Surfaces

and the Number of UHMWPE Large (ECD ≥4µm) Wear Particles

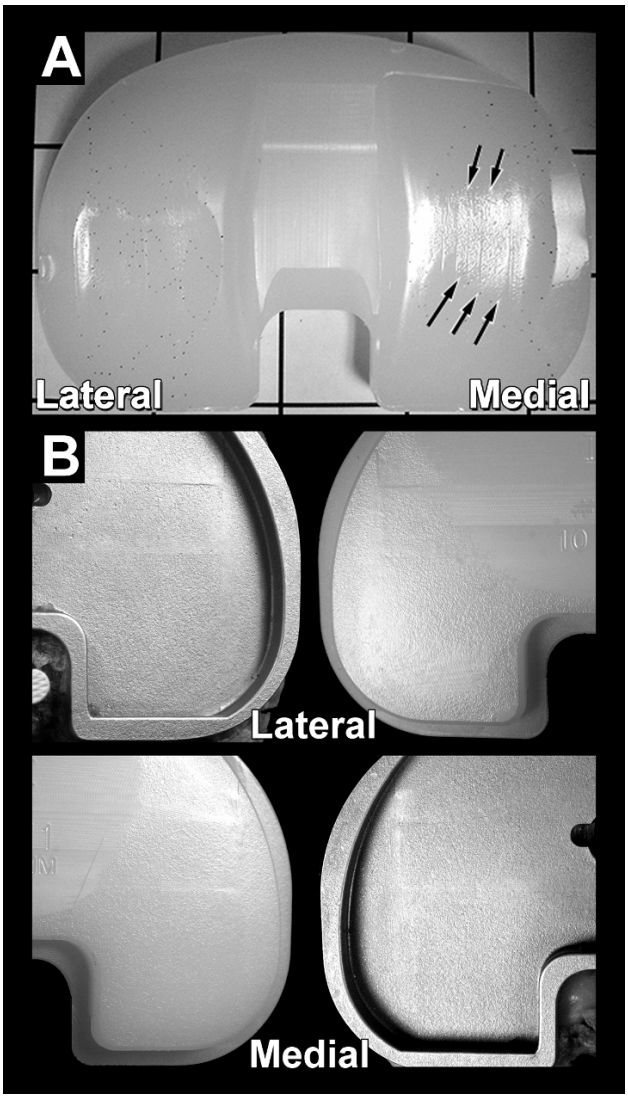

Figure 5.6: Photographs of Damage Patterns on Articular and Backside Surfaces of UHMWPE Tibial Inserts

[A] Burnishing, scratching and striations were seen on the articulating surface, especially, striations covered large area in this knee 10 (arrows). [B] Dimpling was seen on the backside surface for 100% of the modular inserts (knee 9).

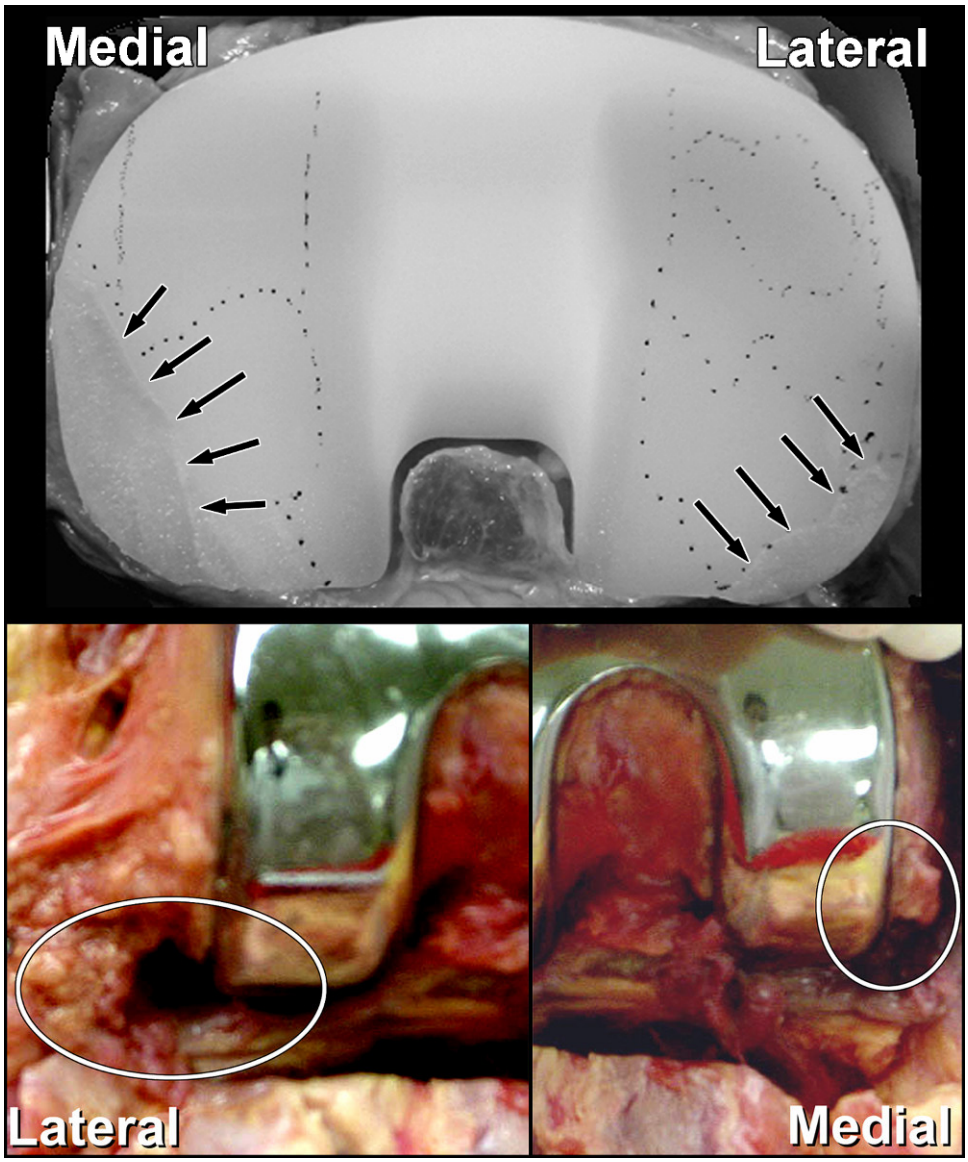

Figure 5.7: Abrasive Wear on a UHMWPE Tibial Insert

Medial and lateral posterior edges (arrows) on an insert retrieved from 82 year old female after 81 months in vivo (knee 11). At autopsy, the femoral component showed a prominent posterior medial osteophyte and calcification in the posterior lateral soft tissues (ovals).

6 POLYETHYLENE DAMAGE AREA AND DEFORMATION ON UNICONDYLAR KNEE PROSTHESES RETRIEVED AFTER 2 TO 13 YEARS OF FUNCTIONAL DURATION

6.1 Introduction

There is renewed interest in unicondylar knee replacement (UKR) as a less invasive surgical procedure for knee arthroplasty. UKR survivorship exceeds 85% at 10 years, with unconstrained (non-conforming) designs showing significantly better survivorship than conforming designs.[21,39] However, progressive component subluxation in non-conforming tibio-femoral articulations is associated with potentially poor wear performance[5] and more conforming, mobile-bearing UKR designs have been advocated.[13] Others have suggested that the occurrence of plastic deformation, or "dishing" on the polyethylene articular surface in non-conforming designs has positive consequences for articular wear.[2,9]

Progressive osteoarthritis (OA) and loosening can limit the longevity of UKR during long term follow-up. Similarly, component alignment on post-operative radiographs is associated with clinical outcome,[19,20,37,40] and tibiofemoral subluxation has been linked to catastrophic wear and failure in unconstrained UKR.[5] However, the decision to revise UKR is complex as radiographic findings are not always consistent with clinical symptoms.[41]

The primary objective of this research was to assess component alignment, fixation and wear of non-conforming UKR. It was hypothesized that clinical outcomes and radiographic evaluations prior to revision surgery would correlate to intraoperative assessments of progressive OA and component fixation and to damage patterns on polyethylene bearings retrieved after *in vivo* function.

6.2 Materials and Methods

Twenty-seven UKR from one manufacturer (WALDEMAR LINK GmbH & Co. KG, Hamburg, Germany) were identified within a larger group of 43 UKR retrieved through an established Implant Retrieval Program.[15] The components were retrieved during revision surgery at one institution (Mannheim University Hospital, Mannheim, Germany) from 1999 to 2003. Index arthroplasty was performed previously at various regional medical centers from 1987 to 1998. There were 22 female and 5 male patients with an average age of 69 (SD 6) (range, 58 to 82) years at index surgery and 76(SD 6) (range, 68 to 87) years at the time of retrieval. Duration of function averaged 79 (SD 34) (range, 25 to 156) months.

Surgical technique at index arthroplasty included implantation in the medial compartment in all knees and cement fixation of the tibial and femoral components. Clinical outcome scores[24] and retrospective radiographic review of radiolucent lines and component alignment[12,26] were completed according to Knee Society guidelines. Angular measurements in the frontal plane included limb alignment and tibial component tilt relative to the long tibial axis (negative angles indicate a medial tilt in component position). Angular measurements in the sagittal plane included femoral component tilt relative to the femoral axis (negative angles indicate a flexed component position) and

tibial component slope relative to the long tibial axis (negative angles indicate a posterior sloped component position). During revision surgery, component fixation was manually assessed and graded as well-fixed or loose, and progressive OA was graded using Outerbridge classification.[33] Intraoperative and radiographic assessments were completed independently.

The components consisted of non-conforming tibiofemoral articulations with fixed polyethylene tibial bearings (Figure 6.1). The inferior surface of all metal tibial baseplates was beaded with a 10 mm fin oriented in the anteroposterior direction (Endosled, WALDEMAR LINK GmbH & Co. KG). The non-articular surface of the femoral components was smooth with one peg and a central fin oriented in the anteroposterior direction (Tönnis, WALDEMAR LINK GmbH & Co. KG). The polyethylene inserts were machined from ram-extruded stock (Grade 2000 resin, Hoechst, Germany) and sterilized using gamma radiation in air, consistent with manufacturing practices prior to 1999. The thickness of the polyethylene tibial insert was 5 mm in 23 knees and 7 mm in four knees.

All components were gently cleaned with mild soap and a dilute sodium hypochlorite solution after retrieval. One observer evaluated damage area and location on the polyethylene articular surface using an optical stereomicroscope (model Z30L, Cambridge Instruments, Cambridge, MA) at 7 to 30 times magnification. The prevalence of nine damage modes was determined using published visual identification methods.[16,22,36] Abrasion was visualized as rough, tufted regions. Burnishing was visualized as smooth regions that were highly reflective of incident light. Delamination was visualized as thin sheets of material separated from the surface. Subsurface

delamination appeared as cracks and/or discoloration located inferior and generally parallel to articular plane without discontinuity of the articular surface material. Embedded debris was visualized as particles that differed in color and/or texture relative to the surrounding polyethylene surface. Pitting was visualized as depressions with rough surfaces typically 1-2 mm in diameter. Scratching was visualized as thin lines in irregular or ordered directions across the surface. Striations were visualized as highly oriented, longitudinal, smooth peaks and troughs on the articular surface.[43] Fractures were visualized as complete cracks or wear-through of the polyethylene insert, typically resulting in exposure of the metal baseplate in these modular components.

The circumference of the damage regions was outlined on calibrated digital images of the articular surface and the damage area was measured using published digital image analysis techniques and custom programs.[10,14,16,18] The technique is 98.6% accurate with a precision of 0.4 mm for linear distances and 3.9 mm^2 for areas. Damage area is presented as a percentage of the total articular surface area. The damage location (area centroid) was calculated relative to a normalized coordinate system referencing the mediolateral (ML location) and anteroposterior (AP location) edges of the insert, with 0% indicating the posterior and medial edges.

Surface deformation (depth) was measured using a hand-held stylus (Microscribe 3DX, Immersion Corp., San Jose, CA) interfaced with a personal computer and surfacing software (Rhinoceros, Robert McNeel & Associates, Seattle, WA). Surface topography was digitized on the articular surface of each retrieved insert and on unused control inserts of the same design. Approximately 1000 points were digitized and exported for each insert to represent the three-dimensional articular geometry. Precision error for set-

up and digitizing was 103 μm using repeated measurements on objects with known dimensions. Image analysis routines were implemented to correct specimen tilt and alignment within the same normalized coordinate system previously established. Surface deformation was calculated as the thickness difference between the articular geometry of the worn inserts compared to unused control inserts. Maximum deformation was measured and the associated damage mode recorded. The deformation rate was calculated as maximum deformation divided by duration of function for each insert.

Strength of association between variables was determined using Spearman's bivariate rank order correlation and multiple regression. Correlation coefficients >0.6 were considered to indicate strong correlation, and values of 0.4 to 0.6 were considered to indicate moderate correlation. Differences between pre-operative and post-operative alignment were analyzed using a paired t-test. The level of significance was $p<0.05$.

6.3 Results

Average Knee Society Scores initially improved from the pre-operative to post-operative evaluation, consistent with successful treatment of the patients' symptoms, but declined more than 30 points at the pre-revision evaluation (Table 6.1). Limb alignment averaged 3° (SD 3°) varus on pre-operative radiographs, consistent with medial compartment osteoarthritis, and 3° (SD 3°) valgus on immediate post-operative radiographs (Table 6.2). Changes in limb alignment, component position, damage area or articular deformation were not significantly correlated with patient sex, age, height, weight, body mass index, or reason for revision ($p>0.05$). Larger damage areas were moderately correlated with lower Knee Society Scores for pain prior to revision (correlation coefficient = -0.45, $p=0.02$).

Changes in limb alignment and component position were evident when immediate post-operative and pre-revision radiographs were compared. Pre-revision limb alignment was significantly different from immediate post-operative alignment (Wilcoxon signed rank test, $p=0.005$), with varus limb alignment in nine (33%) knees at revision. The extent of recurrent varus alignment at revision was significantly correlated with limb alignment on immediate post-operative radiographs (correlation coefficient = 0.64, $p<0.001$). On immediate post-operative radiographs, tibial component posterior slope was greater than 7° in 22 (81%) knees, and 19 (70%) femoral components and 16 (59%) tibial components had more than 3° deviation from 90° in the sagittal and frontal planes, respectively. Tibial or femoral component alignment migrated 5° to 9° in 12 (44%) knees and $\geq$10° in five (19%) knees, including eight knees graded as loose during intra-operative assessment.

Evaluations from pre-revision radiographs did not correspond to intraoperative assessment of progressive OA. Suspected revision reasons based on clinical and radiographic evaluation included aseptic loosening (63%), progressive OA (22%), and wear (15%). The prevalence of progressive OA at revision surgery was more than double the occurrence suspected from radiographs. At revision surgery, there were Grade III or Grade IV changes in the lateral compartment of 15 (56%) knees and patellofemoral compartment of 16 (59%) knees (Table 6.3).

Interpreting indications for loosening from pre-revision radiographs was unpredictable. Revision reason was not correlated with radiographic measurements of limb alignment or component position ($p>0.05$). Intraoperative assessment of component fixation at revision surgery revealed aseptic loosening in 20 (74%) knees (Table 6.4).

There was femoral component loosening in 19 (70%) knees and tibial component loosening in 9 (33%) knees, inclusive of eight (30%) knees in which both components were loose. Radiolucent lines correctly predicted loosening in 46% of the components intraoperatively graded as loose (8 of 19 loose femoral components and 5 of 9 loose tibial components). However, radiolucent lines were absent in 54% of the components intraoperatively graded as loose (11 of 19 loose femoral components and 4 of 9 loose tibial components). In addition, radiolucent lines falsely predicted loosening in 35% of the components intraoperatively graded as well-fixed (3 of 8 well-fixed femoral components and 6 of 18 well-fixed tibial components).

Clinical outcomes and UKR component migration evident on follow-up radiographs corresponded to damage patterns on the polyethylene articular surfaces. Damage area on the polyethylene articular surfaces averaged 64% (SD 21%) (range, 27% to 98%) and was concentrated in the central and posterior regions of the articular surface. Higher grades of lateral OA at revision surgery were moderately correlated with smaller polyethylene damage areas (correlation coefficient = -0.40, p=0.04). Changes in femoral component tilt (correlation coefficient = 0.58, p=0.002) and tibial slope (correlation coefficient = 0.50, p=0.008) between immediate post-operative and pre-revision radiographs were significantly correlated with larger damage areas. The largest and most prevalent damage modes were abrasion, pitting and scratching (Figures 6.2, 6.3). There was abrasive damage on 24 (86%) inserts, including 17 (61%) inserts with damage consistent with impingement between the polyethylene insert and peripheral cement or bone (Figure 6.4). Such abrasion was concentrated on the articular periphery (Figure 6.5) and was significantly correlated with longer duration of function (correlation coefficient

= 0.45, p=0.02), larger damage area (correlation coefficient = 0.59, p=0.001), and lower Knee Society Scores for pain at the pre-revision evaluation (correlation coefficient = -0.47, p=0.01). Seventy eight percent of the tibial components that were loose at revision surgery had evidence of peripheral abrasion. There was a moderate correlation between abrasive damage and a change in femoral component tilt (correlation coefficient = 0.40, p=0.04).

Deformation of polyethylene articular surface corresponded to limb alignment and component position. Contact with the femoral component resulted in a concave depression on the polyethylene articular surface (Figure 6.6), with maximum deformation occurring in regions of abrasion (6 inserts), burnishing, striations or fracture (5 inserts each), pitting (4 inserts) or scratching (3 inserts). These depressions were externally rotated on 17 (61%) inserts, consistent with tibial external rotation relative to the femoral component, neutrally aligned on 7 (25%) inserts, internally rotated on 1 (4%) inserts, and indeterminate on 3 (11%) inserts. Maximum surface deformation averaged 1.251 (SD 0.979) mm (range, 0.079 to 3.932 mm). Changes in limb alignment (correlation coefficient = 0.42, p=0.03) and tibial component slope (correlation coefficient = 0.64, p<0.001) were moderately correlated with greater deformation rates. Five (18%) inserts had complete polyethylene wear-through to the metal surface, corresponding to the highest magnitude and rate of surface deformation (Figure 6.7). Excluding those five inserts, the surface deformation rate averaged 0.145 (SD 0.065) mm/year and gradually decreased with longer duration of function (linear regression, R^2=0.3, p=0.013).

6.4 Conclusions

This study compared clinical and radiographic outcomes after UKR with polyethylene damage patterns on unconstrained UKR retrieved after an average of 79

months of *in vivo* function. Intraoperative assessments of component loosening and progressive degenerative changes were not correctly predicted by evaluation of radiolucent lines and OA on pre-revision radiographs. Limb alignment and component position corresponded to damage patterns on the polyethylene articular surfaces. Osteolysis at the implant-bone interface was largely absent in this series, occurring at the tibial interface in only one knee. This suggests that factors other than biological degradation of the bone interface contributed to the observed loosening.

Although initial limb alignment was restored in a majority of the knees, femoral and tibial component position varied widely and changes in component position were associated with increased polyethylene wear. Aseptic loosening was the most common reason for revision, similar to previous studies of UKR prostheses,[7,8,19] occurring with approximately two-thirds of the femoral components and one-third of the tibial components at revision surgery. Component loosening and progressive degenerative changes were difficult to predict from radiolucent lines and OA on pre-revision radiographs.

Surgical alignment was acceptable as evidenced by the achievement of initial valgus limb alignment for all but two UKR on immediate post-operative radiographs. However, there was a shift to varus in approximately one-third of the knees on radiographs obtained prior to revision surgery. Recurrent varus limb alignment at revision was predicted by initial correction of limb alignment at the index UKR, similar to previous reports.[20] Tibial and femoral component tilt varied widely on post-operative radiographs, with 59% to 70% of the tibial and femoral components aligned with more than 3°deviation from 90°. Initial tibial component slope averaged 12° and was greater than 7° in 78% of knees with loose tibial components assessed at revision surgery.

This magnitude of deviation in initial component alignment has consequences for altered load distribution and wear at the tibiofemoral articulation,[20,23] and is associated with poor clinical outcomes.[11,19,38,40] Such variability in position reflects the difficulty of the surgical technique and is typical of bone cutting errors reported for knee arthroplasty instrumentation contemporary to that used in the current study.[34] However, some of the success of unconstrained UKR designs[1,8,21,39] may be related to the freedom of placement available to the surgeon due to the flat tibial articular geometry, accommodating a range of initial component positions.

Although femoral component loosening after UKR is considered rare,[7,29] some designs have historically poor results related to lack of femoral component fixation.[21,25,27,29,37] Femoral component design and the orientation of the fixation surfaces relative to the joint load are significant factors affecting cement stress and femoral component loosening after UKR.[37] In the current study, the prevalence of femoral component loosening of the Tönnis prostheses was more than double that of tibial component loosening. Poor cement interlock on the flat, smooth femoral component surfaces, combined with femoral components placed in a flexed orientation, may have affected the long-term fixation for the Tönnis femoral components.

Accommodation of varied component positions and tibiofemoral axial rotation during activity was demonstrated by the rotated concave deformations on the polyethylene articular surfaces due to femoral contact (Figure 6.6). This deformation is inclusive of articular damage due to visco-plastic deformation (creep) and material loss due to wear. Increased magnitude of surface deformation was exponentially related to longer duration of function and corresponded to limb alignment and component position, similar

to previous reports.[2] Although initial tibiofemoral incongruity of unconstrained UKR has led to concerns of high contact stress,[5] these deformations may have reduced polyethylene contact stresses by increasing tibio-femoral congruity.[9]

The number of inserts with delamination or subsurface cracks was low compared to the prevalence of other damage modes (Figure 6.4) and there was little evidence of gamma radiation induced degradation. This is consistent with the maintenance of contact stresses below the range associated with material failure.[4,31] Alternately, embrittled polyethylene material may have been removed due to abrasive wear mechanisms. Five inserts with wear-through to metal had some of the highest deformation rates (Figure 6.7), similar to previous reports.[30,42] Exclusion of those five inserts resulted in a mean deformation rate of 145 μm/year, with a gradual decline in deformation rate with longer duration of function (Figure 6.7). This magnitude is similar to the 0.15 mm/year previously reported for the St. Georg Sled UKR[2] and within the range previously reported for other UKR designs.[2,3,30,35,42]

Abrasive damage on the articular periphery (Figure 6.5) due to contact between the polyethylene insert and extra-articular bone or cement are not unique to fixed-bearing UKR. Retrieved mobile bearing UKR show a 63%-83% prevalence of impingement,[3,35] resulting in five times higher rate of polyethylene deformation compared to bearings without impingement.[35] In total knee replacement (TKR), component size and posterior offset of the femoral condyle are correlated with component impingement and abrasive damage.[6,17,18,32] Possible etiology for extra-articular bone includes degenerative stenosis of the intracondylar notch after UKR.[11] Maintaining proper component alignment is essential for reducing this type of wear, as femoral component migration was correlated with peripheral abrasive damage. Unintended contact between rough surfaces and the

tibial insert has consequences for polyethylene debris generation and transmission of shear forces to the bone-implant interface.

In conclusion, UKR remains an infrequent procedure for many surgeons, with TKR prostheses utilized seven times more frequently than UKR prostheses.[39] Rigorous attention to clinical symptoms and careful interpretation of radiographic phenomena are needed to determine indications for revision in UKR patients. Providing surgical techniques and instrumentation to aid alignment and fixation may prove useful toward increasing the longevity of UKR.[25,40,41]

6.5 Acknowledgement

The author thanks Sabine Schmitt, MD, Sven Rössing, MD, Scott A. Banks, PhD, Hans-Peter Sharf, MD, and W. Andrew Hodge, MD for co-authoring publication of this work. The author thanks Sabine Schmitt, MD for providing retrieved UKR components, radiographic data and for translating patient medical records. This work was supported by funding from The BioMotion Foundation in Palm Beach, Florida, with partial funding provided by an institutional research grant from WALDEMAR LINK GmbH & Co., Hamburg, Germany, and University Hospital Mannheim, Mannheim, Germany.

Note: This work has been submitted for publication and is referenced as follows.

Melinda K. Harman, Sabine Schmitt, Sven Rössing, Scott A. Banks, Hans-Peter Sharf, W. Andrew Hodge: Polyethylene damage area and deformation on unicondylar knee prostheses retrieved after 2 to 13 years of functional duration. *ACTA Orthop*. 2006; submitted.

6.6 References Cited

1. Ackroyd CE, Whitehouse SL, Newman JH, Joslin CC. Survivorship of the St. Georg Sled medial unicompartmental knee replacement beyond 10 years. *J Bone Joint Surg Br.* 2006; 88(9):1164-8.

2. Ashraf T, Newman JH, Desai VV, Beard D, Nevelos JE. Polyethylene wear in a non-congruous unicompartmental knee replacement: A retrieval analysis. *The Knee*. 2004; 11:177-81.

3. Argenson JN, O'Connor JJ. Polyethylene wear in meniscal knee replacement: A one to nine year retrieval analysis of the Oxford knee. *J Bone Joint Surg Br*. 1992; 74(2):228-32.

4. Bartel DL, Rawlinson JJ, Burstein AH, Ranawat CS, Flynn WF. Stresses in polyethylene components of contemporary total knee replacements. *Clin Orthop*. 1995; 317:76-82.

5. Bartley RE, Stulberg SD, Robb WJ, Sweeney HJ. Polyethylene wear in unicompartmental knee arthroplasty. *Clin Orthop*. 1994; 299:18-24.

6. Bellemans J, Banks SA, Victor J, Vandenneuker H, Moermans A. Fluoroscopic analysis of deep flexion kinematics in total knee arthroplasty: The influence of posterior condylar offset. *J Bone Joint Surg Br*. 2002; 84:50-3.

7. Bohm I, Landsiedl F. Revision surgery after failed unicompartmental knee arthroplasty: A study of 35 cases. *J Arthroplasty*. 2000; 15(8):982-9.

8. Callahan CM, Drake BG, Heck DA, Dittus RS. Patient outcomes following unicompartmental or bicompartmental knee arthroplasty: A meta-analysis. *J Arthroplasty*. 1995; 10(2):141-50.

9. Cho CH, Murakami T, Sawae Y, Sakai N, Miura H, Kawano T, Iwamoto Y. Elasto-plastic contact analysis of ultra-high molecular weight polyethylene tibial component based on geometrical measurement from a retrieved knee prosthesis. *Proc Instn Mech Engrs Part H: J Engineering in Medicine.* 2004; 218:251-259.

10. Cornwall GB, Bryant JT, Hansson CM, Rudan J, Kennedy LA, Cooke TD. A quantitative technique for reporting surface degradation patterns of UHMWPE components of retrieved total knee replacements. *J Appl Biomater*. 1995; 6:9-18.

11. Emerson RH, Head WC, Peters PC. Soft-tissue balance and alignment in medial unicompartmental knee arthroplasty. J Bone Joint Surg Br 1992; 74(6):807-10.

12. Ewald FC. The Knee Society total knee arthroplasty roentgenographic evaluation and scoring system. *Clin Orthop*. 1989; 248:9-12.

13. Goodfellow JW, Kershaw CJ, D'a Benson MK, O'Connor JJ. The Oxford knee for unicompartmental osteoarthritis: The first 103 cases. *J Bone and Joint Surg Br*. 1988; 70(5):692-701.

14. Harman MK, Markovich GD, Banks SA, Hodge WA. Wear patterns on tibial plateaus from varus and valgus osteoarthritic knees. *Clin Orthop*. 1998; 352:149-58.

15. Harman MK, Banks SA, Hodge WA. Organization of a post-mortem implant retrieval program. 67th Annual Meeting of the American Academy of Orthopaedic Surgeons, San Francisco, CA, 2000.

16. Harman MK, Banks SA, Hodge WA. Polyethylene damage and knee kinematics after total knee arthroplasty. *Clin Orthop*. 2001; 392:383-93.

17. Harman MK, Banks SA, Hodge WA. Component size selection in total knee replacement: Implications for impingement and abrasive polyethylene wear. Proceedings of the 15th Annual Symposium of the International Society for Technology in Arthoplasty (ISTA), Oxford, England, 2002.

18. Harman MK, Banks SA, Hodge WA. Does backside damage correspond to articular damage in retrieved TKA polyethylene inserts? *Clin Orthop*. 2007; in press.

19. Hernigou P, Deschamps G. Posterior slope of the tibial implant and the outcome of unicompartmental knee arthroplasty. *J Bone and Joint Surg Am*. 2004; 86(3):506-11.

20. Hernigou P, Deschamps G. Alignment influences wear in the knee after medial unicompartmental arthroplasty. *Clin Orthop*. 2004; 423:161-5.

21. Hodge WA, Chandler HP. Unicompartmental knee replacement: A comparison of constrained and unconstrained designs. *J Bone Joint Surg Am*. 1992; 74(6):877-83.

22. Hood RW, Wright TM, Burstein AH. Retrieval analysis of total knee prostheses: A method and its application to 48 total condylar prostheses. *J Biomed Mater Res*. 1983; 17:829-42.

23. Hsu HP, Garg A, Walker PS, Spector M, Ewald FC. Effect of knee component alignment on tibial load distribution with clinical correlation. *Clin Orthop*. 1989; 248:135-44.

24. Insall JN, Dorr LD, Scott RD, Scott WN. Rationale of the Knee Society clinical rating system. *Clin Orthop*. 1989;248:13-14.

25. Jenny JY, Boeri C. Unicompartmental knee prosthesis implantation with a non-image-based navigation system: Rationale, technique, case-control comparative study with a conventional instrumented implantation. *Knee Surg Sports Traumatol Arthrosc*. 2003; 11:40-5.

26. Jonsson GT. Compartment arthroplasty for gonarthrosis. *Acta Orthop Scand*. 1981; 193-210.

27. Lewold S, Godman S, Knutson K, Robertsson O, Lidgren L. Oxford meniscal bearing knee versus the Marmor knee in unicompartmental arthroplasty for arthrosis: A Swedish multicenter survival study. *J Arthroplasty*. 1995; 10(6):722-31.

28. Lewold S, Robertsson O, Knutson K, Lidgren L. Revision of unicompartmental knee arthroplasty: Outcome in 1,135 cases from the Swedish Knee Arthroplasty study. *Acta Orthop Scand*. 1998; 69(5):469-74.

29. Lindstrand A, Stenström A, Lewold S. Multicenter study of unicompartmental knee revision: PCA, Marmor, and St. Georg compared in 3,777 cases of arthrosis. *Acta Orthop Scand*. 1992; 63:256-9.

30. McGovern TF, Ammeen DJ, Collier JP, Currier BH, Engh GA. Rapid polyethylene failure of unicondylar tibial components sterilized with gamma radiation in air and implanted after a long shelf life. *J Bone Joint Surg Am*. 2002; 84(6):901-6.

31. Morra EA, Harman MK, Greenwald AS. Computational models can predict polymer insert damage in total knee replacements. In: Insall & Scott Surgery of the Knee, 4th edition (Ed. Scott WN) Churchill Livingstone Elsevier Philadelphia 2005; 13: 271-83.

32. Noble PC, Conditt MA, Thompson MT, Stein JA, Kreuzer S, Parsley BS, Mathis KB. Extraarticular abrasive wear in cemented and cementless total knee arthroplasty. *Clin Orthop*. 2003; 416:120-8.

33. Outerbridge RE. The etiology of chondromalacia patellae. *J Bone Joint Surg Br*. 1961; 43:752-7.

34. Plaskos C, Hodgson AJ, Inkpen K, McGraw RW. Bone cutting errors in total knee arthroplasty. *J Arthroplasty*. 2002; 17(6):698-705.

35. Psychoyios V, Crawford RW, O'Connor JJ, Murray DW. Wear of congruent meniscal bearings in unicompartmental knee arthroplasty. *J Bone Joint Surg Br*. 1998; 80(6):976-82.

36. Rao A, Engh G, Collier M, Smain L. Tibial interface wear in retrieved total knee components and correlations with modular insert motion. *J Bone Joint Surg Am*. 2002; 84(10):1849-55.

37. Riebel GD, Werner FW, Ayers DC, Bromka J, Murray DG. Early failure of the femoral component in unicompartmental knee arthroplasty. *J Arthroplasty*. 1995; 10(5):615-21.

38. Ritter MA, Faris PM, Keating EM, Meding JB. Postoperative alignment of total knee replacement: Its effect on survival. *Clin Orthop*. 1994; 299:153-6.

39. Robertsson O, Knutson K, Lewold S, Lidgren L. The Swedish knee arthroplasty register: Outcomes with special emphasis on 1988-1997. 68th Annual Meeting of the American Academy of Orthopaedic Surgeons, San Francisco, CA, 2001.

40. Swienckowski J, Page BJ. Medial unicompartmental arthroplasty of the knee: Use of the L-cut and comparison with the tibial inset method. *Clin Orthop*. 1989; 239:161-7.

41. Weale AE, Murray DW, Baines J, Newman JH. Radiological changes five years after unicompartmental knee replacement. *J Bone Joint Surg Br*. 2000; 82(7):996-1000.

42. Williams IR, Mayor MB, Collier JP. The impact of sterilization method on wear in knee arthroplasty. *Clin Orthop*. 1998; 356:170-80.

43. Wimmer M, Andriacchi T, Natarajan R, Loos J, Karlhuber M. A striated pattern of wear in ultrahigh-molecular-weight polyethylene components of Miller-Galante total knee arthroplasty. *J Arthroplasty*. 1998; 13(1):8-16.

Table 6.1: Knee Society Scores (mean, standard deviation)

	Pain	Function
Pre-operative	37±14 (range, -5 to 65)	44±9 (range, 20 to 55)
Post-operative	87±10 (range, 46 to 97)	76±10 (range, 50 to 90)
Pre-revision	53±18 (range, 13 to 90)	43±11 (range, 30 to 60)

Table 6.2: Radiographic Data for Retrieved UKR (mean, standard deviation, range)

	Frontal Plane		Sagittal Plane	
	Limb alignment[1]	Tibial tilt[2]	Femoral tilt[3]	Tibial slope[4]
Pre-operative (n=25)	3°±3° varus (-3° to 10°)	-	-	-
Post-operative (n=26)	-3°±3° valgus (-8° to 5°)	-3°±5° (-14° to 8°)	-7°±6° (-20° to 5°)	12°±6° (-21° to 3°)
Pre-revision (n=27)	0°±6° (-9° to 14°)	-2°±7° (-15° to 15°)	-7°±7° (-20° to 5°)	14°±5° (-21° to -4°)
Change post-operative to pre-revision	3°±4° (0° to 17°)	4°±5° (0° to 20°)	3°±3° (0° to 10°)	4°±5° (0° to 23°)

[1] negative = valgus, positive = varus

[2] negative = medial tilt, positive = lateral tilt

[3] negative = femoral flexion, positive = femoral extension

[4] negative = posterior slope, positive = anterior tilt

Table 6.3: Frequency (% Total Number of Knees) of Osteoarthritis Grades at Revision Surgery

Degeneration	Grade I	Grade II	Grade III	Grade IV
Lateral compartment	11%	33%	33%	22%
Retropatellar compartment	4%	37%	33%	26%

Table 6.4: Frequency (% Total Number of Knees) of Radiographic Phenomena and Intraoperative Assessments of Component Fixation

	Osteolysis	Radiolucent Lines	Intraoperative Loosening
None	96%	37%	26%
Femoral Component Only	0	22%	41%
Tibial Component Only	4%	22%	4%
Both Femoral and Tibial Components	0	19%	30%

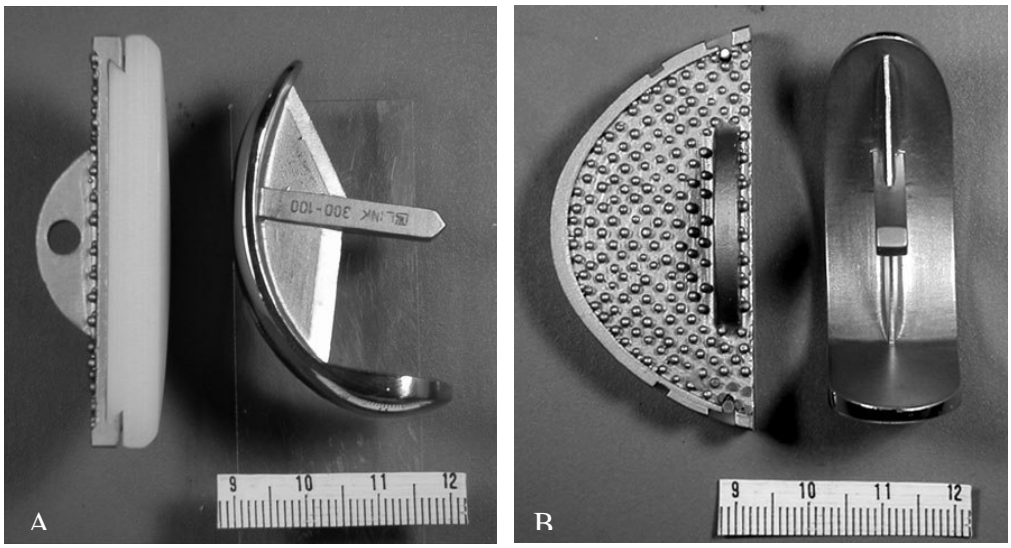

Figure 6.1: Articular Geometry (A) and Fixation Surfaces (B)

of the Femoral and Tibial Components

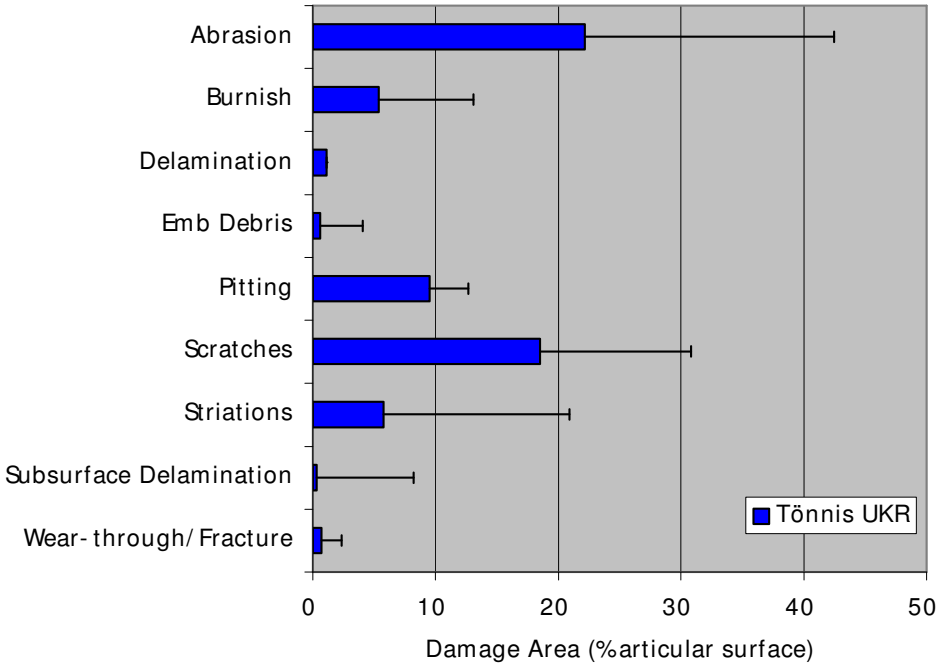

Figure 6.2: Damage Areas on the Retrieved UKR Tibial Components

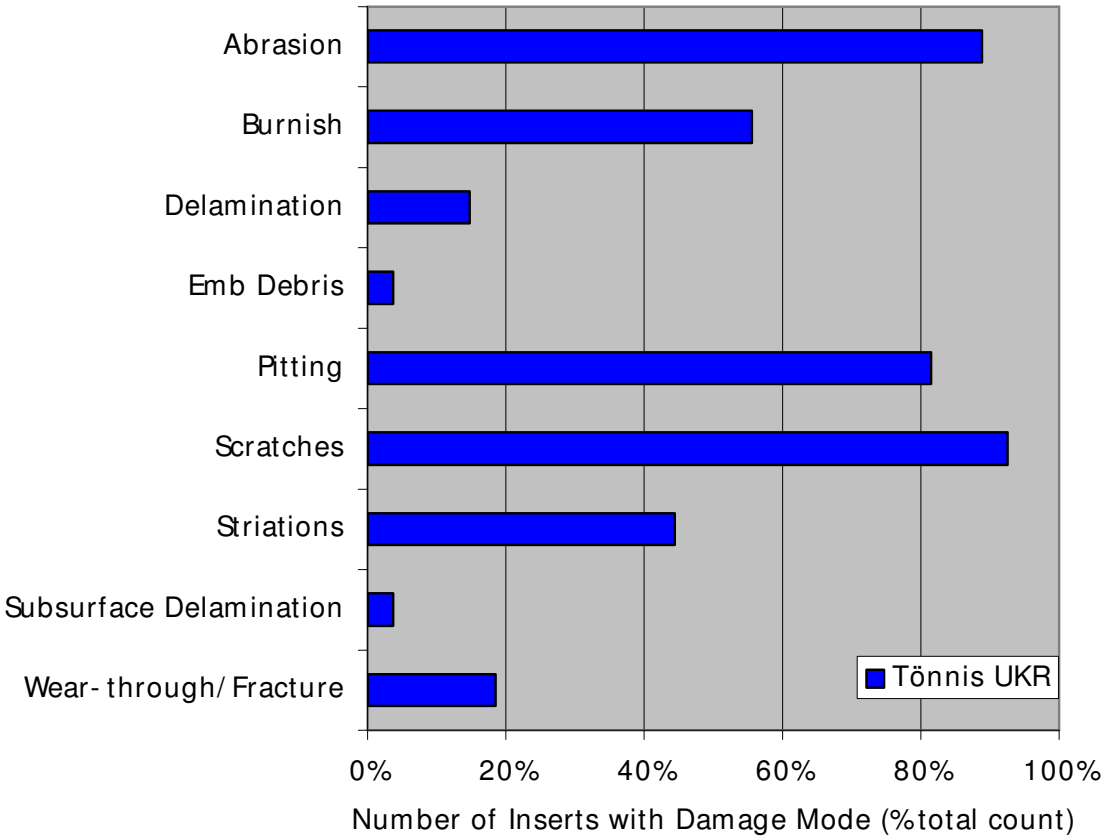

Figure 6.3: Prevalence of Different Damage Modes on the Retrieved UKR Tibial Components

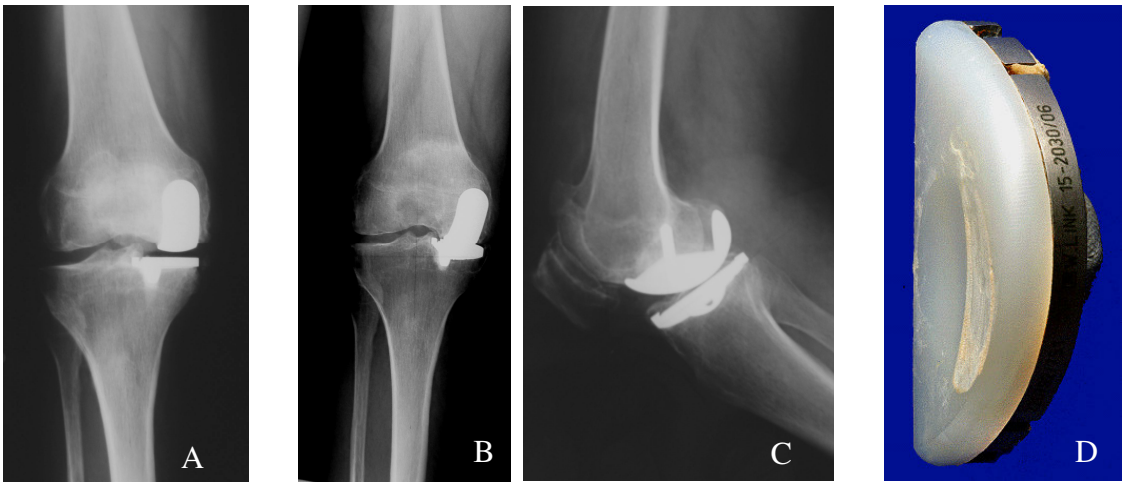

Figure 6.4: Pre-operative (A) and Pre-revision (B, C) Radiographs of Retrieved UKR UKR was retrieved from an 87 year old female (weight=60 kg, height=150 cm) whose right knee prosthesis was revised for aseptic loosening after 89 months (specimen #K2027_04L). Prominent surface deformation and abrasive damage was noted on the polyethylene articular surface (D).

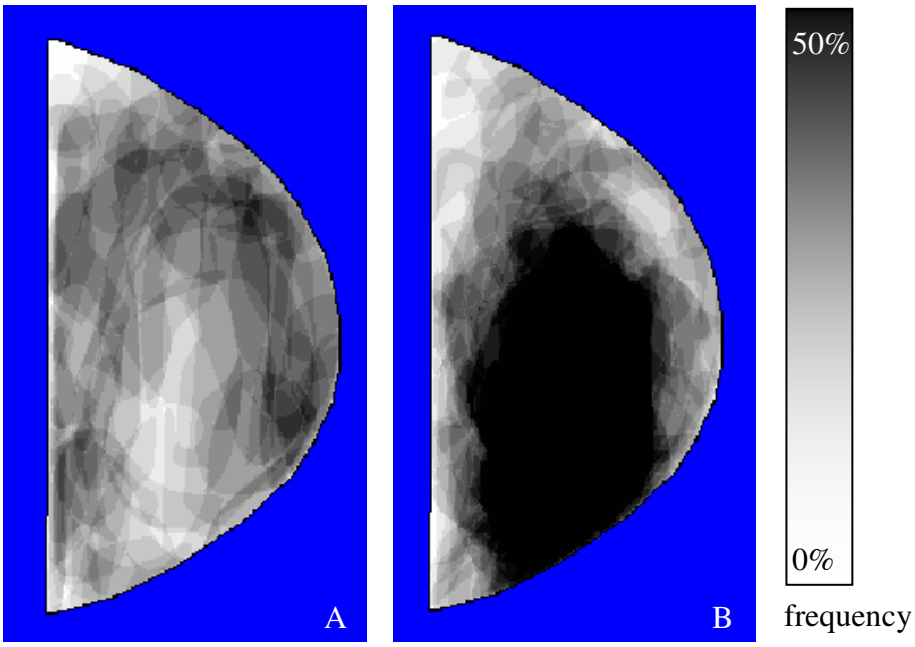

Figure 6.5: Graphic Overlay Depicting Damage Patterns for All UKR Inserts Increasing grayscale density (darker) indicates a greater number of inserts had damage in a given location, with black consistent with at least 50% of inserts having damage. Abrasive damage was concentrated on the periphery of the articular surface (A). All other damage modes were concentrated in the central and posterior articular surface (B).

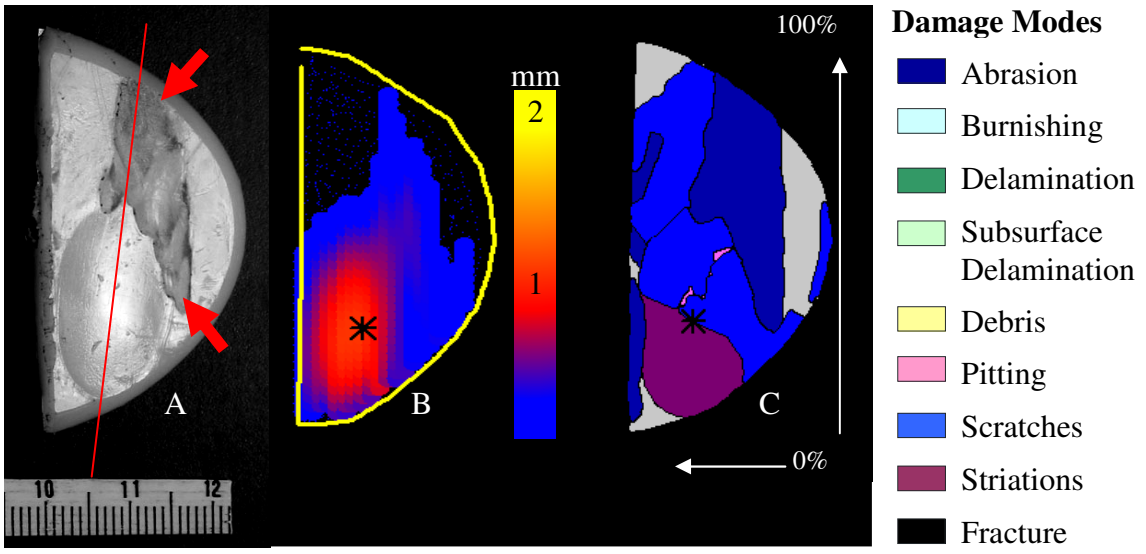

Figure 6.6: Left Medial UKR Polyethylene Insert

This insert (#K2022_04L) was retrieved from an 81 year old male after revision for aseptic loosening after 72 months. Prominent surface deformation (A) was oriented consistent with tibial external rotation (red line) adjacent to abrasive wear (red arrows), with maximum deformation (*) of 1.227 mm (B). 81% of the articular surface was damaged with scratches, striations and pitting occurring in the deformed region, surrounded by scratches and abrasion (C).

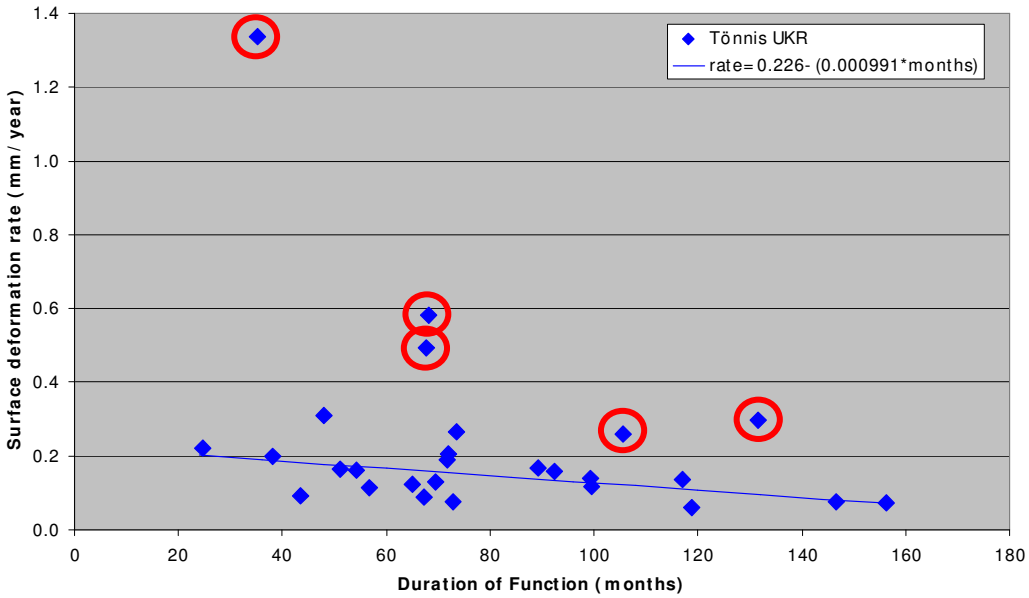

Figure 6.7: Surface Deformation Rate Versus Duration of Function

Five inserts with polyethylene wear-through to the metal surface (red circled data points) had high deformation rates. Excluding those components, the deformation rate averaged 0.145±0.065 mm/year, decreasing linearly with time.

7 ASSOCIATION BETWEEN DISLOCATION, IMPINGEMENT AND ARTICULAR GEOMETRY IN RETRIEVED ACETABULAR POLYETHYLENE CUPS

7.1 Introduction

Dislocation occurs in 2% to 11% of primary total hip replacements (THR) and its prevalence is affected by many clinical[5,6,11,12,17,22] and component design[1,2,3,4,16,19] factors. Design parameters specific to the polyethylene liner, such as elevating the rim or deepening the articular surface, affect THR stability through greater femoral head coverage and larger moments resisting dislocation.[16,19] These parameters alter the head center inset, which is the distance between the polyethylene liner rim and the femoral head center in the articular surface, potentially decreasing the available range of motion before prosthetic impingement.[16,19] However, the relationship between impingement and dislocation is unclear, as impingement can occur in THR with or without a clinical history of dislocation.[20,24]

The prevalence of impingement damage ranges from 39% to 56% among retrieved acetabular polyethylene liners.[10,20,24] Liners with elevated rims exhibit a higher frequency of impingement damage compared to liners with neutral rim elevation.[20,24] However, the magnitude of head center inset is an infrequently reported design parameter,[16,21] making it difficult to discern its role in impingement and dislocation.

The primary objective of this study is to assess relationships between impingement damage, dislocation history and acetabular polyethylene liner geometry using a consecutive series of retrieved liners with neutral rim elevation. It was hypothesized that: 1) liners with impingement damage would have a deeper head center inset than liners without impingement; and 2) liners with dislocation would have a shallower head center inset than stable liners.

7.2 Materials and Methods

Modular and all-polyethylene acetabular components from multiple manufacturers were consecutively retrieved[9] from 1994 through 2003. Forty eight polyethylene liners with neutral rim elevation and mated with 28 mm (30 liners) or 32 mm (18 liners) femoral heads were included. Liners with extended or elevated rims, those with severe removal damage, those without available medical records and all others not meeting inclusion criteria were excluded. Femoral head modularity was monoblock (14 liners), modular (29 liners), and unknown (5 liners), including three heads with extended flanged necks. The head/neck ratio was known for 26 THR and averaged 2.18 (range, 1.63 to 3.36). There were 21 male and 27 female patients with a mean age of 69 years (44 to 88) at retrieval and a mean body weight of 78 kg (42 to 122). Median duration of function was 108 months (1 to 288). Twelve of 48 hips had a documented history of dislocation. Reasons for removal were loosening in 24 hips (including 1 dislocated hip), instability in 9 hips (including 9 dislocated hips), polyethylene wear in 7 hips, infection in 4 hips, osteolysis in 3 hips (including 2 dislocated hips), and autopsy in 1 hip.

Liner design was classified into three types depending on the presence of an inner rim chamfer or bevel (Figure 7.1). Peripheral rim damage consistent with impingement between the liner rim and the femoral head or stem neck[20,24] was assessed at up to 30 times magnification using an optical stereomicroscope (Figure 7.2). The extent of impingement damage into the liner rim was measured in the direction of the liner radius and graded as minimum if it extended <4 mm, moderate if it extended 4 mm to 7 mm; and severe if it extended to the outer edge or >7 mm.[24]

Liner articular geometry was measured using a digital stylus (MicroScribe 3DX; Immersion Corp., San Jose, CA) with an instrument resolution of 0.13 mm and an accuracy of 0.30 mm. Each liner was secured to a horizontal work surface with the articular surface directed upward. Three-dimensional coordinate points were digitized with the stylus tip contacting the inner liner rim and outer liner rim, taking care to avoid damaged regions. Surface deformation was measured using a spherical 28 mm or 32 mm diameter femoral head attached to the stylus tip, matching each liner's inner diameter (Figure 7.3). The sphere was positioned in two distinct contours for each liner, consistent with unworn and worn articular regions. The worn contour was visually distinguished by its highly reflective and polished appearance compared to the less polished and discolored unworn contour.[13,14] The worn contour was also distinguished by manually sensing the transition ridge creating a well-formed demarcation between the worn and unworn contour, as reported in previous retrieval studies.[13,14]

Geometric relationships between the liner rim and femoral head were characterized by lip height and head center inset (Figure 7.3). A curve fitting routine using the linear least-square method was applied to the outer and inner rim points, with a

residual error of 0.018 mm. Image analysis routines were implemented to correct liner tilt such that the outer rim curve was oriented level with the horizontal plane of the work surface (cup tilt < 0.01°). All other digitized points were then transformed using the same rotation matrix and the geometric centroids of the outer rim and inner rim curves were calculated in the horizontal plane. Lip height was the distance between the outer rim centroid and head center (ORu and ORw). Head center inset was the distance between the inner rim centroid and head center (IRu and IRw). The three-dimensional magnitude of head penetration into the polyethylene liner was calculated as the vector length between the head center positioned in the unworn and worn contours (HCw) and normalized to duration of function as penetration rate (HCw/year). The method repeatability was assessed by measuring six acetabular liners on seven different occasions. Measurement repeatability was 0.125 mm for lip height and head center inset and 0.203 mm for head center penetration (HCw), inclusive of error due to set-up, digitizing and image analysis.

Statistical relationships between patient demographic variables, liner geometry type, impingement damage, dislocation history, and measured liner articular geometry were determined using analysis of variance with appropriate post hoc multiple comparisons for parametric (Tukey test) or nonparametric (Dunn's method) data. Strength of associations between variables were determined using Spearman's bivariate rank order correlation and distributions of categorical data were compared using Chi Square or Fisher's Exact test.

7.3 Results

Seventy one percent of retrieved acetabular liners were chamfered rim (type A), 10% were beveled rim (type B), and 19% were flat-rimmed (Type C). Liner design was significantly correlated with the unworn lip height (ORu) ($p=0.003$) and head center inset (IRu) ($p=0.007$), (Table 7.1). However, liner design was not correlated with the presence of impingement damage ($p=0.193$) or dislocation ($p=0.734$). Type C designs had significantly shorter functional duration, less head penetration (HCw) and a lower penetration rate (HCw/year) than Type A and Type B designs (Table 7.1). There were no significant differences between Type A and Type B designs comparing functional duration, HCw or HCw/year. There was a significant correlation between HCw and the duration of function ($r=0.7$, $p=0.001$) and liners mated with 32 mm diameter heads had significantly greater HCw/year compared to liners mated with 28 mm diameter heads (Dunn's method, $p=0.003$). HCw/year was significantly greater in liners revised for polyethylene wear or osteolysis compared to those revised for loosening or instability ($p=0.005$). HCw and HCw/year were not significantly correlated to patient demographics, including age, gender, or body weight.

Impingement damage on the liner rim was noted on 13 (27%) liners and was graded as minimum for 9 liners and moderate for 4 liners. Contrary to the stated hypothesis, liners with impingement did not have a deeper head center inset. Head center inset in the unworn (IRu) and worn contours (IRw), lip height (ORu and ORw), head penetration (HCw and HCw/year), and duration of function were not significantly different for liners with impingement and those without impingement (Table 7.2). Impingement occurred on 27% of both the loose and well-fixed cups, and one of the three

modular heads with a flanged neck had impingement. Impingement was not correlated with duration of function, reason for revision, liner design type or head size.

Similar to the results for impingement damage, dislocation was not correlated to head size or liner design type, with similar lip height for dislocated and stable liners (Table 7.3). However, dislocation was significantly correlated with a shallower head center inset, consistent with the stated hypothesis. Head center inset in the unworn (IRu) and worn contours (IRw) was significantly lower for dislocated liners. IRu was less than 0.95 mm in all dislocated liners, including 10 dislocated liners with IRu less than 0.57 mm. Dislocated liners had significantly shorter duration of function, shorter HCw and shorter HCw/year than stable liners. Only three of the 12 dislocated hips had a functional duration longer than five years.

There was a weak correlation between liners with impingement damage and a clinical history of dislocation ($r=0.3$, $p=0.04$). Six of the 12 (50%) dislocated liners had impingement damage compared to seven of 36 (19%) stable liners. However, the proportion of liners with impingement was not significantly different among dislocated and stable liners (Fisher's Exact Test, $p=0.06$). Head/neck ratio was known for only two liners with impingement and one liner with dislocation precluding statistical analysis of that stem design feature.

7.4 Conclusions

This study evaluated the relationship between impingement damage, THR dislocation history and liner geometry using a consecutive series of retrieved polyethylene liners with neutral rim elevation. The magnitude of lip height and head center inset was measured in an effort to discern the role of these design parameters in

impingement and dislocation. The novel method provided a direct, three-dimensional measurement of femoral head penetration into the polyethylene liners. This method avoided the complexities of making two-dimensional measurements from acrylic casts of worn liners[14,23] or identifying hundreds of articular points.[7]

Femoral head penetration into polyethylene liners, due to wear and creep deformation, effectively increases the distance between the femoral head center and liner rim. Such head penetration is associated with late dislocation,[18] decreased range of motion,[1,23] and rim impingement damage on retrieved acetabular liners.[10,20,24] In the current study, head penetration was not a factor in impingement damage (Table 7.2) and increased penetration did not exist in dislocated liners (Table 7.3). Rather, initial head center inset was a significant factor associated with the prevalence of dislocation in these THR patients.

Although several studies have explored the relationships between liner geometry and dislocation,[1,15,19,20,23] few report the magnitude of head center inset.[16,19,21] Using finite element analysis, Scifert, et al.[19] showed that the peak moment resisting dislocation increases 5.8% for every millimeter of increased head center inset. Letournel and Lagrange[16] described an acetabular component with an articular surface 3 mm deeper than a hemisphere to capture the femoral head and prevent dislocation. Despite improved stability, both of those studies[16,19] reported reduced range of motion, with greater head center inset increasing the potential risk of impingement damage.

It is difficult to estimate the magnitude of head center inset needed to have an impact on clinical stability. In the current study, head center inset was 0.53 mm deeper in stable liners than dislocated liners. According to analytical models,[19] this magnitude of

increase in head center inset would approximate a 3% increase in the torque necessary to dislocate the femoral head. An equivalent change in the moment has been estimated for a 21% increase in the head/neck ratio,[19] with associated increased range of motion and decreased impingement damage.[24] Tanino, et al.[21] reported a 24% decrease in dislocation rate in patients receiving 1 mm head center inset liners compared to patients with 0 mm head center inset liners. These results from retrieved acetabular liners,[24] analytical models[19] and clinical studies[21] support using head center inset as a design parameter relevant to THR dislocation.

Liner design, as characterized by rim shape (Figure 7.1) and lip height, was not a factor in impingement damage or dislocation. Rather, the geometric relationship between the femoral head and the liner's inner rim was a significant factor in the prevalence of dislocation. Liners retrieved from patients with a dislocation history had significantly shallower articular surfaces (Table 7.3). The head center inset (IRu) was less than 0.57 mm in 83% and less than 0.95 mm in 100% of the dislocated liners. Thus, designing THR polyethylene liners with a sufficiently deep articular surface that exceeds 0.95 mm may prove beneficial for decreasing the prevalence of early dislocation, independent of impingement damage.

While retrieved polyethylene liners have been used to investigate the association between impingement damage and dislocation,[10,20,24] variations in rim elevation, smaller head sizes and the absence of head center inset measurements can preclude direct comparisons between studies. In the current study, there was a 27% incidence of impingement damage among the retrieved non-lipped polyethylene liners and impingement damage occurred on both dislocated and stable liners, similar to other

studies.[20,24] There was a 50% incidence of impingement among unstable THR and only a weak correlation between impingement and dislocation. In a study cohort of 99 retrieved liners, of which 94 had extended rims, Yamaguchi, et al.[24] reported a similar incidence of impingement in retrieved non-lipped liners (20%). Sixty-four percent of the unstable hips had impingement damage, but no association between impingement and dislocation was reported.[24] Retrieved Charnley cups with neutral rims and smaller (22 mm) head diameter have a higher incidence (48% to 64%) of impingement.[10,23] In a study cohort of 170 retrieved liners, Shon, et al.[20] reported a lower incidence of impingement in retrieved non-lipped liners (47%) compared to extended-rim liners (81%), with dislocated cups having a significantly higher prevalence (94%) of impingement damage.

Adding beveled rims on polyethylene liners[2] and increasing the head-to-neck diameter ratio[1,3,4] have been advocated to reduce the likelihood of impingement. Larger head diameters are associated with a lower prevalence of impingement damage,[24] but increased polyethylene wear rates.[14] High stresses and rim fracture due to impingement can occur even when large (40 mm) diameter heads are used.[8] In the current study, head/neck ratio averaged 2.18, similar to the 2.21 ratio reported for retrieved liners without impingement damage[24] and the 2.2 ratio considered as a transition value below which neck impingement against the liner can contribute to dislocation and decreased range of motion.[4,24]

Limitations with the current study are common to most studies of retrieved components. Confounding factors that can affect the prevalence of impingement and dislocation, such as surgical approach and initial component alignment,[5,6,17,22] could not be investigated in the current study. Included patients were referred from surgeons at

outside institutions and the original surgical notes, clinical follow-up records and adequate serial radiographs were unavailable in a majority of cases. Similarly, identification of component design and measurement of head/neck ratio were incomplete as components submitted for analysis were often limited to the liner and modular head. Duration of function exceeded 5 years for 60% and exceeded 10 years for 48% of the retrieved liners in this series. Therefore, the reported findings reflect intermediate to long-term performance.

It is recognized that impingement and dislocation are complex problems requiring many factors to be considered simultaneously. Our results suggest that acetabular liner articular geometry, specifically the depth of the articular surface relative to the polyethylene liner rim, is related to the prevalence of dislocation. These findings support using head center inset as a design criterion toward improving stability after THR. This study also reveals that in the observed range of head center insert for both the worn and unworn contours, impingement is not increased from shallow to deep liner geometry.

7.5 Acknowledgements

The author thanks Hiromasa Tanino, MD, Scott A. Banks, PhD, and W. Andrew Hodge, MD for co-authoring publication of this work. The author thanks W. Andrew Hodge, MD for providing retrieved THA components; Hiromasa Tanino, MD for summarizing clinical records and completing THR liner geometry measurements. This work was supported by funding from The BioMotion Foundation of Palm Beach, Florida.

Note: This work has been submitted for publication and is referenced as follows.

Hiromasa Tanino, MD; Melinda K. Harman, MSc; Scott A. Banks, PhD; and W. Andrew Hodge, MD: Association between dislocation, impingement and articular geometry in retrieved acetabular polyethylene cups. J Orthop Res 2007, in press.

7.6 References Cited

1. Amstutz HC, Lodwig RM, Schurman DJ, Hodgson AG. Range of motion studies for total hip replacements. *Clin Orthop*. 1975; 111:124-30.
2. Amstutz HC, Kody MH. Hip Arthroplasty. Amstuz HC ed. New York, NY: Churchill Livingstone 1991; 429-47.
3. Barrack RL. Dislocation after total hip arthroplasty: implant design and orientation. *J Am Acad Orthop Surg*. 2003; 11(2):89-99.
4. Bartz RL, Noble PC, Kadakia NR, Tullos HS. The effect of femoral component head size on posterior dislocation of the artificial hip joint. *J Bone Joint Surg Am*. 2000; 82(9):1300-7.
5. Berry DJ, von Knoch M, Schleck CD, Harmsen WS. The cumulative long-term risk of dislocation after primary Charnley total hip arthroplasty. *J Bone Joint Surg Am*. 2004; 86(1):9-14.
6. D'Lima DD, Urquhart AG, Buehler KO, et al. The effect of the orientation of the acetabular and femoral components on the range of motion of the hip at different head-neck ratios. *J Bone Joint Surg Am*. 2000; 82(3):315-21.
7. Hall RM, Unsworth A, Craig PS, et al. Measurement of wear in retrieved acetabular sockets. *Proceeding Instn Mech Engrs, Part H*. 1995; 209(4):233-42.
8. Halley D, Glassman A, Crowninshield RD. Recurrent dislocation after revision total hip replacement with a large prosthetic femoral head. *J Bone Joint Surg Am* 2004; 86(4):827-30.
9. Harman MK, Banks SA, Hodge WA. Organization of a post-mortem implant retrieval program. Transaction of the 67th Annual Meeting of the American Orthopaedic Surgeons 2000; 1: 610.
10. Isaac GH, Wroblewski BM, Atkinson JR, Dowson D. A tribological study of retrieved hip prostheses. *Clin Orthop*. 1992; 276:115-25.
11. Ito H, Matsuno T, Minami A, Aoki Y. Intermediate-term results after hybrid total hip arthroplasty for the treatment of dysplastic hips. *J Bone Joint Surg Am* 2003; 85(9):1725-32.
12. Ito H, Matsuno T, Aok Y, Minami A. Total hip arthroplasty using an Omniflex modular system: 5 to 12 years follow-up. *Clin Orthop*. 2004; 419:98-106.

13. Jasty M, Goetz DD, Bragdon CR, et al. Wear of polyethylene acetabular components in total hip arthroplasty. *J Bone Joint Surg Am*. 1997; 79(3):349-58.

14. Kabo JM, Gebhard JS, Loren G, Amstuz HC. In vivo wear of polyethylene acetabular components. *J Bone Joint Surg Br* 1993; 75(2):254-8.

15. Kelley SS, Lachiewicz PF, Hickman JM, Paterno SM. Relationship of femoral head and acetabular size to the prevalence of dislocation. *Clin Orthop*. 1998; 355:163-70.

16. Letournel E, Lagrange J. Lagranege-Letournel hip prosthesis: results of 1,355 cases. Proceeding of the third open scientific meeting of the Hip Society. 1975; 278-99.

17. Li E, Meding JB, Ritter MA, et al. The natural history of a posteriorly dislocated total hip replacement. *J Arthroplasty*. 1999; 14(8):964-8.

18. Orozco F, Hozack WJ. Late dislocations after cementless total hip arthroplasty resulting from polyethylene wear. *J Arthroplasty*. 2000; 15(8):1059-63.

19. Scifert CF, Brown TD, Pedersen DR, Callaghan JJ. A finite element analysis of factors influencing total hip dislocation. *Clin Orthop*. 1998; 355:152-62.

20. Shon WY, Baldini T, Peterson MG, Wright TM, Salvati EA. Impingement in total hip arthroplasty: A study of retrieved acetabular components. *J Arthroplasty*. 2005; 20(4):427-35.

21. Tanino H, Ito H, Banks S, Harman M, et al. Acetabular liner design affects clinical dislocation rate after THA. Transactions of the Orthop Res Soc. 2006; 31: 489.

22. Woo RY, Morrey BF. Dislocations after total hip arthroplasty. *J Bone Joint Surg Am.* 1982; 64(9):1295-306.

23. Wroblewski BM. Direction and rate of socket wear in Charnley low-friction arthroplasty. *J Bone Joint Surg Br* 1985; 67(5):757-61.

24. Yamaguchi M, Akisue T, Bauer TW, Hashimoto Y. The spatial location of impingement in total hip arthroplasty. *J Arthroplasty*. 2000; 15(3):305-13.

Table 7.1: Functional Duration, Lip Height, Head Center Inset, Penetration and Penetration Rate for Acetabular Liners Grouped According to Liner Design

	Type A	Type B	Type C	Total
n	34	5	9	48
Median Duration (months)	126	204	15[a]	108
ORu (mm)	2.53	4.44	0.98[a]	2.44±1.43
ORw (mm)	2.90	5.13	0.99[a]	2.77±1.69
IRu (mm)	0.55	0.76	0.98[b]	0.66±0.67
IRw (mm)	0.93	1.45	0.99	0.99±0.88
HCw (mm)	0.94	1.70	0.06[a]	0.85±0.95
HCw / year (mm)	0.08	0.19	0.01[a]	0.07±0.10

[a] Significantly different from Type A and Type B ($p<0.05$)

[b] Significantly different from Type A ($p<0.05$)

Table 7.2: Results of Acetabular Liners With and Without Impingement Damage

	Impingement	No Impingement	p
n	13	35	
Median Duration (months)	120	96	0.601
Head size (28/32 mm)	8/5	22/13	
Liner class (A/B/C)	11/1/1	23/4/8	
ORu (mm)	2.39±1.45	2.45±1.44	0.899
ORw (mm)	2.66±1.77	2.82±1.68	0.781
IRu (mm)	0.52±0.65	0.71±0.68	0.393
IRw (mm)	0.79±1.05	1.07±0.81	0.132
HCw (mm)	0.84±1.02	0.86±0.94	0.990
HCw / year (mm)	0.08±0.09	0.08±0.10	0.703

Table 7.3: Results of Acetabular Liners With and Without Dislocation

	Dislocation	No Dislocation	p
n	12	36	
Median Duration (months)	23	144	0.002
Head size (28/32 mm)	10/2	20/16	
Liner class (A/B/C)	9/1/2	25/4/7	
ORu (mm)	1.99±0.93	2.58±1.55	0.225
ORw (mm)	2.12±0.83	2.99±1.85	0.134
IRu (mm)	0.26±0.48	0.79±0.68	0.017
IRw (mm)	0.39±0.53	1.20±0.89	0.005
HCw (mm)	0.38±0.91	1.01±0.92	0.020
HCw / year (mm)	0.05±0.09	0.09±0.10	0.049

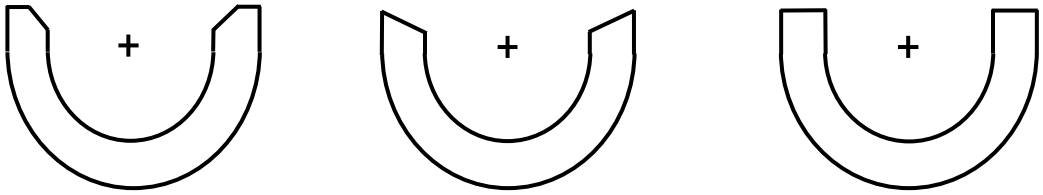

Figure 7.1: Three Types of Polyethylene Liner Designs

Type A had an inner chamfer, Type B had a bevel and Type C had neither an inner chamfer nor bevel.

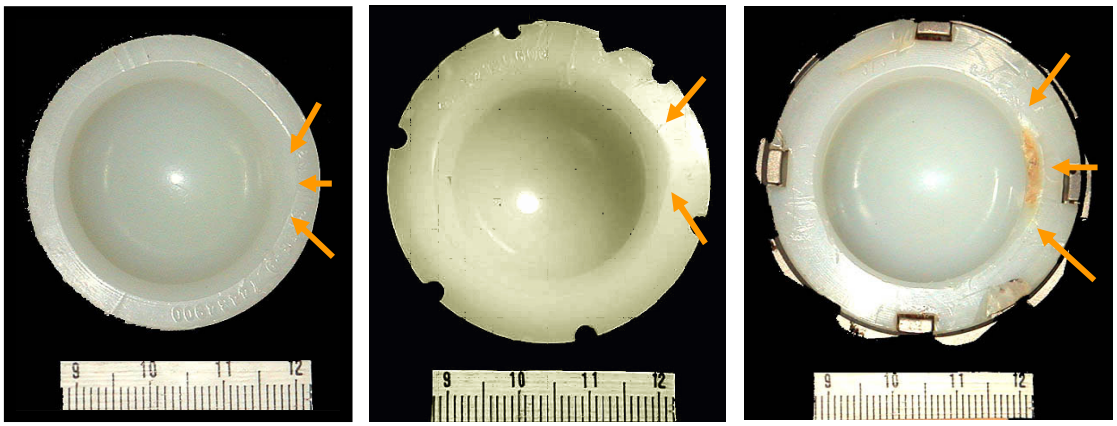

Figure 7.2: Acetabular Liners with Peripheral Rim Damage Consistent with Impingement

Liners were retrieved at autopsy after 70 months (left), for recurrent dislocation after 13 months (center), and for cup and stem loosening after 156 months (right).

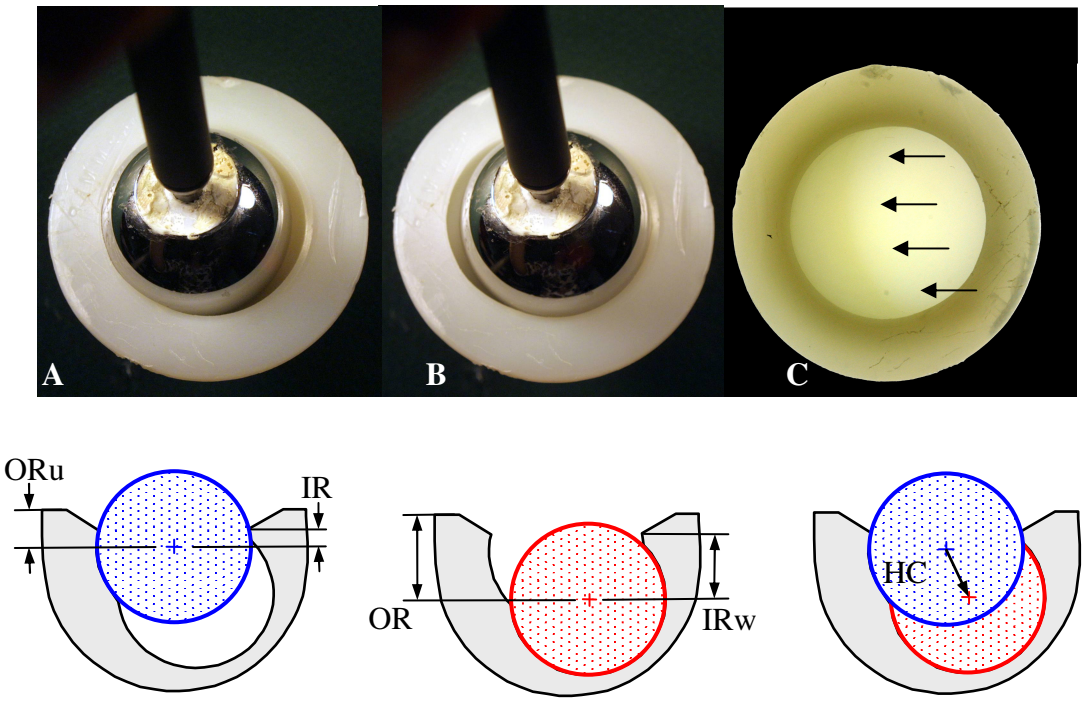

Figure 7.3: Measurement of Liner Geometry and Head Penetration

The measurement technique included locating a femoral head sphere in the unworn (A) and worn (B) contours of the polyethylene liner as demarked by a transitional ridge (C, arrows). Lip height was measured from the outer rim to the head center in the unworn (ORu) and worn (ORw) contours. Head center inset was measured from the inner rim to the head center in the unworn (IRu) and worn (IRw) contours. Head penetration (HCw) was the three-dimensional vector length between the sphere center in the unworn (shaded blue) and worn (shaded red) contours.

8 COMPARISON OF POLYETHYLENE TIBIAL INSERT DAMAGE FROM IN VIVO FUNCTION AND IN VITRO WEAR SIMULATION

8.1 Introduction

Knee joint wear simulation is used to mimic relevant *in vivo* physiologic function and to evaluate the wear properties of the tibiofemoral articulation in total knee replacements (TKR). In order for wear simulators to be useful in prospective evaluations, they should be able to reproduce clinical wear rates and wear mechanisms under conditions which replicate appropriate loads and displacements occurring in patient populations.[8,14,42,52,54] While methods exist for comparison of *in vitro* simulator and *in vivo* clinical wear rates in total hip replacements,[14,43] developing comparable methods for TKR has proven difficult.[8,15,37,50,51]

Considering that knee mechanics contribute substantially to articular damage,[26,30,58,59] evaluation of damage patterns occurring on polyethylene tibial inserts after wear simulation is one method for verifying a simulator's kinematic and load input parameters. Comparison of damage patterns on simulated and retrieved TKR inserts can demonstrate that simulated TKR kinematics and loading are comparable to physiologic TKR function during activities of daily living in patients.

Methods for evaluating TKR insert wear after *in vitro* knee joint wear simulation typically have been different from those methods used for assessing TKR inserts retrieved after *in vivo* function in patients. This can preclude direct comparison of damage patterns

on simulated and retrieved TKR inserts. Gravimetric assessment, the standard metric for quantifying polyethylene wear in knee simulator studies,[3] is difficult to apply to retrieved polyethylene inserts.[8] Consequently, visual identification of damage patterns and damage modes are more commonly used in retrieval studies.[18,30,31,33,52,55,59] Articular damage area and surface deformation have been reported separately in the literature for simulated[47] and retrieved[1,2,10,28,31,32,49,57] polyethylene tibial inserts. However, there are only a few studies[8,50,52] comparing the damage on retrieved polyethylene tibial inserts to damage after *in vitro* knee joint wear simulation.

The purpose of this study was to determine if TKR wear simulators with specific kinematic and load input parameters could produce damage patterns comparable to those observed on polyethylene tibial inserts that were retrieved from patients after *in vivo* physiologic function. Two different simulator loading profiles were evaluated, including a walking profile and a walking plus stair descent profile.[11] It was hypothesized that: 1) simulated inserts and retrieved inserts of the same design would have similar damage size and location; 2) simulated inserts and retrieved inserts would have similar surface deformation rates; and 3) simulated inserts subjected to a walking load profile would have different damage size and location compared to simulated inserts subjected to a combined walking and stair load profiles.

8.2 Materials and Methods

Three groups of tibial inserts from PCL-retaining TKR (Natural Knee, Sulzer Medica, Inc., Austin, TX) were analyzed. Group R included nine polyethylene tibial inserts (Natural Knee I Standard Congruent, Sulzer Medica, Inc.) retrieved after an average of 4.3±3.8 (range, 1.1 to 10.3) years of *in vivo* physiologic loading in patients. The average

patient age at retrieval was 68±20 (range, 32 to 87) years. The inserts were retrieved at autopsy (n=7) and at revision surgery for pain (n=2). Prostheses retrieved for loosening, instability, malposition, and those *in situ* for <6 months were excluded. Group W consisted of three inserts (Natural Knee II Standard Congruent, Sulzer Medica, Inc.) subjected to five million cycles of simulated *in vitro* walking loads on an Instron/Stanmore knee wear simulator (Instron Corp., Norwood, MA) using inputs programmed by the simulator manufacturer.[20,54] Group W+S consisted of four inserts (Natural Knee I Standard Congruent, Sulzer Medica, Inc.) subjected to five million cycles of simulated *in vitro* walking loads based on the amended proposed 1999 ISO force-controlled testing standard[34] and simulated *in vitro* stair descent loads. A ratio of 70:1 walking cycles to stair descent cycles[44] was used to represent a more severe loading pattern with high axial loads occurring at high flexion angles. In addition, the peak loads applied for walking cycles in Group W+S were approximately 19% higher than in Group W.[11] All simulator tests were cycled at 1 Hz and a 50% bovine serum solution was used as the lubricant and replaced every 100,000 cycles. Specific details of the knee simulator set-up and loading protocols have been reported elsewhere.[11]

The articular geometry of the simulator inserts and retrieved inserts were similar.[11] The articulation was flat in the coronal plane and sagittal planes, with slight anterior and posterior dishing. Group W and Group W+S inserts were machined with a 7.6 mm minimum thickness, sterilized using gamma radiation and packaged with an oxygen scavenger prior to testing. Group R inserts were machined with an average 7.1±1.2 mm minimum thickness, sterilized using gamma radiation and stored in ambient air prior to implantation.

Polyethylene articular surfaces were visually assessed by one observer (MKH) using an optical microscope (model Z30L, Cambridge Instruments, Cambridge, MA) at 7 to 30 times magnification. The prevalence of nine distinct damage modes were evaluated on the UHMWPE surfaces using published visual identification methods.[30,33,59] Abrasion is typically visualized as rough, tufted regions. Burnishing is visualized as smooth regions that are highly reflective of incident light. Non-articular deformation is visualized as a permanent change in shape from the original surface in regions not intended as a bearing surface. Delamination is visualized as thin layers of UHMWPE material separated from the surface. Embedded debris is visualized as particles that differed in color and/or texture relative to the surrounding UHMWPE surface, consistent with embedded particles of bone, cement fragments or metal particles. Pitting is visualized as depressions with rough surfaces typically 1 to 2 mm in diameter. Scratching is visualized as thin lines in irregular or ordered directions across the surface. Striations are visualized as highly oriented, longitudinal, smooth peaks and troughs on the articular surface.[59] Fractures are visualized as complete cracks or wear-through of the polyethylene insert.

Damage patterns were assessed separately on the medial and lateral articular surfaces of all inserts. The circumference of each identified damage mode region was outlined on digital images using published techniques.[16,30] Based on measurement of calibrated images of shapes with known dimensions, the technique had an absolute error of 0.4 mm for linear distances and 3.5 mm^2 for areas and was 98.6% accurate. Damage mode frequency was calculated as the number of inserts showing a given damage mode divided by the total number of inserts in each group. The damage area was calculated as

a percentage of the total medial or lateral articular surface area. The anterior-posterior (AP) extent of damage was calculated as the distance between the maximum anterior and posterior damage normalized to the dimensions of a medium (size 3) insert. The medial and lateral damage area centroids were calculated. The AP damage location was measured as the distance from the area centroids to an axis bisecting the tibial component into anterior and posterior halves, with a positive sign for anterior damage and a negative sign for posterior damage.

Maximum linear surface deformation, inclusive of damage due to visco-plastic deformation (creep) and material loss due to wear,[13,37,47] on the medial and lateral articular surfaces of all inserts was measured using a hand-held digital stylus (Microscribe 3DX, Immersion Corp., San Jose, CA) with a 3.2 mm ball tip. The instrument resolution is 0.13 mm and accuracy is 0.30 mm. Approximately 4000 to 7000 points were digitized for the worn inserts and unused control inserts of the same design to represent the three-dimensional articular surface geometry (Rhinoceros, Robert McNeel & Associates, Seattle, WA). Custom analysis software (PV-Wave, Version 6.0, Visual Numerics, Inc., Boulder, CO) was used to implement algorithms to correct specimen tilt and alignment and to generate a 1 mm contour grid across each articular surface, fitting a polynomial least-squares fit line to the digitized points within the grid. Surface deformation was calculated as the thickness difference between the best-fit articular contour grid lines of the worn inserts compared to unused control inserts.[32,47] The deformation rate was calculated as maximum deformation divided by duration of function for each insert, with duration defined as the number of years *in situ* for Group R and the number of repetitions of one million cycles of *in vitro* loading for Group W and Group W+S.

Differences in damage area, AP extent, AP location and deformation rate were compared between the groups using analysis of variance with appropriate post hoc multiple comparisons. Differences in medial and lateral damage within each group were compared using a paired t-test.

8.3 Results

Differences in the damage modes and area were observed between all the groups (Figures 8.1-8.2). Burnishing and striation damage were the largest damage modes on Group R inserts, occupying more than 25% of the medial and lateral plateau. Burnishing and scratching damage were the largest and most frequent damage modes for Group W and Group W+S. Striations were common (frequency >60%) on Group W inserts, but were not observed on any Group W+S inserts. Three (33%) Group R inserts had delamination covering an average of 23% of the articular surface, and seven (78%) Group R inserts had deformation on the tibial eminence. In contrast, none of the inserts in Group W or Group W+S had delamination or deformation.

There was considerable variation in damage area for Group R, ranging from 27% to 81% of the articular surfaces (Figure 8.3). Group R inserts had significantly greater lateral damage area compared to Group W ($p=0.017$) and Group W+S ($p=0.014$), whereas the medial damage areas were similar for all groups (Table 8.1). The AP extent of damage averaged approximately 35 mm on the Group R inserts, which was significantly greater than the AP extent for Group W and Group W+S (Table 8.1).

Damage pattern locations occurred predominantly in the central medial and lateral regions of the polyethylene articular surfaces of all groups (Figure 8.3). Lateral damage was located more posterior than medial damage for all groups, corresponding to an

externally rotated damage pattern, but average AP damage locations were not significantly different between the three groups (Table 8.1).

Comparison of the medial and lateral damage patterns revealed significant differences for Group W and Group W+S, but not for Group R. The medial surface of Group W inserts had significantly greater damage area and greater AP extent compared to the lateral surface. The medial surface of Group W+S inserts had significantly greater damage area, greater AP extent, more anterior AP damage location and lower deformation rate compared to the lateral surface.

The deformation rate for Group R inserts decreased with duration of physiologic loading in patients (linear regression, R^2=0.43, $p<0.003$), consistent with an initial creep response (Figure 8.4). Deformation rate decreased 0.03 mm for every year of *in vivo* function in patients. There was good agreement between the deformation rates for Group R, Group W and Group W+S inserts, assuming simulation for 5 million cycles is representative of 5 years of physiologic function in patients (Figure 8.4). One Group R insert with notable delamination showed an increased deformation rate (> 0.4 mm/year). This type of damage was not observed on simulator inserts. The average deformation rate for Group R was more than double the deformation rate for Groups W and W+S (Table 8.1) and was significantly greater on the medial plateau compared to Group W (p=0.027). Deformation rates for Group R and Group W+S were not significantly different.

Simulated walking and stair climbing activities in a ratio of 70:1 cycles altered the damage patterns on the Group W+S inserts, but no significant differences between the Group W and the Group W+S damage patterns were detected (Table 8.1). Group W+S showed 21% to 40% greater AP extent of damage compared to Group W, with 50%

greater deformation rate and a more posterior damage location on the lateral plateau. Medial and lateral damage areas were not significantly different for Group W or Group W+S inserts.

8.4 Conclusions

The load-controlled knee joint wear simulator produced damage patterns on the simulator's polyethylene tibial inserts that were comparable to those observed on well-functioning inserts of the same design that were retrieved from patients. Although the simulator inserts had smaller damage sizes, the damage regions for all simulated inserts were completely overlapped by the damage regions on retrieved inserts. Deformation rates of simulated inserts were analogous to five years of physiologic function in TKR patients (Figure 8.4). Simulated walking and stair climbing activities in a ratio of 70:1 cycles resulted in a 21% to 40% greater AP extent of damage compared to simulated walking only, with 50% greater deformation rate and a more posterior damage location on the lateral plateau. Variations in the AP extent of damage were consistent with the differences in tibiofemoral contact kinematics of the simulator and those known to occur in patients during activities of daily living.[19]

Knee joint wear simulators can generate tibiofemoral contact kinematics that compare well with knee kinematics derived from TKR patients during walking.[19,20,54] However, it is recognized that activities other than walking[56] and variability in surgical technique and patient habitus[9,48] affect dynamic TKR function. These variations, and higher demand activities of daily living for TKR patients, manifest different tibiofemoral contact patterns[4-7] and joint loads[22,23,38,41,44,46] in TKR patients, which correlate to different damage patterns evident on retrieved polyethylene inserts.[30] Such altered

kinematic and load profiles are included in simulator test methods in an effort to better replicate load and displacement variations occurring in patient populations[11,26,21,45] and to generate more clinically relevant polyethylene wear.[11,21,35,40]

In the current study, simulator inputs for Group W+S were modified to exceed what has previously been considered physiologic, including a 50% greater AP excursion of the lateral femoral contact, greater peak axial load and rotational torque with the addition of a stair descent loading profile.[11] Despite the modifications, damage patterns on the simulated inserts underestimated the damage patterns observed on the retrieved inserts. Group R inserts had a larger variety of damage modes (Figure 8.1) that covered a larger area on the articular surface compared to the Group W and Group W+S inserts (Table 8.1, Figure 8.3). The lateral damage size for Group R inserts was more than double the lateral damage size on Group W and Group W+S inserts. Similarly, Group R inserts had a significantly larger AP extent of damage than Group W and Group W+S inserts. The significant differences between the medial and lateral damage areas for Group W and Group W+S, but not Group R inserts, are consistent with asymmetry in the simulator's contact pathways. These differences suggest that there is greater variability in the "contact envelope", or range of tibiofemoral contact, during TKR function in patients than in the two simulated activities.

Variations in the damage patterns on the retrieved and simulated inserts were consistent with differences in the tibiofemoral contact kinematics of the simulator and those known to occur *in vivo* in patients.[19] Group W+S showed 21% to 40% greater AP extent of damage compared to Group W, with 50% greater deformation rate and a more posterior damage location on the lateral plateau. These damage patterns are consistent

with the simulator's greater AP excursion of the lateral femoral contact and greater loads in Group W+S.[11] As previously reported, greater AP excursion corresponds to larger damage areas on both simulated[50] and retrieved inserts.[30,50]

Simulation using the ISO force-controlled testing standard (Group W) and the amended ISO force-controlled testing standard and stair descent loading (Group W+S) each generated polyethylene deformation rates that were comparable to the deformation rate measured for these well-functioning retrieved inserts (Figure 8.4). Assuming simulation for 5 million cycles is representative of 5 years of function in patients, there was good agreement in the deformation rates for Group R, Group W and Group W+S inserts. The deformation rate for Group R inserts averaged 0.27 mm/year and 0.31 mm/year on the medial and lateral articular surface, respectively. These magnitudes are within the 0.13 mm/year to 0.35 mm/year range previously reported for retrieved polyethylene tibial inserts.[2,10,37] Average deformation rates for the Group W and Group W+S inserts ranged from 0.10 mm/year to 0.15 mm/year and were lower than those measured for the Group R inserts. However, the deformation rate decreased with time *in situ* up to 10 years in Group R inserts, consistent with previous retrieval studies.[2,10,32]

Given that TKR kinematics and loads are principal determinants of damage on polyethylene tibial inserts,[9,12,21,24,27,29,30,36,39,52,58] observations from retrieved TKR inserts are useful for verifying the predictive capabilities of musculoskeletal models and *in vitro* simulations.[8,26,45,50,52] In a patient-specific dynamic contact model,[26] the magnitude of predicted damage was in close agreement with measured damage on the polyethylene tibial insert later retrieved at autopsy from the same patient whose *in vivo* kinematics were used as model inputs. In a TKR finite element model, predicted peripheral pitting

damage was comparable to the location of pitting observed on retrieved inserts of the same design.[45] In the current study, damage patterns on simulated inserts were directly related to the known simulator loads and motions, providing a complete functional assessment loop between TKR simulation and the resulting damage patterns. Modification of the knee joint wear simulator inputs was a step toward developing methodologies inclusive of the cumulative range of dynamic contact and loading that occurs in TKR patients. Continued rigorous evaluation of biomechanical models is essential to verify that the knee simulation methods accurately represent the *in vivo* conditions they are meant to simulate.

8.5 Acknowledgements

The author thanks John D. DesJardins, PhD, Lisa C. Benson, PhD, Scott A. Banks, PhD, Martine LaBerge, PhD, and W. Andrew Hodge, MD for co-authoring publication of this work. The author thanks Roy D. Bloebaum for access to retrieved tibial inserts; Sulzer Medica, Inc. for simulator inserts. This work was supported by funding from The BioMotion Foundation of Palm Beach, Florida, the Fullerton Foundation, and the National Science Foundation (EPS-9871943).

Note: This work has been submitted for publication and is referenced as follows.

Melinda K. Harman, John D. DesJardins, Lisa C. Benson, Scott A. Banks, Martine LaBerge, W. Andrew Hodge: Comparison of polyethylene tibial insert damage from in vivo function and in vitro wear simulation. J Orthop Res, submitted March 2007.

8.6 References Cited

1. Argenson JN, O'Connor JJ. Polyethylene wear in meniscal knee replacement: A one to nine year retrieval analysis of the Oxford knee. *J Bone Joint Surg Br*. 1992; 74(2):228-32.
2. Ashraf T, Newman JH, Desai VV, et al. Polyethylene wear in non-congruous unicompartmental knee replacement: A retrieval analysis. *Knee.* 2004; 11:177-81
3. ASTM F1715-00. Standard guide for wear assessment of prosthetic knee designs in simulator devices. Annual Book of ASTM Standards. West Conshohocken: ASTM International 2002.
4. Banks SA, Markovich GD, Hodge WA. In Vivo kinematics of cruciate-retaining and -substituting knee arthroplasties. *J Arthroplasty*. 1997; 12(3):297-304.
5. Banks SA, Bellemans J, Nozaki H, et al. Knee motions during maximum flexion in fixed and mobile-bearing arthroplasties. *Clin Orthop*. 2003; 410:131-8.
6. Banks SA, Hodge WA. Implant design affects knee arthroplasty kinematics during stair-stepping. *Clin Orthop*. 2004; 426:187-193.
7. Banks SA, Hodge WA. 2003 Hap Paul Award paper of the International Society for Technology in Arthroplasty. Design and activity dependence of kinematics in fixed and mobile-bearing knee arthroplasties. *J Arthroplasty*. 2004; 19(7):809-16.
8. Beaule PE, Campbell PA, Walker PS, et al. Polyethylene wear characteristics in vivo and in a knee simulator. *J Biomed Mater Res*. 2002; 60:411-9.
9. Bei Y, Fregly BJ. Multibody dynamic simulation of knee contact mechanics. *Med Eng Phys*. 2004; 26(9):777-89.
10. Benjamin J, Szivek J, Dersam G, et al. Linear and volumetric wear of tibial inserts in posterior cruciate-retaining knee arthroplasties. *Clin Orthop*. 2001; 392:131-8.
11. Benson LC, DesJardins JD, Harman MK, LaBerge M. Effect of stair descent loading on ultra-high molecular weight polyethylene wear in a force-controlled knee simulator. Proc Instn Mech Engrs: *Proc Instn Mech Engrs: J Eng Med [Part H]*. 2002; 216: 409-18.
12. Blunn GW, Walker PS, Joshi A, Hardinge K. The dominance of cyclic sliding in producing wear in total knee replacements. *Clin Orthop*. 1991; 273:253-60.
13. Cho CH, Murakami T, Sawae Y, et al. Elasto-plastic contact analysis of ultra-high molecular weight polyethylene tibial component based on geometrical measurement from a retrieved knee prosthesis. *Proc Instn Mech Engrs: J Eng Med (Part H).* 2004; 218(Part H):251-9.
14. Clarke IC, Gustafson A, Jung H, Fujisawa A. Hip-simulator ranking of polyethylene wear. *Acta Orthop Scand*. 1996; 67(2):128-32.

15. Collier MB, Jewett BA, Engh CA Jr. Clinical assessment of tibial polyethylene thickness: comparison of radiographic measurements with as-implanted and as-retrieved thicknesses. *J Arthroplasty*. 2003; 18(7):860-6.

16. Cornwall GB, Bryant JT, Hansson CM, et al. A quantitative technique for reporting surface degradation patterns of UHMWPE components of retrieved total knee replacements. *J Appl Biomater*. 1995; 6:9-18.

17. Currier JH, Bill MA, Mayor MB. Analysis of wear asymmetry in a series of 94 retrieved polyethylene tibial bearings. *J Biomech*. 2005; 38:367-75.

18. Currier JH, Duda JL, Sperling DK, et al. In vitro simulation of contact fatigue damage found in ultra-high molecular weight polyethylene components of knee prostheses. *Proc Inst Mech Eng: J Eng Med (Part H)*. 1998; 212(H):293-302.

19. DesJardins JD, Banks SA, LaBerge M. Validation of TKR wear testing contact sliding velocities using in vivo TKR fluoroscopy. Proceedings of the 48th Annual Meeting of the Orthopaedic Research Society. Dallas, 2002.

20. DesJardins JD, Walker PS, Haider H, Perry J. The use of a force-controlled dynamic knee simulator to quantify the mechanical performance of total knee replacement designs during functional activity. *J. Biomech.* 2000; 33:1231-42.

21. D'Lima DD, Jermida JC, Chen PC, Colwell CSJ. Polyethylene wear and variations in knee kinematics. *Clin Orthop*. 2001; 392:124-30.

22. D'Lima DD, Patil S, Steklov N, et al. Tibial forces measured in vivo after total knee arthroplasty. *J Arthroplasty*. 2006; 21(2):255-62.

23. D'Lima DD, Patil S, Steklov N, et al. The Chitranjan Ranawat Award: In vivo knee forces after total knee arthroplasty. *Clin Orthop*. 2005; 440:45-9.

24. Estupinan JA, Bartel DL, Wright TM. Residual stresses in ultra-high molecular weight polyethylene loaded cyclically by a rigid moving indenter in nonconforming geometries. *J Orthop Res*. 1998; 16:80-8.

25. Fregly BJ, Bei Y, Sylvester ME. Experimental evaluation of an elastic foundation model to predict contact pressures in knee replacements. *J Biomech*. 2003; 36(11):1659-68.

26. Fregley BJ, Sawyer WG, Harman MK, Banks SA. Computational wear prediction of a total knee replacement from in vivo kinematics. *J Biomech*. 2005; 38:305-14.

27. Gevaert MR, LaBerge M, Gordon JM, DesJardins. The quantification of physiologically relevant cross-shear wear phenomena on orthopaedic bearing materials using the MAX-Shear wear testing system. *J Tribology*. 2005; 127(4):740-9.

28. Hailey JL, Fisher J, Dowson D, et al. A tribological study of a series of retrieved accord knee explants. *Med Eng Phys*. 1994; 16(3):223-8.

29. Hamilton MA, Sucec MC, Fregly BJ, et al. Quantifying multidirectional sliding motions in total knee replacements. *J Tribology*. 2005; 127(2):280-6.

30. Harman MK, Banks SA, Hodge WA. Polyethylene damage and knee kinematics after total knee arthroplasty. *Clin Orthop*. 2001; 392:383-93.

31. Harman MK, Banks SA, Hodge WA. Does backside damage correspond to articular damage in retrieved TKA polyethylene inserts? *Clin Orthop*. 2007; in press.

32. Harman MK, Schmitt S, Rössing S, et al. Predicting progressive degeneration, component fixation and polyethylene wear from radiographs of 27 UKR retrieved after 2 to 13 years of functional duration. *Acta Orthopaedica*. 2006; in review.

33. Hood RW, Wright TM, Burstein AH. Retrieval analysis of total knee prostheses: A method and its application to 48 total condylar prostheses. *J Biomed Mater Res*. 1983; 17:829-42.

34. ISO 14243-1. Implants for Surgery: Wear of Total Knee Joint Prostheses. Part 1: Loading and Displacement Parameters for Wear Testing Machines with Load Control and Corresponding Environmental Conditions for Test. London: International Organization for Standardization, 1999.

35. Johnson TS, Laurent MP, Yao JQ, Gilbertson LN. The effect of displacement control input parameters on tibiofemoral prosthetic knee wear. *Wear*. 2001; 250:222-6.

36. Kawanabe K, Clarke IC, Tamura J, et al. Effects of A-P translation and rotation on the wear of UHMWPE in a total knee joint simulator. *J Biomed Mater Res*. 2001; 54(3):400-6.

37. Kellett CF, Short A, Price A, et al. In vivo measurement of total knee replacement wear. *The Knee*. 2004; 11:183-7.

38. Kuster MS; Wood GA, Stachowiak GW Gachter A. Joint load considerations in total knee replacement. *J Bone Joint Surg Br*. 1997; 79(1):109-13.

39. Landry ME, Blanchard CR, Mabrey JD, et al. Morphology of in vitro generated ultrahigh molecular weight polyethylene wear particles as a function of contact conditions and material parameters. *J Biomed Mater Res (Appl Biomater)*. 1999; 48:61-9.

40. McEwen HM, Barnett PI, Bell CJ, et al. The influence of design, materials and kinematics on the in vitro wear of total knee replacements. *J Biomech*. 2005; 38(2):357-65.

41. McFadyen BJ, Winter DA. An integrated biomechanical analysis of normal stair ascent and descent. *J Biomechanics*. 1988; 21(9):733-44.

42. McKellop HA, Clarke IC. Evolution and evaluation of materials-screening machines and joint simulators in predicting in vivo wear phenomena. In: Ducheyne P. and Hastings GW. Functional Behavior of Orthopaedic Biomaterials, Vol. II: Applications. Chap. 3:51-85. Boca Raton: CRC Press 1983.

43. McKellop H, Shen FW, Lu B, et al. Effect of sterilization method and other modifications on the wear resistance of acetabular cups made of ultra-high

molecular weight polyethylene. A hip-simulator study. *J Bone Joint Surg Am*. 2000; 82(12):1708-25.

44. McLeod PC, Kettlekamp DB, Srinivasan V, Henderson OL. Measurements of repetitive activities of the knee. *J Biomech*. 1975; 8:369-73.

45. Morra EA, Harman MK, Greenwald AS. Computational models can predict polymer insert damage in total knee replacements. In: Insall JN, Scott WN. Surgery of the Knee. 4th ed. New York: Elsevier 2005.

46. Morrison JB. Function of the knee joint in various activities. *Biomed Engr*. 1969; 4(12):573-80.

47. Muratoglu OK, Perinchief RS, Bragdon CR, et al. Metrology to quantify wear and creep in polyethylene tibial inserts. *Clin Orthop*. 2003; 410:155-64.

48. Nozaki H, Banks SA, Suguro T, Hodge WA. Observations of femoral rollback in cruciate-retaining knee arthroplasty. *Clin Orthop*. 2002; 404:308-14.

49. Price AJ, Short A, Kellett C, et al. Ten year in vivo wear measurement of a fully congruent mobile bearing unicompartmental knee arthroplasty. *J Bone Joint Surg Br*. 2005; 87(11):1493-7.

50. Rawlinson JJ, Furman BD, Li S, et al. Retrieval, experimental, and computational assessment of the performance of total knee replacements. *J Orthop Res*. 2006; 24:1384-94.

51. Short A, Gill HS, Marks B, et al. A novel method for in vivo knee prosthesis wear measurement. *J Biomech*. 2005; 38:315-22.

52. Tamura J, Clarke IC, Kawanabe K, et al. Micro-wear patterns on UHMWPE tibial inserts in total knee joint simulation. *J Biomed Mater Res*. 2002; 61(2):218-25.

53. Rawlinson JJ, Furman BD, Li S, et al. Retrieval, experimental, and computational assessment of the performance of total knee replacement. *J Orthop Res*. 2006; 24:1384-94.

54. Walker PS, Blunn GW, Perry JP, et al. Methodology for long-term wear testing of total knee replacements. *Clin Orthop*. 2000; 372:290-301.

55. Wasielewski RC, Galante JO, Leighty RM, et al. Wear patterns on retrieved polyethylene tibial inserts and their relationship to technical considerations during total knee arthroplasty. *Clin Orthop*. 1994; 299:31-43.

56. Weiss JM, Noble PC, Conditt MA, et al. What functional activities are important to patients with knee replacements? *Clin Orthop*. 2002; (404):172-88.

57. Williams IR, Mayor MB, Collier JP. The impact of sterilization method on wear in knee arthroplasty. *Clin Orthop*. 1998; 356:170-80.

58. Wimmer MA, Andriacchi TP. Tractive forces during rolling motion of the knee: Implications for wear in total knee replacement. *J Biomech*. 1997; 30(2):131-7.

59. Wimmer M, Andriacchi T, Natarajan R, et al. A striated pattern of wear in ultrahigh-molecular-weight polyethylene components of Miller-Galante total knee arthroplasty. *J Arthroplasty*. 1998; 13(1):8-16.

Table 8.1: Comparison of Damage Patterns on the Medial and Lateral Plateaus of Simulated and Retrieved Tibial Inserts (mean, standard deviation)

		Medial	Lateral	paired t-test
Group R	Damage Area (%)	46±14	57±19 [a,b]	p=0.180
	AP extent (mm)	34.4±5.2 [a,b]	35.9±7.2 [a,b]	p=0.896
	AP Damage Location (mm)	0.7±2.9	-1.5±3.2	p=0.112
	Deformation Rate (mm/year)	0.27±0.15 [a]	0.31±0.18	p=0.077
Group W	Damage Area (%)	35±3	26±2 [a]	p=0.008
	AP extent (mm)	21.9±0.5 [a]	16.7±0.7 [a]	p=0.014
	AP Damage Location (mm)	3.0±0.8	0.0±0.6	p=0.062
	Deformation Rate (mm/year)	0.10±0.01 [a]	0.10±0.02	p=0.544
Group W+S	Damage Area (%)	36±2	28±1 [b]	p=0.005
	AP extent (mm)	26.6±1.2 [b]	23.3±0.2 [b]	p=0.006
	AP Damage Location (mm)	2.3±0.6	-2.3±0.4	p<0.001
	Deformation Rate (mm/year)	0.11±0.02	0.15±0.02	p=0.006

[a] significant difference between Group R and Group W inserts (ANOVA, $p<0.05$)

[b] significant difference between Group R and Group W+S inserts (ANOVA, $p<0.05$)

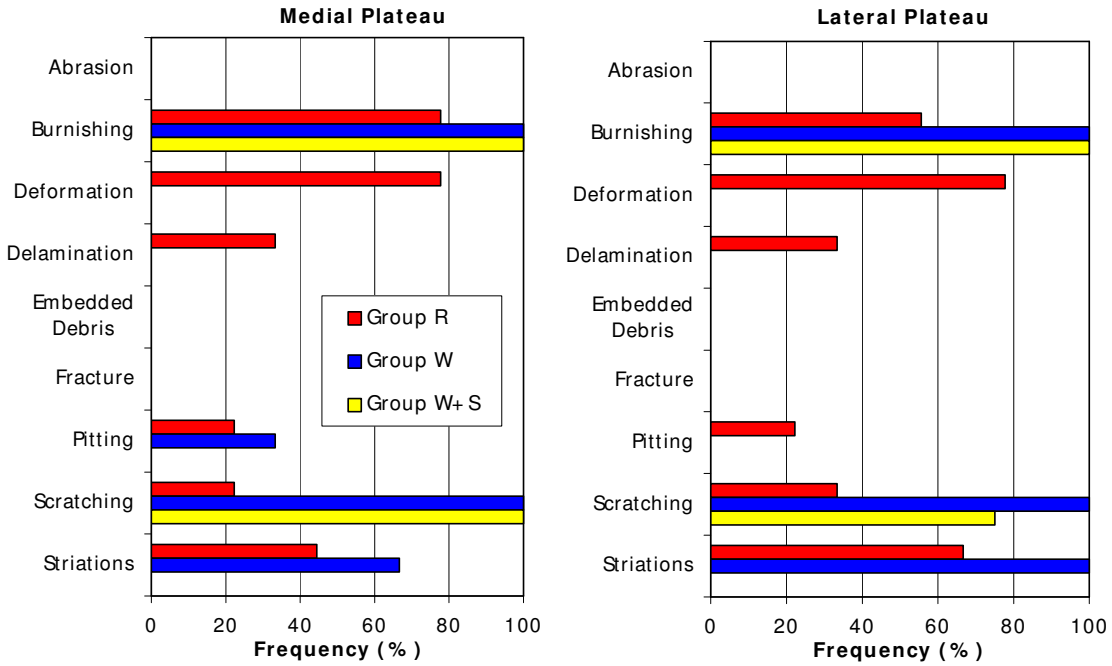

Figure 8.1: Damage Mode Frequency on Polyethylene Inserts Obtained After *In vivo* Function (Group R) and After *In vitro* Simulation with Two Loading Conditions (Group W, Group W+S)

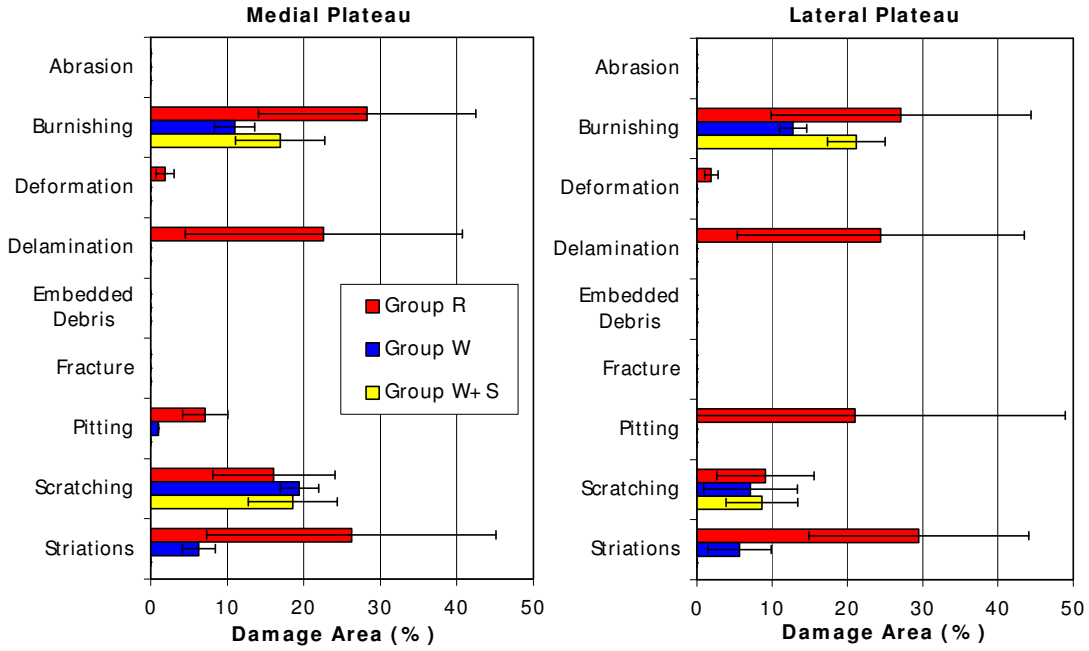

Figure 8.2: Damage Area of Different Damage Modes on Polyethylene Inserts Obtained After *In vivo* Function (Group R) and After *In vitro* Simulation with Two Loading Conditions (Group W, Group W+S)

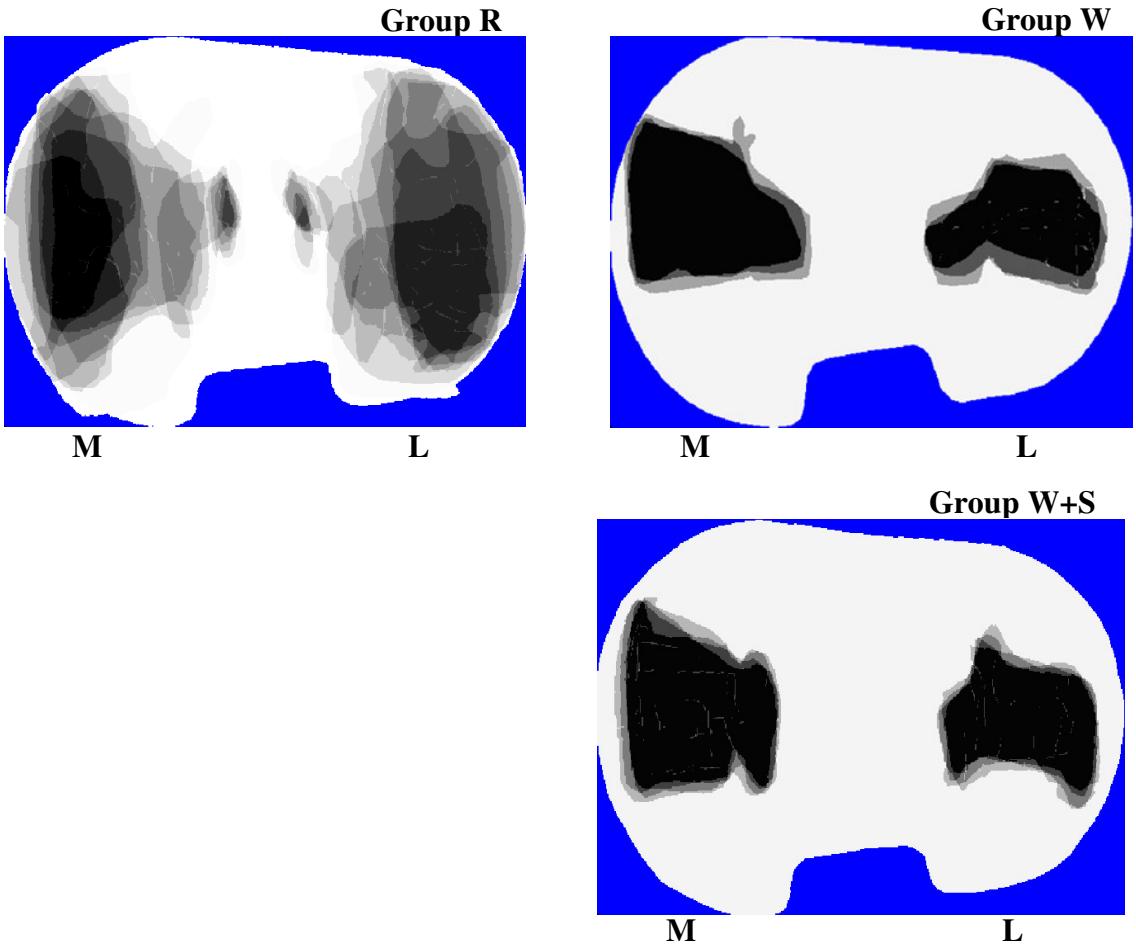

Figure 8.3: Graphic Overlays Depict Articular Damage Patterns

from All Retrieved Inserts (Group R) and Simulated Inserts

with Two Loading Conditions (Group W, Group W+S)

Increasing grayscale density (darker) indicates a greater number of inserts

had damage in a given location, with black indicating 100% of inserts had damage.

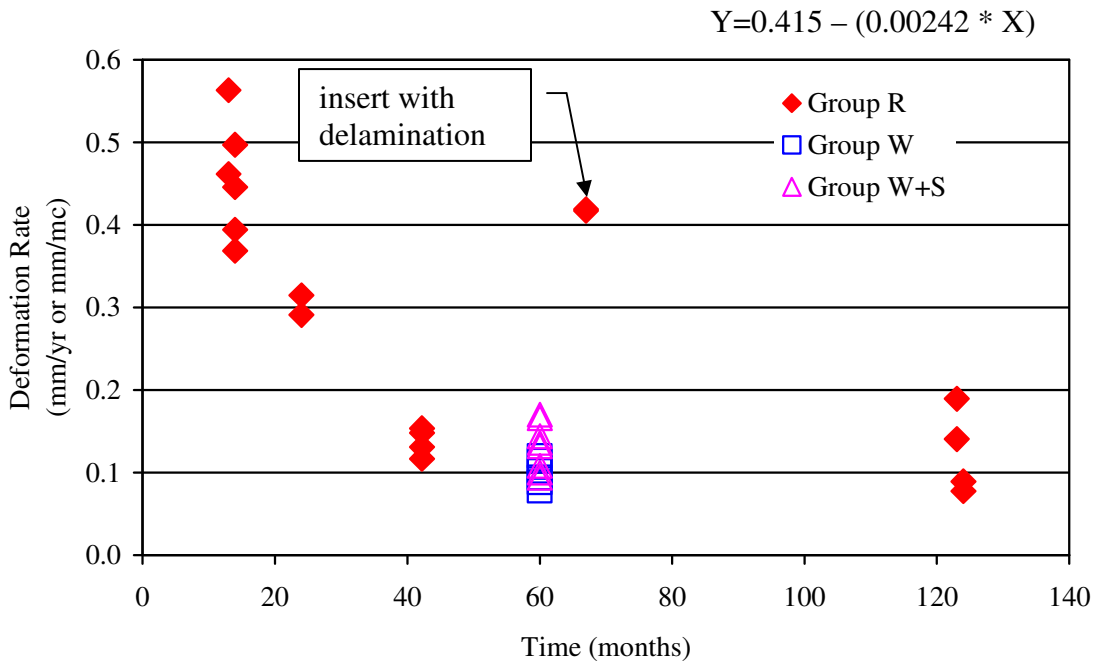

Figure 8.4: Deformation Rate for Group R Inserts and Group W and Group W+S Inserts

The rate for Group R decreased linearly with time *in situ* (R^2=0.43, p<=0.003).

Deformation rate decreased 0.03 mm for every year of *in vivo* functional duration

according to the regression equation

(deformation rate = 0.415 - (0.00242 * months of duration).

9 COMPUTATIONAL WEAR PREDICTION OF A TOTAL KNEE REPLACEMENT FROM IN VIVO KINEMATICS

9.1 Introduction

Wear of ultra-high molecular weight polyethylene (UHMWPE) in total knee replacements remains a major limitation to the longevity of these clinically successful devices.[14,30,44,52] Improvements over the past decade in sterilization techniques have reduced oxidative degradation of the UHMWPE bearing, with potentially dramatic long-term reductions in fatigue related pitting and delamination wear.[39,59] However, abrasive-adhesive wear mechanisms remain, with the potential to generate large numbers of submicron debris particles of osteolytic potential.[19,31,37] Efforts to reduce abrasive-adhesive or ‘‘mild’’ wear have resulted in the introduction of more highly crosslinked polymer bearings[42,62] and more scratch-resistant, highly wettable femoral articular surfaces.[27,57] These technologies may reduce, but cannot eliminate, mild wear mechanisms.

Because mild wear is a function of contact pressure, material properties, and kinematics,[11,26,47,60,61] efforts to minimize it must necessarily address these three determinants. Unfortunately, the relationships between contact pressure, kinematics, and wear have been poorly understood for implant-scale systems, making prediction of clinical wear performance a historically daunting challenge. Recent advances in computational mechanics, tribology, and in vivo assessment might now provide the required tools to permit accurate prediction of clinical implant wear performance.

The goal of the present effort was to demonstrate the feasibility of combining in vivo measurement of knee kinematics (Figure 9.1a), computation of the resulting dynamic contact pressures (Figure 9.1b), and tribological modeling (Figure 9.1c) to accurately predict clinical wear in a patient-specific model. The effort was guided by the concept that no tuning of model parameters would be done, and only previously published values for material properties and other input parameters would be used. Predicted damage was compared to the autopsy retrieved tibial insert from the same patient whose in vivo kinematics were used as model inputs (Figure 9.1d). Despite uncertain parameters and simplified modeling methods, the proposed computational wear methodology is able to capture many of the significant characteristics observed upon retrieval.

9.2 Materials and Methods

9.2.1. In vivo kinematic data

Fluoroscopic kinematic data previously collected from one total knee arthroplasty patient (female, age 65 at time of surgery, height 170 cm, mass 70 kg) were used in this study.[26] The patient received a cemented posterior cruciate ligament retaining prosthesis (Series 7000, Stryker Howmedica Osteonics, Inc., Allendale, NJ) with a 6.8mm thick insert machined from slab molded polyethylene sheets sterilized with gamma radiation in air. The insert geometry was essentially flat in the sagittal and coronal planes, with slight dishing at the anterior and posterior borders. The multi-radius femoral component had three separate sagittal plane radii. The angle created by the femoral and tibial shaft axes was 172° and the tibial component alignment in the sagittal plane was 90° on postoperative radiographs.[18] Knee Society Clinical Rating System[29] scores were 97 (knee) and 80 (function) after 1 year and 99 (knee) and 100 (function) after 2 years. The

patient gave written informed consent to participate in the kinematic and retrieval studies as previously described.[26]

The patient performed treadmill gait and stair rise/ descent activities during fluoroscopic motion analysis[3-6] 21 months after surgery (Figure 9.1a). This analysis method matches three-dimensional computer-aided design (CAD) models of the prosthetic components provided by the manufacturer to the two-dimensional fluoroscopic images and is accurate to approximately 1° for all rotations and 0.5mm for translations in the sagittal plane.[6] Kinematic data from one representative cycle of each activity were averaged in 5° increments of knee flexion for stair and 1% increments for gait including stance and swing phases. The duration of the cycle was 1.22 s for gait and 4.6 s for stair.

9.2.2. Dynamic contact model

A multi-body dynamic contact model was constructed from the same implant CAD model used in the fluoroscopic motion analysis. A commercial software program (Pro/MECHANICA MOTION, Parametric Technology Corporation, Waltham, MA) provided the multi-body dynamics framework, and an elastic contact model was integrated into this framework using user supplied routines[21] (Figure 9.1b). The contact model utilized elastic foundation theory[1,10,33,38] which scatters a ‘‘bed of springs’’ over the three-dimensional surfaces to push them apart. The springs represent an elastic layer of known thickness covering one or both bodies, where each spring is independent from its neighbors. For a rigid femur contacting a deformable tibial insert of finite thickness, the contact pressure p for any spring can be calculated from[1,10,33]

$$p = \frac{(1-\nu)E}{((1+\nu)((1-2\nu)h}d \tag{9.1}$$

where E is Young's modulus of the elastic layer, ν is Poisson's ratio of the layer, h is the layer thickness at the spring location, and d is the spring deflection, defined as the interpenetration of the undeformed surfaces in the direction of the local surface normal. E was chosen to be 463MPa[34] corresponding to gamma radiation crosslinked virgin GUR 1050 polyethylene and ν was chosen as 0.46.[8] All geometry calculations were performed using the ACIS 3D Toolkit (Spatial Corporation, Westminster, CO). The original CAD geometry in the regions of contact was re-surfaced using Geomagic Studio (Raindrop Geomagic, Research Triangle Park, NC) to eliminate potential problems caused by seams between surface patches. The tolerance between the original and resurfaced geometry was $\pm$002 mm. No faceting of the geometry was required for the contact calculations.

The dynamic contact model used in vivo fluoroscopic measurements (anterior–posterior translation, internal– external rotation, and flexion; Figures 9.2a–c, respectively) as prescribed kinematic inputs. The model predicted the remaining degrees of freedom (axial translation, varus – valgus rotation, and medial–lateral translation) via forward dynamic simulation to ensure compatibility with the applied loads (see below). All prescribed and predicted motions were for the femur moving with respect to a fixed tibia.

Four loads applied to the femoral component affected the predicted motions. The first was an axial force applied vertically downward and positioned to produce either a 70–30 or 50–50 medial–lateral load split at 0° flexion.[28,32,50] With two activities (gait and stair) and two load splits (70–30 and 50–50), this produced four cases for dynamic simulation. The axial force curve for each activity was defined by scaling the vertical ground reaction force curve to be between 0.25 and 3.0 BW[41,50,53,54] (Figure 9.2d). Ground reaction force data were not available from the fluoroscopy/retrieval patient, so

vertical forces during gait and stair activities from a patient of similar age, height, weight, and knee flexion characteristics were used.[7] The stance phase of the gait force data was extended from 62% to 68% of the cycle to match the treadmill kinematics. The second load was a medial–lateral nonlinear spring force of the form

$$k(ax)^b, \tag{9.2}$$

where k = 100; a = 2; and b = 4; which produces a small restoring force in the region $|x| \leq$ 0:5mm and ramps up quickly for $|x| >$ 0:5mm: This force was included to prevent the femoral component from ‘‘riding’’ the medial eminence of the tibial insert in the 70–30 load split simulations and had little effect on the 50–50 simulations. The third load was comprised of the net force and torque due to elastic contact in the medial and lateral tibiofemoral compartments. The final load was comprised of the inertial force and torque, which was made negligible by choosing small values for the femoral component mass and inertia.

The dynamic contact model generated wear model inputs in two steps. A forward dynamics simulation with a coarse contact element grid was used to predict accurate contact forces and kinematics, since the contact forces and torques were highly insensitive to grid density. A subsequent inverse dynamics analysis with a finer element grid was used to predict accurate contact pressures and slip velocities from these kinematics, since the peak and average contact pressures are much more sensitive to grid density. Though accurate kinematics and contact pressures could be predicted simultaneously, this two-stage approach minimized CPU time. To determine the necessary resolution of the coarse grid, the predicted contact forces and torques were

investigated using the lightest load (0.25 BW) and smallest contact area (90° flexion). For a fixed static configuration, convergence to within 3% relative error occurred for a 35×20 grid on each side. The accuracy of the dynamic simulation results produced with this grid was verified by repeating the simulations using a denser 50×35 grid. With the coarse 35×20 grid, each forward dynamics simulation required between 10 and 15 min of CPU time on a 2.4GHz Pentium IV workstation, while the finer 50×35 grid required between 18 and 21 min of CPU time. The subsequent inverse dynamics analysis used a 50×50 element grid (Figure 9.5) and required less than 2 min of CPU time for each case.

9.2.3. Computational wear model

A computational wear model was developed to produce element-by-element damage predictions given the predicted time history of contact pressures and slip velocities experienced by each element. The model computes total damage depth for each element as the sum of material removal due to mild wear and surface deformation due to compressive creep:

$$\delta_{Damage} = N\delta_{Wear} + \delta_{Creep} \tag{9.3}$$

where δ_{Damage} is the total damage, δ_{Wear} is the damage per cycle due to mild wear, N is the total number of cycles, and δ_{Creep} is the damage due to creep. N was calculated from the number of months of implantation (see below) assuming 1 million cycles per year of gait or stair.[51] The depth of material removed from an element over one cycle due to mild wear was predicted using Archard's classic wear law:[2]

$$\delta_{Wear} = k\sum_{i=1}^{n} p_i d_i = k\sum_{i=1}^{n} p_i |v_i| \Delta t \tag{9.4}$$

where k is the material wear rate, i is a discrete time instant in an activity measured at n instants, p_i is the contact pressure on the element at that instant, and d_i is the sliding distance experienced by the element, calculated as the product of slip velocity magnitude $|v_i|$ at that instant and increment Δt between time instants. To determine an appropriate value of k, the articulating surface of the retrieved metal femoral component was examined under a white-light optical interferometer (Wyko NT1000, Veeco Instruments, Woodbury, NY). The average roughness R_a measured at multiple locations on the contact surfaces varied between 46 and 275 nm with a mean value of 131 nm. Published wear rates as a function of R_a were examined for UHMWPE of similar age to that implanted in the patient and subjected to similar contact pressure, slip velocity, and environmental conditions.[20] Since the reported wear rates vary dramatically with R_a; the average value of R_a was used to select an average wear rate of $k = 220 \pm 10^{-9}$ mm^3/Nm.

Because UHMWPE is a viscoelastic material that deforms in a time-dependent manner under load,[36,55,56] not all surface profile changes in retrieved components are a result of wear. Experiments to determine the compressive creep characteristics of medical grade extruded UHMWPE were performed by Lee and Pienkowski.[36] Their results can be formulated into the following equation for the depth of element surface deformation due to creep over the total time of implantation:

$$\delta_{Creep} = \left[3.491x10^{-3} + 7.996x10^{-4}\left(Log\left(N\sum_{i=1}^{n} \Delta t_{ci} \right) - 4 \right) \right] \frac{\sum_{i=1}^{n} p_{ci}\Delta t_{ci}}{\sum_{i=1}^{n} \Delta t_{ci}} h \tag{9.5}$$

where all notations are as defined previously with the exceptions that the subscript *c* denotes use of only those time instants *i* when the contact pressure p_i is non-zero, *h* is the minimum thickness of the tibial insert, the unit for pressure must be MPa, the unit for time minutes, and the unit for thickness mm. Since no data were found in the literature that could be used to form a creep recovery equation similar to Eq. (9.5), zero relaxation was assumed rather than estimating a relaxation percentage that could not be justified. Thus, the predicted values of δ_{Creep} will be overestimates.

Implanted components see a wide spectrum of activities depending on the age and lifestyle of the patient, with different activities placing different tribological demands on the joint. To account for the varying spectrum of activities, a linear damage model (linear rules-of-mixture) was used to predict the total damage δ_{Damage} produced by any combination of gait δ_{Gait} and stair δ_{Stair} activities. With the fraction of each activity denoted by x_{Gait} and x_{Stair} for gait and stair, respectively, where $x_{Gait} + x_{Stair} = 1$; the total damage depth for any assumed partitioning of activities is given by:

$$\delta_{Damage} = x_{Gait}\delta_{Gait} + (1 - x_{Gait})\delta_{Stair} \tag{9.6}$$

where δ_{Gait} and δ_{Stair} are computed from Eq. (9.3) assuming all cycles are either gait or stair.

9.2.4. Comparison with retrieval

Five computational wear predictions (two activities with two load splits, and one partition of activities: 85% gait and 15% stair) were compared to the actual damage depths and patterns measured on the tibial insert retrieved from the patient post-mortem. The total time of implantation at retrieval was 51 months. For both the predictions and

the retrieval, visualizations of the wear contours were generated using commercial automatic inspection software (Geomagic Qualify, Raindrop Geomagic, Research Triangle Park, NC). For the wear predictions, the center of each contact element on the tibial insert surface was displaced by the calculated damage depth δ_{Damage} in the direction of the local surface normal. A ‘‘worn’’ polygonal surface model was created from these points, and a contour plot of the deviations between the original and worn surfaces was generated by the software. The retrieval showed scratching, burnishing, and tractive striations on the articular surfaces.[26] Pitting and delamination were not observed. A three-dimensional scan was obtained of the worn insert (Figure 9.3a) and a matched unworn insert using a laser scanner (Vivid 900, Minolta Corporation, Ramsey, NJ) possessing a manufacturer-reported accuracy of $\pm$0.04 mm. Once the point clouds generated by the laser scans were converted to polygonal surface models and aligned by the software, a retrieval wear contour plot was also generated (Figure 9.3b). To determine a threshold for reporting retrieval wear, the unworn insert was aligned with the insert CAD model and the maximum deviation between contact surfaces (0.25 mm) determined.

9.3 Results

Qualitatively, the damage regions predicted by the computer simulations were in good agreement with the clinical damage regions (compare Figure 9.4 with Figure 9.3). The medial damage scars for the 70–30 gait case (Figure 9.4a) extended to the anterior medial corner of the insert, similar to the retrieval. In contrast, the medial damage scars for the 70–30 (Figure 9.4b) stair case extended broadly to the posterior rim of the insert, enlarging the region predicted by the gait cases. The lateral damage scars for the 70–30

gait case extended more anteriorly than in the retrieval, whereas the anterior border on the lateral side in the 70–30 stair case corresponded well with the retrieval. Altering the load split to 50–50 decreased medial damage while increasing lateral damage for both gait (Figure 9.4c) and stair (not shown). For an 85% gait, 15% stair partitioning of activities based on linear rules of mixture, the damage area for a 70–30 load split (Figure 9.4d) was a combination of the gait (Figure 9.4a) and stair (Figure 9.4b) damage areas. For both gait and stair, the lateral wear regions were more central in the anterior–posterior direction than were the medial regions, similar to the retrieval, and possessed a posterior border of similar shape and location to the retrieval.

The predicted locations of maximum damage were in good agreement with the retrieval (stars in Figures 9.3b and 9.4). On the lateral side, the location of maximum damage was the same in all four simulations and was consistent with the retrieval. On the medial side, the maximum damage location was shifted anteriorly for the gait simulations (Figures 9.4a and c) and posteriorly for the stair simulations (Figure 9.4b). However, when an 85% gait, 15% stair partitioning of activities was considered (Figure 9.4d), the predicted maximum damage location on the medial side also became consistent with the retrieval.

Quantitatively, the simulations predicted maximum total damage depths on the same order of magnitude as those measured from the retrieved insert (Table 9.1). The predicted maximum damage depths ranged from 0.7 to 2.7 mm. The predicted creep deformation was a substantial portion of the total damage. The 70–30 load split for gait and stair activities exhibited the deepest damage on the medial side, whereas the 50–50 load cases produced the deepest damage on the lateral side. Total damage area was

greater for gait than for stair, while total damage volume was approximately 50% larger for stair than for gait. Smaller medial loads (50–50 split) decreased the damage volume in the medial compartment and increased damage volume in the lateral compartment such that the total damage volume was unaffected by load split.

Combining damage predictions from the two activities (85% gait, 15% stair) resulted in damage similar to the retrieved implant (Table 9.2). The predicted locations of maximum damage depth were the same as on the retrieved insert (Figure 9.4d). Maximum damage depths for the retrieval were 0.7mm medial and 0.8mm lateral versus 0.8 and 0.9mm for the simulation. The combined case predicted 112% of the total damage area on the retrieval, 114% medially and 108% laterally. The medial–lateral ratio for damage depth was 0.88 for the retrieval and 0.89 for the simulation while for damage area it was 1.38 for the retrieval and 1.47 for the simulation.

9.4. Conclusions

This study used a novel combination of in vivo measurements, post-mortem observations, and computational tools to predict patient-specific damage in a total knee replacement. This approach allows researchers to ‘‘close the loop’’ on damage predictions by validating them against the tibial insert retrieved from the same patient whose in vivo kinematics were used as model inputs. Though the methodology requires a number of uncertain input parameters and modeling assumptions, integration of these approaches into a single cohesive framework leads to damage predictions that capture the important features of retrieval observations. With continuing refinements, this methodology may be useful for improving implant designs through virtual prototyping or predicting in vivo damage prior to clinical use.

Using knee kinematics from two activities (85% gait, 15% stair), it was possible to create bearing surface damage similar to the retrieved insert. The locations of maximum damage were the same (Figure 9.4d), as were the ratios of damage between medial and lateral sides (Table 9.2). The maximum damage depth was greater for the simulations than the retrieval, in part because the model did not include creep relaxation. Similarly, predicted volumetric damage was 42–64mm^3 per year, higher than published retrieval series. Lavernia, et al.[35] reported 31mm^3 per year on autopsy retrieved devices of similar geometry, and Price, et al.[45] reported 8mm3 per year on fully conforming, mobile-bearing unicondylar knee replacements. It was somewhat surprising to find greater damage depth under the lateral condyle for both simulation and retrieval, but this was explained by the kinematics, where little translation of the lateral condyle focused damage in a smaller area. The medial condyle showed greater translations for both activities, creating greater damage areas, but shallower damage depths, both in simulation and in vivo.

Obviously, patients do not spend 15% of their weight-bearing cycles climbing stairs. It is reasonable to assume, however, that stair data provides an approximation to other activities involving the flexed knee under high load, such as sitting and rising from a chair or bed, using a toilet, entering and exiting a car, etc. The composite of these relatively less frequent, but highly demanding, activities could play a significant role in the damage experience of the prosthetic bearing.

The major difference between damage on the retrieved implant and the simulations was a modest amount of apparent damage at the periphery of the retrieved insert (Figure 9.3b). Visual inspection of this region of the retrieval revealed negligible

damage. One explanation of this apparent damage is that the implant had warped, upward at the tibial eminence, as has been observed on similar implants at autopsy.[31] The inspection software registered the worn and unworn parts at the central eminence, so the periphery of the retrieval appeared lower, and consequently worn. The dynamic contact modeling approach used in this study is extremely efficient computationally. Recent studies of knee wear simulator machines have used dynamic finite element analyses (FEA) to predict knee replacement kinematics and contact pressures simultaneously.[22,24] An advantage of dynamic FEA is that it also predicts internal stresses. However, a high computational price is paid for this benefit, with CPU times ranging from 1.4 days[24] to between 2.4 and 3.2 days.[22] Predicting kinematics alone requires 6–7 h of CPU time.[24] To improve computational performance, a simplified dynamic FEA method that combines rigid body analysis with an elastic foundation contact model, similar to our approach, has recently been proposed.[25] By sacrificing internal stress calculations, this method can achieve CPU times comparable to those of the present study. Consequently, when only kinematics, contact forces, and/or contact pressures are of interest, hybrid rigid body/elastic contact approaches can provide faster alternatives to traditional dynamic FEA.

Despite its computational advantages, the current contact model formulation has limitations. It does not account for viscoelastic material properties,[55,56] friction,[46] or how pressure applied at one location affects the displacement of other locations.[33] However, the most significant issue is the use of a linear material model. This model was chosen over a nonlinear model for two reasons. First, a linear model is more in line with the guiding concept of using models with previously published, well-established parameter

values. Second, in recent simulations of a different knee implant using the same dynamic contact model, a linear model matched static contact pressure measurements better than did a nonlinear material model[15] for 16 different loading conditions (loads of 750, 1500, 2250, and 3000N and flexion angles of 0°, 30°, 60°, and 90°).[21] The value of Young's modulus that reproduced the experimental data (400MPa) was close to the value reported by Kurtz, et al.[34] as used here. Use of a nonlinear material model[15] in the simulations produces more uniform contact pressures across a broader patch (Figure 9.5). Thus, a nonlinear material model with well established parameter values would produce broader damage predictions in the anterior–posterior direction, similar to the retrieval, but would not likely cause dramatic changes in the depth or distribution of predicted damage.

The spatially discrete nature of the predicted damage scars in the anterior–posterior direction, especially on the medial side, was due to variations in the input kinematics during a single motion cycle. Since the damage predictions integrate the combined effects of motion and loads on each element over the cycle, high loads during sliding at any point in the cycle will produce localized damage regions. Use of multiple experimental motion cycles or more accurate axial load inputs, if available, could produce more continuous anterior–posterior variation in predicted damage.

A constant 70–30 or 50–50 load split was used in the simulations as a simple approximation to the in vivo loads. It is tempting to use the external varus–valgus moment from gait analysis to define a variable load split throughout the gait or stair cycle. However, muscles play a significant role in balancing external moments at joints,[17,23,40,41] and the adduction moment resisted by tibiofemoral contact forces is likely much smaller than the external knee adduction moment.[41] Knowledge of muscle and

ligament forces would be needed to calculate the variable contact moment from the external moment. For these reasons, a conservative 50–50 load split was used along with a 70–30 load split based on data in the literature.[28,32,50]

The damage computations required a number of input parameters that are not known with certainty. For pin-on-flat tribometer experiments using material pairs and loading conditions similar to joint replacements, measured values of the wear rate k for UHMWPE vary by orders of magnitude as a function of the average roughness R_a of the counterface. For R_a values between 18 and 72 nm, Fisher, et al.[20] reported k values ranging from 7.9×10^{-9} to 457×10^{-9} mm^3/Nm with a sudden increase in k at approximately R_a = 50 nm: This rapid increase is the motivation for highly polished and scratch-resistant femoral components. Wear rates have also been shown to be highly dependent on the extent of crossing motion.[12,13,43,48] For the implant and patient used in the present study, subsequent analyses performed by the authors suggest that no element on the tibial insert surface experienced bi-directional crossing motion greater than about 10°.[49] Thus, adjusting the wear factor for crossing severity would have little effect on the damage predictions. By using accurate k values measured from pin-on-disk tribometer experiments, the wear performance of new femoral component materials could be predicted via computer simulation for specific knee designs prior to physical testing and clinical trials.

The precise number of load cycles of gait and stair was also unknown for the patient. Using an electronic pedometer, Schmalzried, et al.[51] measured the number of steps per day taken by hip and knee replacement patients. The average data extrapolated to 0.9 million cycles per year, ranging from 0.1 million to 3.2 million cycles per year.

Since the wear per cycle δ_{Wear} is multiplied by the number of cycles per year *N*; the wear predictions can vary substantially based on the patient's assumed activity level.

Finally, simulations of a single cycle of gait and/or stair were used to develop all damage predictions, with no changes in surface geometry due to repeated loading taken into account. In many mechanisms, accurate wear prediction requires accounting for the coupled evolution of wear, kinematics, and load.[9, 16,48] To determine the number of cycles that a single simulation could be extrapolated for wear prediction before changes in surface geometry were required, Dickrell, et al.[16] used a combined experimental, analytical, and computer simulation approach. They found that if loads and surface geometry change little, extrapolation of a single simulation over a large number of cycles is reasonable. For patients with knee replacements, the loads during daily activities are relatively constant, and the damage depths are orders of magnitude smaller than the radii of curvature of the components. Thus, the effect of form changes on subsequent kinematics, slip velocities, slip distances, and contact pressures is expected to be low, making the system weakly coupled and extrapolation errors small.

This study has presented a novel approach for performing computational wear predictions of total knee replacements. Despite a large number of simplifying assumptions, the methodology produces damage predictions reasonably consistent with retrieval observations. Using in vivo kinematic data from fluoroscopy to drive a dynamic contact model, damage on differential elements of the tibial insert surface can be predicted. Modeling knee simulator machines, where the load and kinematic inputs are better defined, will provide a valuable avenue for refining the methodology and validating its predictions. Eventually, it may be possible to use similar computational

tools to augment traditional in vitro mechanical testing, predict damage performance of novel implants or materials in early clinical trials, and evaluate systematically the effects of variable surgical positioning on subsequent implant performance.

9.5. Acknowledgements

The author thanks Benjamin J. Fregley, PhD, W. Gregory Sawyer, PhD, and Scott A. Banks, PhD for co-authoring publication of this work; Stryker Howmedica Osteonics for providing the CAD models used in the simulations; Yanhong Bei for assistance with elastic contact model development; and Matt Hamilton for assistance with computational wear model development. This study was supported by new faculty start-up funds from the University of Florida and by The Biomotion Foundation of Palm Beach, Florida.

Note: This work has been published and is referenced as follows.

Benjamin J. Fregley, PhD; W. Gregory Sawyer, PhD; Melinda K. Harman, MSc; Scott A. Banks, PhD: Computational wear prediction of a total knee replacement from in vivo kinematics. J Biomech 38:305-314, 2005.

9.6. References Cited

1. An KN, Himenso S, Tsumura H, Kawai T, and Chao EYS. Pressure distribution on articular surfaces: application to joint stability analysis. *J Biomech*. 1990; 23:1013-20.
2. Archard JF and Hirst W. The wear of metals under unlubricated conditions. *Proc Royal Soc.* 1956; A236:397-410.
3. Banks SA. Model based 3D kinematic estimation from 2D perspective silhouettes: Application with total knee prostheses. PhD Dissertation, Massachusetts Institute of Technology, Cambridge, MA, 1992.
4. Banks SA, Markovich GD, and Hodge WA. In vivo kinematics of cruciate-retaining and substituting knee arthroplasties. *J Arthroplasty.* 1997; 12:297-304.

5. Banks SA, Markovich GD, and Hodge WA. The mechanics of knee replacements during gait: In vivo fluoroscopic analysis of two designs. *Am J Knee Surg*. 1997; 10:261-7.

6. Banks SA and Hodge WA. Accurate measurement of three-dimensional knee replacement kinematics using single-plane fluoroscopy. *IEEE Trans Biomed Eng*. 1996; 43:638-49.

7. Banks SA, Otis JC, Backus SI, Furman GL, and Haas SB. Function of total knee replacements during activities of daily living. In *Proceedings of the 67th Annual Meeting of the American Academy of Orthopaedic Surgeons*. 2000; Orlando, FL.

8. Bartel DL, Rawlinson JJ, Burstein AH, Ranawat CS, and Flynn WF. Stresses in polyethylene components of contemporary total knee replacements. *Clin Orthop*. 1995; 317:76-82.

9. Blanchet TA. The interaction of wear and dynamics of a simple mechanism. *J Tribology.* 1997; 119:597-9

10. Blankevoort L, Kuiper JH, Huiskes R, and Grootenboer HJ. Articular contact in a three-dimensional model of the knee. *J Biomech.* 1991; 24:1019-31.

11. Blunn GW, Walker PS, Joshi A, and Hardinge K. The dominance of cyclic sliding in producing wear in total knee replacements. *Clin Orthop* 1991; 273:253-60.

12. Bragdon CR, O'Conner DO, Lowenstein JD, Jasty M, Syniuta WD. The importance of multidirectional motion on the wear of polyethylene. *IMechE Part H: J Eng Med*. 1996; 210:157–65.

13. Burroughs BR, Blanchet TA. Factors affecting the wear of irradiated UHMWPE. *Tribology Trans*. 2001; 44:215–23.

14. Cadambi A, Engh GA, Dwyer KA, and Vinh TN. Osteolysis of the distal femur after total knee arthroplasty. *J Arthoplasty.* 1994; 9:579-94.

15. Cripton PA. Compressive characterization of ultra-high molecular weight polyethylene with applications to contact stress analysis of total knee replacements. Master of Science Thesis. 1993; Queen's University, Kingston, Ontario.

16. Dickrell DJ, Dooner DB, and Sawyer WG. The evolution of geometry for a wearing circular cam: Analytical and computer simulation with comparison to experiment. *J Tribology.* 2003; 125:1878-92.

17. Duda GN, Schneider E, and Chao EYS. Internal forces and moments in the femur during walking. *J Biomechanics.* 1997; 30:933-41.

18. Ewald FC. The Knee Society total knee arthroplasty roentgenographic evaluation and scoring system. *Clin Orthop.* 1989; 248;9-12.

19. Ezzet KA, Garcia R, and Barrack RL. Effect of component fixation method on osteolysis in total knee arthroplasty. *Clin Orthop.* 1995; 321:86-91.

20. Fisher J, Dowson D, Hamdzah H, and Lee HL. The effect of sliding velocity on the friction and wear of UHMWPE for use in total artificial joints. *Wear.* 1994; 175:219-25.

21. Fregly BJ, Bei Y, and Sylvester ME. Experimental evaluation of an elastic foundation model to predict contact pressures in knee replacements. *J Biomechanics.* 2003; 36:1659-68.

22. Giddings VL, Kurtz SM, and Edidin AA. Total knee replacement polyethylene stresses during loading in a knee simulator. *J Tribology.* 2001; 123:842-7.

23. Glitsch U, and Baumann W. The three-dimensional determination of internal loads in the lower extremity. *J Biomechanics.* 1997; 30:1123-31.

24. Godest AC, Meaugonin M, Haug E, Taylor M, and Gregson PJ. Simulation of a knee joint replacement during a gait cycle using explicit finite element analysis. *J Biomechanics*. 2002; 35:267-76.

25. Halloran JP, Easley SK, Penmetsa J, Laz PJ, Petrella AJ, Rullkoetter PJ. Efficient dynamic finite element rigid body analysis of TJR. In: *Proceedings of the 2003 ASME Summer Bioengineering Conference*. 2003; Key Biscayne, FL.

26. Harman MK, Banks SA, and Hodge WA. Polyethylene damage and knee kinematics after total knee arthroplasty. *Clin Orthop.* 2001; 392:383-93.

27. Heimke G, Leyen S, and Willmann G. Knee arthroplasty: recently developed ceramics offer new solutions. *Biomaterials.* 2002; 23:1539-51.

28. Hurwitz DE, Sumer DR, Andriacchi TP, and Sugar DA. Dynamic knee loads during gait predict proximal tibial bone distribution. *J Biomechanics*. 1998; 31:423-30.

29. Insall JN, Dorr LD, Scott RD, and Scott WN. Rationale of the Knee Society clinical rating system. *Clin Orthop.* 1989; 248:13-14.

30. Jacobs JJ, Shanbhag A, Glant TT, Black J, and Galante JO. Wear debris in total joint replacements. *J Am Acad Orthop Surg* 1994; 2:212-20.

31. Jacobs JJ, Surace MF, Berzins A, Urban RM, Berger RA, Natarajan RN, Andriacchi TP, and Galante JO. Backsided tibial polyethylene wear and osteolysis in modular tibial components. In *Proceedings of the Knee Society.* 2002; Dallas, TX.

32. Johnson F, Scarrow P, and Waugh W. Assessments of loads in the knee joint. *Medical and Biological Engineering and Computing.* 1981; 19:237-43.

33. Johnson KL. *Contact Mechanics.* 1985; Cambridge University Press, Cambridge.

34. Kurtz SM, Jewett CW, Bergström JS, Foulds JR, and Edidin AA. Miniature specimen shear punch test for UHMWPE used in total joint replacements. *Biomatierals.* 2002; 23:1907-19.

35. Lavernia CJ, Sierra RJ, Hungerford DS, Krackow K. Activity level and wear in total knee arthroplasty: a study of autopsy retrieved specimens. *J Arthroplasty*. 2001; 16:446-53.

36. Lee KY, and Pienkowski D. Compressive creep characteristics of extruded ultrahigh-molecular-weight polyethylene, *J Biomed Mater Res.* 1998; 39:261-5.

37. Lewis G. Polyethylene wear in total hip and knee arthroplasties. *J Biomed Mater Res (Applied Biomaterials).* 1997; 38:55-75.

38. Li G, Sakamoto M, and Chao EYS. A comparison of different methods in predicting static pressure distribution in articulating joints. *J Biomechanics.* 1997; 30:635-8.

39. Li S. and Burstein AH. Ultra-high molecular weight polyethylene: The material and its use in total joint implants. *J Bone Joint Surg Am.* 1994; 76:1080-90.

40. Lu TW, O'Connor JJ, Taylor SJG, and Walker PS. Validation of a lower limb model with *in vivo* femoral forces telemetered from two subjects. *J Biomechanics.* 1998; 31:63-9.

41. Lu TW, Taylor SJG, O'Connor JJ, and Walker PS. Influence of muscle activity on the forces in the femur: an in vivo study. *J Biomechanics.* 1997; 30:1101-06.

42. McKellop H, Shen FW, Lu B, Campbell P, and Salovey R. Development of an extremely wear-resistant ultra high molecular weight polyethylene for total hip replacements. *J Orthop Res.* 1999; 17:157-67.

43. Muratoglu OK, Bragdon CR, O'Conner DO, Jasty M, Harris WH, Gul R, McGarry F. Unified wear model for highly crosslinked ultra-high molecular weight polyethylenes UHMWPE. *Biomaterials*. 1999; 20:1463–70.

44. Peters PC, Engh GA, Dwyer KA, and Vinh TN. Osteolysis after total knee arthroplasty without cement. *J Bone Joint Surg* Am. 1992; 74:864-76.

45. Price A, Short A, Kellett C, Beard D, Gill H, Dodd C, and Murray D. Ten-year in vivo wear measurement of a fully congruent mobile-bearing unicompartmental knee arthroplasty. *J Bone Joint Surg Br.* 2005; 87(11):1493-7.

46. Sathasivam S. and Walker PS. Computer model with surface friction for the prediction of total knee kinematics. *J Biomechanics.* 1997; 30:177-84.

47. Sathasivam S and Walker PS. Computer model to predict subsurface damage in tibial inserts of total knees. *J Orthop Res.* 1998; 16:564-71.

48. Sawyer WG, Diaz KI, Hamilton MA, and Micklos B. Evaluation of a model for the evolution of wear in a scotch-yoke mechanism. *J Tribology.* 2003; 125:678-81.

49. Sawyer WG, Hamilton MA, Succec MC, Fregly BJ, Banks SA. Quantifying multidirectional sliding motions in total knee replacements. *J Tribology*. 2004; 127:280-6.

50. Schipplein OD and Andriacchi TP. Interaction between active and passive knee stabilizers during level walking. *J Orthop Res*. 1991; 9:113-9.

51. Schmalzried TP, Szuszczewicz ES, Northfield MR, Akizuki KH, Frankel RE, Belcher G, and Amstutz HC. Quantitative assessment of walking activity after total hip or knee replacement. *J Bone Joint Surg Am.* 1998; 80:54-9.

52. Sharkey PF, Hozack WJ, Rothman RH, Shastri S, Jacoby SM. Why are total knee arthroplasties failing today? *Clin Orthop.* 2002; 404:7-13.

53. Taylor SJG and Walker PS. Force and moments telemetered from two distal femoral replacements during various activities. *J Biomech.* 2001; 34:839-48.

54. Taylor SJG, Walker PS, Perry JS, Cannon SR, and Woledge R. The forces in the distal femur and the knee during walking and other activities measured by telemetry. *J Arthroplasty.* 1998; 13:428-37.

55. Waldman SD and Bryant JT. Compressive stress relaxation behabvior of irradiated ultra-high molecular weight polyethylene at 37ºC. *J Applied Biomat.* 1994; 5:333-8.

56. Waldman SD and Bryant JT. Dynamic contact stress and rolling resistance model for total knee arthroplasties. *J Biomech Eng.* 1997; 119:254-60.

57. Walker PS, Blunn GW, and Lilley PA. Wear testing of materials and surfaces for total knee replacements. *J Biomed Mater Res*. 1996; 33:159-75.

58. Wang A. A unified theory of wear for ultra-high molecular weight polyethylene in multi-directional sliding. *Wear.* 2001; 248:38–47.

59. Williams IR, Mayor MB, and Collier JP. The impact of sterilization method on wear in knee arthroplasty. *Clin Orthop.* 1998; 356:170-80.

60. Wimmer MA and Andriacchi TP. Tractive forces during rolling motion of the knee: Implications for wear in total knee replacement. *J Biomech.* 1997; 30:131-7.

61. Wimmer MA, Andriacchi TP, Natarajan RN, Loos J, Karlhuber M, Petermann J, Schneider E, and Rosenberg AG. A striated pattern of wear in ultrahigh-molecular-weight polyethylene components of Miller-Galante knee arthoplasty. *J Arthroplasty.* 1998; 13:8-16.

62. Wroblewski BM, Siney PD, and Fleming PA. Low friction arthroplasty of the hip using alumina ceramic and crosslinked polyethylene: A ten-year follow-up report. *J Bone Joint Surg Br.* 1999; 81:54-5.

Table 9.1: Quantitative Summary of Damage Results Predicted by the Computer Simulations for Gait and Stair Activities with 70-30 and 50-50 Load Splits

Load Split	Damage	Gait			Stair		
		Medial	Lateral	Total	Medial	Lateral	Total
70-30	Wear depth (mm)	0.5	0.5	—	0.6	0.7	—
	Creep depth (mm)	0.5	0.3	—	2.1	0.5	—
	Damage depth (mm)	1.0	0.8	—	2.7	1.2	—
	Area (mm^2)	372	321	693	337	206	543
	Damage volume (mm^3)	123	54	177	200	74	274
50-50	Wear depth (mm)	0.3	0.7	—	0.5	0.9	—
	Creep depth (mm)	0.4	0.4	—	0.6	0.7	—
	Damage depth (mm)	0.7	1.1	—	1.1	1.6	—
	Area (mm^2)	359	352	711	318	233	551
	Damage volume (mm^3)	94	85	179	147	113	260

Maximum wear, creep and total damage may occur at different locations on the surface.

Table 9.2: Quantitative Comparison Between Retrieval Damage and Simulation Damage Predicted by an Activity Partition of 85% Gait, 15% Stair with a 70-30 Load Split

Damage	Retrieval[a]			Simulation		
	Medial	Lateral	Total	Medial	Lateral	Total
Total depth (mm)	0.7	0.8	—	0.8	0.9	—
Area (mm^2)	422	305	727	483	329	812

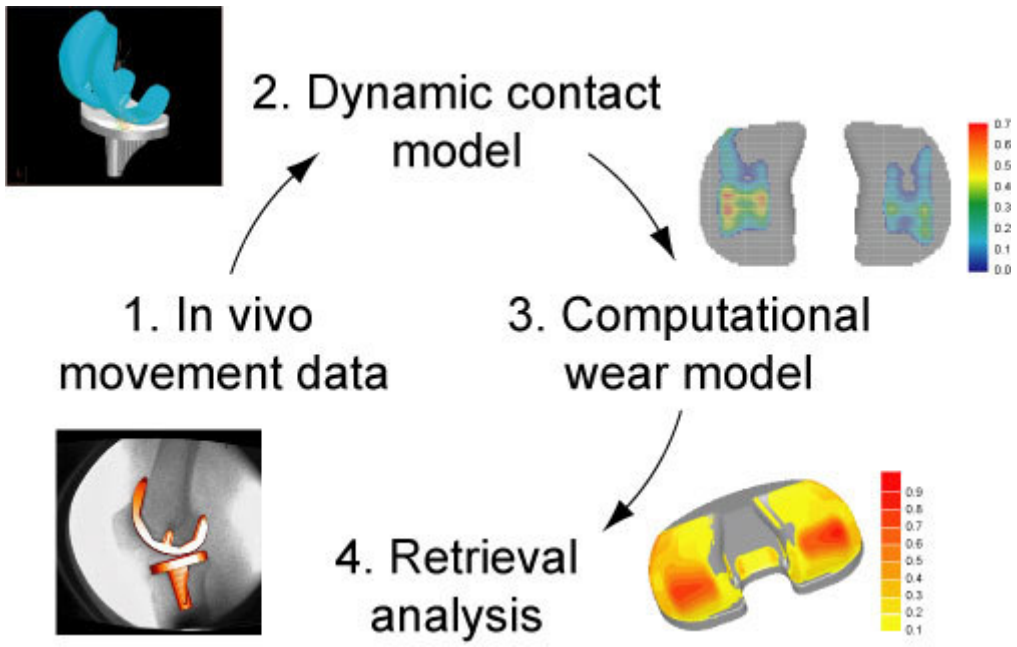

Figure 9.1: Overview of the Experimental and Computer Modeling Methods Used to Develop and Evaluate Wear Predictions

(1) In vivo fluoroscopic data provide patient-specific kinematic inputs to a dynamic contact model of the same knee design and size; (2) the dynamic model predicts contact pressures and slip velocities experienced by individual elements on the tibial insert surface and outputs these data to a computational wear model; (3) the wear model performs wear and creep analyses to calculate the total damage depth for each element and outputs the worn geometry to computer aided inspection software; and (4) the inspection software produces color contour maps of the predicted damage regions, which are compared with a damage contour map produced from a laser scan of the tibial insert retrieved from the same patient whose fluoroscopic data were used as model inputs.

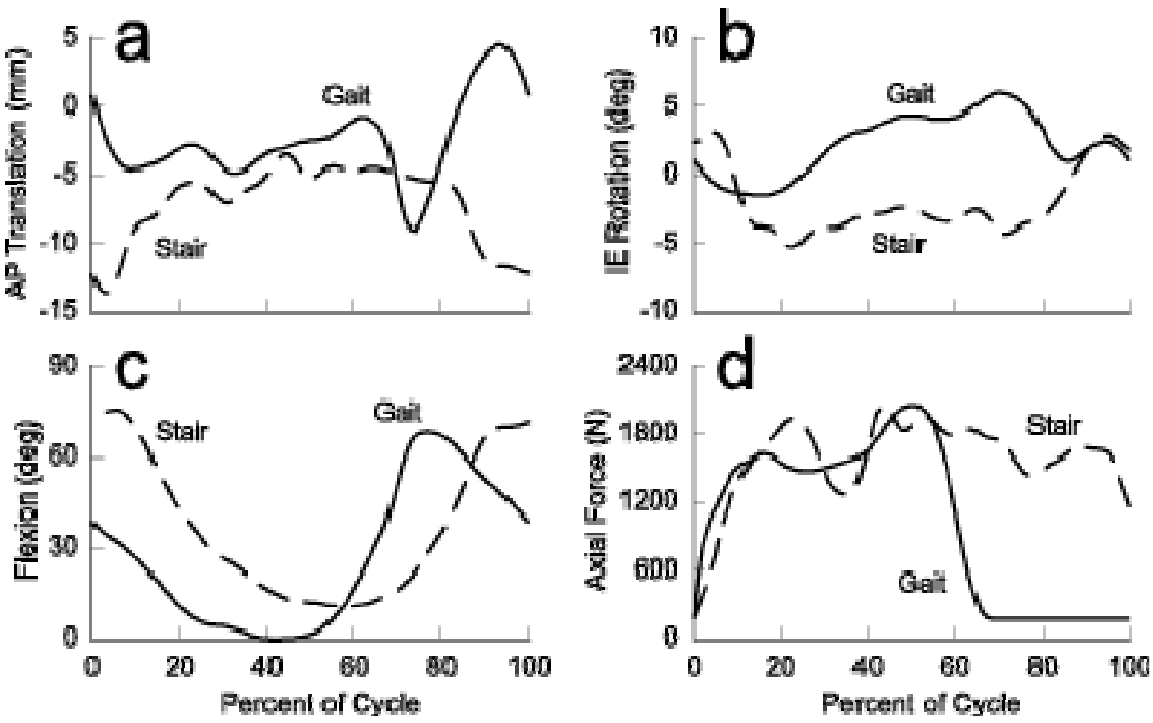

Figure 9.2: In vivo Experimental Data Used as Inputs to the Dynamic Contact Model (a) Anterior–posterior (AP) translation; (b) internal–external (IE) rotation; (c) Flexion; and (d) axial force. Kinematic data are from pre-retrieval video fluoroscopy gait and stair experiments with the femur moving with respect to the tibia. Anterior translation and external rotation are positive. Axial force data are scaled vertical ground reaction force data from a patient of similar age, height, weight, and knee flexion characteristics.

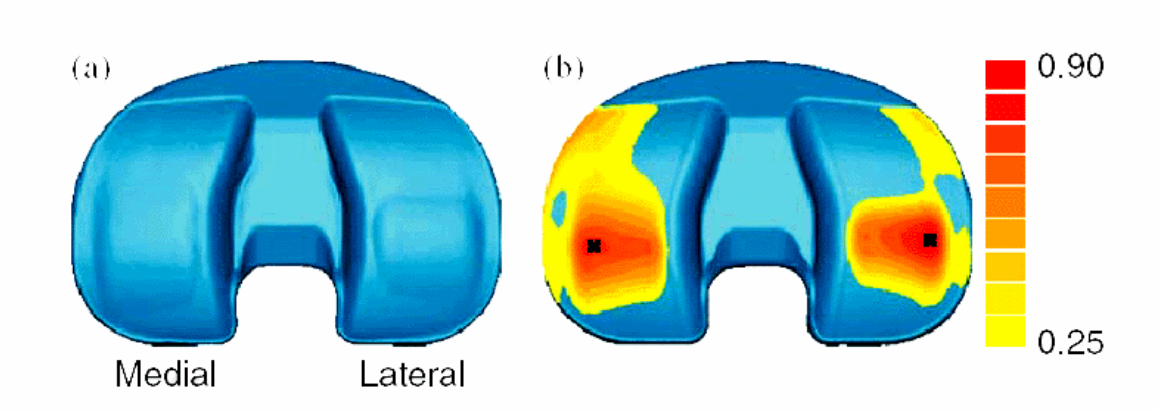

Figure 9.3: Damage Visualization of the Retrieved Tibial Insert

(a) Laser scan showing damage regions visible to the naked eye; and (b) contour map indicating depth of damage zones. Color bar indicates depth in mm. Stars indicate location of maximum damage on each side.

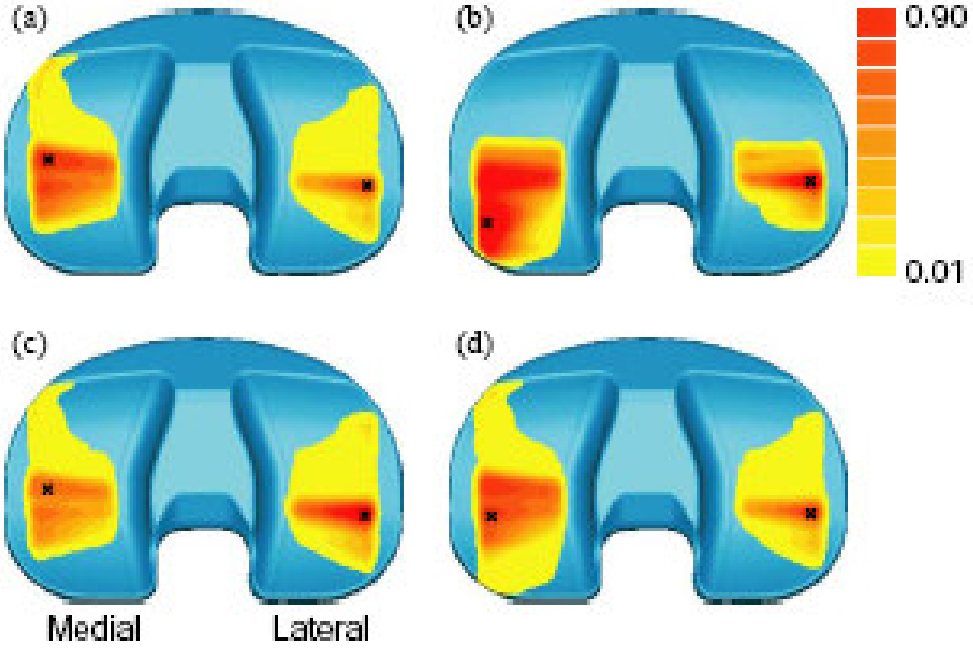

Figure 9.4: Damage Contour Maps Predicted by the Computer Simulations (a) Gait with 70–30 load split; (b) stair with 70–30 load split; (c) gait with 50–50 load split; and (d) combined activity assuming 85% gait, 15% stair with 70–30 load split. Color bar indicates depth in mm. Stars indicate location of maximum damage on each side. Both gait and stair accurately predicted the location of maximum damage on the lateral side, while only combined activity predicted the correct location on the medial side.

10 COMPUTATIONAL MODELS CAN PREDICT POLYTHYLENE INSERT DAMAGE IN TOTAL KNEE REPLACEMENTS

10.1 Introduction

A computational model that accurately predicts clinically observed damage occurring in the polymer bearings of total knee replacements (TKR) is a powerful predictive tool. Analytical models use the finite element (FE) method to visualize the magnitude and location of stress on and within polyethylene tibial inserts. Such models enhance the visualization of mechanisms associated with bearing wear and facilitate evaluation of innovative design changes on the wear mechanisms.

Primary to TKR longevity is the durability of the ultra-high molecular weight polyethylene (UHMWPE) tibial insert component.[10,31] Sharkey *et al.*[31] found that UHMWPE wear was the primary reason for 25% of revision TKR surgeries. UHMWPE bearing wear contributes to TKR failure through mechanisms of bearing creep, debris generation, "wear through", delamination and fracture.[7,17] Many researchers[4,18,27,28] have associated accumulated damage observed in UHMWPE to specific states of cyclic stress that arise when a femoral component articulates with a tibial insert. Abrasive/adhesive wear mechanisms are related to the magnitude and distribution of compressive normal (contact) stresses on the surface of the tibial insert and relative tangential velocities between components. Delamination cracks that propagate parallel to, but just below, the articulating surface are associated with Von Mises stresses. Pitting (cracks that develop in a

direction perpendicular to the articulating surface) is a function of the range of maximum principal stresses that any given point in the polymer experiences in a gait cycle.

Although contact area is a simple and often used performance benchmark, it can be a poor predictor of wear performance. Contact stress and its distribution on the articulating surface is directly related to abrasion, pitting and delamination of the tibial insert and is a far more reliable predictor of long term wear performance than contact area. The objective of this study was to verify computational results of contact areas and contact stresses from FE models with damage patterns observed on UHMWPE tibial bearings retrieved after TKR

10.2 Materials and Methods

Three-dimensional, finite element (FE) models of a fixed-bearing TKR (Duracon, Howmedica, Rutherford, NJ) and a rotating-platform TKR (LCS, DePuy, Warsaw, IN) were created by measuring the articular surfaces of implantable quality parts using a coordinate measuring machine and laser profilometer.[22] The resulting cloud of data points represented the actual manufactured surfaces and was imported into the FE software to define the geometries of both the femoral and tibial insert components.[21] The modeled tibial insert was positioned in the computer according to the specified surgical procedure from each manufacturer.

The femoral surface was treated as a rigid body and was articulated with the modeled tibial insert using the average values for the heel-strike portion of the level walking cycle[23,24,26] (1,950 N) and flexion angle[1,16,25] (0° flexion). All polymer inserts were characterized by the same gamma irradiated, nonlinear material[32] of 10 mm thickness maintained at 37° Celsius. The virtual components were allowed to settle into

their preferred alignments without consideration of friction or soft tissue constraints. The resulting stress distributions on and within the polymer insert were then photorealistically imaged allowing visual comparison of the different implant designs.

Two groups of retrieved UHMWPE tibial components were evaluated,[13,14] including 17 fixed-bearing TKR (Group FB) and 13 rotating-platform TKR (Group RP) that were the same designs as used in the FE models. The index TKR surgical technique for Group FB included implantation of one prosthesis design (Duracon) using retention of the posterior cruciate ligament and cement fixation. The index TKR surgical technique for Group RP included implantation of one prosthesis design (LCS) using resection of the posterior cruciate ligament and cementless fixation. The UHMWPE bearings in both groups exceeded 6 mm in thickness and were sterilized using gamma radiation in air.

Group FB consisted of 15 female and 2 male patients with a mean age of 69±6 years (range, 55-76) at revision. Functional duration for Group FB averaged of 16±11 months (1-37 months) and reasons for revision included loosening (7 knees), infection (4 knees), instability (3 knees), and pain (3 knees). Group MB consisted of 6 female and 7 male patients with a mean age of 69±11 years (range, 55-79) at revision. Functional duration for Group MB averaged 53±52 months (11-162 months) and reasons for revision included loosening (4 knees), pain and/or stiffness (4 knees), UHMWPE wear (3 knees), infection (1 knee), and unknown (1 knee).

Articular surfaces of the retrieved bearings were visually inspected at 10 to 30 times magnification and the prevalence of nine distinct damage modes (abrasion, burnishing, creep deformation, delamination, embedded debris, pits, scratches, striations

and fracture) was assessed.[12,15,34] Damage mode areas and locations were measured from digital images of the articular surfaces using published image analysis techniques.[8,12]

10.3 Results

Differences in the computed contact area and stresses were noted between the groups (Table 10.1). Contact area for Group FB was 76% smaller than Group RP, with associated higher peak contact stress. Stresses associated with delamination damage (Von Mises stress) and pitting damage (principal stress) were also higher for Group FB compared to Group RP (Figure 10.1).

Damage patterns were centrally located and occupied 59%$\pm$16% and 72%$\pm$16% of the articular surfaces of Group FB and Group RP, respectively (Figure 10.2). Scratching, pitting, burnishing and striations were the largest and most common damage modes for Group FB, with a frequency of 62% to 79% for the retrieved bearings in that group (Figure 10.3). Only one Group FB bearing had delamination occupying less than 1% of the articular surface. Scratching, pitting, burnishing, striations and abrasion were the largest and most common damage modes for Group RP, with a frequency of 69% to 85% for the retrieved bearings in that group (Figure 10.3). Three Group RP bearings had delamination occupying up to 35% of the articular surfaces.

10.4. Conclusions

A feature common to analytical and computational models is the inclusion of simplifying assumptions meant to reduce a complex problem to one that is more easily understood. It is important to check the effect of a model's simplifying assumptions against a set of relevant benchmarks to assure that an oversimplification does not lead to errant conclusions. Similarity between a model result and benchmark increases

confidence in the validity of the model. When modeling TKR wear, comparison with damage patterns observed on UHMWPE TKR bearings retrieved after in vivo function is a widely accepted standard benchmark.

A model also is more valuable if it can be validated to several extreme cases, providing confidence that the model can be exercised in a range of circumstances and still yield accurate and useful results. The current study characterized the predicted contact stresses and in vivo wear performance of two very different TKR designs, each with highly successful clinical outcomes reported in the medical literature. [5,6,19,20] Group FB was characteristic of nonconforming, fixed bearing TKR with a relatively small predicted contact area. Group RP was characteristic of a conforming, mobile bearing TKR with a relatively large predicted contact area. The average articular damage area on bearings retrieved after in vivo function was greater in Group RP bearings than Group FB bearings (Figures 10.2 and 10.3), consistent with the larger predicted contact area in the FE model for Group RP. The ability of the FE model to predict clinically relevant damage patterns was verified for each of these extremes based on these comparisons with retrieved bearings.

Material failure theories for polymers[33] suggest that pitting and delamination in a UHMWPE tibial insert is unlikely to develop when cycled through a stress range less than 9 MPa. As stresses experienced by a given point within a UHMWPE bearing exceed this threshold, there is a higher potential for crack development at that point. In contrast, a minimum contact stress threshold that initiates abrasive damage under physiologic cyclic loading is not universal for UHMWPE[27,28] and is likely to vary with material properties, design characteristics and the articular loading environment. As the cyclical

nature of patient kinematics repeatedly moves the areas of contact around on a tibial insert, a given point of polymer may be at one moment under great tension followed by a moment of large compression, fatiguing the material.

In the current study, both Group FB and Group RP bearings had predicted principal stresses exceeding a 9 MPa range (Table 10.1) and the area of pitting damage averaged 10% to 15% on retrieved bearings in both groups (Figure 10.3), consistent with the FE model predictions. Pitting damage around the periphery of Group RP TKR was predicted by the FE model, similar to the pattern of pitting damage observed on the retrieved Group RP bearings (Figure 10.4). However, the maximum principal stress range for Group FB was twice as large as the range predicted for Group RP, without an associated change in observed pitting damage. Confounding factors associated with material properties and duration of function, as well as contact stress, likely affected the observed damage patterns on retrieved bearings.

It is recognized that the FE results in this study represent best-case scenarios, due to average heel-strike loads being applied to optimally aligned components. The effects of soft tissues and kinematic phenomena like femoral rollback and anteroposterior sliding were not considered and only the intrinsic curvatures of the components guided their optimal alignment. Contact areas at heel-strike, if subjected to typical patient kinematics,[2,3] would predict a similar damage pattern to that seen on the retrieved Group FB bearings (Figure 10.5). The kinematics of component articulation during cyclical activities such as walking gait and stair climb would propel the visualized stress patterns about the tibial insert, with associated changes in shape and intensity.

Knee kinematics are an important determinant in the wear mechanisms that occur in patients after TKA and must be considered in any model predicting the wear scars observed in clinical retrievals of TKA UHMWPE bearings. FE models have been recently extended to consider damage accumulation in the tibial insert[29,30] and kinematics using an explicit analysis.[11] In addition, dynamic contact models[9] have been used to address surface deformation due to compressive creep and material removal due to mild wear. Mild wear is consistent with the adhesive-abrasive damage modes observed on the retrieved bearings in the current study, including scratching, burnishing and striations. Both FE models and dynamic contact models have proven useful for predicting the different types of damage observed on retrieved TKR bearings.[9,21]

Determination of optimal tibiofemoral conformity for stable TKR function and long-term durability is aided by FE model predictions for a wide range of TKR articular geometries.[21] FE computational models in the current study successfully predicted the damage patterns observed on retrieved bearings with largely different articular geometries, and as such, may prove to be a valuable tool for determining *a priori* the wear performance of new TKR designs. These models may also prove useful in the manufacturers design stage to vet product concepts computationally prior to the time and expense required by physical laboratory wear testing and clinical trials.

10.5. Acknowledgements

The author thanks Edward Morra, MSME and A. Seth Greenwald, D.Phil.(Oxon) for co-authoring publication of this work; and George D. Markovich and Sabine Schmitt, MD for providing retrieved TKR components. This work was supported by The Biomotion

Foundation of Palm Beach, Florida and Orthopaedic Research Laboratories of Cleveland, Ohio.

Note: This chapter is an abstracted version of the full published work as referenced.

Morra EA, Harman MK, Greenwald AS: Computational models can predict polymer insert damage in total knee replacements. In *Insall & Scott Surgery of the Knee, 4th edition*, Vol. 1 (13):271-283, Scott WN (ed.) Elsevier Inc., Philadelphia, PA, 2005.

10.6. References Cited

1. Apkarian J, Naumann S, Cairns B. A three-dimensional kinematic and dynamic model of the lower limb. *J Biomech*. 1989; 22(2):143-55.
2. Banks SA, Hodge WA. Hap Paul Award paper of the International Society for Technology in Arthroplasty. Design and activity dependence of kinematics in fixed and mobile-bearing knee arthroplasties. *J Arthroplasty*. 2004; 19(7):809-16.
3. Banks SA, Hodge WA. Implant design affects knee arthroplasty kinematics during stair-stepping. *Clin Orthop*. 2004; 426:187-93.
4. Bartel DL, Bicknell MS, Wright TM. The effect of conformity, thickness, and material on stresses in UHMWPE components for total joint replacement. *J Bone Joint Surg*. 1986; 68A(7):1041-51.
5. Buechel FF Sr, Buechel FF Jr, Pappas MJ, D'Alessio J. Twenty-year evaluation of the New Jersey LCS rotating platform knee replacement. *J Knee Surg*. 2002; 15(2):84-9.
6. Buechel FF Sr, Buechel FF Jr, Pappas MJ, D'Alessio J. Twenty-year evaluation of meniscal bearing and rotating platform knee replacements. *Clin Orthop*. 2001; 388:41-50.
7. Collier JP, Mayor MB, McNamara JL, Surprenant VA, Jensen RE. Analysis of the failure of 122 polyethylene inserts from uncemented tibial knee components. *Clin Orthop*. 1991; 273:232-42.
8. Cornwall GB, Bryant JT, Hansson CM, Rudan J, Kennedy LA, Cooke TD. A quantitative technique for reporting surface degradation patterns of UHMWPE components of retrieved total knee replacements. *J Appl Biomater*. 1995; 6:9-18.
9. Fregly B, Sawyer W, Harman M, Banks S. Computational wear prediction of a total knee replacement from in vivo kinematics. *J Biomech*. 2005; 38:305-14.

10. Furnes O, Espehaug B, Lie SA, Vollset SE, Engesaeter LB, Havelin LI. Early failures among 7,174 primary total knee replacements: A follow-up study from the Norwegian arthroplasty register 1994-2000. *Acta Orthop Scand*. 2002; 73(2):117-29.

11. Halloran JP, Petrella AJ, Rullkoetter PJ. Explicit finite element modeling of total knee replacement mechanics. *J Biomech*. 2005; 38(2):323-31.

12. Harman MK, Banks SA, Hodge WA. Polyethylene damage and knee kinematics after total knee arthroplasty, *Clin Orthop*. 2001; 392:383-93.

13. Harman MK, Banks SA, Schmitt S, Hedley AK, Hodge WA. Total knee replacement performance beyond 5 years: Can in vivo fluoroscopy and retrieved implant analysis lead the way? *69th Annual Meeting of the American Academy of Orthopaedic Surgeons*. 2002; Dallas, TX.

14. Harman MK, Markovich GD, Banks SA, Hodge WA. Cementless LCS total knee arthroplasty after 9 years in-situ: Articular and backside wear on retrieved meniscal and rotating platform polyethylene bearings. *71st Annual Meeting of the American Academy of Orthopaedic Surgeons*. 2004; San Francisco, CA.

15. Hood RW, Wright TM, Burstein AH. Retrieval analysis of total knee prostheses: A method and its application to 48 total condylar prostheses. *J Biomed Mater Res*. 1983; 17:829-42.

16. LaFortune MA, Cavanaugh PR, Sommer HJ, Kalenack A. Three-dimensional kinematics of the human knee during walking. *J Biomech*. 1992; 25(4):347-57.

17. Landy MM, Walker PS. Wear of ultra-high molecular-weight polyethylene components of 90 retrieved knee prostheses. *J Arthroplasty*. 1988; 3:S73-S85.

18. Mazzucco D, Spector M: Effects of contact area and stress on the volumetric wear of ultrahigh molecular weight polyethylene. *Wear*. 2003; 254(5-6):514-22.

19. Mont MA, Becher OJ, Lee CW, LaPorte DM, Hungerford DS. Patellofemoral complications after total knee arthroplasty: A comparison of modular Porous-Coated Anatomic with Duracon prostheses. *Am J Orthop*. 1999; 28:241-7.

20. Mont MA, Yoon TR, Krackow KA, Hungerford DS. Eliminating patellofemoral complications in total knee arthroplasty. Clinical and radiographic results of 121 consecutive cases using the Duracon system. *J Arthroplasty*. 1999; 14:446-55.

21. Morra EA, Harman MK, Greenwald AS. Computational models can predict polymer insert damage in total knee replacements. In *Insall & Scott Surgery of the Knee, 4th edition*, Vol. 1 (13):271-283, Scott WN (ed.) Elsevier Inc., Philadelphia, PA, 2005.

22. Morra EA, Postak PD, Plaxton MS, Greenwald AS. The effects of external torque on polyethylene tibial insert damage patterns. *Clin Orthop*. 2003; 410:90-100.

23. Morrison JB: Function of the knee joint in various activities, *Biomed Eng*, 4:573-580, 1969.

24. Morrison JB. The mechanics of the knee joint in relation to normal walking. *J Biomech*. 1970; 3:51-61.

25. Murray MP, Drought AB, Kory RC. Walking patterns in normal men. *J Bone Joint Surg*. 1964; 46A:335-360.

26. Paul JP. Forces transmitted by joints in the human body. *Proc Inst Mech Eng*. 1967; 181:358.

27. Rose RM, Goldfarb HV. On the pressure dependence of the wear of ultrahigh molecular weight polyethylene. *Wear*. 1983; 92:99-111.

28. Rostoker W, Galante JO. Contact pressure dependence of wear rates of ultra high molecular weight polyethylene. *J Biomed Mater Res*. 1979; 13:957-964.

29. Sathasivam S, Walker PS. The conflicting requirements of laxity and conformity in total knee replacement. *J Biomech*. 1999; 32(3):239-47.

30. Sathasivam S, Walker PS, Campbell PA, Rayner K. The effect of contact area on wear in relation to fixed bearing and mobile bearing knee replacements. *J Biomed Mater Res*. 2001; 58(3):282-90.

31. Sharkey PF, Hozack WJ, Rothman RH, Shastri S, Jacoby SM. Why are total knee arthroplasties failing today? *Clin Orthop.* 2002; 404:7-13.

32. Waldman SD, Bryant JT. Compressive stress relaxation behavior of irradiated ultra-high molecular weight polyethylene at 37° C. *J Appl Biomater*. 1994; 5:333-338.

33. Williams JG. *Stress Analysis of Polymers*. Halstead Press, John Wiley & Sons, 1984.

34. Wimmer MA, Andriacchi TP, Natarajan RN, Loos J, Karlhuber M, Petermann J, Schneider E, Rosenberg AG. A striated pattern of wear in ultrahigh- molecular-weight polyethylene components of Miller-Galante total knee arthroplasty. *J Arthroplasty*. 1998; 13:8-16.

Table 10.1: Contact Area and Stresses Computed in FE Model

	Group FB	Group RP
Model year evaluated	1995	1996
Contact area (mm^2)	212	875
Peak contact stress (MPa)	30.7	10.4
Von Mises peak stress (MPa)	21.8	15.4
Compressive principal peak stress (MPa)	-17.2	-5.9
Tensile principal peak stress (MPa)	13.8	9.5
Principal peak stress range (MPa)	31.0	15.4

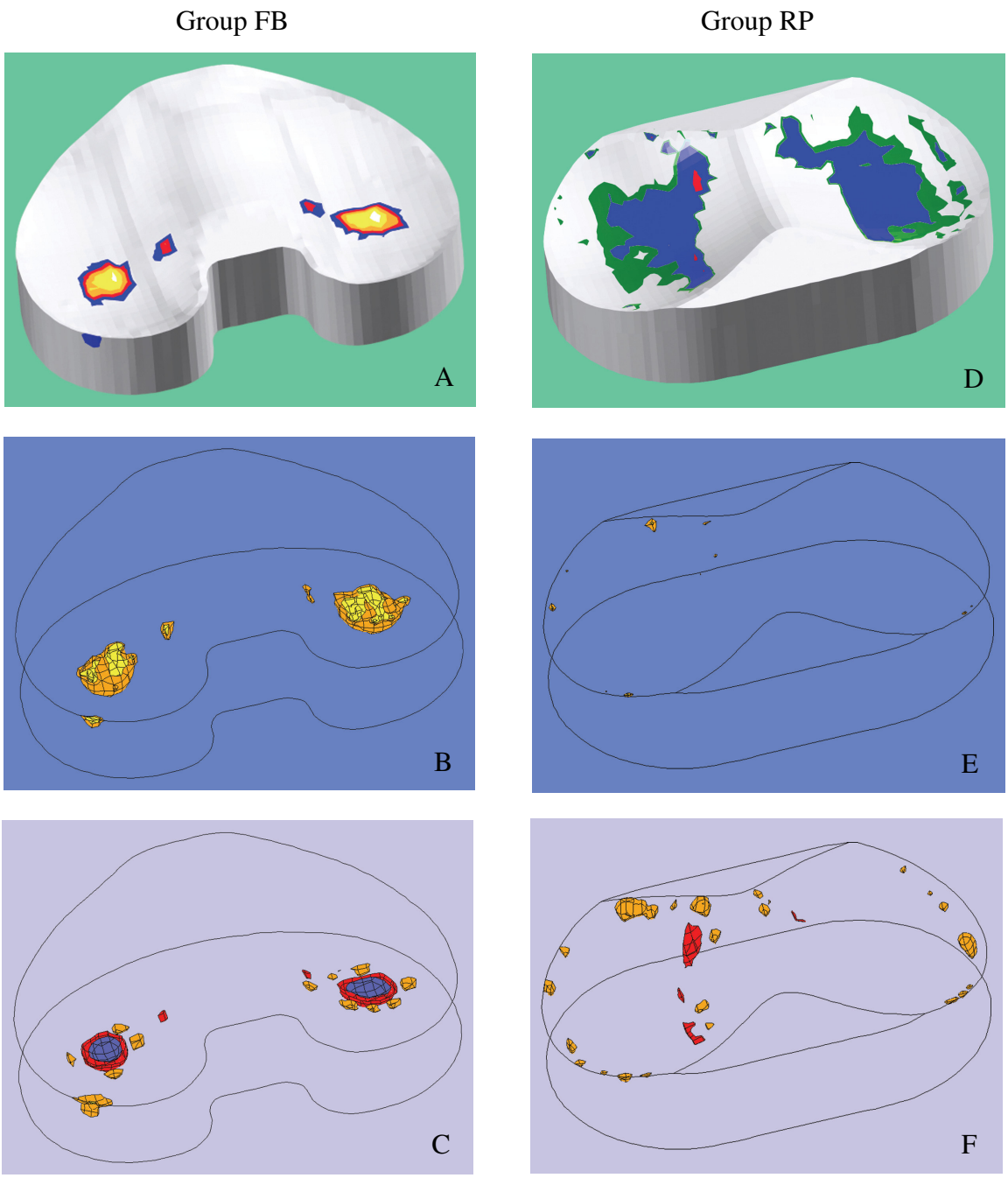

Figure 10.1: Peak Stresses for Group FB and Group RP TKA Designs

Graphical representation of peak contact stresses (A,D),

peak von Mises stresses (B, E) and peak principal stresses (C, F).

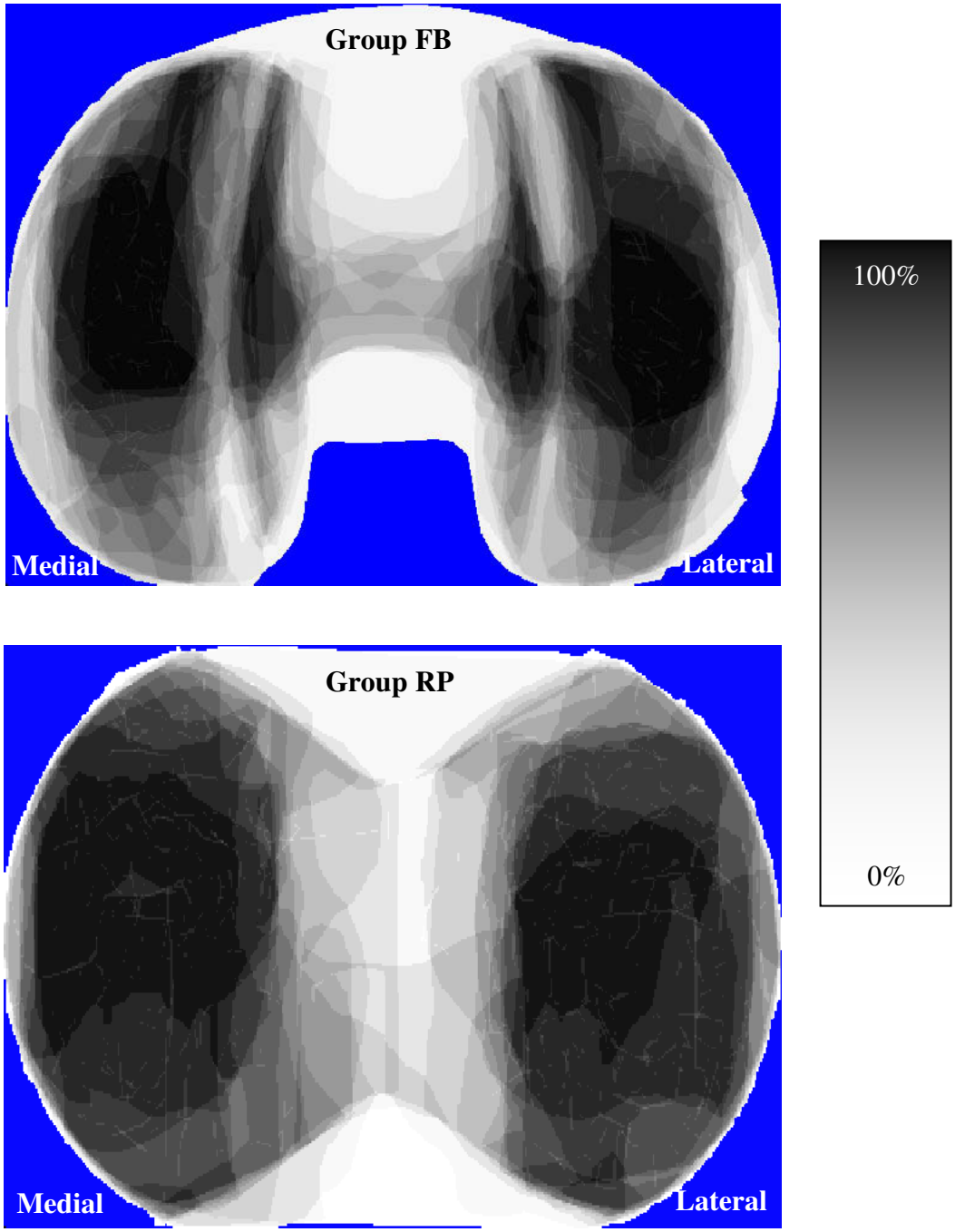

Figure 10.2: Overlay Graphic of Damage Patterns for Group FB

and Group RP UHMWPE Bearings

Darker patterns indicate a greater number of inserts had damage in a given region.

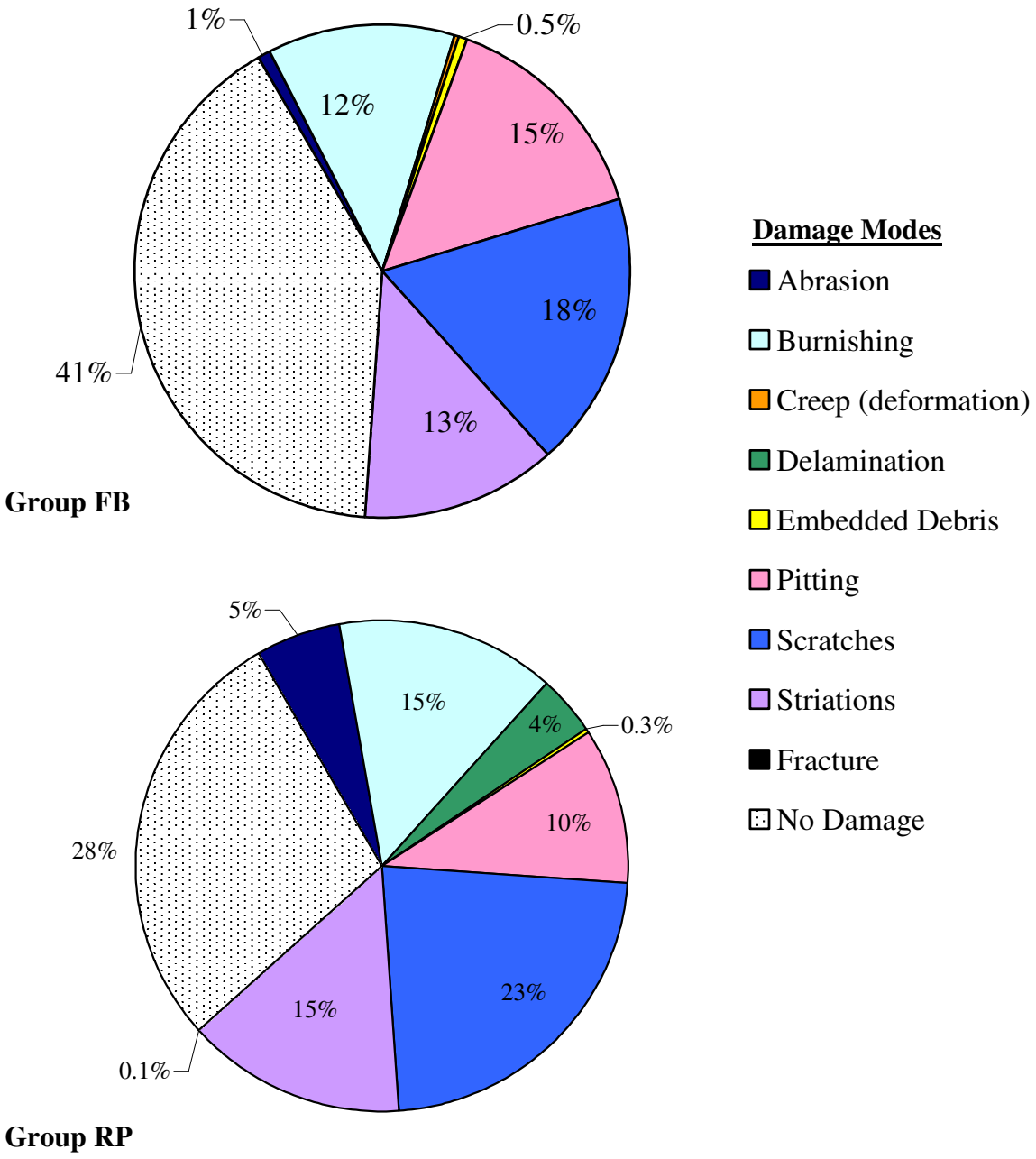

Figure 10.3: Articular Damage Area for Different Damage Modes

on the Retrieved UHMWPE Bearings from Each Group

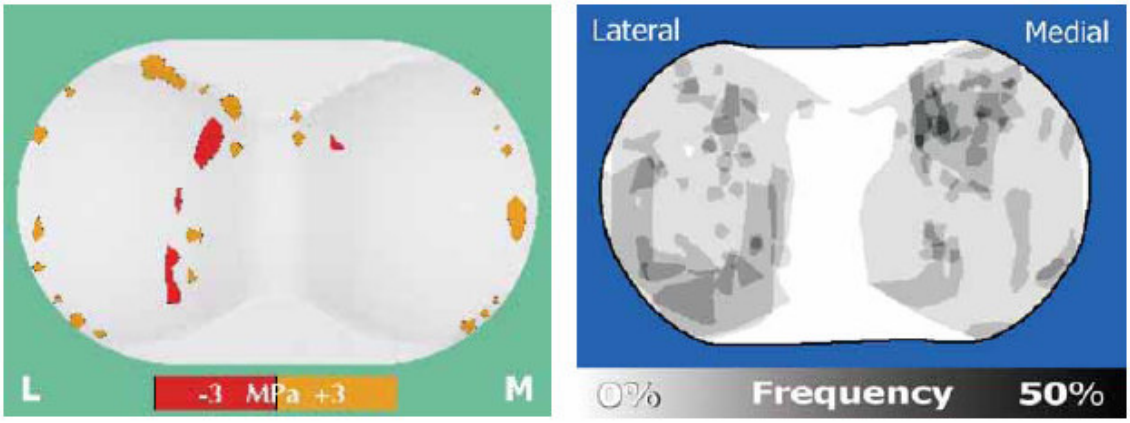

Figure 10.4: Compressive (red) and Tensile (orange) Peak Principal Stresses for Group RP and Overlay Graphic of Pitting Damage for Retrieved Group RP Bearings

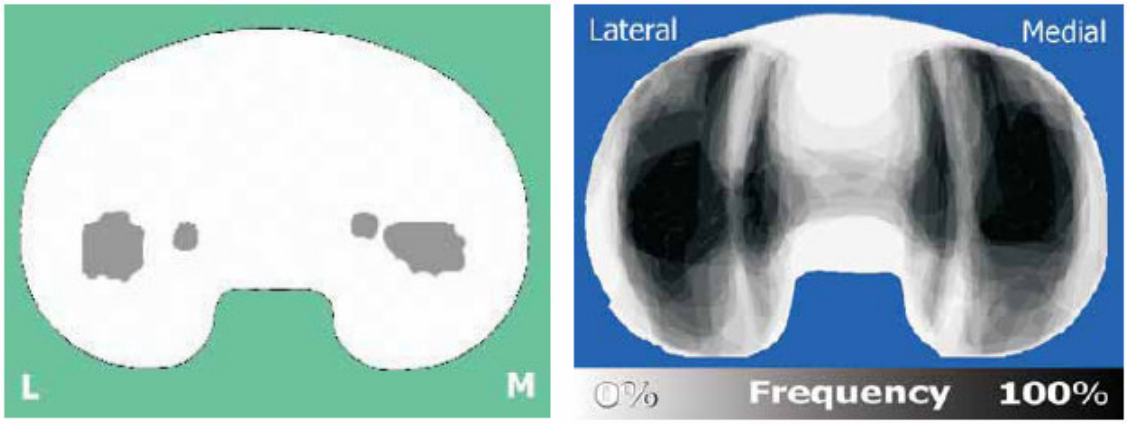

Figure 10.5: Contact Locations Predicted for Group FB at Heel Strike and Overlay Graphic of All Damage Modes for Retrieved Group FB Bearings

11 ESTIMATING TIBIOFEMORAL KINEMATICS FROM THE ARTICULAR GEOMETRY OF POLYETHYLENE TIBIAL INSERTS

11.1 Introduction

Articular damage patterns on polyethylene tibial inserts retrieved after *in vivo* function have been attributed to different wear mechanisms and femoral contact locations during total knee arthroplasty (TKA) motion.[10,11,15,17,18,21,27,28,29] However, identifying the relationships between articular damage and joint mechanics can be difficult.[2,14,15,19,20,22,27,28,29] Without accurate descriptions of tibial-femoral articular contact during *in vivo* function, varied interpretations of contact conditions and damage mechanisms can be inferred from a given damage pattern.

Fluoroscopic analysis of patients' knee function after TKA has emerged as a useful *in vivo* technique for evaluating three dimensional kinematics of the femoral and tibial components during dynamic activities.[1-9,12,13,23,24] In patients that have participated in fluoroscopic evaluation prior to implant retrieval, the location of tibiofemoral contact is significantly correlated to the articular damage location on the polyethylene inserts retrieved from the same patients.[15] Those findings[15] suggest that articular damage patterns can be used to estimate the "contact envelope", or range of tibiofemoral contact that existed during *in vivo* function.

The objective of this study was to develop a novel measurement technique to estimate three-dimensional femoral component kinematics relative to the tibial component after implant retrieval. It was hypothesized that the femoral component could

be optically tracked as a spatial sensor, using the polyethylene articular geometry to guide its position and orientation.

The objective of this study was to develop a novel measurement technique to estimate three-dimensional femoral component kinematics relative to the tibial component after implant retrieval. It was hypothesized that the femoral component could be optically tracked as a spatial sensor, using the polyethylene articular geometry to guide its position and orientation.

11.2 Materials and Methods

Tibiofemoral kinematics of a fixed bearing prosthesis design (Series 7000, Stryker Orthopaedics, Mahwah, NJ) were assessed using the articular geometry of the tibial insert to guide the relative motions of the femoral and tibial TKA components. A motion capture system consisting of four high-speed digital video cameras (MX-40, Vicon, Los Angeles, CA) interfaced with a computer and image capture software (Nexus 1.0, Vicon, Los Angeles, CA) optically tracked a series of 11 reflective marker spheres rigidly attached to the femoral components and tibial inserts (Figure 11.1). The cameras were positioned on a frame above the calibrated working volume and a global coordinate system was established (Figure 11.2). The cameras recorded at 50 frames/second with a resolution of 0.343 mm/pixel, resulting in approximately 0.200 mm error when the markers were tracked by two or more cameras.

The geometric positions of the spheres were measured relative to identifiable landmarks on the femoral and tibial components using the hand-held digital stylus (MicroScribe 3DX Immersion Corp., San Jose, CA) interfaced with a computer and surfacing software (Rhinoceros, Robert McNeel & Associates, Seattle, WA). Femoral

component and tibial insert geometry were registered within the global coordinate system by digitizing specific landmarks on each component and the marker spheres. This established a static model of each component specific to geometry and size and a component-based coordinate system, according to previously established conventions for TKA prostheses[3] (Figures 11.3). The positions and orientations of the femoral and tibial components in laboratory coordinates were given by the time varying 4x4 matrix of

$$^{Lab}T_{Fem\_implant} = {}^{Lab}T_{Fem\_array} * {}^{Fem\_array}T_{Fem\_implant} \text{ and} \quad (11.1)$$

$$^{Lab}T_{Tib\_implant} = {}^{Lab}T_{Tib\_array} * {}^{Tib\_array}T_{Tib\_implant}, \quad (11.2)$$

respectively.

Once the static models were created, the femoral and tibial components were positioned in an anatomic configuration (femur component superior, tibial component inferior) and moved by hand using the articular geometry on the polyethylene tibial inserts to guide the relative motions. The three-dimensional position coordinates (x, y, z) of each marker sphere were recorded by the motion capture system as the femoral and tibial components were articulated throughout two physiologic knee motions that commonly occur during activities of daily living, namely flexion-extension and anterior-posterior translation. This generated a point cloud for the incremental motions and the position and orientation of the femoral component in tibial component coordinates was given by the 4x4 matrix of

$$^{Fem\_implant}T_{Tib\_implant} = {}^{Fem\_implant}T_{Lab} * {}^{Lab}T_{Tib\_implant} = \left({}^{Lab}T_{Fem\_array} * {}^{Fem\_array}T_{Fem\_implant}\right)^{-1} * {}^{Lab}T_{Tib\_array} * {}^{Tib\_array}T_{Tib\_implant}. \quad (11.3)$$

The outputs of this technique were the kinematics of the femoral component relative to the tibial component, as given by the absolute translations and rotations of the component within a component-based coordinate system. The relative angles between the two components were determined using the Cardan angle convention as a 3-1-2 ordered sequence[26] from the computed tibiofemoral pose. The locations of femoral contact were determined as the lowest point on each femoral condyle with respect to the transverse plane of the tibial baseplate.[3,7] For visual presentation, the positions and orientations of the femoral and tibial components were used to pose computer-aided design (CAD) models of both components, replicating the actual arrangement of the components throughout the dynamic motions.[3] The technique was 92.5% accurate with a precision of 0.008 mm for linear translations.

11.3 Results

The ranges of femoral component kinematics were quantified (Table 11.2), corresponding to the CAD model poses (Figures 11.4 and 11.6). The femoral component motions in the first trial approximated 90° of flexion-extension with limited (~ 1 cm) of anterior-posterior translation (Figures 11.4 and 11.5). The femoral component motions in the second trial approximated 75° of flexion-extension and 4 cm of anterior-posterior translation (Figures 11.6 and 11.7). The range of superior-inferior translation was 0.6 cm to 0.8 cm, consistent with slight dishing of the polyethylene articular surface in the sagittal plane.

11.4 Conclusions

A novel measurement technique to estimate three-dimensional TKA kinematics has been developed. This technique demonstrates that the femoral and tibial components

can be optically tracked as spatial sensors using conventional motion capture technology. The articular geometry of the polyethylene tibial insert was successfully used to guide femoral component motion through a physiologic range of motion. These results complement previous studies that used articular surface wear and deformation on retrieved hip and knee polyethylene bearings to guide the positioning of measurement sensors.[16,25]

The preliminary data in the current study support the use of articular damage patterns on retrieved tibial inserts to estimate the "contact envelope", or range of tibiofemoral contact, that existed during *in vivo* function, prior to implant retrieval. Objective, quantitative estimates of tibial-femoral kinematics and articular contact during *in vivo* function should prove useful for interpreting damage patterns evident on retrieved TKR. Continuing to expand the utility of this spatial sensor can provide quantitative estimates of knee kinematics to other test methodologies based on the variety of contact pathways evident on retrieved TKA bearings.

11.5 Acknowledgement

The author thanks Scott A. Banks, PhD and James C. Coburn, ScM for technical contributions; and Osteonics Corp. (now Stryker Orthopaedics), Mahwah, New Jersey for providing CAD models. This work was supported by funding from The BioMotion Foundation in Palm Beach, Florida.

11.6 References Cited

1. Banks SA, Fregly BJ, Boniforti F, Reinschmidt C, Romagnoli S. Comparing *in vivo* kinematics of unicondylar and bi-unicondylar knee replacements. *Knee Surg Sports Traumatol Arthros*c. 2005; 13(7):551-6.

2. Banks SA, Harman MK, Hodge WA. Mechanism of anterior impingement damage in total knee arthroplasty. *J Bone Joint Surg Am*. 2002; 84(suppl 2):37-42.

3. Banks SA, Hodge WA. Accurate measurement of three-dimensional knee replacement kinematics using single-plane fluoroscopy. *IEEE Trans Biomed Eng*. 1996; 43:638-49.

4. Banks SA, Hodge WA. Design and activity dependence of kinematics in fixed and mobile-bearing knee arthroplasties. *J Arthroplasty*. 2004; 19(7):809-16.

5. Banks SA, Hodge WA: Implant design affects knee arthroplasty kinematics during stair-stepping. *Clin Orthop*. 2004; 426:187-93.

6. Banks SA, Markovich GD, Hodge WA. In vivo kinematics of cruciate-retaining and substituting knee arthroplasties. *J Arthroplasty*. 1997; 12:297-304.

7. Banks SA, Markovich GD, Hodge WA. The mechanics of knee replacements during gait: *In vivo* fluoroscopic analysis of two designs. *Am J Knee Surg*. 1997; 10(4):261-7.

8. Banks, SA. Model based 3D kinematic estimation from 2D perspective silhouettes: Application with total knee prostheses [doctoral dissertation]. 1992; Massachusetts Institute of Technology, Cambridge, MA.

9. Banks SA. Understanding knee arthroplasty kinematics: News you can use. In *Insall & Scott Surgery of the Knee, 4th edition*, Scott WN (ed.). 2005; 1(11):258-64, Elsevier Inc., Philadelphia, PA.

10. Blunn GW, Joshi AB, Minns RJ, Lidgren L, Lilley P, Ryd L, Engelbrecht E, Walker PS. Wear in retrieved condylar knee arthroplasties: A comparison of wear in different designs of 280 retrieved condylar knee prostheses. *J Arthroplasty.* 1997; 12:281-90.

11. Cameron HU. Tibial component wear in total knee replacement. *Clin Orthop*. 1994; 309:29-32.

12. Dennis DA, Komistek RD, Hoff WA, Gabriel SM. In vivo knee kinematics derived using an inverse perspective technique. *Clin Orthop*. 1996; 331:107-17.

13. Dennis DA, Komistek RD, Colwell CE, Ranawat CS, Scott RD, Thornhill TS, Lapp MA. In vivo anteroposterior femorotibial translation of total knee arthroplasty: a multicenter analysis. *Clin Orthop*. 1998; 356:47-57.

14. Feng EL, Stulberg SD, Wixson RL. Progressive subluxation and polyethylene wear in total knee replacements with flat articular surfaces. *Clin Orthop*. 1994; 229:60-71.

15. Harman MK, Banks SA, Hodge WA. Polyethylene damage and knee kinematics after total knee arthroplasty. *Clin Orthop.* 2001; 392:383-93.

16. Harman MK, Schmitt S, Rössing S, Banks S, Sharf HP, Hodge WA. Polyethylene damage area and deformation on unicondylar knee prostheses retrieved after 2 to 13 years of functional duration. *ACTA Orthop*. 2006, in review.

17. Hirakawa K, Bauer TW, Yamaguchi M, Stulberg BN, Wilde AH. Relationship between wear debris particles and polyethylene surface damage in primary total knee arthroplasty. *J Arthroplasty*. 1999; 14(2):165-71.

18. Knight JL, Gorai PA, Atwater RD, Grothaus L. Tibial polyethylene failure after primary porous-coated anatomic total knee arthroplasty: Aids to diagnosis and revision. *J Arthroplasty*. 1995; 10:748-57.

19. Lewis P, Rorabeck CH, Bourne RB, et al: Posteromedial tibial polyethylene failure in total knee replacements. *Clin Orthop*. 1994; 299:11-17.

20. Puloski SK, McCalden RW, MacDonald SJ, Rorabeck CH, Bourne RB. Tibial post wear in posterior stabilized total knee arthroplasty: An unrecognized source of polyethylene debris. *J Bone Joint Surg Am*. 2001; 83:390-7.

21. Sathasivam S, Walker PS. Computer model to predict subsurface damage in tibial inserts of total knees. *J Orthop Res.* 1998; 16:564-71.

22. Silva M, Kabbash CA, Tiberi JV III, Park SH, Reilly DT, Mahoney OM, Schmalzried TP. Surface damage on open box posterior-stabilized polyethylene tibial inserts. *Clin Orthop*. 2003; 416:135-44.

23. Stiehl JB, Dennis DA, Komistek RD, Keblish PA. In vivo kinematic analysis of a mobile bearing total knee prosthesis. *Clin Orthop*. 1997; 345:60-6.

24. Stiehl JB, Komistek RD, Dennis DA, Paxson RD. Fluoroscopic analysis of kinematics after posterior-cruciate-retaining knee arthroplasty. *J Bone Joint Surg Br*. 1995; 77:884-9.

25. Tanino H, Harman MK, Banks SA, Hodge WA. Relationship between polyethylene liner design, impingement and dislocation on retrieved acetabular components. *J Orthop Res*. 2005; in press.

26. Tupling S, Pierrynowski M. Use of Cardan angles to locate rigid bodies in three-dimensional space. *Med. & Biol. Eng. & Comp.* 1987; 25:527-32.

27. Wasielewski RC, Galante JO, Leighty RM, Natarajan RN, Rosenberg AG. Wear patterns on retrieved polyethylene tibial inserts and their relationship to technical considerations during total knee arthroplasty. *Clin Orthop.* 1994; 299:31-43.

28. Wimmer MA, Andriacchi TP. Tractive forces during rolling motion of the knee implications for wear in total knee replacement. *J Biomech*. 1997; 30:131-7.

29. Wimmer M, Andriacchi T, Natarajan R, Loos J, Karlhuber M. A striated pattern of wear in ultrahigh-molecular-weight polyethylene components of Miller-Galante total knee arthroplasty. *J Arthroplasty*. 1998; 13(1):8-16.

Table 11.1: Range of Femoral Component Kinematics Relative to the Tibial Component During the Trial Physiologic Motions

	Rotations (°)			Translations (cm)		
	Flex/Ext[a]	Abd/Add[b]	Int/Ext[c]	Ant/Post[d]	Sup/Inf[e]	Med/Lat[f]
Trial 1	65	8	9	1.3	0.6	0.1
Trial 2	47	5	4	3.8	0.8	0.4

[a] Flex/Ext = flexion/extension

[b] Abd/Add = abduction/adduction

[c] Int/Ext = internal/external

[d] Ant/Post = anterior/posterior

[e] Sup/Inf = superior/inferior

[f] Med/Lat = medial/lateral

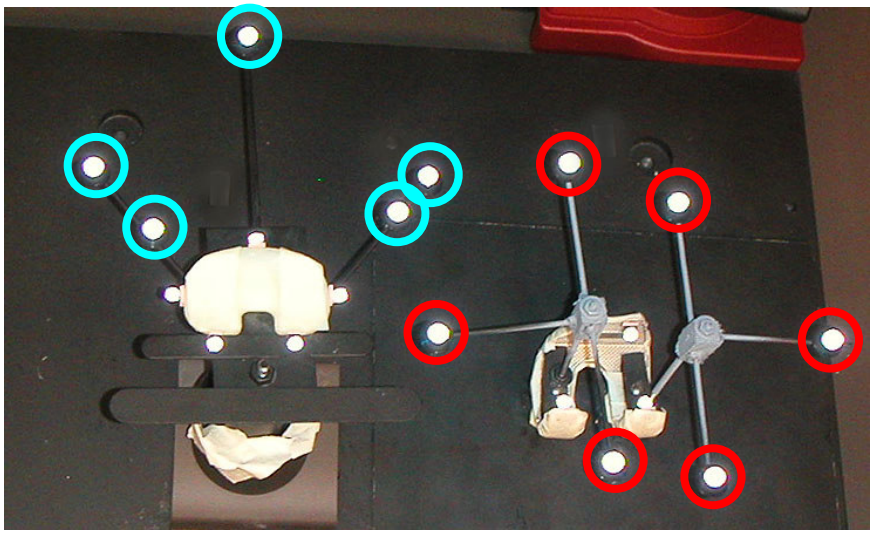

Figure 11.1: Marker Spheres Defining the Femoral and Tibial Components' Geometry Five markers (cyan) were oriented on rigid wire outriggers about the tibial insert and six markers (red) were oriented on rigid wire outriggers about the femoral component.

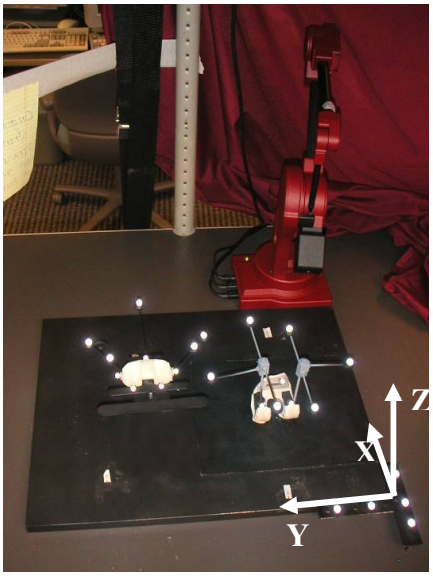

Figure. 11.2: Tibial and Femoral Components Positioned in the Calibrated Volume with Reflective Marker Spheres

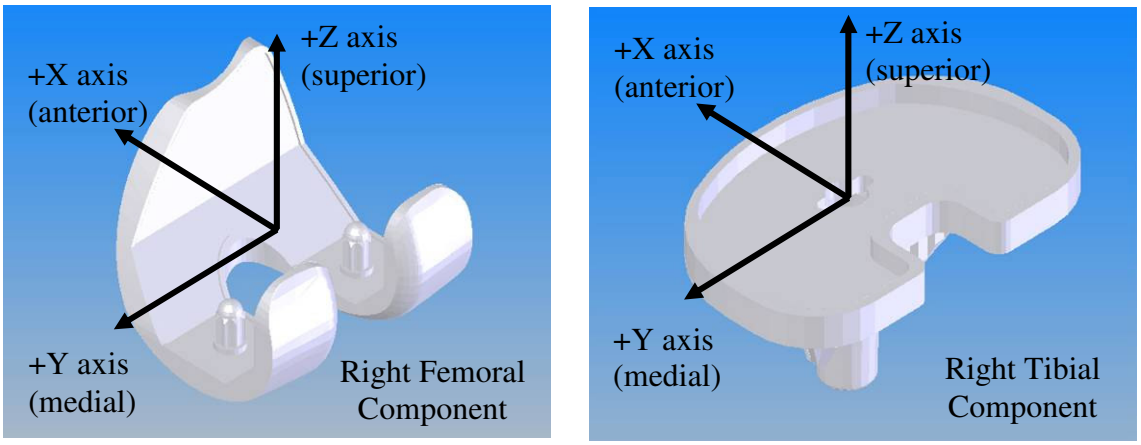

Figure. 11.3: Femoral and Tibial Component-Based Coordinate Systems

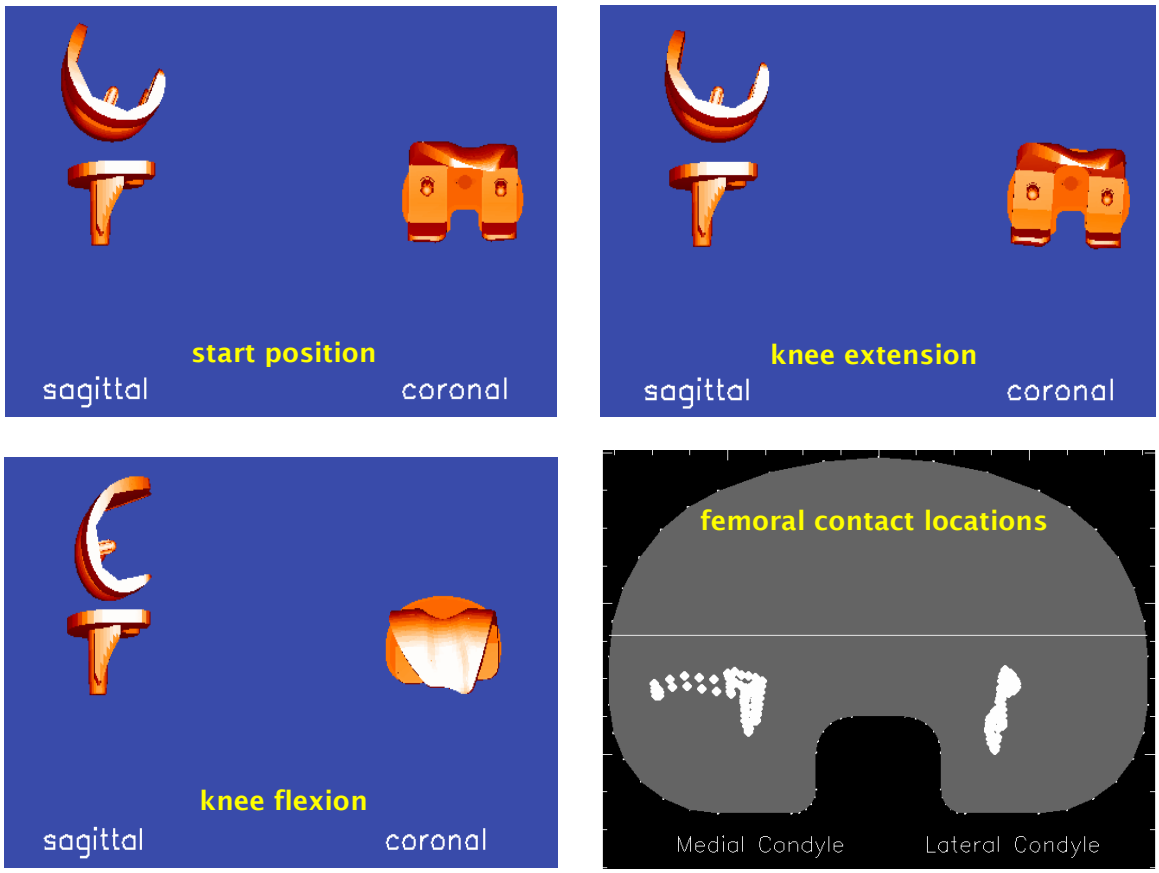

Figure 11.4: Right Femoral and Tibial CAD Models Replicating the Components' Configurations and Contact Locations During Increments of Dynamic Flexion/Extension Motion

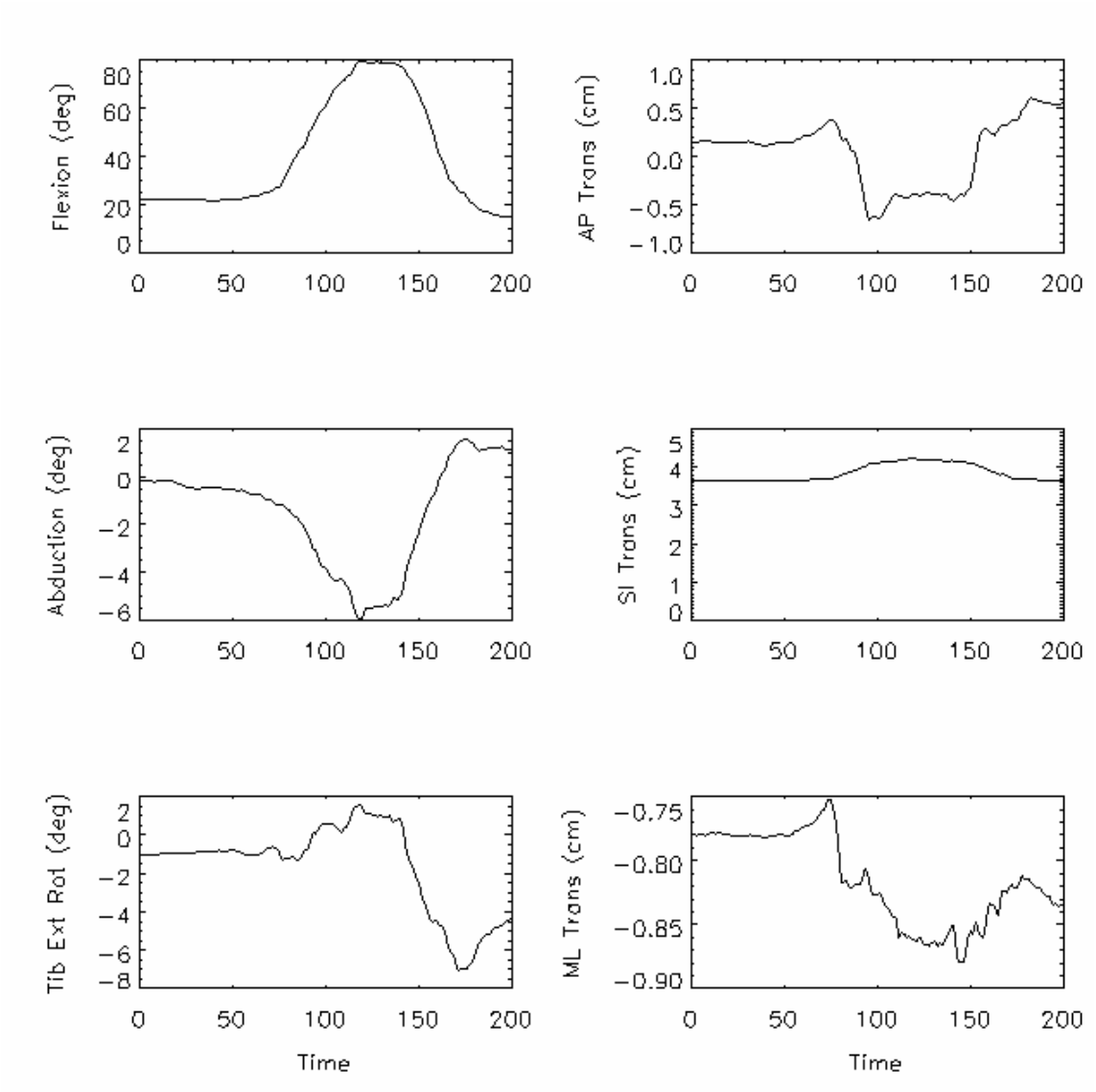

Figure 11.5: Time Varying Kinematics Measured Throughout

the Dynamic Flexion/Extension Motion

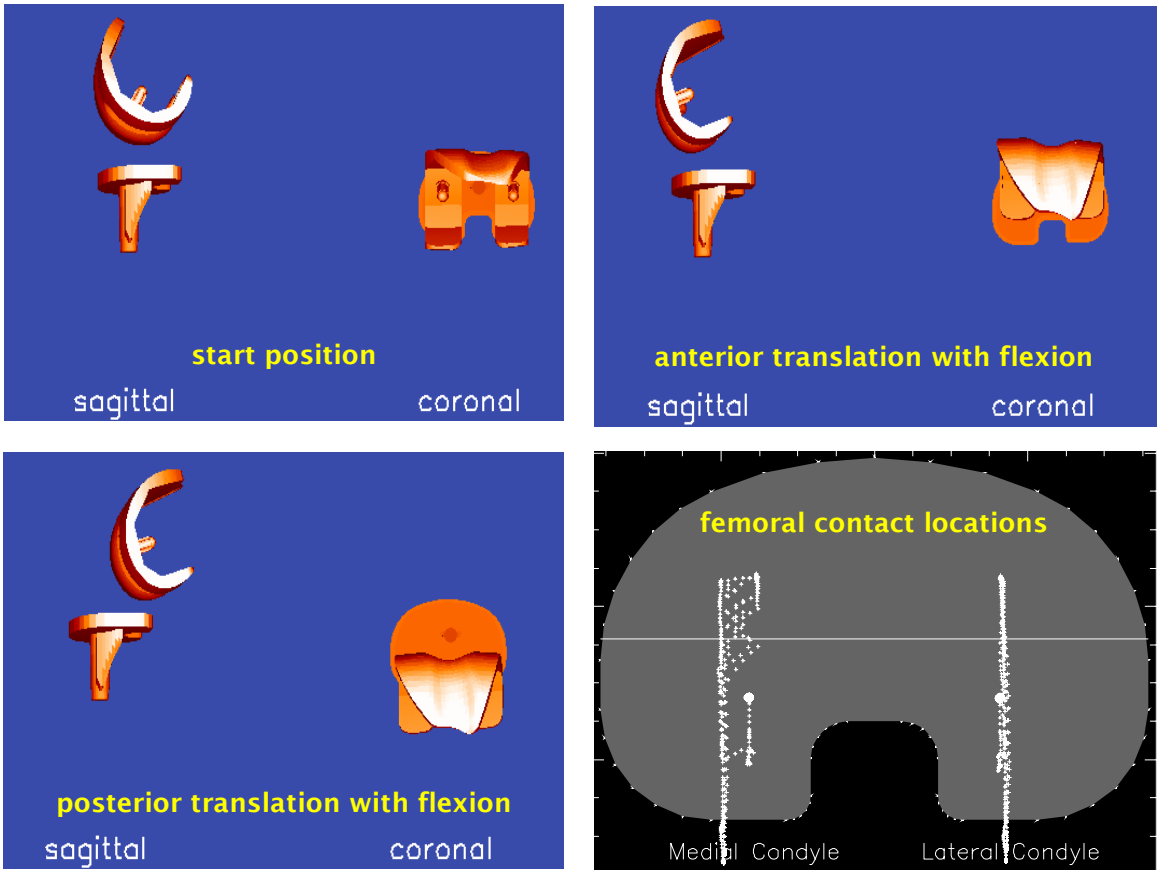

Figure 11.6: Right Femoral and Tibial CAD Models Replicating the Components' Configurations and Contact Locations During Increments of Dynamic Flexion/Extension and Anterior/Posterior Translation Motions

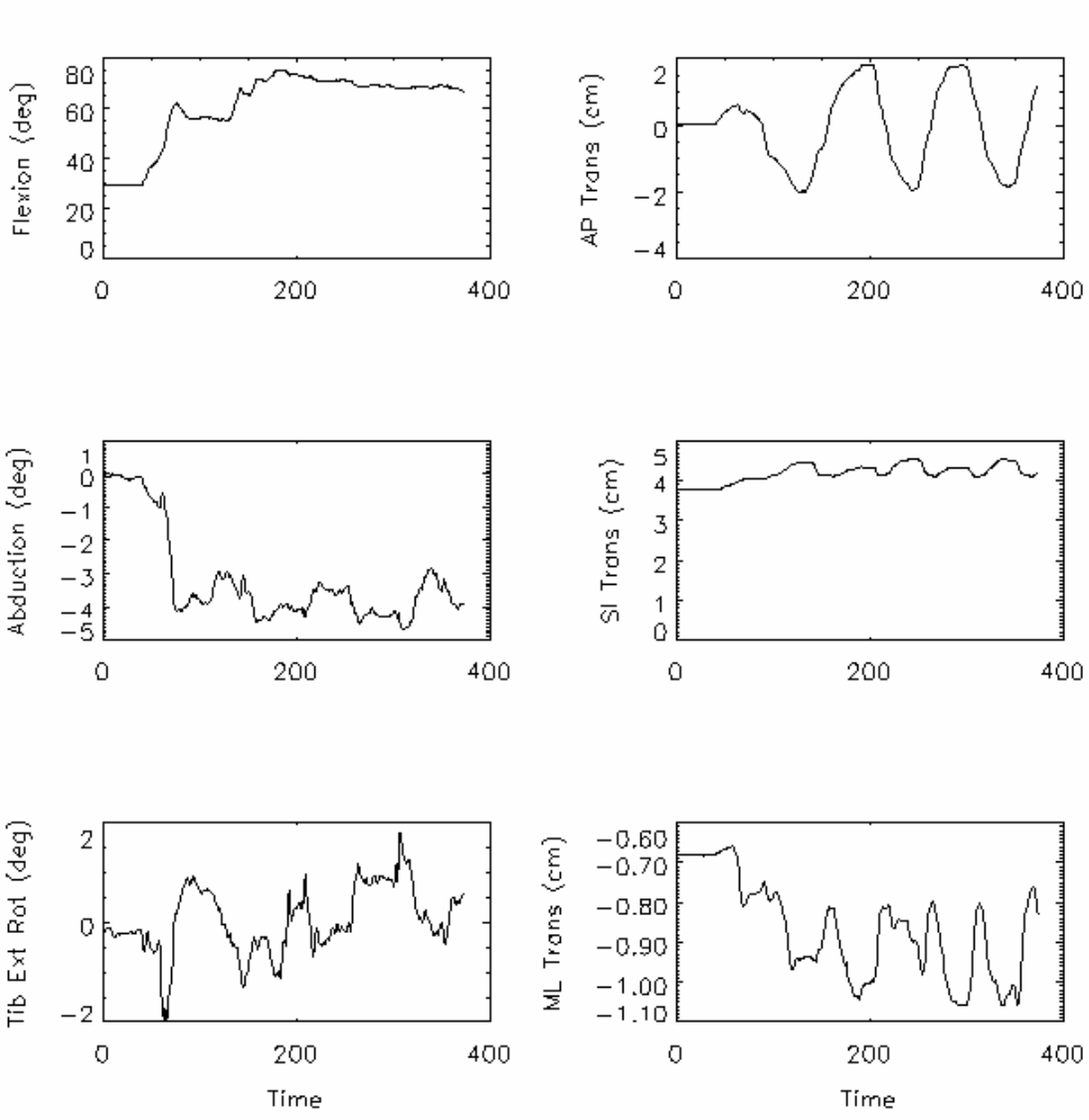

Figure 11.7: Time Varying Kinematics Measured Throughout the Dynamic Flexion/Extension and Anterior/Posterior Translation Motions

CONCLUSIONS AND RECOMMENDATIONS

Evaluation of retrieved joint arthroplasty bearings provides unique evidence related to the physiological environment in which bearing materials are expected to perform. This dissertation described the development of novel spatial sensors and measurement strategies for standardized, quantitative assessments of arthroplasty bearings, with particular emphasis toward understanding the biomechanical conditions specific to bearing function in patients. These quantitative assessments proved complementary to outcome evaluations commonly applied to TJA patients in a clinical setting and complementary to existing preclinical methodologies for prospective evaluation of bearing performance.

This dissertation presented experimental techniques in Chapter 1 that were applied to a series of 10 individual studies, each with unique hypotheses originating from the context of the retrieved bearing performance. Chapter 2 through Chapter 7 characterized TKR and THR bearing performance under physiologic conditions by quantifying the cumulative damage that occurred at the bearing surfaces. Those assessments of *in vivo* performance were then compared with results from contemporary joint wear simulation in Chapter 8 and contact modeling in Chapters 9 and 10, with the objectives of those studies verifying that the biomechanical simulations and analytical models accurately represent the in vivo conditions they are meant to simulate. Finally, Chapter 11 explored the relationship between tibiofemoral kinematics and articular geometry. This dissertation provides useful, quantitative endpoints benefiting the

development of simulations and musculoskeletal models that better mimic *in vivo* conditions and challenge what is considered to be normal function for joint replacements.

Chapter 2 utilized optical sensors combined with biomechanical testing to demonstrate that duration of physiological loading affects modularity features and the distribution of damage patterns on TKA polyethylene bearings retrieved at autopsy. Contrary to conventional thought, modularity did not degrade with duration of function and there was evidence that polyethylene deformation into the textured tibial baseplate enhanced the interlock at the modular interface. The backside damage area and location corresponded to articular damage, consistent with transmission of loading conditions through the full insert thickness. However, substantial differences between the articular and backside damage modes suggest different wear mechanisms exist at the two interfaces during physiological loading. Based on these observations, it is recommended that modular TKA designs include full peripheral rim capture mechanisms.

Chapter 3 utilized optical sensors and reported apparent contradictions between predicted performance and actual in vivo performance of mobile-bearing TKA retrieved after 1 to 15 years in-situ. Anticipated clinical consequences of bearing wear, such as osteolysis, were not realized despite bearing wear and bearing fracture. Observed fatigue-related damage modes provided evidence of degraded material properties and a changing radius of tibial-femoral contact during dynamic knee motion. Based on these data from retrieved TKA, it is recommended that multiple flexion positions and dynamic loading conditions be included in analytical models of contact area and contact stress in an effort to improve the predictive power of the models. The inclusion of varied material

properties in predictive models also is recommended, as the physiological environment generated wear modes consistent with degraded material properties.

In Chapter 4, relationships between patellar-femoral geometry and TKA biomechanics were explored using optical sensors to assess damage patterns on two different patellar bearing designs. Evidence of compromised bearing mobility and deleterious loading conditions were observed on retrieved mobile-bearing patellae, resulting in severe polyethylene wear and fracture. Furthermore, both dome-shaped and fully congruent patellar component designs had damage modes consistent with small areas of contact enduring high contact stresses. It is recommended that preclinical biomechanical models of patellar-femoral function after TKA include variations in bearing alignment to better predict the observed damage on these retrieved patellar components.

Chapter 5 used optical sensors to evaluate twelve well-functioning knee prostheses retrieved at autopsy from TKA patients. This study supported the observation that different articular wear mechanisms correspond to visibly different articular wear modes and different wear particle sizes with associated biological response. It was hypothesized that different wear modes on retrieved polyethylene bearings would correspond to wear particle size and shape and the corresponding histological responses. Although the majority of polyethylene particles recovered from periprosthetic tissues were <4 μm in diameter, which is within the range for stimulating a bone resorbing biological response, there was a noted absence of osteolysis. Abrasive bearing wear associated with extra-articular bone contact impacted the accumulation of polyethylene debris in the tissues and demonstrated that unanticipated contact mechanisms can affect

bearing performance. Continued effort to obtain autopsy retrieved prostheses is recommended, since these retrievals provide context for our understanding of "well-functioning" joint replacement.

Chapter 6 utilized optical and spatial sensors to assess articular damage on nonconforming UKA bearings. Variations in prosthesis alignment, due to surgical technique and dynamic knee motions, were evident by the distribution of damage patterns on the bearing surfaces. Different articular wear mechanisms contributed to visibly different wear modes and bearing deformation. Deformity of the bearing surface was consistent with contact stresses exceeding the yield strength of polyethylene, but fatigue-related damage mechanisms were infrequent. The inclusion of time-dependent material properties in analytical models is recommended in an effort to improve the models' abilities to predict clinical performance of nonconforming polyethylene bearings.

Chapter 7 explored the association between THA bearing geometry and the clinical consequences of hip instability. A spatial sensor applied to retrieved polyethylene acetabular bearings proved useful for assessing initial bearing geometry and the change in bearing shape as a consequence of femoral head penetration and bearing wear. This study showed a relationship between bearing articular geometry and hip dislocation, as predicted by analytical models and demonstrated by instability and poor THA performance in some clinical outcome studies. Based on these results, it is recommended that head center inset be used as a liner design parameter for improved hip stability. Furthermore, the geometry of the THA bearings assessed in this study provided unique wear paths to guide the positioning of the spatial sensor. The concept of using wear patterns to estimate contact pathways warrants further exploration to expand its utility.

Chapter 8 utilized optical and spatial sensor to compare well-functioning retrieved polyethylene TKA bearings to bearings tested in a knee joint wear simulator. This study demonstrated the value of spatial sensors to generate uniform, quantitative assessments from both retrieved and simulator worn bearings. The effect of altered input controls was evident in the results. Observed differences in damage extent on the retrieved and simulator worn inserts were consistent with differences in the tibiofemoral contact mechanics of the simulator and those known to occur in patients during functional activities. Based on these comparisons, it is recommended that knee joint wear simulators continue to be evaluated against *in vivo* assessments to assure the simulation methodologies accurately represent the *in vivo* conditions they are meant to simulate.

In Chapter 9, quantitative assessments of damage patterns on a retrieved TKA polyethylene bearing were part of the verification process for an analytical modeling approach to predict patient-specific bearing damage. This approach incorporated in vivo measures of dynamic knee function and dynamic contact and wear models into one framework for preclinical predictions of bearing performance. Despite a number of necessary simplifying assumptions in the analytical models, the damage predictions were consistent with the damage patterns measured from the retrieved insert. It is recommended that objective, quantitative design assessment tools be developed to combine *in vivo* evaluations, such as dynamic kinematics or wear, with computational analyses.

Verification of the predictive capabilities of computational modeling was further explored in Chapter 10, with comparison of finite element modeling and damage assessments of TKA polyethylene bearings. Stresses in polyethylene bearings predicted for the stance phase of walking gait were used to compare TKA designs and explore the

relationships between articular conformity and contact stress. It is recommended that assessments from retrieved bearings be used to provide relevant benchmarks for verifying models' simplifying assumptions and to provide some confidence in the clinical relevance of the resulting predictions. Extending finite element models to consider damage accumulation from cyclic loading and the role of knee kinematics in stress distribution is also recommended.

The objective of Chapter 11 was to develop measurement techniques capable of exploring relationships between articular damage on TKA polyethylene bearings and the range of *in vivo* knee kinematics contributing to such damage. Optical and spatial sensors developed in Chapters 6 and 7 and applied to THA were explored for use with TKA, using the articular geometry of polyethylene tibial inserts to guide the position and orientation of the femoral component counterface. The results were consistent with the more complex kinematic pathway in TKA compared to THA. Continuing to expand the utility of the spatial sensors presented in this chapter is recommended to provide quantitative estimates of knee kinematics to other test methodologies based on the variety of contact pathways evident on retrieved TKA bearings. Furthermore, it is recommended that articular damage patterns on retrieved tibial inserts be used to estimate the "contact envelope", or range of tibiofemoral contact, that exists during *in vivo* function, prior to implant retrieval. Of critical importance, this measurement technique will allow the massive historical databank of retrieved implants to be reassessed to infer knee kinematics and this information is complementary to surface damage characterizations already performed.

The results presented in this dissertation achieve the objective of developing novel spatial sensors for quantitative assessment of retrieved arthoplasty bearings. Bearings that had endured a finite duration of function in patients were assessed, with particular emphasis on expanding our understanding of the biomechanical conditions contributing to bearing wear. Several quantifiable parameters were identified that proved comparable to pre-clinical *in vitro* wear tests, including knee wear simulation and analytical modeling. These comparisons provided clinical relevance to the existing methodologies, advancing the prospective evaluation of bearing materials and designs for total joint arthroplasty.

Limitations with the methods used in this dissertation are common to most studies of retrieved joint arthroplasty bearings, as detailed in the various individual chapters. It is recognized that conditions existing at the time of retrieval may not always reflect the lifetime functional performance of the bearing and confounding factors affecting the observed damage patterns could not always be investigated to the extent desired. Clinical context was provided in as much detail as was available from medical records, including duration of function and whether the retrieved bearings were well-functioning at the time of procurement. However, patients referred into our Implant Retrieval Program sometimes lacked complete follow-up records and serial radiographs. As this dissertation focused on biomechanical factors, the effects of material properties often were left unexplored or were grossly classified based on the performance of well-characterized bearing materials, e.g. polyethylene sterilized using gamma radiation and stored in an ambient environment prior to implantation. New bearing materials introduced in the previous five years hold the promise for improved bearing durability. Applying the spatial sensors and measurement techniques developed in this dissertation to retrieved

bearings manufactured from the new materials will provide useful metrics for assessing that durability after function in the physiologic environment. Finally, the approximately 225 retrieved bearings included in this dissertation represent only a fraction of the total number of bearings used in orthopaedic medicine. Although this small number cannot be considered representative of the entire population, the information gained proved useful for challenging the general rationale for bearing design concepts based on unique quantitative assessments.

REFERENCES CITED

1. Argenson JN, O'Connor JJ. Polyethylene wear in meniscal knee replacement. A one to nine-year retrieval analysis of the Oxford knee. *J Bone Joint Surg Br*. 1992; 74(2):228-32.

2. ASTM F 75-01. Standard specification for cobalt-28 chromium-6 molybdenum alloy castings and casting alloy for surgical implants. Annual Book of ASTM Standards. 2002; ASTM International, West Conshohocken, PA.

3. ASTM F 648-00. Standard specification for ultra-high-molecular-weight polyethylene powder and fabricated form for surgical implants. Annual Book of ASTM Standards. 2002; ASTM International, West Conshohocken, PA.

4. ASTM F 1715-00. Standard guide for wear assessment of prosthetic knee designs in simulator devices. Annual Book of ASTM Standards. 2002; ASTM International, West Conshohocken, PA.

5. ASTM F 2033-00. Standard specification for total hip joint prosthesis and hip endoprosthesis bearing surfaces made of metallic, ceramic and polymeric materials. Annual Book of ASTM Standards. 2002; ASTM International, West Conshohocken, PA.

6. Banks SA, Fregly BJ, Boniforti F, Reinschmidt C, Romagnoli S. Comparing *in vivo* kinematics of unicondylar and bi-unicondylar knee replacements. *Knee Surg Sports Traumatol Arthros*c. 2005; 13(7):551-6.

7. Banks SA, Harman MK, Hodge WA. Mechanism of anterior impingement damage in total knee arthroplasty. *J Bone Joint Surg Am*. 2002; 84(suppl 2):37-42.

8. Banks SA, Hodge WA. Accurate measurement of three-dimensional knee replacement kinematics using single-plane fluoroscopy. *IEEE Trans Biomed Eng*. 1996; 43:638-49.

9. Banks SA, Hodge WA. Design and activity dependence of kinematics in fixed and mobile-bearing knee arthroplasties. *J Arthroplasty*. 2004; 19(7):809-16.

10. Banks SA, Hodge WA: Implant design affects knee arthroplasty kinematics during stair-stepping. *Clin Orthop*. 2004; 426:187-93.

11. Banks SA, Markovich GD, Hodge WA. In vivo kinematics of cruciate-retaining and substituting knee arthroplasties. *J Arthroplasty*. 1997; 12:297-304.

12. Banks SA, Markovich GD, Hodge WA. The mechanics of knee replacements during gait: *In vivo* fluoroscopic analysis of two designs. *Am J Knee Surg*. 1997; 10(4):261-7.

13. Banks, SA. Model based 3D kinematic estimation from 2D perspective silhouettes: Application with total knee prostheses. 1992; Massachusetts Institute of Technology, Cambridge, MA.

14. Banks SA. Understanding knee arthroplasty kinematics: News you can use. In *Insall & Scott Surgery of the Knee, 4th edition*, Scott WN (ed.). 2005; 1(11):258-64, Elsevier Inc., Philadelphia, PA.

15. Bargmann LS, Bargmann BC, Collier JP, Currier BH, Mayor MB. Current sterilization and packaging methods for polyethylene. *Clin Orthop*. 1999; (369):49-58.

16. Bartel DL, Bicknell VL, Wright TM. The effect of conformity, thickness, and material on stresses in ultra-high molecular weight components for total joint replacement. *J Bone Joint Surg Am*. 1986; 68:1041-51.

17. Beaule PE, Campbell PA, Walker PS, Schmalzried TP, Dorey FJ, Blunn GW, Bell CJ, Yahia, Amstutz HC. Polyethylene wear characteristics in vivo and in a knee simulator. *J Biomed Mater Res*, 2002; 60:411-9.

18. Bei, Y., Fregly, B. J., Sawyer, W. G., Banks, S. A., and Kim, N. H. The relationship between contact pressure, insert thickness, and mild wear in total knee replacements. *Comp Modeling Eng & Sci*, 2004; 6:145-152.

19. Bei Y, Fregly BJ. Multibody dynamic simulation of knee contact mechanics. *Med Eng Phys*. 2004; 26(9):777-89.

20. Bellemans J, Banks SA, Victor J, Vandenneuker H, Moermans A. Fluoroscopic analysis of deep flexion kinematics in total knee arthroplasty: The influence of posterior condylar offset. *J Bone Joint Surg Br*, 2002; 84(1):50-3.

21. Benevenia J, Lee FY-I, Buechel F, Parsons JR. Pathologic supracondylar fracture due to osteolytic pseudotumor of knee following cementless total knee replacement. *J Biomed Mater Res (Appl Biomater)* 1998; 43:473-7.

22. Benson LC, DesJardins JD, LaBerge M. Effects of *in vitro* wear of machined and molded UHMWPE tibial inserts on TKR kinematics. *J Biomed Mater Res (Appl Biomater)*. 2001; 58:496-504.

23. Bergmann G, Graichen F, Rohlmann A. Hip joint loading during walking and running, measured in two patients. *J Biomech*. 1993; 26(8):969-90.

24. Bloebaum RD, Bachus KN, Rubman MH, Dorr LD. Postmortem comparative analysis of titanium and hydroxyapatite porous-coated femoral implants retrieved from the same patient: A case study. *J Arthroplasty*. 1993; 8(2):203-11.

25. Bloebaum RD, Nelson K, Dorr L, Hofmann AA; Lyman DJ. Investigation of early surface delamination observed in retrieved heat-pressed tibial inserts. *Clin Orthop.* 1991; 269:120-7.

26. Bloebaum RD, Rhodes DM, Rubman MH, Hofmann AA. Bilateral tibial components of different cementless designs and materials. Microradiographic, backscattered imaging, and histologic analysis. *Clin Orthop*. 1991; 268:179-87.

27. Blunn GW, Walker PS, Joshi A, Hardinge K. The dominance of cyclic sliding in producing wear in total knee replacements. *Clin Orthop.* 1991;273:253-60.

28. Blunn GW, Joshi AB, Minns RJ, et al: Wear in retrieved condylar knee arthroplasties: A comparison of wear in different designs of 280 retrieved condylar knee prostheses. *J Arthroplasty.* 1997; 12:281-90.

29. Blunn GW, Walker PS, Joshi A, Hardinge K. The dominanace of cyclic sliding in producing wear in total knee replacements. *Clin Orthop*. 1991; 273:253-60.

30. Bohl JR, Bohl WR, Postak PD, Greenwald AS. The effects of shelf life on clinical outcome for gamma sterilized polyethylene tibial components. *Clin Orthop.* 1999; 367:28-38.

31. Bosco J, Benjamin J, Wallace D. Quantitative and qualitative analysis of polyethylene wear particles in synovial fluid of patients with total knee arthroplasty. A preliminary report. *Clin Orthop*. 1994; 309:11-9.

32. Cadambi A, Engh GA, Dwyer KA, Vinh TN. Osteolysis of the distal femur after total knee arthroplasty. *J Arthroplasty*. 1994; 9(6):579-94.

33. Clarke IC, Johnson S, Phipatanakul W, Good V. Effects of hip-loading input on simulated wear of Al2O3-PTFE materials, *Wear.* 2001; 250:159-66.

34. Clarke I. Wear-screening and joint simulation studies versus materials selection and prosthesis design. *CRC Critical Rev Biomed En*g. 1982; 8(1):29-91.

35. Clarke IC, Gustafson A, Jung H, Fujisawa A. Hip-simulator ranking of polyethylene wear. *ACTA Orthop Scand*. 1996; 67(2):128-32.

36. Collier JP, Bauer TW, Bloebaum RD, Bobyn JD, Cook SD, Galante JO, Harris WH, Head WC, Jasty MJ, Mayor MB. Results of implant retrieval from postmortem specimens in patients with well-functioning, long-term total hip replacement. *Clin Orthop*. 1992; 274:97-112

37. Collier JP, Currier BH, Kennedy FE, Currier JH, Timmins GS, Jackson SK, Brewer RL. Comparison of cross-linked polyethylene materials for orthopaedic applications. *Clin Orthop*. 2003; 414:289-304.

38. Collier MB, Jewett BA, Engh CA. Clinical assessment of tibial polyethylene thickness: comparison of radiographic measurements with as-implanted and as-retrieved thicknesses. *J Arthroplasty*. 2003; 18(7):860-6.

39. Collier JP, Sperling DK, Currier JH, Sutula LC, Saum KA, Mayor MB. Impact of gamma sterilization on clinical performance of polyethylene in the knee. *J Arthroplasty*. 1996; 11(4):377-89.

40. Collier JP, Sutula LC, Currier BH, Currier JH, Wooding RE, Williams IR, Farber KB, Mayor MB. Overview of polyethylene as a bearing material: comparison of sterilization methods. *Clin Orthop*. 1996; 333:76-86.

41. Currier BH, Currier JH, Collier JP, Mayor MB. Effect of fabrication method and resin type on performance of tibial bearings. *J Biomed Mater Res*. 2000; 53(2):143-51.

42. Currier BH, Currier JH, Collier JP, Mayor MB, Scott RD. Shelf life and in vivo duration. Impacts on performance of tibial bearings. *Clin Orthop*. 1997; 342:111-22.

43. Currier JH, Duda JL, Sperling DK, Collier JP, Currier BH, Kennedy FE. In vitro simulation of contact fatigue damage found in ultra-high molecular weight polyethylene components of knee prostheses. *Proc Inst Mech Eng [H]*. 1998; 212(4):293-302.

44. Dannenmaier WC, Haynes DW, Nelson CL. Granulomatous reaction and cystic bony destruction associated with high wear rate in a total knee prosthesis. *Clin Orthop.* 1985; 198:224-30.

45. Deluzio KJ, Banks SA, Costigan PA, Ladouceur D, O'Flynn H, Wyss UP, Jasty M, Rubash H, Harris WH. Kinematics and kinetics of total knee replacement patients; fluoroscopy, motion analysis, and forceplate data. *Arch Physiol Biochem*. 2000. 108 (1):2-33.

46. Dennis D, Komistek R, Scuderi G, Argenson JN, Insall J, Mahfouz M, Aubaniac JM, Haas B. In vivo three-dimensional determination of kinematics for subjects with a normal knee or a unicompartmental or total knee replacement. *J Bone Joint Surg Am*. 2001; 83(Suppl 2):104-15.

47. Dennis DA, Komistek RD, Hoff WA, Gabriel SM. In vivo knee kinematics derived using an inverse perspective technique. *Clin Orthop*. 1996; 331:107-17.

48. Dennis DA, Komistek RD, Colwell CE Jr, Ranawat CS, Scott RD, Thornhill TS, Lapp MA. In vivo anteroposterior femorotibial translation of total knee arthroplasty: a multicenter analysis. *Clin Orthop*. 1998; 356:47-57.

49. Dennis DA, Komistek RD, Mahfouz MR, Haas BD, Stiehl JB. Multicenter determination of in vivo kinematics after total knee arthroplasty. *Clin Orthop*. 2003; 416:37-57.

50. Dennis DA, Komistek RD, Mahfouz MR. In vivo fluoroscopic analysis of fixed-bearing total knee replacements. *Clin Orthop*. 2003; 410:114-30.

51. DesJardins J, Aurora A, Tanner SL, Pace TB, Acampora KB, LaBerge M. Increased total knee arthroplasty ultra-high molecular weight polyethylene wear using clinically relevant hyaluronic acid simulator lubricant. *Proc Inst Mech Eng [H]: J Eng Med*. 2005; 220:1-16.

52. DesJardins JD, Walker PS, Haider H, Perry J. The use of a force-controlled dynamic knee simulator to quantify the mechanical performance of total knee replacement designs during functional activity. *J Biomech*. 2000; 33(10):1231-42.

53. D'Lima DD, Jermida JC, Chen PC, Colwell CSJ. Polyethylene wear and variations in knee kinematics. *Clin Orthop*. 392:124-130, 2001.

54. D'Lima DD, Patil S, Steklov N, Slamin JE, Colwell CW. Tibial forces measured in vivo after total knee arthroplasty. J Arthroplasty. 2006; 21(2):255-62.

55. D'Lima DD, Patil S, Steklov N, Slamin JE, Colwell CW. The Chitranjan Ranawat Award: In vivo knee forces after total knee arthroplasty. *Clin Orthop*. 2005; 440:45-9.

56. D'Lima DD, Townsend CP, Arms SW, Morris BA, Colwell CW. An implantable telemetry device to measure intra-articular tibial forces. *J Biomech*. 2005; 38(2):299-304.

57. Engh G, Dwyer K, Hanes C. Polyethylene wear of metal-backed tibial components in total and unicompartmental knee prostheses. *J Bone Joint Surg Br*. 1992; 74:9-17.

58. Estupinan JA, Bartel DL, Wright TM. Residual stresses in ultra-high molecular weight polyethylene loaded cyclically by a rigid moving indenter in nonconforming geometries. *J Orthop Res*. 1998; 16:80-8.

59. Fantozzi S, Leardini A, Banks SA, Marcacci M, Giannini S, Catani F. Dynamic in-vivo tibio-femoral and bearing motions in mobile bearing knee arthroplasty. *Knee Surg Sports Traumatol Arthrosc*, 2004; 12(2):144-51.

60. Fantozzi S, Benedetti MG, Leardini A, Banks SA, Cappello A, Assirelli D, Catani F. Fluoroscopic and gait analysis of the functional performance in stair ascent of two total knee replacement designs. *Gait Posture*. 2003; 17(3):225-34.Fehring TK, Murphy JA, Hayes TD, Roberts DW, Pomeroy DL, Griffin WL. Factors influencing wear and osteolysis in press-fit condylar modular total knee replacements. *Clin Orthop*. 2004; 428:40-50.

62. Feng EL, Stulberg SD, Wixson RL. Progressive subluxation and polyethylene wear in total knee replacements with flat articular surfaces. *Clin Orthop*. 1994; 229:60-71.

63. Fisher J, Chan KL, Hailey JL, Shaw D, Stone M. Preliminary study of the effect of aging following irradiation on the wear of ultrahigh-molecular-weight polyethylene. *J Arthroplasty*. 1995; 10(5):689-92.

64. Fregly BJ, Bei Y, Sylvester ME. Experimental evaluation of an elastic foundation model to predict contact pressures in knee replacements. *J Biomech*. 2003; 36(11):1659-68.

65. Furnes O, Espehaug B, Lie SA, Vollset SE, Engesaeter LB, Havelin LI. Early failures among 7, 174 primary total knee replacements: A follow-up study from the Norwegian Arthroplasty register 1994-2000. *ACTA Orthop Scand*. 2002; 73(2):117-29.

66. Gevaert MR, LaBerge M, Gordon JM, DesJardins. The quantification of physiologically relevant cross-shear wear phenomena on orthopaedic bearing materials using the MAX-Shear wear testing system. *J Tribology*. 2005; 127(4):740-9.

67. Gioe TJ, Killeen KK, Grimm K, Mehle S, Scheltema K. Why are total knee replacements revised?: Analysis of early revision in a community knee implant registry. *Clin Orthop*. 2004; 428:100-6.

68. Godest AC, Beaugonin M, Haug E, Taylor M, Gregson PJ. Simulation of a knee joint replacement during a gait cycle using explicit finite element analysis. *J Biomech.* 2002; 35(2):267-75.

69. Good VD, Clarke IC, Gustafson GA, Downs B, Anissian L, Sorensen K. Wear of ultra-high molecular weight polyethylene and polytetrafluoroethylene in a hip simulator: a dose-response study of protein concentration. *ACTA Orthop Scand*. 2000; 71(4):365-9.

70. Hahn DW, Wolfarth DL, Parks NL. Characterization of submicron polyethylene wear debris from synovial-fluid samples of revised knee replacements using a light-scattering technique. *J Biomed Mater Res*. 1996; 31:355-63.

71. Hailey JL, Fisher J, Dowson D, Sampath SA, Johnson R, Elloy M. A tribological study of a series of retrieved accord knee explants. *Med Eng Phys*. 1994; 16(3):223-8.

72. Hamilton MA, Sucec MC, Fregly BJ, Banks SA, Sawyer WG: Quantifying multidirectional sliding motions in total knee replacements. *J Tribology*. 2005; 127(2):280-6.

73. Harman MK, Banks SA, Hodge WA. Polyethylene damage and knee kinematics after total knee arthroplasty. *Clin Orthop*. 2001; 392:383-93.

74. Harrysson OL, Robertsson O, Nayfeh JF. Higher cumulative revision rate of knee arthroplasties in younger patients with osteoarthritis. *Clin Orthop*. 2004; (421):162-8.

75. Herberts P, Malchau H, Garellick G. The Swedish national hip arthroplasty register: Annual report 2003. www.jru.orthop.gu.se

76. Hide IG, Grainger AJ, Wallace IW, Hui A, Campbell RS. A radiological technique for the assessment of wear in prosthetic knee replacements. *Skeletal Radiol*. 2000; 29(10):583-6.

77. Hirakawa K, Bauer TW, Stulberg BN, et al. Characterization of debris adjacent to failed knee implants of 3 different designs. *Clin Orthop*. 1996; 331:151-8.

78. Hirakawa K, Bauer TW, Stulberg BN, et al: Comparison and quantitation of wear debris of failed total hip and total knee arthroplasty. *J Biomed Mater Res.* 1996; 31:257-63.

79. Hirakawa K, Bauer TW, Yamaguchi M, Stulberg BN, Wilde AH. Relationship between wear debris particles and polyethylene surface damage in primary total knee arthroplasty. *J Arthroplasty*. 1999; 14(2):165-71.

80. Hirakawa K, Yamaguchi, Bauer T. Characterization and quantitation of wear debris in primary total knee arthroplasty. *Semin Arthroplasty.* 1996; 7:285-92.

81. Hodge WA, Carlson KL, Fijan RS, Burgess RG, Riley PO, Harris WH, Mann RW. Contact pressures from an instrumented hip endoprosthesis. *J Bone Joint Surg Am*. 1989; 71(9):1378-86.

82. Hoff, W.A., Komistek, R.D., Dennis, D.A., Gabriel, S.M., Walker, S.A. Three-dimensional determination of femoral-tibial contact positions under in vivo conditions using fluoroscopy. *Clin Biomech.* 1998; 13:455-72.

83. Hood RW, Wright TM, Burstein AH. Retrieval analysis of total knee prostheses: A method and its application to 48 total condylar prostheses. *J Biomed Mater Res.* 1983; 17: 829-42.

84. Hosip-Flor S, Lester DK. Human postmortem retrieval of total hip arthroplasty. *J Arthroplasty*. 1997; 12(5)562-7.

85. Howling GI, Barnett PI, Tipper JL, et al. Quantitative characterization of polyethylene debris isolated from periprosthetic tissue in early failure knee implants and early and late failure Charnley hip implants. *J Biomed Mater Res (Appl Biomater)*. 2001; 58: 415-20.

86. Huang CH, Ho FY, Ma HM, Yang CT, Liau JJ, Kao HC, Young TH, Cheng CK. Particle size and morphology of UHMWPE wear debris in failed total knee arthroplasties- a comparison between mobile bearing and fixed bearing knees. *J Orthop Res*. 2002; 20:1038-41.

87. Incavo SJ, Mullins ER, Coughlin KM, Banks S, Banks A, Beynnon BD. Tibio-femoral kinematic analysis of kneeling after total knee arthroplasty. *J Arthroplasty*. 2004; 19(7):906-10.

88. Ingham E, Fisher J. The role of macrophages in osteolysis of total joint replacement. *Biomaterials*. 2005; 26:1271-86.

89. ISO 5832-4. Implants for surgery: Metallic materials. Part 4: Cobalt-chromium-molybdenum casting alloy. International Organization for Standardization, 1996; Geneva, Switzerland.

90. ISO 5834-1. Implants for surgery: Ultra-high molecular weight polyethylene. Part 1: Powder form. International Organization for Standardization, 1998; Geneva, Switzerland.

91. ISO 5834-2. Implants for surgery: Ultra-high molecular weight polyethylene. Part 1: Moulded forms. International Organization for Standardization, 1998; Geneva, Switzerland.

92. ISO 7206-2. Implants for surgery: Partial and total hip joint prostheses. Part 2: Articulating surfaces made of metallic, ceramic and plastic materials. International Organization for Standardization, 1998; Geneva, Switzerland.

93. ISO 7207-2. Implants for surgery: Components for partial and total knee prostheses. Part 2: Articulating surfaces made of metal, ceramic and plastic materials. International Organization for Standardization, 1998; Geneva, Switzerland.

94. ISO 14243-1. Implants for Surgery: Wear of Total Knee Joint Prostheses. Part 1: Loading and displacement parameters for wear testing machines with load control and corresponding environmental conditions for tests. International Organization for Standardization, 2000; Geneva, Switzerland.

95. ISO 14243-2. Implants for Surgery: Wear of Total Knee Joint Prostheses. Part 2: Methods of measurement. International Organization for Standardization, 2000; Geneva, Switzerland.

96. Isaac GH, Wroblewski BM, Atkinson JR, Dowson D. A tribological study of retrieved hip prostheses. *Clin Orthop*. 1992; 276:115-25.

97. Jacobs JJ, Patterson LM, Skipor AK, Hall Debra J, Urban RM, Black J, Galante JO. Postmortem retrieval of total joint replacement components. *J Biomed Mater Res (Appl Biomater)*. 1999; 48:385-91.

98. James SP, Lee KR, Beauregard GP, Rentfrow ED, McLaughlin JR. Clinical wear of 63 ultrahigh molecular weight polyethylene acetabular components: effect of starting resin and forming method. *J Biomed Mater Res*. 1999; 48(3):374-84.

99. Jasty M, Goetz DD, Bragdon CR, et al. Wear of polyethylene acetabular components in total hip arthroplasty. *J Bone Joint Surg Am*. 1997; 79(3):349-58.

100. Jones CA, Voaklander DC, Johnston DW, Suarez-Almazor ME. Health related quality of life outcomes after total hip and knee arthroplasties in a community based population. *J Rheumatol*. 2000; 27(7):1745-52.

101. Jones SMG, Pinder IM, Moran CG, et al. Polyethylene wear in uncemented knee replacements. *J Bone Joint Surg Br.* 1992; 74:18-22.

102. Kadoya Y, Revell PA, Al-Saffar N, Kobayashi A, Scott G, Freeman MAR. Bone formation and bone resorption in failed total joint arthroplasties: Histomorphometric analysis with histochemical and immunohistochemical technique. *J Ortho Res*. 1996; 14:473-82.

103. Kanekasu K, Banks SA, Honjo S, Nakata O, Hiromi K. Fluoroscopic analysis of knee arthroplasty kinematics during deep flexion kneeling. *J Arthroplasty.* 2004; 19(8):998-1003.

104. Kaneyama R, Suzuki M, Moriya H, Banks SA, Hodge WA. Fluoroscopic analysis of knee kinematics after total knee arthroplasty in osteoarthritis and rheumatoid arthritis. *Chiba Med J*. 2002; 78:193-201.

105. Karrholm J, Jonsson H, Nilsson KG, et al. Kinematics of successful knee prostheses during weight-bearing: Three-dimensional movements and positions of screw axes in the Tricon-M and Miller-Galante designs. *Knee Surg Sports Traumatol Arthrosc.* 1994; 2:50-59,.

106. Kawanabe K, Clarke IC, Tamura J, Akagi M, Good VD, Williams PA, Yamamoto K. Effects of A-P translation and rotation on the wear of UHMWPE in a total knee joint simulator. *J Biomed Mater Res*. 2001; 54(3):400-6.

107. Kellett CF, Short A, Price A, Gill HS, Murray DW. In vivo measurement of total knee replacement wear. *The Knee.* 2004; 11:183-7.

108. Kilgus D, Moreland JR, Finerman GA, et al: Catastrophic wear of tibial polyethylene inserts. *Clin Orthop*. 1991; 273:223-231.

109. Kirking B, Krevolin J, Townsend C, Colwell CW Jr, D'Lima DD. A multiaxial force-sensing implantable tibial prosthesis. *J Biomech*. 2006; 39(9):1744-51.

110. Knight JL, Gorai PA, Atwater RD, et al: Tibial polyethylene failure after primary porous-coated anatomic total knee arthroplasty: Aids to diagnosis and revision. *J Arthroplasty*. 1997; 12(1):11-20.

111. Kobayashi A, Bonfield W, Kadoya Y, et al: The size and shape of particulate polyethylene wear debris in total joint replacements. *Proc Instn Mech Engrs [H]*. 1997; 211: 11-15.

112. Komistek RD, Scott RD, Dennis DA, Yasgur D, Anderson DT, Hajner ME. In vivo comparison of femorotibial contact positions for press-fit posterior stabilized and posterior cruciate-retaining total knee arthroplasties. *J Arthroplasty*. 2002; 17(2):209-16.

113. Kotzar GM, Davy DT, Goldberg VM, Heiple KG, Berilla J, Heiple KG Jr, Brown RH, Burstein AH. Telemeterized in vivo hip joint force data: a report on two patients after total hip surgery. *J Orthop Res*. 1991; 9(5):621-33

114. Kurtz S, Mowat F, Ong K, Chan N, Lau E, Halpern M. Prevalence of primary and revision total hip and knee arthroplasty in the United States from 1990 through 2002. *J Bone Joint Surg Am*. 2005; 87(7):1487-97.

115. Kurtz SM, Lau E, Zhao K, Mowat F, Ong K, Halpern M: The future burden of hip and knee revisions: U.S. projections from 2005 to 2030. Annual Meeting of the American Academy Orthopaedic Surgeons, 2005; Chicago, IL.

116. Kurtz SM, Muratoglu OK, Evans M, Edidin AA. Advances in the processing, sterilization, and cross-linking of ultra-high molecular weight polyethylene for total joint arthroplasty. *Biomaterials*. 1999; 20:1659-88.

117. Landry ME, Blanchard CR, Mabrey JD, Wang X, Agrawal CM. Morphology of in vitro generated ultrahigh molecular weight polyethylene wear particles as a function of contact conditions and material parameters. *J Biomed Mater Res (Appl Biomater).* 1999; 48:61-9.

118. Lemons JE. Bone-biomaterial interfaces of retrieved implants. In: *The Bone Biomaterial Interface*. JE Davies (ed). 1991; University of Toronto Press, Toronto.

119. Lewis, G. Polyethylene wear in total hip and knee arthroplasties. *J Biomed Mater Res (Appl Biomater).* 1997; 38:55-75.

120. Lewis P, Rorabeck CH, Bourne RB, et al. Posteromedial tibial polyethylene failure in total knee replacements. *Clin Orthop*. 1994; 299:11-17.

121. Li S, Burstein AH. Ultra-high molecular weight polyethylene: The material and its use in total joint implants. *J Bone Joint Surg Am*. 1994; 76(7):1080-90.

122. Lingard EA, Sledge CB, Learmonth ID. Kinemax Outcomes Group. Patient expectations regarding total knee arthroplasty: differences among the United States, United kingdom, and Australia. *J Bone Joint Surg Am*. 2006; 88(6):1201-7.

123. Lidgren L, Knutson K, Robertsson O. The Swedish knee arthroplasty register: Annual report 2004. www.ort.lu.se/knee/

124. Lombardi AV Jr, Mallory TH, Dennis DA, Komistek RD, Fada RA, Northcut EJ. An in vivo determination of total hip arthroplasty pistoning during activity. *J Arthroplasty*. 2000; 15(6):702-9.

125. Mabrey JD, Keshmiri AA, Engh GA, et al. Standardized analysis of UHMWPE wear particles from failed total joint arthroplasties. *J Biomed Mater Res (Appl Biomater)*. 2002; 63:475-83.

126. MacIntosh DL. Arthroplasty of the knee in rheumatoid arthritis. *J Bone Joint Surg Br*. 1966; 48(1):179.

127. McEwen HM, Barnett PI, Bell CJ, Farrar R, Auger DD, Stone MH, Fisher J. The influence of design, materials and kinematics on the in vitro wear of total knee replacements. *J Biomech*. 2005; 38(2):357-65.

128. McGovern TF, Ammeen DJ, Collier JP, Currier BH, Engh GA. Rapid polyethylene failure of unicondylar tibial components sterilized with gamma irradiation in air and implanted after a long shelf life. *J Bone Joint Surg Am*. 2002; 84(6):901-6.

129. McKeever DC. Tibial plateau prosthesis. *Clin Orthop*. 1960; 18:86.

130. McKellop H, Shen FW, Lu B, Campbell P, Salovey R. Effect of sterilization method and other modifications on the wear resistance of acetabular cups made of ultra-high molecular weight polyethylene. A hip-simulator study. *J Bone Joint Surg Am*. 2000; 82(12):1708-25.

131. McKellop HA, Campbell P, Park S, et al. The origin of submicron polyethylene wear debris in total hip arthroplasty. *Clin Orthop*. 1995; 311: 3-20.

132. McKellop HA, Clarke IC. Evolution and evaluation of materials-screening machines and joint simulators in predicting in vivo wear phenomena. In: Ducheyne P. and Hastings GW (eds.). Functional Behavior of Orthopaedic Biomaterials, Vol. II: Applications. 1983; 3:51-85, CRC Press, Boca Raton, FL.

133. Muratoglu OK, Perinchief RS, Bragdon CR, O'Connor DO, Konrad R, Harris WH. Metrology to quantify wear and creep in polyethylene tibial inserts. *Clin Orthop*. 2003; 410:155-64.

134. Murray DW, Rushton N. Macrophages stimulate bone resorption when they phagocytose particles. *J Bone Joint Surg Br*. 1990; 72(6):988-92.

135. Nilsson KG, Karrholm J, Ekelund L. Knee motion in total knee arthroplasty. A roentgen stereophotogrammetric analysis of the kinematics of the Tricon-M knee prosthesis. *Clin Orthop*. 1990. 256:147-161.

136. Noble PC, Gordon MJ, Weiss JM, Reddix RN, Conditt MA, Mathis KB. Does total knee replacement restore normal knee function? *Clin Orthop*. 2005; 431:157-65.

137. Noble PC, Conditt MA, Thompson MT, Stein JA, Kreuzer S, Parsley BS, Mathis KB. Extraarticular abrasive wear in cemented and cementless total knee arthroplasty. *Clin Orthop.* 2003; 416:120-8.

138. Nozaki H, Banks SA, Suguro T, Hodge WA. Observations of femoral rollback in cruciate-retaining knee arthroplasty. *Clin Orthop*. 2002; 404:308-14.

139. Oakeshott R, Stiehl JB, Komistek RA, Anderson DT, Haas BD. Kinematic analysis of a posterior cruciate retaining mobile-bearing total knee arthroplasty. *J Arthroplasty*. 2003; 18(8):1029-37.

140. Peters PC, Engh G A, Dwyer K, Vinh TN. Osteolysis after total knee arthroplasty without cement. *J Bone Joint Surg Am.* 1992; 74:864-76.

141. Premnath V, Harris WH, Jasty M, Merrill EW. Gamma sterilization of UHMWPE articular implants: An analysis of the oxidation problem. *Biomaterials*. 1996; 17:1741-53.

142. Puloski SK, McCalden RW, MacDonald SJ, Rorabeck CH, Bourne RB. Tibial post wear in posterior stabilized total knee arthroplasty: An unrecognized source of polyethylene debris. *J Bone Joint Surg Am.* 2001; 83A:390-7.

143. Ranawat CS, Komistek RD, Rodriguez JA, Dennis DA, Anderle M. In vivo kinematics for fixed and mobile-bearing posterior stabilized knee prostheses. *Clin Orthop*. 2004;418:184-90.

144. Rand J, Ilstrup D. Survivorship analysis of total knee arthroplasty. Cumulative rates of survival of 9200 total knee arthroplasties. *J Bone Joint Surg Am*. 1991; 73:397.

145. Rand JA, Trousdale RT, Ilstrup D, Harmsen WS. Factors affecting the durability of primary total knee prostheses. *J Bone Joint Surg Am.* 2003; 85:259.

146. Rao A, Engh G, Collier M, Smain L. Tibial interface wear in retrieved total knee components and correlations with modular insert motion. *J Bone Joint Surg Am.* 2002; 84(10):1849-24.

147. Rawlinson JJ, Furman BD, Li S, Wright TM, Bartel DL. Retrieval, experimental, and computational assessment of the performance of total knee replacements. *J Orthop Res*. 2006; 24(7):1384-94.

148. Riley LH, Healy WL. History and evolution of total knee replacement. In: *Total Knee Arthroplasty: A Comprehensive Approach*. DS Hungerford, KA Krackow, RV Kenna (eds.). 1984; 1:1-4,Williams & Wilkins, Baltimore, MD.

149. Sanzen L, Sahlstrom A, Gentz CF, Johnell IR. Radiographic wear assessment in a total knee prosthesis. 5- to 9-year follow-up study of 158 knees. *J Arthroplasty*. 1996; 11(6):738-42.

150. Sathasivam S, Walker PS. Computer model to predict subsurface damage in tibial inserts of total knees. *J Orthop Res*. 1998; 16(5):564-71.

151. Sathasivam S, Walker PS. A computer model with surface friction for the prediction of total knee kinematics. *J Biomech*. 1997; 30(2):177-84.

152. Sauer WL, Anthony ME. Predicting the clinical wear performance of orthopaedic bearing surfaces. In: Jacobs JJ, Craig TL (eds.). Alternative bearing surfaces in total joint replacement. American Society for Testing and Materials, 1998; West Conshohoken, PA.

153. Schmalzried TP, Jasty M, Rosenberg A, et al. Polyethylene wear debris and tissue reactions in knee as compared to hip replacement prostheses. *J Appl Biomater.* 1994; 5:185-190.

154. Schmalzried TP, Campbell P, Schmitt AK, Brown IC, Amstutz HC. Shapes and dimensional characteristics of polyethylene wear particles generated in vivo by total knee replacements compared to total hip replacements. *J Biomed Mater Res (Appl Biomater)*. 1997; 38:203-10.

155. Scuderi MG, Mayor MB. The value of postmortem retrievals in the analysis of long-term, well-functioning cemented femoral stems. *Am J Orthop*. 1997; 826-35.

156. Shanbhag AS, Jacobs JJ, Glant TT, et al. Composition and morphology of wear debris in failed uncemented total hip replacmnent. *J Bone Joint Surg Br*. 1994; 76:60-7.

157. Shanbhag AS, Bailey HO, Hwang D-S, Cha CW, Eror NG, Rubash HE. Quantitative analysis of ultrahigh molecular weight polyethylene(UHMWPE) wear debris associated with total knee replacements. *J Biomed Mater Res (Appl Biomater)*. 2000; 53:100-110.

158. Short A, Gill HS, Marks B, Waite JC, Kellett CF, Price AJ, O'Connor JJ, Murray DW. A novel method for in vivo knee prosthesis wear measurement. *J Biomech*. 2005; 38:315-22.

159. Sierra RJ, Cooney WP 4th, Pagnano MW, Trousdale RT, Rand JA. Reoperations after 3200 revision TKAs: rates, etiology, and lessons learned. *Clin Orthop*. 2004; 425:200-6.

160. Silva M, Kabbash CA, Tiberi JV III, Park SH, Reilly DT, Mahoney OM, Schmalzried TP. Surface damage on open box posterior-stabilized polyethylene tibial inserts. *Clin Orthop*. 2003; 416: 135-144.

161. Smith-Peterson MN. Arthoplasty of the hip: A new method. *J Bone Joint Surg Am*. 1939; 21(2):269-88.

162. Stiehl JB, Dennis DA, Komistek RD, Keblish PA. In vivo kinematic analysis of a mobile bearing total knee prosthesis. *Clin Orthop*. 1997; 345:60-6.

163. Stiehl JB, Komistek RD, Dennis DA. Detrimental kinematics of a flat on flat total condylar knee arthroplasty. *Clin Orthop*. 1999; 365:139-48.

164. Stiehl JB, Dennis DA, Komistek RD, Keblish PA. In vivo kinematic comparison of posterior cruciate ligament retention or sacrifice with a mobile bearing total knee arthroplasty. *Am J Knee Surg*. 2000; 13(1):13-8.

165. Surace MF, Berzins A, Urban RM, Jacobs JJ, Berger RA, Natarajan RN, Andriacchi TP, Galante JO. Back surface wear and deformation in polyethylene tibial inserts retrieved postmortem. *Clin Orthop.* 2002; 404:14-23.

166. Tamura J, Clarke IC, Kawanabe K, Akagi M, Good VD, Williams PA, Masaoka T, Schroeder D, Oonishi H. Micro-wear patterns on UHMWPE tibial inserts in total knee joint simulation. *J Biomed Mater Res*. 2002; 61(2):218-25.

167. Tashman S, Anderst W. In-vivo measurement of dynamic joint motion using high speed biplane radiography and CT: application to canine ACL deficiency. *J Biomech Eng*. 2003; 125(2):238-45.

168. Taylor SJ, Walker PS, Perry JS, Cannon SR, Woledge R. The forces in the distal femur and the knee during walking and other activities measured by telemetry. *J Arthroplasty*. 1998; 13(4):428-37.

169. Tsao A, Mintz L, McRae C, et al. Failure of the porous-coated anatomic prosthesis in total knee arthroplasty due to severe polyethylene wear. *J Bone Joint Surg Am*. 1993; 75:19-26.

170. Urban JA, Collier MB, Engh CA Jr, Engh GA. Relationship between product demand, tibial polyethylene insert shelf age, and total knee arthroplasty survival: retrospective review of total knees of one design. *J Arthroplasty*. 2006; 21(3):330-7.

171. Victor J, Banks SA, Bellemans J. Kinematics of posterior cruciate ligament - retaining versus –substituting total knee arthroplasty: A prospective randomised outcome study. *J Bone Joint Surg Br.* 2005; 87(5):646-55.

172. Walker PS, Blunn GW, Perry JP, Bell CJ, Sathasivam S, Andriacchi TP, Paul JP, Haider H, Campbell PA. Methodology for long-term wear testing of total knee replacements. *Clin Ortho*. 2000; 372:290-301.

173. Walker SA, Hoff W, Komistek R, Dennis D. "In vivo" pose estimation of artificial knee implants using computer vision. *Biomed Sci Instrum*. 1996; 32:143-50.

174. Wang A, Stark C, Dumbleton JH. Mechanistic and morphological origins of ultra-high molecular weight polyethylene wear debris in total joint replacement prostheses. *Proc Instn Mech Engrs [H]*. 1996; 210:141-55.

175. Wang A, Polineni VK, Stark C, Dumbleton JH. Effect of femoral head surface roughness on the wear of ultrahigh molecular weight polyethylene acetabular cups. *J Arthroplasty*. 1998; 13(6):615-20.

176. Wasielewski RC, Galante JO, Leighty RM, et al. Wear patterns on retrieved polyethylene tibial inserts and their relationship to technical considerations during total knee arthroplasty. *Clin Orthop*. 1994; 299:31-43.

177. Wasielewski RC, Parks N, Williams I, Surprenant H, Collier JP, Engh G. Tibial insert undersurface as a contributing source of polyethylene wear debris. *Clin Orthop*. 1997; 345:53-9.

178. Weiss JM, Noble PC, Conditt MA, Kohl HW, Roberts S, Cook KF, Gordon MJ, Mathis KB. What functional activities are important to patients with knee replacements? *Clin Orthop*. 2002; 404:172-88.

179. Williams IR, Mayor MB, Collier JP. The impact of sterilization method on wear in knee arthroplasty. *Clin Orthop*. 1998; 356:170-80.

180. Wimmer MA, Andriacchi TP, Natarajan RN, et al. A striated pattern of wear in ultrahigh-molecular-weight polyethylene components of Miller-Galante total knee arthroplasty. *J Arthroplasty*. 1998; 13:8-16.

181. Wimmer MA, Andriacchi TP. Tractive forces during rolling motion of the knee: Implications for wear in total knee replacement. *J Biomech.* 1997; 30(2):131-7.

182. Wolfarth DL, Han DW, Bushar G, et al. Separation and characterization of polyethylene wear debris from synovial fluid and tissue samples of revised knee replacemnts. *J Biomed Mater Res.* 1997; 34: 57-61.

183. Wright TM, Rimnac CM, Stulberg SD, et al. Wear of polyethylene in total joint replacements: Observations from retrieved PCA knee implants. *Clin Orthop*. 1992; 276:126-34

184. Wroblewski BM. Direction and rate of socket wear in Charnley low-friction arthroplasty. *J Bone Joint Surg Br.* 1985; 67(5):757-61.

185. Wrona M, Mayor MB, Collier JP, Jensen RE. The correlation between fusion defects and damage in tibial polyethylene bearings. *Clin Orthop*. 1994; 299:92-103.

186. Young SK, Keller TS, Greer KW, Gorhan MC. Wear testing of UHMWPE tibial components: Influence of oxidation. *J Tribology*. 2000; 122:323-31.

187. Zuffi S, Leardini A, Catani F, Fantozzi S, Cappello A. A model-based method for the reconstruction of total knee replacement kinematics. *IEEE Trans Med Imaging*. 1999; 18(10):981-91.